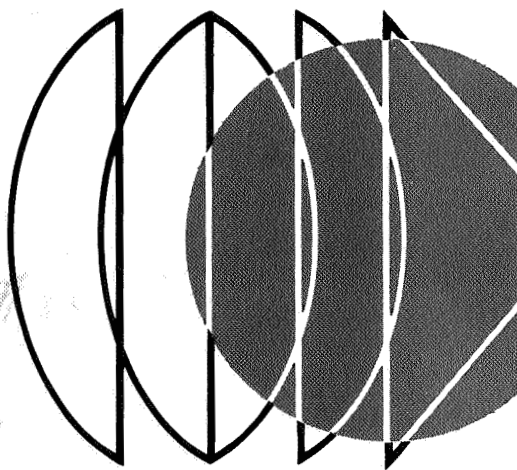


26
PART E ALTERNATIVES AND SYSTEMS A
PART F FUTURE MISSION OPTIONS

*PREPARED FOR THE
NASA-AMSC
CONTRACT NUMBER 952000*

**VOYAGER
CAPSULE
PHASE B
FINAL REPORT**



VOLUME IV ENTRY SCIENCE PACKAGING

JET PROPULSION LABORATORY
PASADENA, CALIFORNIA
CONTRACT NUMBER 952000

15 JPL

REPORT ORGANIZATION

VOYAGER PHASE B FINAL REPORT

The results of the Phase B VOYAGER Flight Capsule study are organized into several volumes. These are:

- Volume I Summary
- Volume II Capsule Bus System
- Volume III Surface Laboratory System
- Volume IV Entry Science Package
- Volume V System Interfaces
- Volume VI Implementation

This volume, Volume IV, describes the McDonnell Douglas selected design for the Entry Science Package. It is arranged in 11 parts, A through K, and bound in 4 separate documents, as noted below.

- Part A Introduction and Summary
- Part B Objectives and Requirements
- Part C Design Criteria and Constraints 1 Document
- Part D Selected Design Concept
- Part E Alternatives and Systems Analysis
- Part F Future Mission Options 1 Document
- Part G Subsystem Equipment 1 Document
- Part H Reliability
- Part I Planetary Quarantine
- Part J Operational Support Equipment 1 Document
- Part K Interface Alternatives

In order to assist the reader in finding specific material relating to the Entry Science Package, Figure 1 cross indexes broadly selected subject matter, at the system and subsystem level, through all volumes.

TABLE OF CONTENTS

	<u>Page</u>
PART E ALTERNATIVES AND SYSTEMS ANALYSIS	
SECTION 1 PRINCIPAL ALTERNATIVES AND SELECTION FACTORS	1-1
1.1 Configuration and Interface	1-1
SECTION 2 EXPERIMENT ANALYSIS	2-1
2.1 Atmospheric Properties Reconstruction	2-1
2.1.1 Alternatives	2-1
2.1.2 Comparison of Alternatives	2-2
2.1.3 Results	2-9
2.2 Entry TV Observations	2-10
SECTION 3 SCIENCE INSTRUMENTS	3-1
3.1 Atmospheric Properties Instruments	3-2
3.1.1 Pressure	3-2
3.1.2 Direct Density Measurements	3-7
3.1.3 Temperature	3-17
3.1.4 Composition Determination by Mars Spectrometer	3-20
3.1.5 Composition Determination by Absorption Methods	3-22
3.1.6 Acceleration	3-35
3.1.7 Capsule Bus Sensor Data	3-39
3.2 Entry TV	3-42
3.2.1 Constraints	3-42
3.2.2 Alternatives	3-42
3.2.3 Comparison	3-42
3.2.4 Selection	3-42
SECTION 4 ENTRY SCIENCE PACKAGE - SUPPORTING SUBSYSTEMS	
4.1 Electrical Power	
4.2 Telecommunications	4-14
4.2.1 Propagation Analysis	4-14
4.2.2 Telemetry Subsystem	4-43
4.2.3 Radio Subsystem	4-59
4.2.4 Antenna Subsystem Analysis	4-64
4.2.5 Data Storage Subsystem	4-74
4.2.6 Interconnection with Capsule Bus	4-79
4.3 Structural/Mechanical Subsystem	4-29
4.4 Packaging and Cabling	4-100
4.5 Thermal Control	4-104

	<u>Page</u>
SECTION 5 CAPSULE BUS/ENTRY SCIENCE	5-1
5.1 Trajectories	5-1
5.2 De-Orbit	5-2
5.3 Aeroshell Properties	5-5
5.4 Capsule Mequencing	5-23
5.5 Aeroshell Separation	5-25
5.6 Attitude Control	5-26
5.7 Radar Altimeter	5-36
5.8 Post Touchdown Operation	5-39
PART F FUTURE MISSION OPTIONS	1

This Document Consists of the Following Pages:

Title Page

i through iv

PART E: 1

 1-1 through 1-9

 2-1 through 2-40

 3-1 through 3-47

 4-1 through 4-107

 5-1 through 5-40

PART F: 1 through 3

PART E

ALTERNATIVES AND SYSTEMS ANALYSIS

This part first summarizes important alternatives and selection considerations, and then discusses configuration alternatives. ,The discussions of entry science, instrumentation, and supporting subsystems follow. These may be supplemented by reading the material presented on the selected design concept in Part D, and the functional descriptions applicable to the selected concept, given in Part G.

VOLUME IV CROSS REFERENCE INDEX

VOLUME IV PARTS ITEM		PART A	PART B	PART C	PART D	PART E
		INTRODUCTION AND SUMMARY	OBJECTIVES AND REQUIREMENTS	DESIGN CRITERIA AND CONSTRAINTS	DESCRIPTION OF PREFERRED CONFIGURATION	PRINCIPAL ALTERNATE AND SELECTIVE FACTOR
ESP ASPECT						
MISSION	Objectives	Sec. 1.0	1.0	-	-	-
	Operations (& Profiles)	2.0 6.3	2.0	-	2.0-d 4.1 5.0	5.1 5.8
DESIGN	Configuration	3.0 6.2	√	√	1.0	1.1
	Functional	4.0	√	√	1.0	1.0
		5.0			2.0	2.0
		6.0			3.0 4.0	3.0 4.0 5.0
Weight	3.0 4.0	-	√	1.4 2.0	3.0 d	
Interfaces (See Also Volume V)		Introduction	-	1.0 2.0 3.0	1.3 2.0-d 3.0-d 4.0 5.3.4	1.1 3.0-d 4.1.3 5.0
Implementation (See Also Volume VI)		-	-	-	6.0	-
ESP EQUIPMENT OR SUBSYSTEM						
Imaging		Sec. 2.0 4.0 6.0	1.2 2.2	6.1	1.2.1 2.1 4.3.2.4	1.1 2.2 3.2 5.3.2.6
Atmospheric Properties Measurement		2.0 4.0 6.0	1.1	6.2	1.2.2 2.0 4.0-d	1.1 2.1 3.1 5.0-d
Engineering Instrumentation		-	-	-	Figure 3.0-1	Figure 4.2-1 4.2.2.2
Data Storage		6.0	-	-	2.5.3 3.2.1	4.2.5
Telecommunications		5.1	-	6.3	2.5.3 3.2	4.2
Power		5.2	-	6.3	2.5.1 3.1	4.1
Structural/Mechanical		-	-	4.0	2.5.4 3.3	4.3
Cabling and Packaging		-	-	5.0 6.3	2.5.1 3.4	4.4
Thermal Control		5.3	-	6.3	2.5.7 3.5 4.3.2	4.5

v Denotes that the part or section generally applies to the topic.

d Denotes that the topic is distributed throughout the part or section.

Figure 1

ii - /

ILLUSTRATIVE ALTERNATIVES AND SELECTION CONSIDERATIONS

ATMOSPHERIC PROPERTIES DETERMINATION

ITEM(S) AFFECTED	ALTERNATIVES	SELECTION CONSIDERATION
Instruments	<ul style="list-style-type: none"> ● Mass Spectrometer Use At High Altitude in Addition to Below Mach 5 ● Additional Instruments UV and Xray Absorbition ● γ Backscatter ● Spherical Nose Differential Pressure Sensors ● High Altitude (Molecular Flow Region) Pressure Measurement ● Accelerometer Location ● Accelerometer Sampling Rate High (10 Samples/Second) or Low (2 Samples/Second) 	<ul style="list-style-type: none"> ● Molecular Leak, Sample Porting and Valving Design ● Contribution to Density Altitude Function and Specific Atmosphere Constituents ● Direct Free Stream Density Measurement Value; Handling Problems ● Value of Redundant Source for Dynamic Pressure ● External Location or Additional Large Port ● Accelerometer Data Correction for Accelerometer Location ● Use of Accelerometer Data To Construct Angle of Attack Time History ● Amount of Data Transmitted ● Acceleration Correction for Frequency and Amplitudes due to Aeroelastic Vibration
Aeroshell	<ul style="list-style-type: none"> ● Sensor Location (Pressure, Temperature and Composition) ● Aeroshell Ports <ol style="list-style-type: none"> 1. Flush Mounted at Stagnation Point or Side Location 2. Extended Ports at Stagnation Point or Side Location Using Either Fixed or Flush Ports Capable of Extension ● Base Region Ports 	<ul style="list-style-type: none"> ● Flow Field Relationships for Sensor Data Interpretation ● Angle of Attack Excursions ● Pressure Coefficient Behavior ● Ablative Products Entering and Recondensing on Sensor Elements ● Design of Extensible Ports ● Base Region Location Measurement after Aeroshell Separation
De-Orbit	<ul style="list-style-type: none"> ● AV Monitoring For Orbit Improvement ● Trajectory Improvement vs Diagnostic Data 	<ul style="list-style-type: none"> ● Data Enhancement - Atmospheric Property Reconstruction
Attitude Control Entry	<ul style="list-style-type: none"> ● Rate Damping or Uncontrolled Rates 	<ul style="list-style-type: none"> ● α Excursion Limit ● Aerodynamic Coefficients Accuracy Enhancement ● Accelerometer Correction Accuracy Enhancement ● Instrument Placement to Avoid Contamination
Radar Altimeter	<ul style="list-style-type: none"> ● Initiate Measurement at 200,000 feet or Initiate Measurement at 30,000 feet 	<ul style="list-style-type: none"> ● Trajectory Reconstruction Accuracy Effects ● Entry Condition for Prediction Accuracy Improvements ● Altimeter Accomodation Considerations ● Attitude Oscillations
Capsule Bus Inertial Sensor	<ul style="list-style-type: none"> ● IMU Attitude Rate Output At 2 Sample/Second for Diagnostic Measurement or IMU Attitude Rate at Output 4 to 12 Sample/Second for Oscillation History 	<ul style="list-style-type: none"> ● Accuracy of Vehicle Oscillations Reconstruction Using Accelerometer and Aerodynamic Information Only
Data Handling	<ul style="list-style-type: none"> ● Mass Spectrometer and Stagnation Temperature Flow Measurements on All the Time, or Mass Spectrometer and Stagnation Temperature Blocked Until 15 to 40 Second After Peak Pressure 	<ul style="list-style-type: none"> ● Molecular Leak and Valving Design ● Thermal Design of Temperature Sensor ● Internal Blockage of Sensors due to Recondensation of Contaminants

IMAGING

ITEM(S) AFFECTED	ALTERNATIVES	SELECTION CONSIDERATION
Instrument	<ul style="list-style-type: none"> ● Camera Installation Location with Respect to Aeroshell ● Retain Camera to Impact or Eject prior to Touchdown 	<ul style="list-style-type: none"> ● Thermal Design ● Mechanical Design ● Optical Coverage/ Resolution ● Cycle Rate ● Design for Avoidance of Interference ● High Resolution Image
Aeroshell	<ul style="list-style-type: none"> ● Window Design Door Cover or Exposed, Multiple or Single Glazing; Recessed Cavity or Flush; Location; Removable Outer Pane or not ● Nose Cap Ablative or Non-Ablative 	<ul style="list-style-type: none"> ● Design and Operation Cover ● Design and Operation of Removable Outer Pane ● Sequencing Door for High Low Altitude Images ● Temperature History ● Outgassing of Ablator ● Recondensation of Ablator Products on Window ● Thermal Heating ● Imaging Periods and Image Quality Uncertainty
Attitude Control-Entry	<ul style="list-style-type: none"> ● Monitor Attitude ● Roll Stobilation 	<ul style="list-style-type: none"> ● Exposure Time and Resolution Loss due to Image Smear ● Rate Monitoring to Control Imagery
Data Handling	<ul style="list-style-type: none"> ● Image Recording Continuously From 800,000 ft, Including Low Quality Images ● Programming for Taking of Images Before and After Peak Heating Only ● Post Touchdown Imaging for Period of UHF Relay Link Availability 	<ul style="list-style-type: none"> ● Design Simplicity ● Image Sequence Value ● Spacecraft Data Storage and Transmiss ● SLS Imaging Backup ● Weight For Camera Re or For an Additional C

ENTRY SCIENCE PACKAGE SUPPORTING SUBSYSTEMS

ITEM(S) AFFECTED	ALTERNATIVES	SELECTION CONSIDERATION
POWER		
Surface Laboratory/Entry Science Package Power Interface	<ul style="list-style-type: none"> ● Internal Battery Redundancy vs Cross Link to SLS 	<ul style="list-style-type: none"> ● Overall ESP Weight ● Overall ESP Reliability ● Interface Complexity
Capsule Bus/Entry Science Package Power Interface	<ul style="list-style-type: none"> ● Provide CB power to the ESP for descent operation vs a separate ESP battery 	<ul style="list-style-type: none"> ● Overall FC Weight ● Reliability ● Future Mission ● Interface Complexity
DATA HANDLING AND TELEMETRY		
Instruments	<ul style="list-style-type: none"> ● Storage Videcon versus Buffer Storage 	<ul style="list-style-type: none"> ● Transmitter Rate Capability
Capsule Bus Telemetry ESP Entry	<ul style="list-style-type: none"> ● Cross Link ESP/CB Telemetry ● Spacecraft-Capsule Doppler Tracking from De-orbit to Entry 	<ul style="list-style-type: none"> ● Backup Telemetry System for ESP ● Improved Entry Conditions Prediction
SPACECRAFT - BORNE EQUIPMENT		
Spacecraft Telemetry	<ul style="list-style-type: none"> ● Use Spacecraft Data Storage or Use Separate Storage 	<ul style="list-style-type: none"> ● ESP/Spacecraft Interface Simplicity

Figure 1-1

1-2

SELECTED ENTRY SCIENCE PACKAGE INSTALLATION

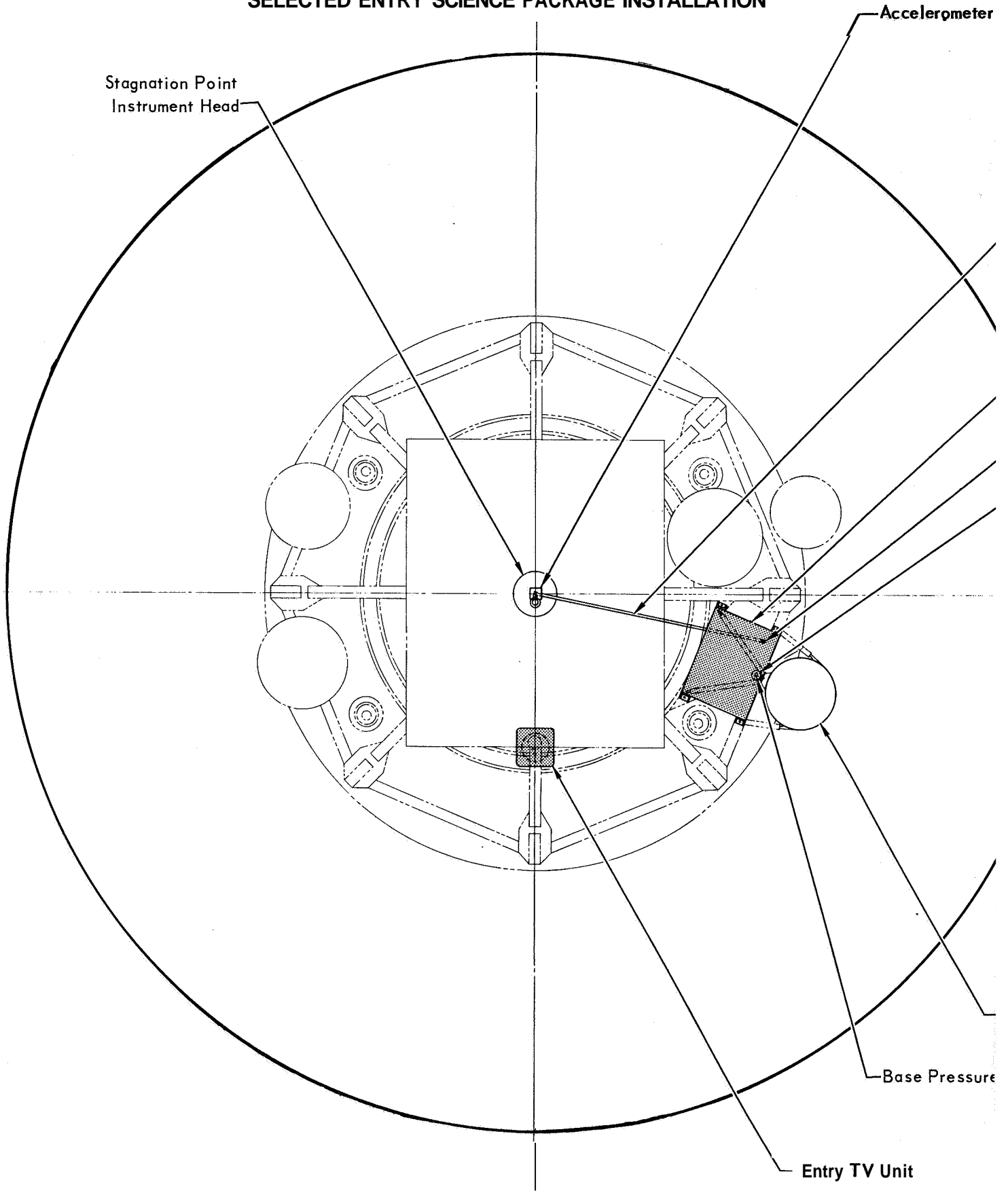
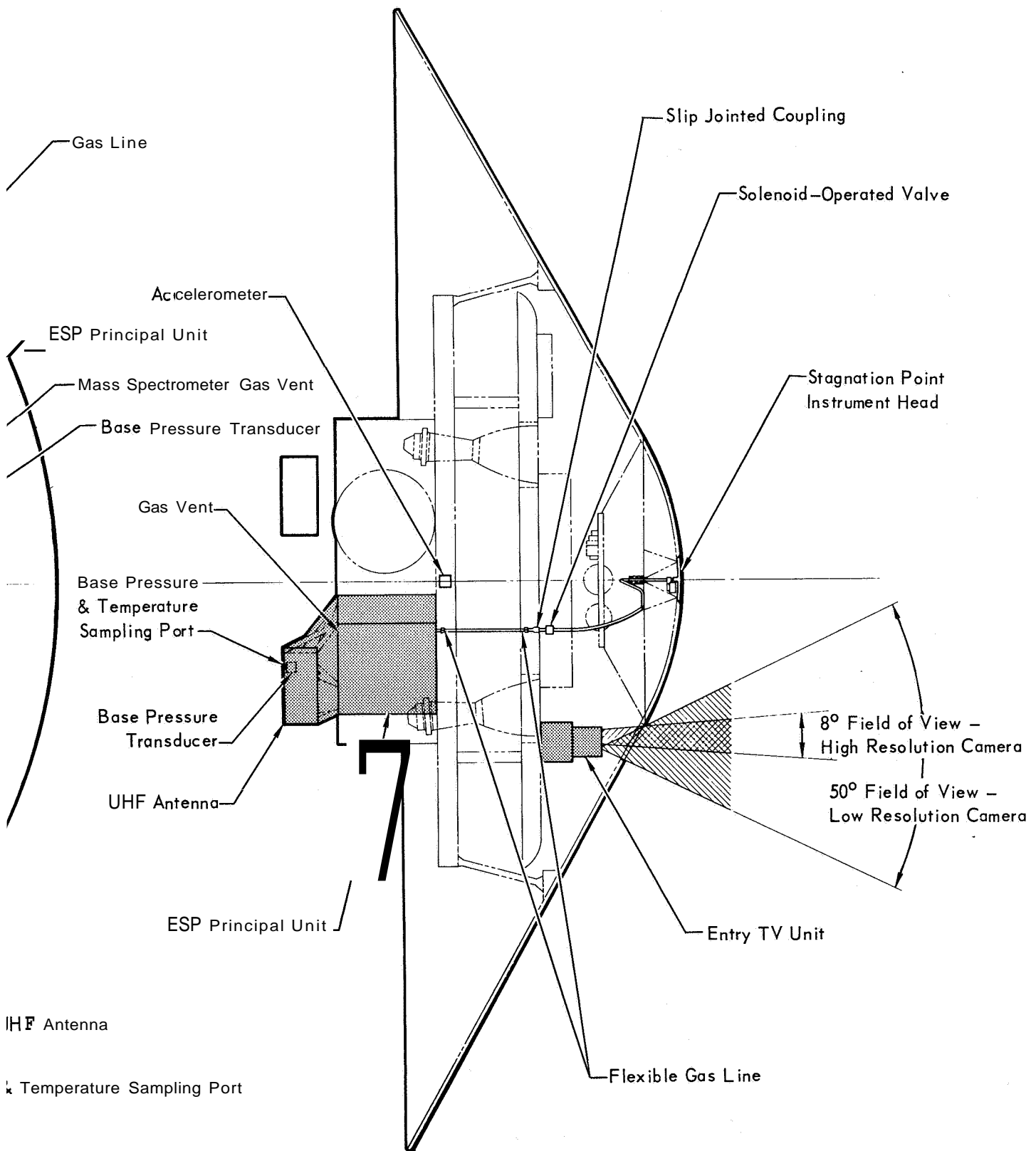


Figure 1-2

1-3-1



1-3-2

PRINCIPLE UNIT WITH SENSORS INCORPORATED

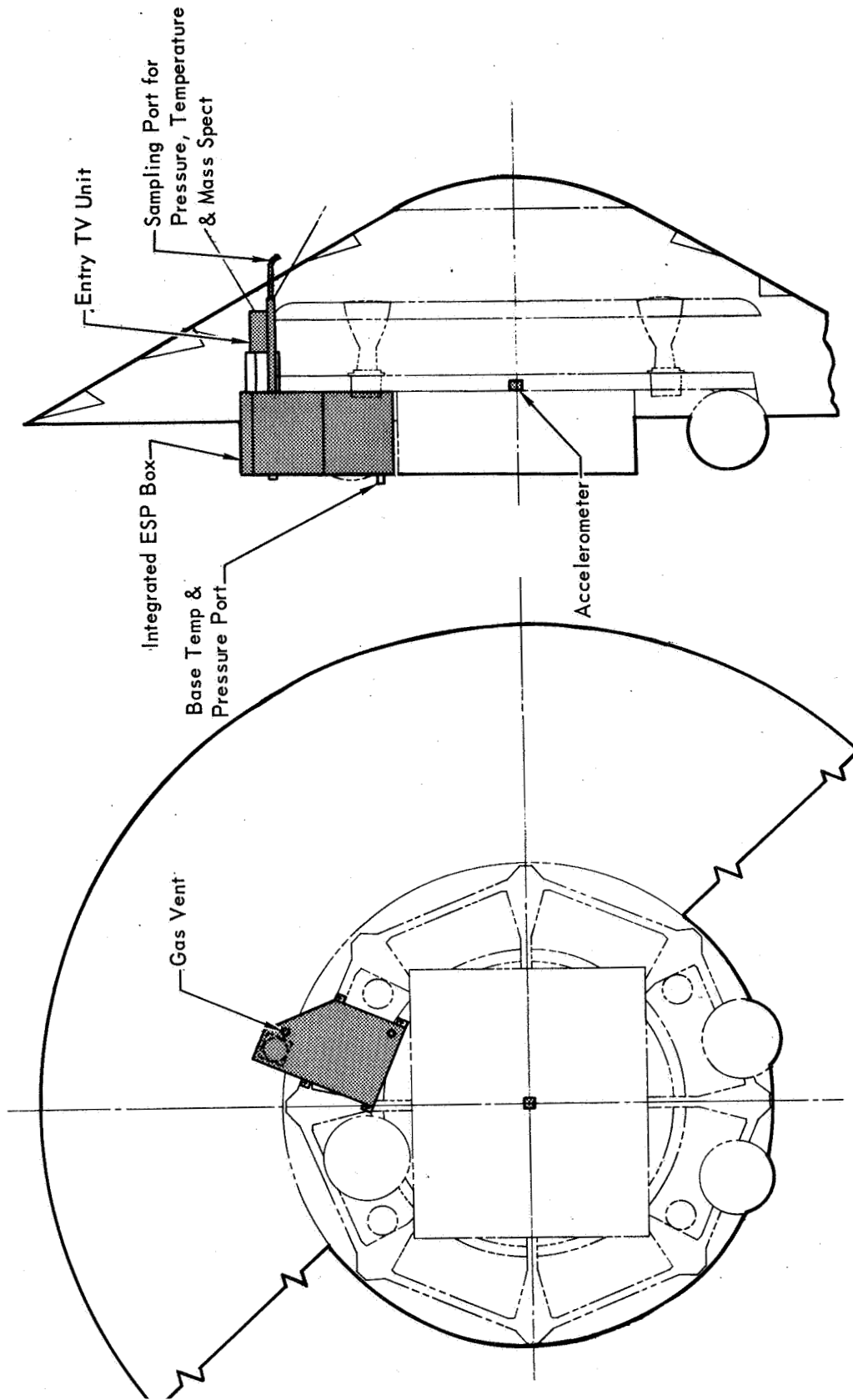


Figure 1-3

1-4

PROVISIONS FOR ADDITIONAL ESP MEASUREMENTS

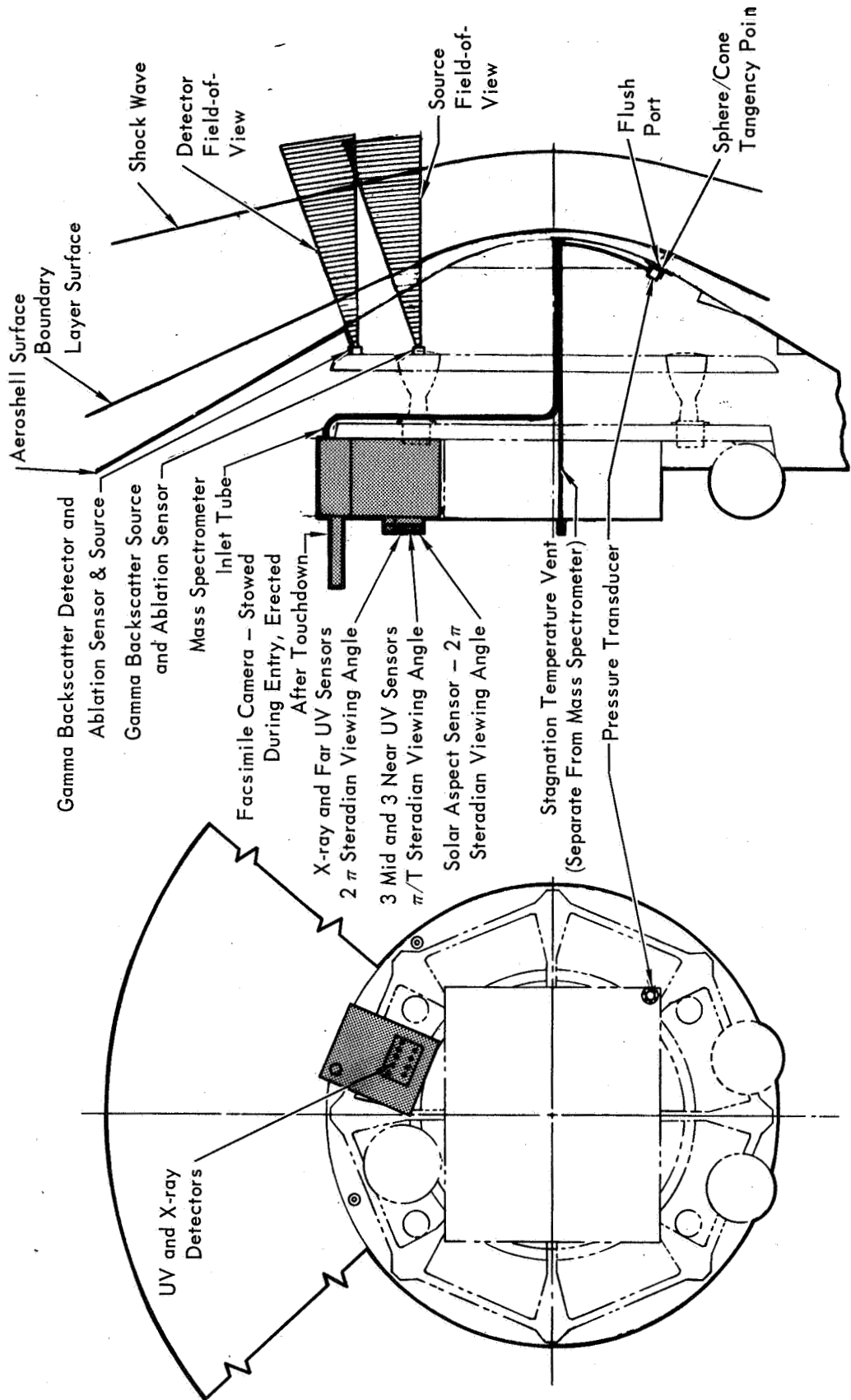


Figure 1-4

STAGNATION REGION ALTERNATIVES

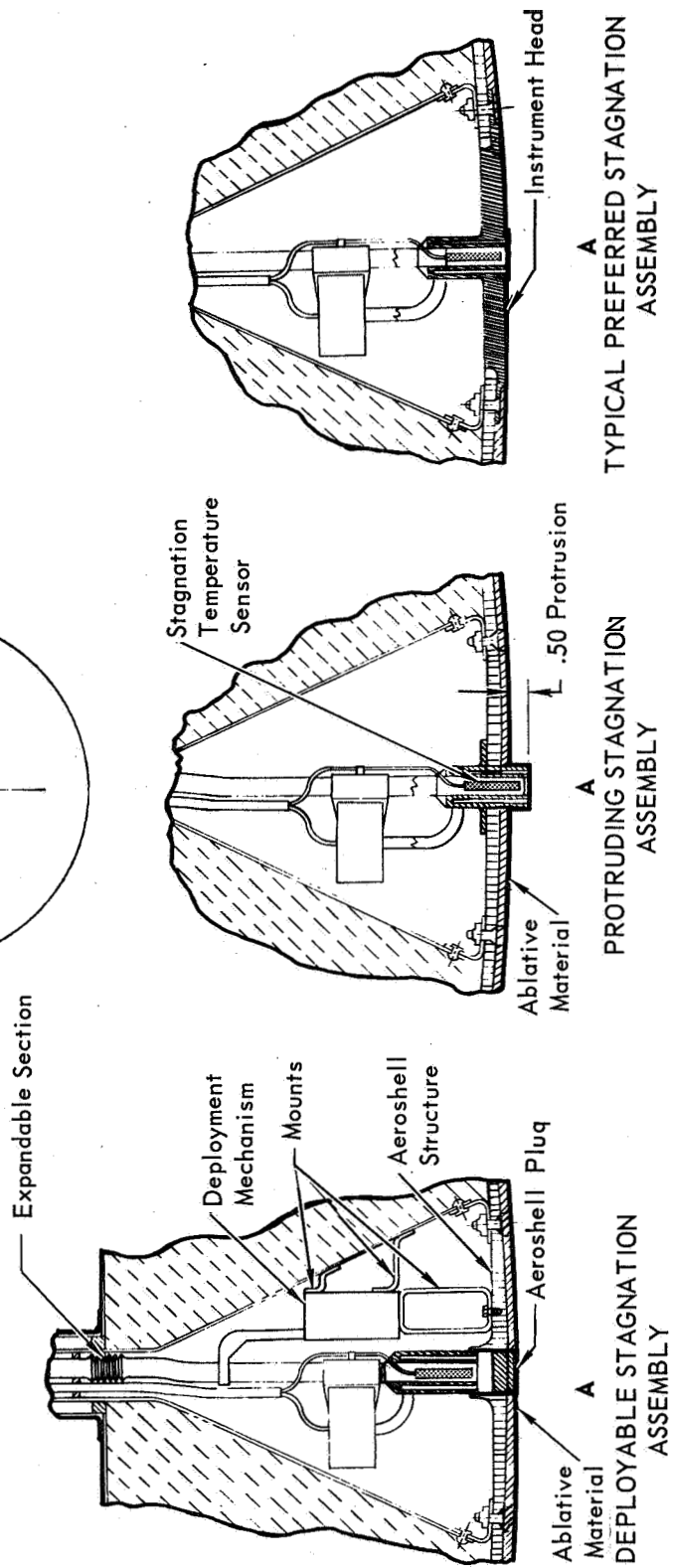
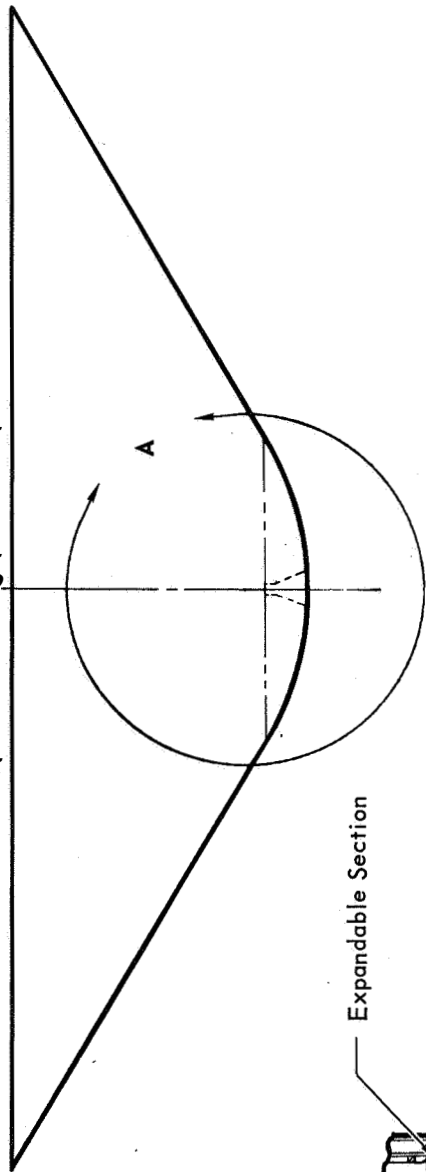


Figure 1-5

Attempts to incorporate the science instruments in the ESP principal unit posed several problems which led to the selection of external science instruments as the preferred approach. Incorporating the sensors into the principal unit as shown in Figure 1-3 poses two immediate problems.

- a. Access is denied to the stagnation region for the total temperature transducer, the mass spectrometer inlet tube, and the forebody pressure port.
- b. The entry TV cameras cannot be located as close to the Aeroshell as would be desirable.

The stagnation region of the Aeroshell is a very desirable measurement area for atmospheric parameter data because the entry-induced influences on these parameters are better defined in this region. Science instruments located in the ESP principal unit would require that the atmospheric access ports be located some 4 to 5 feet from the nominal stagnation point. In this area the effects of varying angle-of-attack, Mach number, attitude rates, etc., are much more difficult to accommodate than they are in the stagnation region. A further problem with the off-stagnation location is that there is a higher probability of ablation product contamination or blockage of the atmospheric access ports.

TV camera location in the ESP principal unit requires that the structure be designed to place the optics of the cameras as near as possible to the inside surface of the Aeroshell. If the cameras are not mounted close enough to the Aeroshell, three undesirable conditions present themselves. (1) The camera window size and weight will be excessive in order to accommodate the 50° field-of-view. (2) The window size may be larger than the space between Aeroshell structural rings thus requiring a local redesign in Aeroshell with an additional weight penalty. (3) And, location of the viewing window at any place other than in or adjacent to the non-ablative portion of the Aeroshell requires another weight increase due to replacing additional ablative material with non-ablative. The weight penalty in this instance is dictated by the 1.2:1 density ratio for the non-ablative to ablative material and the requirement to avoid ablation product deposition on the viewing window.

In summary, the design and operational complexity and increased weight penalty of accommodating the sensors into the ESP principal unit led to the selection of external sensors with the principal unit as the preferred design.

1.1.2 Additional Instruments and Locations - Several instruments or features in addition to those selected in the preferred approach could be used advantageously in the ESP. These include:

- a. Facsimile camera for surface imaging by the ESP
- b. Gamma backscatter densitometer
- c. X-ray and UV detectors
- d. Wall/stagnation differential pressure transducer
- e. Separate mass spectrometer inlet tube.

Figure 1-4 illustrates the location of the instruments in the Capsule Bus and emphasizes some of their prominent features. The facsimile camera is shown in its erected configuration. It will be stowed inside the ESP until after touchdown. This camera could be used to obtain a panoramic scan of the local Martian surface in the first few minutes after touchdown. The information obtained from this instrument could serve two functions:

- a. Provide an early survey of the landing site terrain for use in determining advisability of deploying SL instruments, and
- b. Provide functional redundancy for the SL cameras pre-programmed panoramic scans. In the event that either SL facsimile fails, the ESP facsimile would provide the data required for stereoscopic images of the landing site.

The gamma backscatter densitometer consists of two separate units. One contains the atmospheric backscatter detector and a source/detector system for sensing ablator thickness while the other contains a main source and an ablator thickness detector. The ablator thickness detectors are required to determine the percent loss in both the source and the backscattered gammas so that the data can be corrected to yield the actual count on atmospherically backscattered gammas. Figure 1-4 also illustrates an important requirement imposed on this instrument. The source and detector fields of view must intersect ahead of the shock wave in order to obtain true free stream density measurements because the density behind the shock wave is greater than the free-stream density. As the Mach number approaches 1.0 the shock wave moves farther and farther ahead of the CB, so there would be a small period during the entry where density data would not be interpretable due to the shock wave being in the source/detector intersection zone. Below Mach 1.0 there is no shock so the data will once again be interpretable.

The X-ray and UV detectors are mounted on the aft end of the ESP and are used to :

- a. Determine the number density and altitude distribution of CO_2 , O_3 , N_2 and/or A in the Martian atmosphere, and
- b. Determine the solar flux of biologically significant UV radiation reaching the surface.

The instruments measure the solar constant at the top of the Martian atmosphere in each band of interest and then measure the attenuation until either the instrument threshold is reached or the CB lands on the Martian surface. The detectors have viewing areas corresponding to those shown in Figure 1-4 and sufficient quantities of each sensor band are used to insure that the Sun remains in the sensor field of view during the entire entry.

The addition of a wall/stagnation differential pressure transducer would permit a determination of free stream density independent of free stream pressure. The unit is located just ahead of the sphere/cone tangency point and uses a port flush with the Aeroshell surface to sense the wall pressure.

Use of a separate inlet tube for the mass spectrometer permits the mass spectrometer and the total temperature sensor at the stagnation region to operate in non-simultaneous operating periods and reduces the possibility of temperature transducer outgassing products being seen by the mass spectrometer.

1.1.3 Stagnation Region Alternatives - The preferred approach for the stagnation region sensors is the non-deployable, flush port unit mounted in the non-ablative nose section of the Aeroshell. Two other arrangements were considered and they are shown along with the preferred approach in Figure 1-5.

The deployable unit was considered as a means of protecting the assembly from peak heating condition during entry.

The protruding assembly was considered as a means of overcoming the potential ablation produce contamination and/or blockage problem.

The flush port mounted in the non-ablative Aeroshell nose section, with a downstream valve to inhibit flow through the stagnation temperature transducer vent tube was selected as the best means of obtaining stagnation pressure and temperature, measurements and atmosphere gas samples during entry.

Ref. 1-1 1973 VOYAGER Capsule System Constraints and Requirements Document (Rev. No. 2). JPL SE 003 BB 002-2821, 12 June 1967

SECTION 2

EXPERIMENT ANALYSIS

This section describes the selection of the preferred approach for the entry experiment including (1) a discussion of the preferred maximum likelihood technique for calculating the atmospheric properties from the entry measurements, (2) a discussion of the factors affecting the entry TV observations, (3) the selection of the two TV fields of view, 8" and 50°, (4) the selection of a TV window, and (5) the selection of a non-ablative section of the heat shield to obtain a continuous sequence of photographs over a wide range of altitude during entry. The discussion of the selection of the preferred instruments is discussed in Section 3.

2.1 ATMOSPHERIC PROPERTIES RECONSTRUCTION - This section discusses the post flight calculation of the atmospheric profile from the entry measurements. An evaluation of the preferred atmospheric reconstruction method depends upon the accuracy and applicability of the results obtained by this method, as compared with the desired results and those obtainable from alternative reconstruction methods. The preferred reconstruction method is a maximum likelihood estimator which was selected because it utilizes all the data in an optimum manner and best predicts variations in the Martian atmospheric profile.

Results presented in this section indicate the feasibility of the general computational procedure programmed (IBM 360-50/75 used). However, the final reconstruction program has not been completed.

The most important result desired from the entry experiment is a detailed density vs altitude profile. Pressure and temperature profiles are a by-product of this determination.

The density in the vicinity of maximum dynamic pressure is important for use in entry capsule design for later missions and for planning the descent sequences for the second capsule in 1973 while the density at high altitudes is important in determining orbiter life time.

Determination of the atmospheric properties at altitudes below that at which the aerodynamic decelerator is deployed is difficult because of the uncertain trajectory sensitivities. These sensitivities relate measurements and trajectory states that lie on opposite sides of the point of aerodynamic decelerator deployment. For this reason, measurements taken after deployment are valuable for complete determination of the profile.

2.1.1 Alternatives - A variation of the proposed maximum likelihood method is possible which will conserve computer storage requirements and circumvent much of

the computation errors. This method makes the assumption that the acceleration records are taken over long enough time intervals so that parts of the solution of the optimum filter can be represented as solutions of integral equations. This approach seems to be more realistic than a method which would require grouping of the accelerometer data. A variation of the preferred determination scheme is to add the density history as a state variable rather than acceleration. This is more attractive from a theoretical point of view since density is the real unknown. The derivation of the optimal estimator becomes somewhat more complicated, however. These alternatives are summarized in Figure 2.1-1.

Alternatives exist **also** in the types of measured quantities which enter into the determination. Possibilities exist in the use of such ESP alternatives as descent imaging and gamma ray backscatter for direct determination of density. Monitoring the de-orbit maneuver may reduce the a priori uncertainties at entry. Doppler rate sensing between capsule and spacecraft may also reduce these uncertainties.

An added feature which may be included in the estimation procedure is the estimation of Martian surface variations along the sub-trajectory path. This can be accomplished by appending the surface altitude vs time to the dynamical state vector. Assumed statistics of variations of the surface must be incorporated into the estimator.

2.1.2 Comparison of Alternatives - A pilot computer program has been implemented which processes measurements and predicts the trajectory and atmospheric profile. The equations presented in Part D, Section 2.2.2 of this report were used in this implementation. A study illustrating the operation of this program was performed in order to investigate the effectiveness of the determination method and the effectiveness of the various measurement procedures which might actually be performed. The reference case chosen for the study incorporates acceleration data, altitude data, stagnation pressure and temperature data and an a priori estimation of the entry conditions. The measurements used were generated by the sampling of random numbers representing the expected measurement errors and entry condition errors.

Figures 2.1-2 and 2.1-3 show the actual density and ambient pressure, respectively, which were assumed (corresponding to the VM-10 atmosphere) together with the estimated density and pressure profiles. The illustration given shows the result of a particular sampling of the measurement errors. Another sample may give results which vary from the actual in the opposite way depending in particular upon the

ATMOSPHERIC RECONSTRUCTION ALTERNATIVES
• VARIATIONS OF MAXIMUM LIKLIHOOD METHOD

ALTERNATE ANALYSIS METHODS	ADVANTAGES	DISADVANTAGES	RELATIVE EVALUATION
Acceleration History Appended to State Vector	<ul style="list-style-type: none"> ● Gives optimal smoothing with moderate complexity to extract maximum information about atmosphere. 	<ul style="list-style-type: none"> ● Requires angle of attack determination prior to data smoothing. ● May require grouping of acceleration measurements in computing estimation 	Very Good
Density History Appended to State Vector	<ul style="list-style-type: none"> ● Uses 3 Axis Acceleration in best possible way. 	<ul style="list-style-type: none"> ● Very complicated estimation formulae. ● May require grouping of measurements 	Very Good
Procedure Involving Integral Equations	<ul style="list-style-type: none"> ● Does not require large storage ● Does not accumulate error ● Does not require grouping of data. 	<ul style="list-style-type: none"> ● Cumbersome Formulae ● Neglects finite nature of acceleration history. 	Best
Sequential Estimation Along Trajectory	<ul style="list-style-type: none"> ● Does not require large storage ● Does not require grouping of data. 	<ul style="list-style-type: none"> ● Computational error accumulates excessively 	Not Good
Model Atmosphere	<ul style="list-style-type: none"> ● Simple ● Will estimate parameters which have certain important application. 	<ul style="list-style-type: none"> ● Cannot find unpredicted fluctuations in atmosphere ● May require grouping of data 	Very Good Supporting Program

Figure 2.1-1

ATMOSPHERIC PROPERTIES ESTIMATION

Nominal Measurement Program

- Acceleration 2/sec $\sigma_A = 3.22 \text{ ft/sec}^2$ $a > 5g$
 $\sigma_A = .537 \text{ ft/sec}^2$ $a < 5g$
- Altitude 1/9 sec from 200,000 ft to 18,000 ft
 $\sigma_H \approx 1/3\%$ (Depends on H)
- Pressure 1/sec from 0.05 psi to 18,000 ft
 $\sigma_P = 4.32 \text{ lb/ft}^2$
- Temperature 1/sec from M= 5 to 18,000 ft

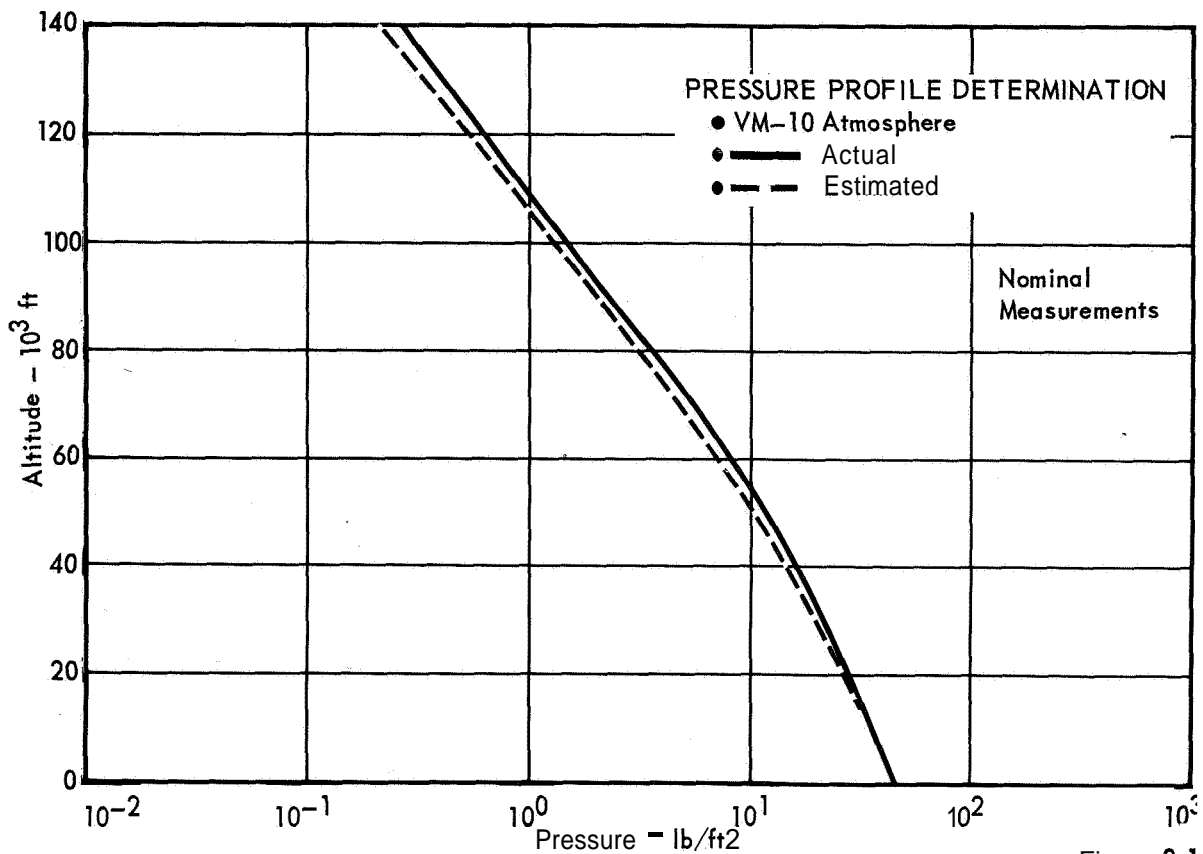


Figure 2.1-3

Figures 2.1-2, 2.1-3

2-47

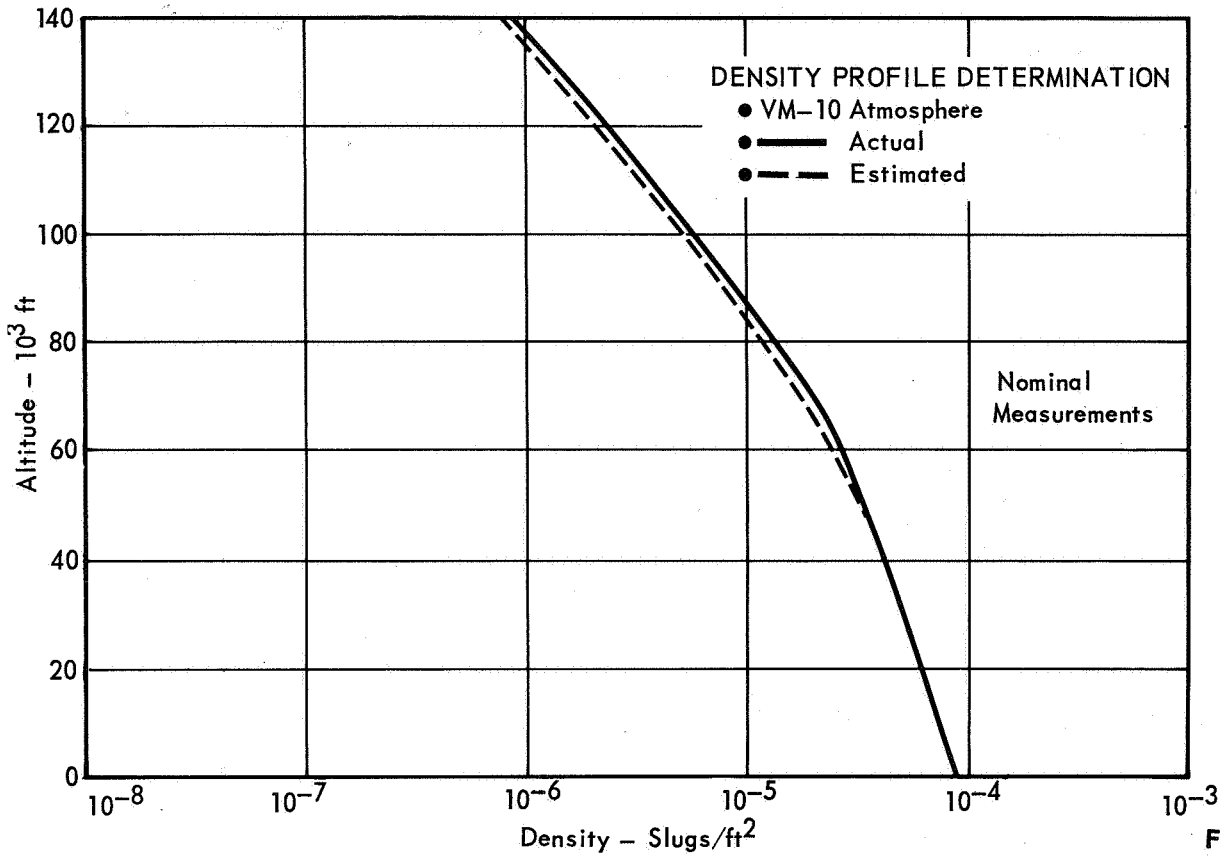


Figure 2.1-2

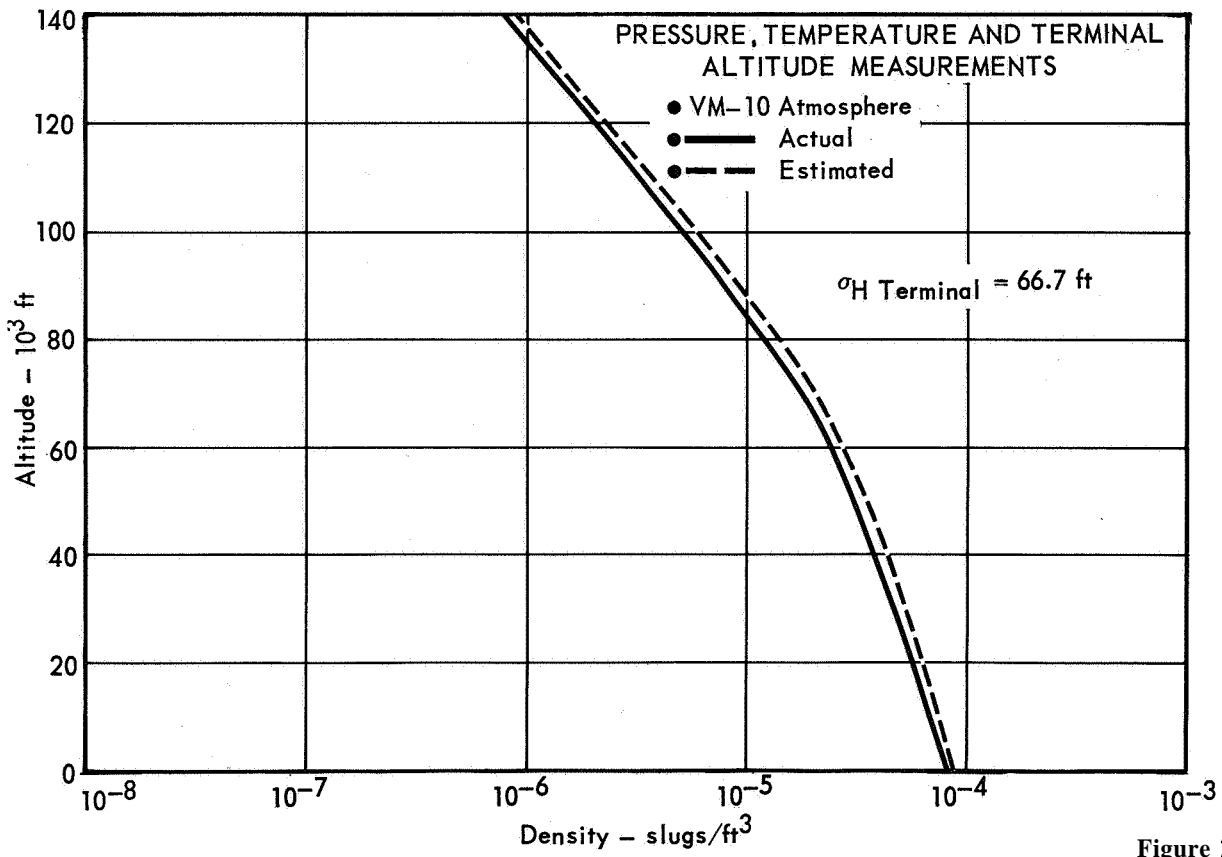


Figure 2.1-4

3, 2.1-4
2+

2-4-2

sampling for the entry condition errors. The curves shown are for the same normalized random sample so that the parametric variations are indicative of the effects produced in general.

If the bulk of the altimeter data is deleted from the estimation, then the results are less accurate as can be seen from Figure 2.1-4. These cases include a terminal altitude measurement, The terminal measurement is by far the most important in the reconstruction of the trajectory since it is very instrumental in reducing large entry altitude errors.

All of the cases so far discussed assume that the entry conditions employed in the trajectory computation are based upon monitoring of the magnitudes and direction of the de-orbit maneuver and that the initial attitude reference error has been reduced by monitoring of the Spacecraft attitude at the time of Capsule Bus reference alignment. Examination of Figure 2.1-5 shows that the improvement due to monitoring is not significant.

Doppler velocity between the Capsule Bus and the Spacecraft taken prior to entry may reduce the entry velocity errors to about one third and entry angle uncertainty to about half of the values attainable without such tracking. The improvement in atmospheric determination resulting from this added data is shown in Figure 2.1-6.

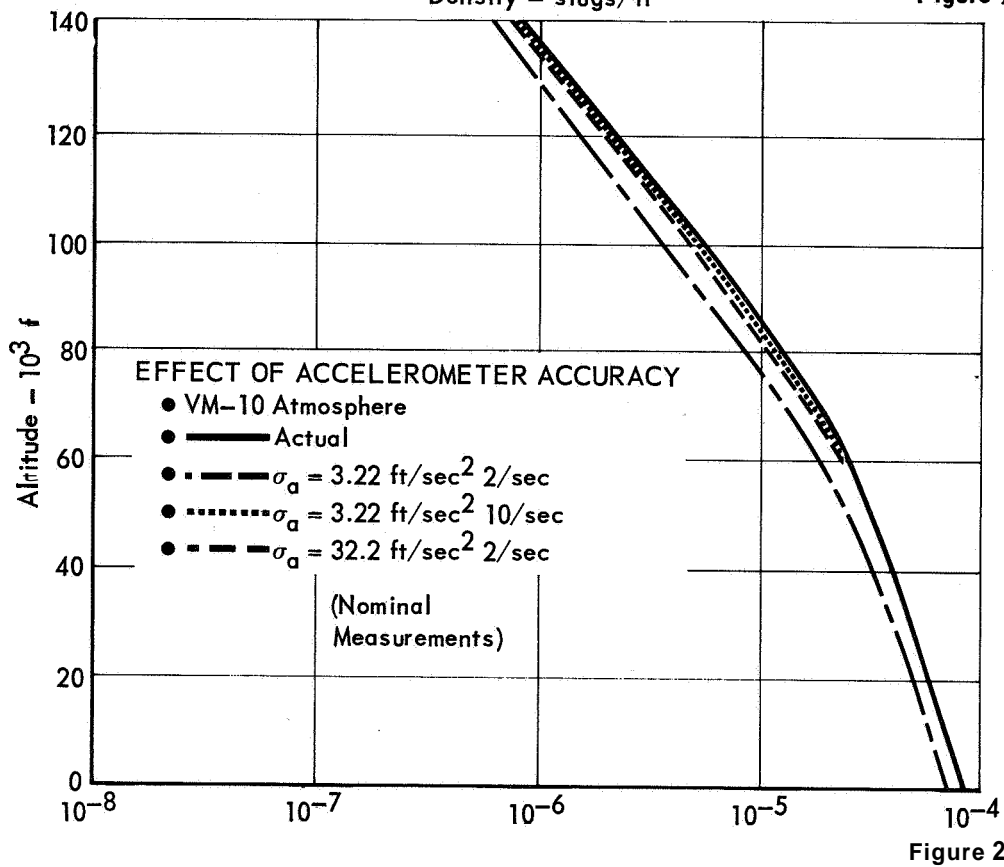
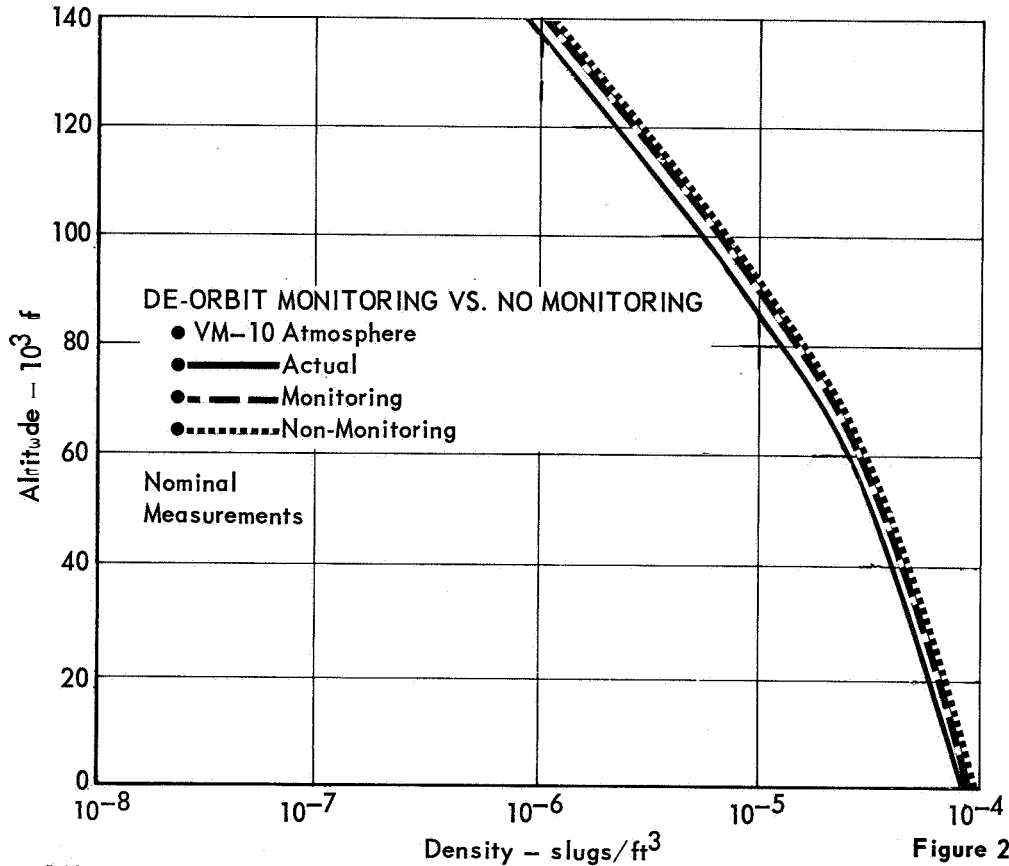
The importance to be attached to the accuracy of the accelerometer data can be seen from examination of Figure 2.1-7 which shows the result of increasing the sample rate by a factor of five and also the result of increasing the instrument standard deviation by a factor of ten.

The importance of the temperature data can be seen from Figure 2.1-8 which shows the estimation for two situations differing only in the accuracy of the temperature data. In these cases the altimeter data was deleted in order to more clearly show the effects of the temperature accuracy variations.

A similar variation in the pressure data failed to give comparable results since the trajectory estimation seemed to be less sensitive to pressure and the computational inaccuracies involved in the inversion of high order matrices. These errors together with large residuals can produce erroneous results unless the a priori trajectory is quite close to the actual trajectory.

Follow on studies to alleviate the computational error problem contemplate using a partly sequential estimation which incorporates the terminal altitude measurement and perhaps a few other very influential measurements to improve the a priori entry conditions and then employ an estimator of the integral equation

ATMOSPHERIC PROPERTIES ESTIMATION (Continued)



2-6-1

Figures 2.1-5, 2.1-6, ;

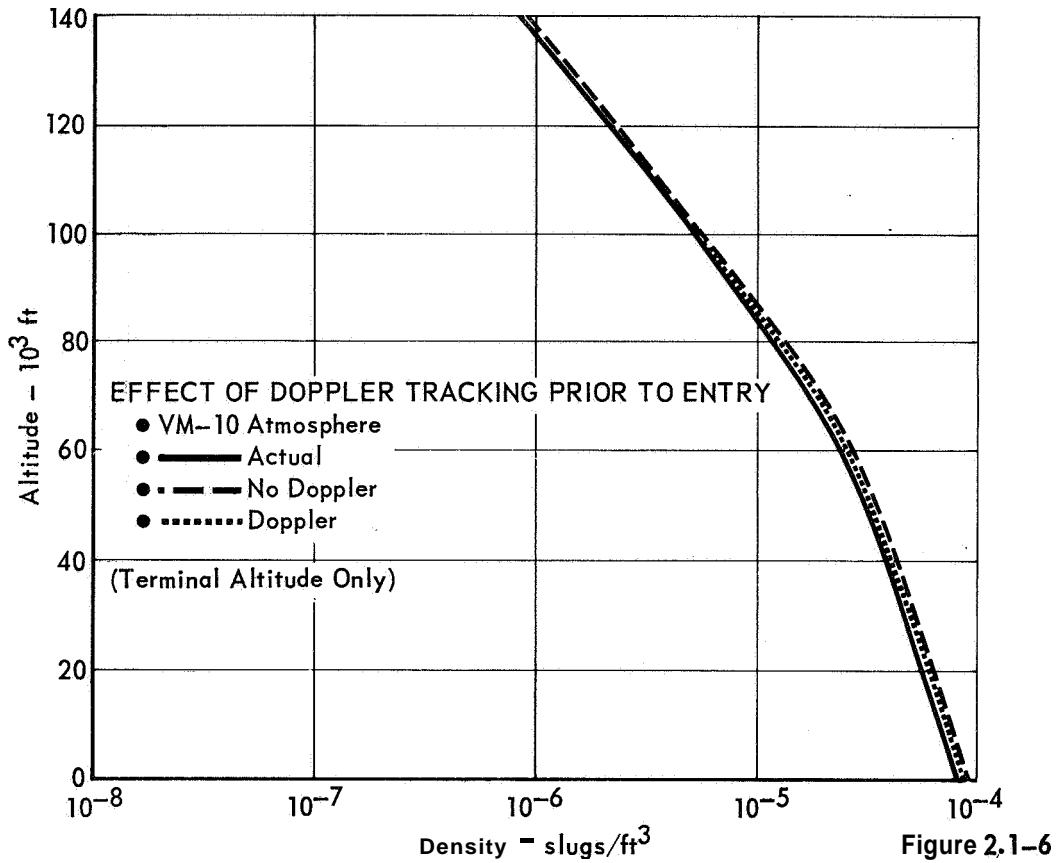


Figure 2.1-6

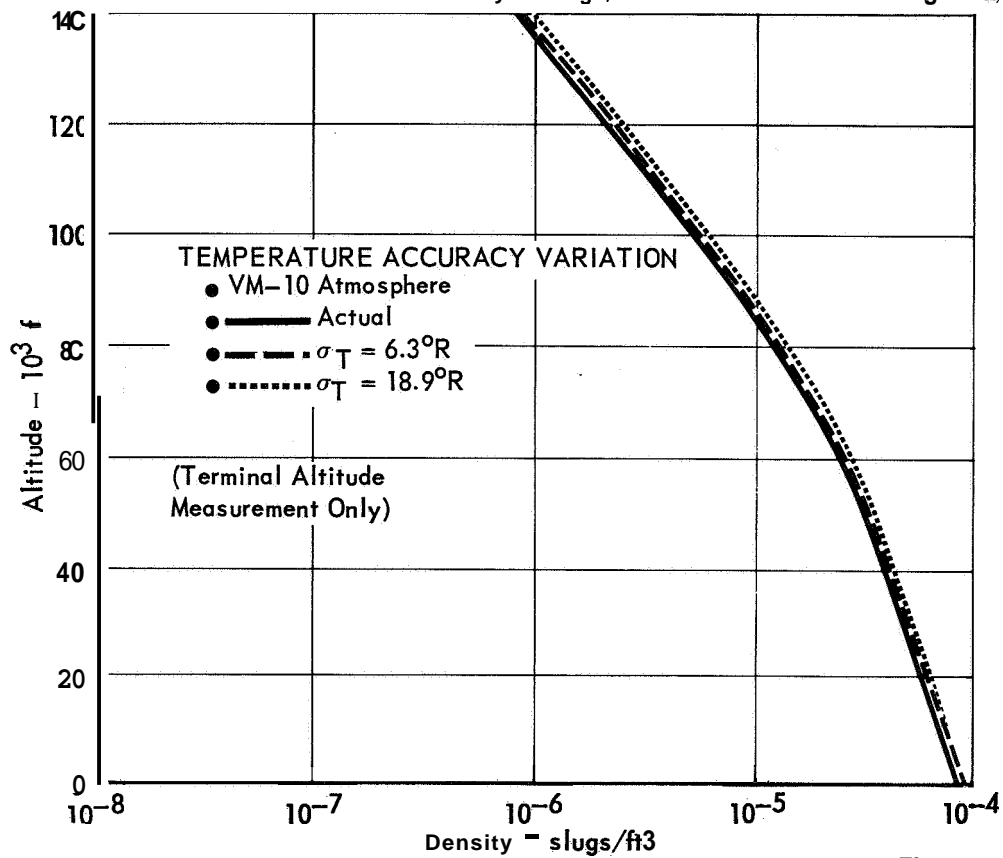


Figure 2.1-8

variety to utilize the remaining data.

A separate estimation accuracy study was performed which did not depend upon the existence of a specific pilot program but merely provides the covariance matrices for the determination accuracy. The primary concern was to develop trade-off results required for the specification of a radar altimeter. These are discussed in detail in Part D, Section 4 of this report. An example of the results for density determination is reproduced in Figure 2.1-9. These results do not include the effects of the acceleration data statistics upon the trajectory or upon the atmospheric profile determination whereas these effects are included in the more general profile reconstruction program.

The acceleration coupling effects are not significant due to the large amounts of altitude data involved.

One area of major importance is that of determining the effect of de-orbit monitoring upon the atmospheric determination.

For no monitoring of the attitude during de-orbit a pointing uncertainty of as much as 0.772 deg is possible. This is mostly an initial alignment uncertainty and an uncertainty due to the ± 0.25 deg deadband of the attitude control system. If monitoring is used to determine the side of the deadband to which the attitude is driven during de-orbit thrusting, then the uncertainty in pointing is reduced to 0.75 deg. If, in addition, spacecraft attitude is monitored at the time the capsule reference is established, then the spacecraft deadband of ± 0.5 deg can be removed, resulting in a pointing uncertainty of 0.532 deg.

The uncertainty in de-orbit ΔV is primarily due to the uncertainty in prediction of the thrust tail off characteristics. This is expected to amount to as much as 0.472 ft./sec. in the uncertainty in the value of ΔV as recorded by the integrated output of an accelerometer. If the total integrated output of the accelerometer during de-orbit is monitored, the ΔV uncertainty is reduced to 0.25 ft./sec.

These de-orbit uncertainties must be related to uncertainties in the entry conditions for purposes of atmospheric determination. The corresponding entry dispersions are as follows:

	No Monitoring	Monitoring	Monitoring of Spacecraft
Entry Altitude Uncertainty 3σ	$.89 \times 10^5$ Ft.	$.843 \times 10^5$ Ft.	$.616 \times 10^5$ Ft.
Entry Anomaly Uncertainty 3σ	1.4 deg	1.32 deg	.963 deg

**ATMOSPHERIC DENSITY ESTIMATION ACCURACY ($3\sigma_{\rho}/\rho$) AS A FUNCTION OF
ALTIMETER ACCURACY ($3\sigma_H$) AND DISTANCE OF FIRST ALTITUDE MEASUREMENT**

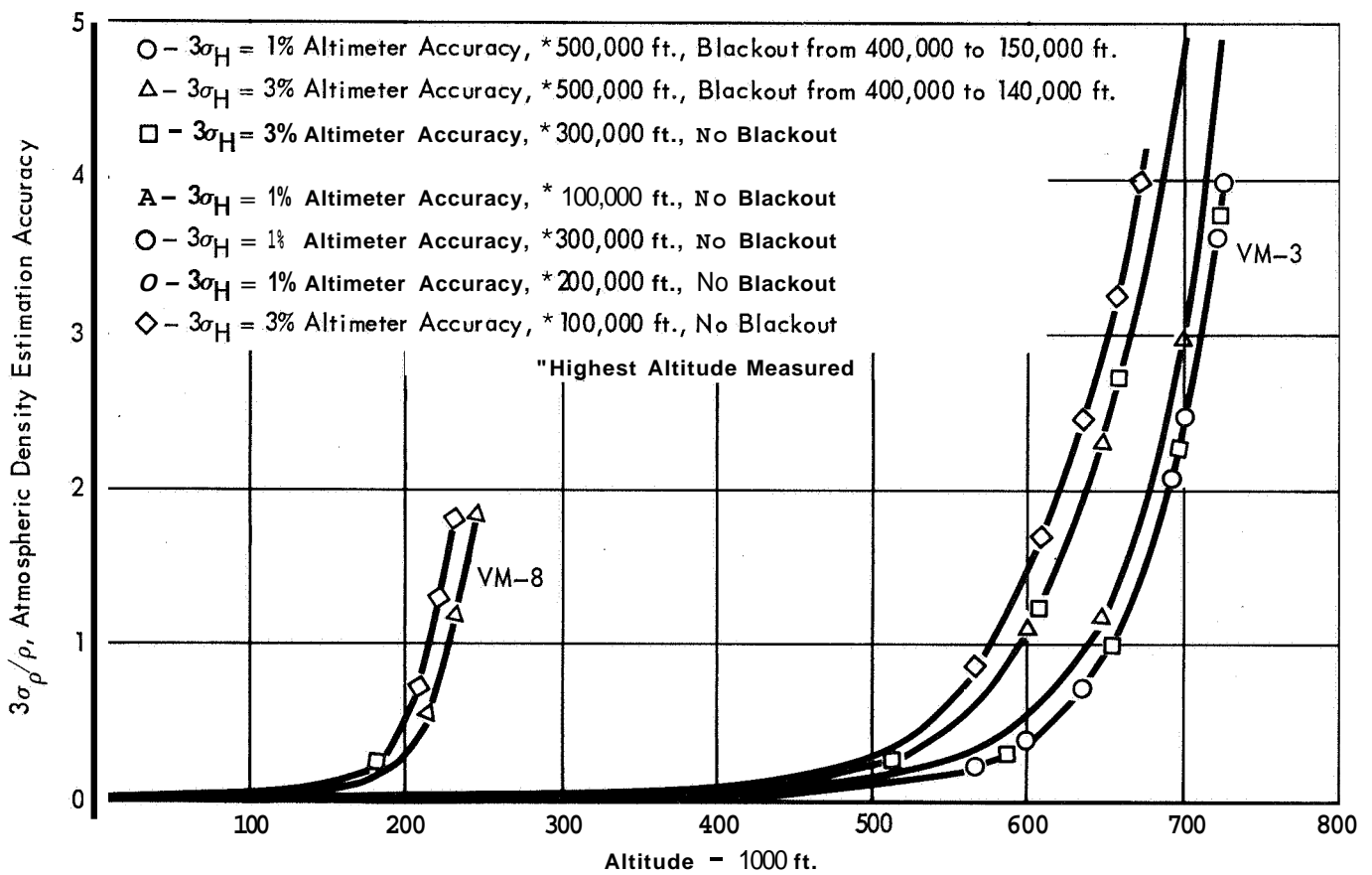


Figure 2.1-9

	No Monitoring	Monitoring	Monitoring of Spacecraft
Entry Velocity Uncertainty 3σ	65.3 Ft./Sec.	61.3 Ft /Sec.	44.8 Ft/ Sec.
Entry Flight Path Uncertainty 3σ	.605 deg	.567 deg	.415 deg

If, in addition, capsule spacecraft doppler data is taken during descent to entry, then the velocity uncertainties can be reduced to within about 3 Ft./Sec.

2.1.3 Results - A maximum likelihood method for trajectory/atmospheric reconstruction, with the acceleration history appended to the dynamical state vector, has been programmed and run to show the feasibility of the specific concept. Results achieved, using VM-10 atmospheres, are believed less sensitive to variations in data sources, than some at the other atmospheres may be. Remaining problems due to inversion of high-order, ill-conditioned matrices may be circumvented by the device of integral equation approximation of parts of the estimation procedure.

2.2 ENTRY TV OBSERVATIONS - The analysis which leads to (1) the selection of the TV camera field of view, 8° and 50°, (2) the use of a window, and (3) a non-ablative section in the heat shield is discussed in this section.

The objectives of the Entry TV experiment are to:

- a. Accurately locate the landing site.
- b. Obtain detailed pictures of the local surface,
- c. Survey the general Martian terrain; from stereo images obtain profiles of surface elevation.
- d. Photometrically evaluate surface reflectivity.
- e. Measure atmospheric attenuation, especially that due to scattering by dust and clouds.
- f. Image limb clouds.
- g. Generate supplementary data for the correction of anomalies in the flight profile.

At least the first two objectives must be met to constitute successful imaging.

Dual vidicons, viewing through a fused silica window in the non-ablative portion of the Aeroshell, gather both the wide angle and high resolution imagery needed to accomplish these objectives.

Documentation in the JPL report, *PD606-4*, calls out the dual vidicon television (TV) installation and establishes a ground resolution requirement ranging from a match of the Orbiter TV resolution to a 1 meter terminal resolution. It was assumed that the 1 meter resolution refers to the resolution of the last frame transmitted before impact if the terminal deceleration fails. Normally the resolution of the last frame is much better than 1 meter. A 0.44 inch vidicon format and 200 x 200 line, slow-scan operation serves to define the basic instrumentation reference conditions. The restrictions in combination with environmental and operational limitations are the descent TV constraints.

Environmental Limitations - Two important factors enter into the environmental considerations. The first relates to whether or not the landing site is in the field of view. The best landing site imagery occurs at altitudes between 50,000 and 200,000 feet. Here coverage is good and resolutions are adequate to satisfy most of the scientific objectives. These altitudes, however, fall in the region where the CBS is pitching over from its nearly horizontal early flight trajectory to a more vertical descent. This change in attitude is rapid and strongly dependent on the type of Martian atmosphere encountered. To include the landing site in the field of view under these conditions, a camera with 50 to 60 degree

viewing cones should be employed, reference Figure 2.2-1. This relatively wide angular coverage is also valuable at altitudes below 25,000 feet where the CBS is undergoing its braking, where deceleration maneuvers and angular rates again tend to be high.

Entry is also accompanied by self-luminous gas emission, and/or generation of ablative products. These two effects could inhibit imagery for a considerable portion of the lower trajectory either by obscuring the viewing window or by blacking out the communications. This fact argues for imagery either at very high altitudes before environmental interference becomes severe, or late in the flight when conditions have improved.

Operational Limitations - Landing site imaging should, for optical reasons, be obtained around 100,000 feet altitude where coverage and resolving power allow optimum identification of ground objects. Surface detail, the second objective, is best procured at altitudes less than 5,000 feet. This latter consideration avoids the need for extremely high resolving powers with their resulting difficulties in pointing and susceptibility to image smear.

Light level, angular resolving power, and platform stability, dictate exposure, coverage, resolution, and data rate requirements. Figures 2.2-2 and 2.2-3 describe the expected lighting conditions and Figure 2.2-4 shows the trade-offs used to set performance parameters. Descent rates are normally adequate to provide a number of useful pictures. However, if the terminal propulsion fails, descent rate will increase to 500 to 750 feet per second and these higher rates will restrict low altitude imaging as shown in Figure 2.2-5.

In order to achieve adequate transmission time and the required 1 meter resolution (for the case of terminal deceleration failure) above 3300 ft. altitude, the field of view must be (using a Kell factor of 0.7):

$$0.7 \frac{3.3 \text{ ft}}{3300} \times 57.3^\circ/\text{radian} \times 200 \text{ lines} = 8''$$

For some entry conditions the impact velocity is approximately 900 ft/sec. To obtain a 1 meter resolution with this velocity, a 6.7° field of view would be required.

Lastly, the image will degrade as the objective distance decreases. Cameras which are optimized for high altitude landing site observation show an increase in image distance at low altitudes which cause defocus and increased sensitivity to motion. Typical loss effects are presented in Figure 2.2-6.

Alternatives - Design options are established more by necessity than by a

'LANDING SITE VISIBILITY

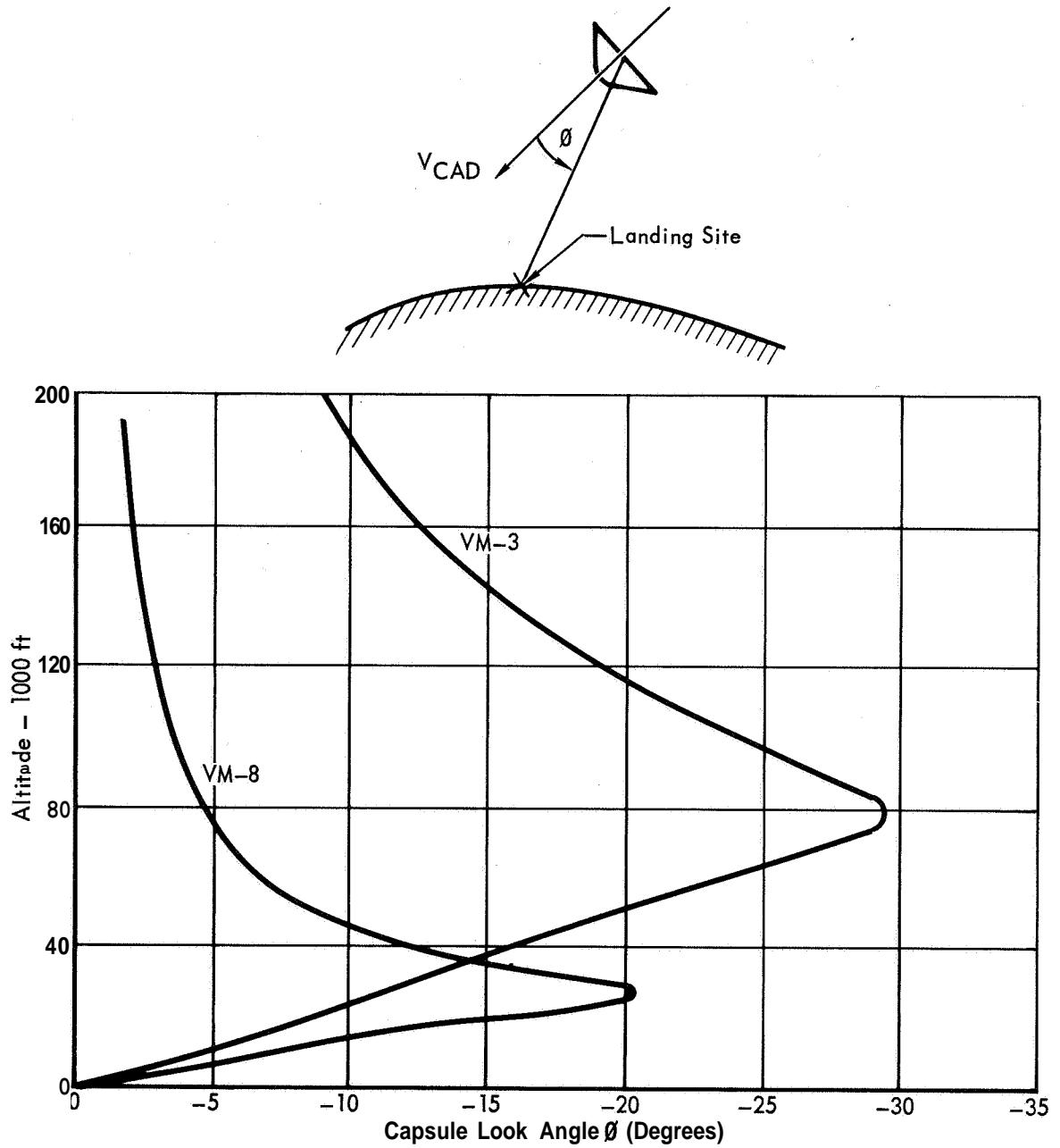


Figure 2.2-1

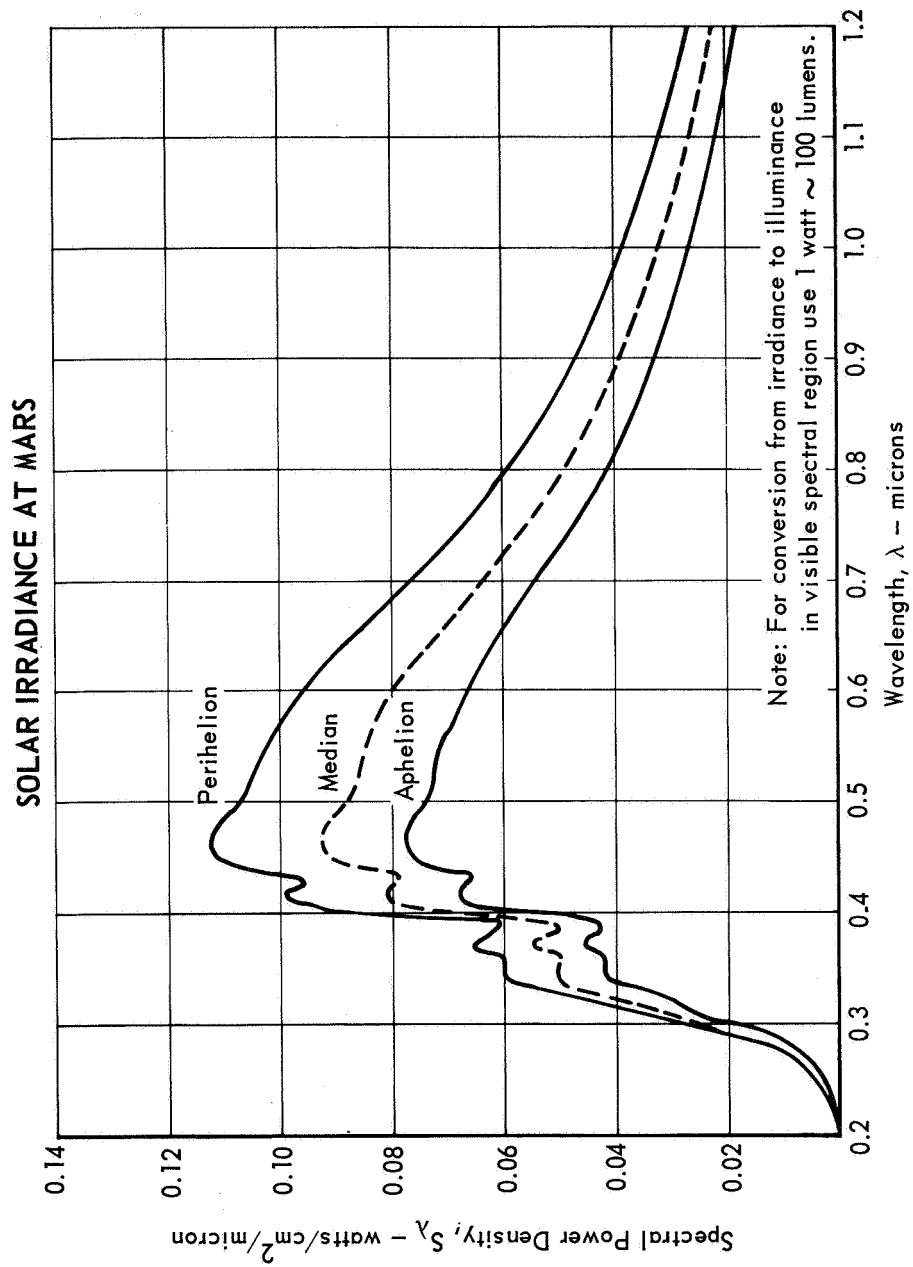


Figure 2.2-2

SURFACE REFLECTIVITY AND ATMOSPHERIC TRANSMISSION OF MARS

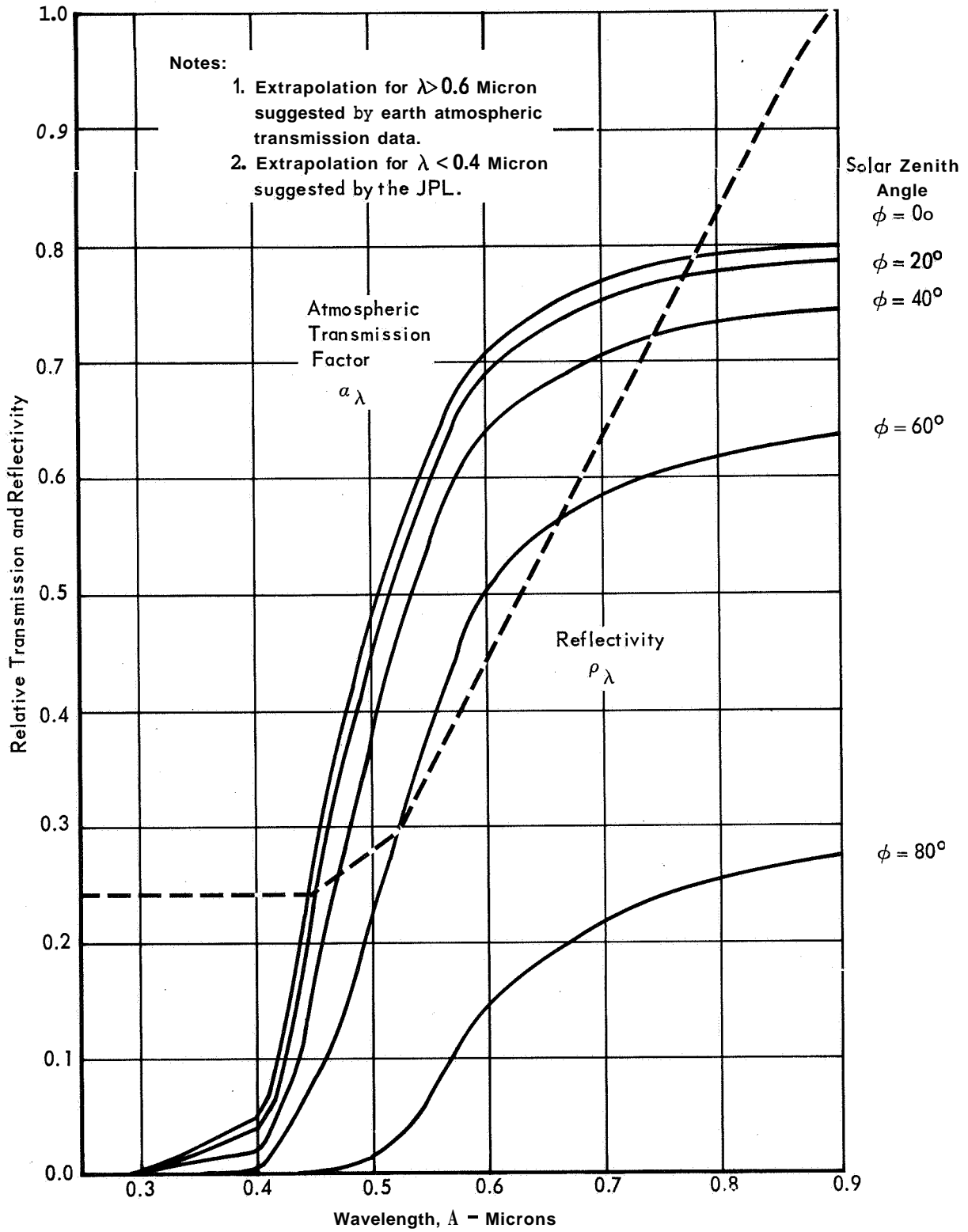


Figure 2.2-3

THE INTERACTION OF RANGE, FOCAL LENGTH, FIELD OF VIEW, ANGULAR MOTION AND EXPOSURE TIME IN DESCENT IMAGING

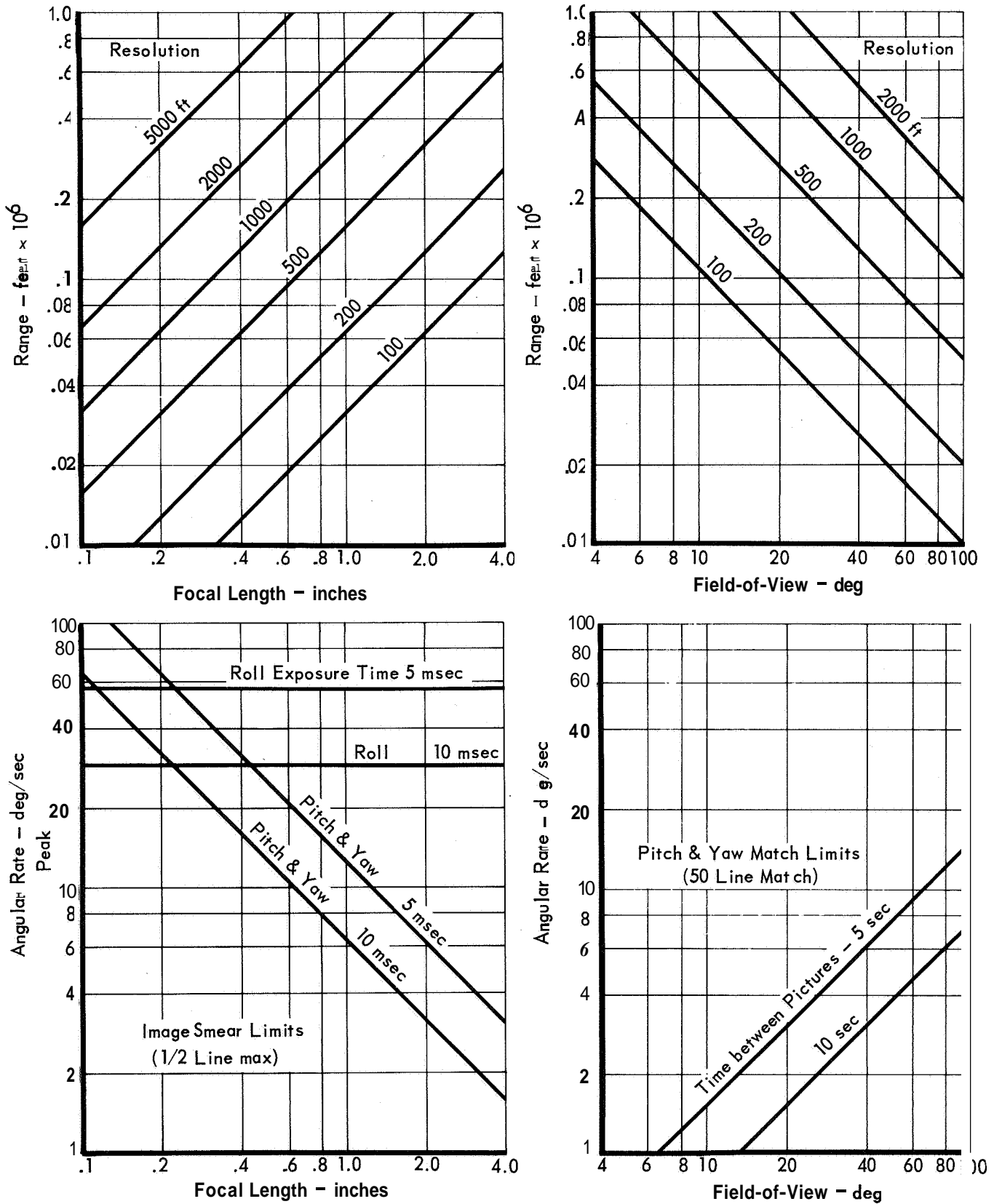


Figure 2.2-4

IMAGING DATA HANDLING REQUIREMENTS IN THE EVENT OF TERMINAL DECELERATOR FAILURE

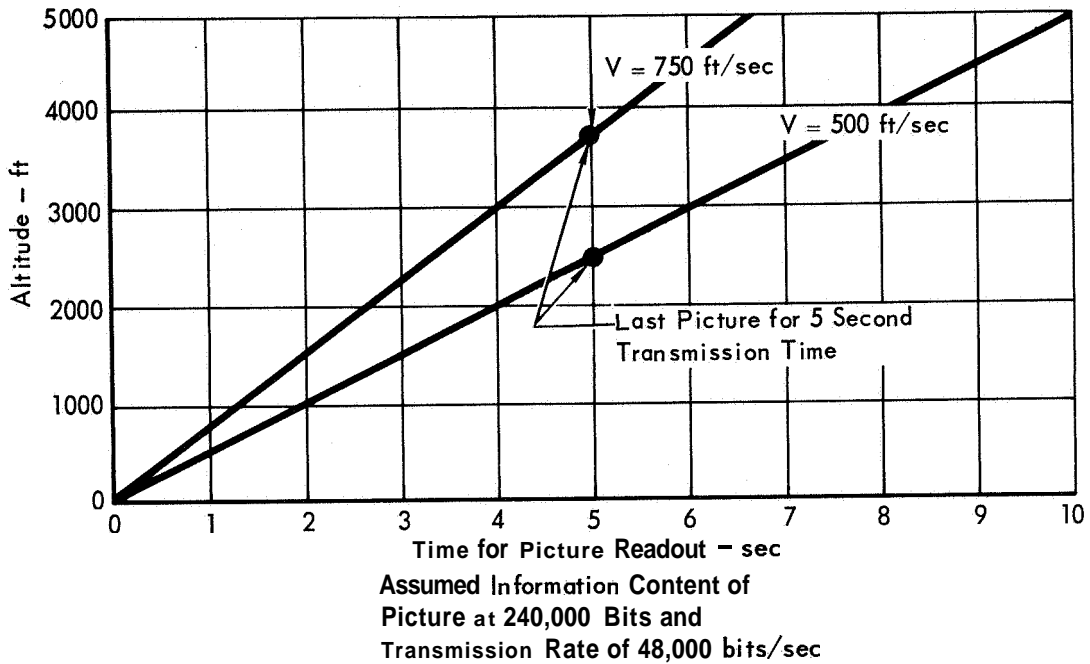


Figure 2.2-5

IMAGE DEGRADATION AT TERMINAL ALTITUDES

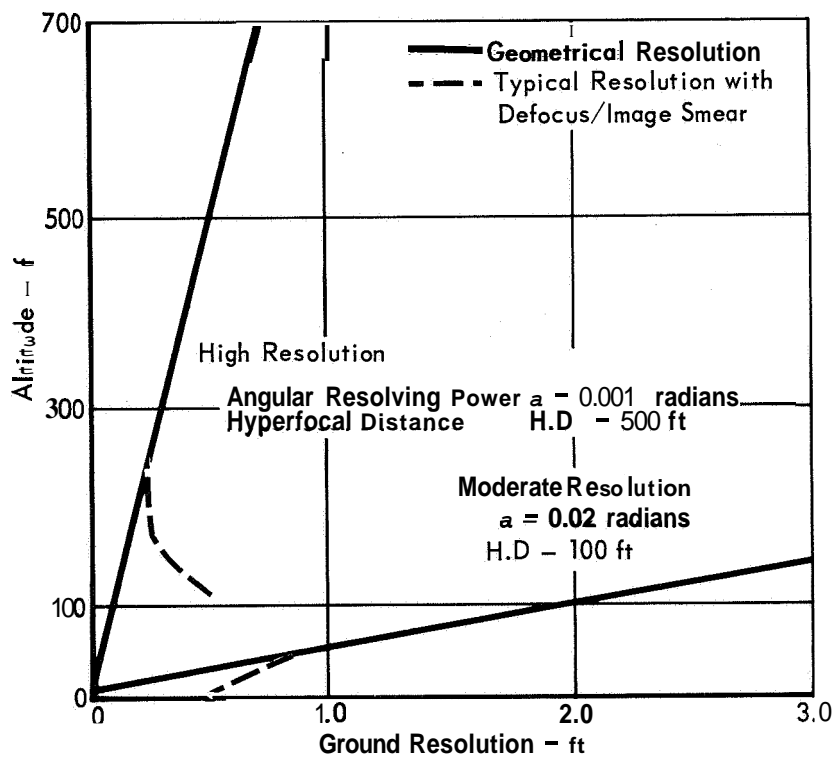


Figure 2.2-6

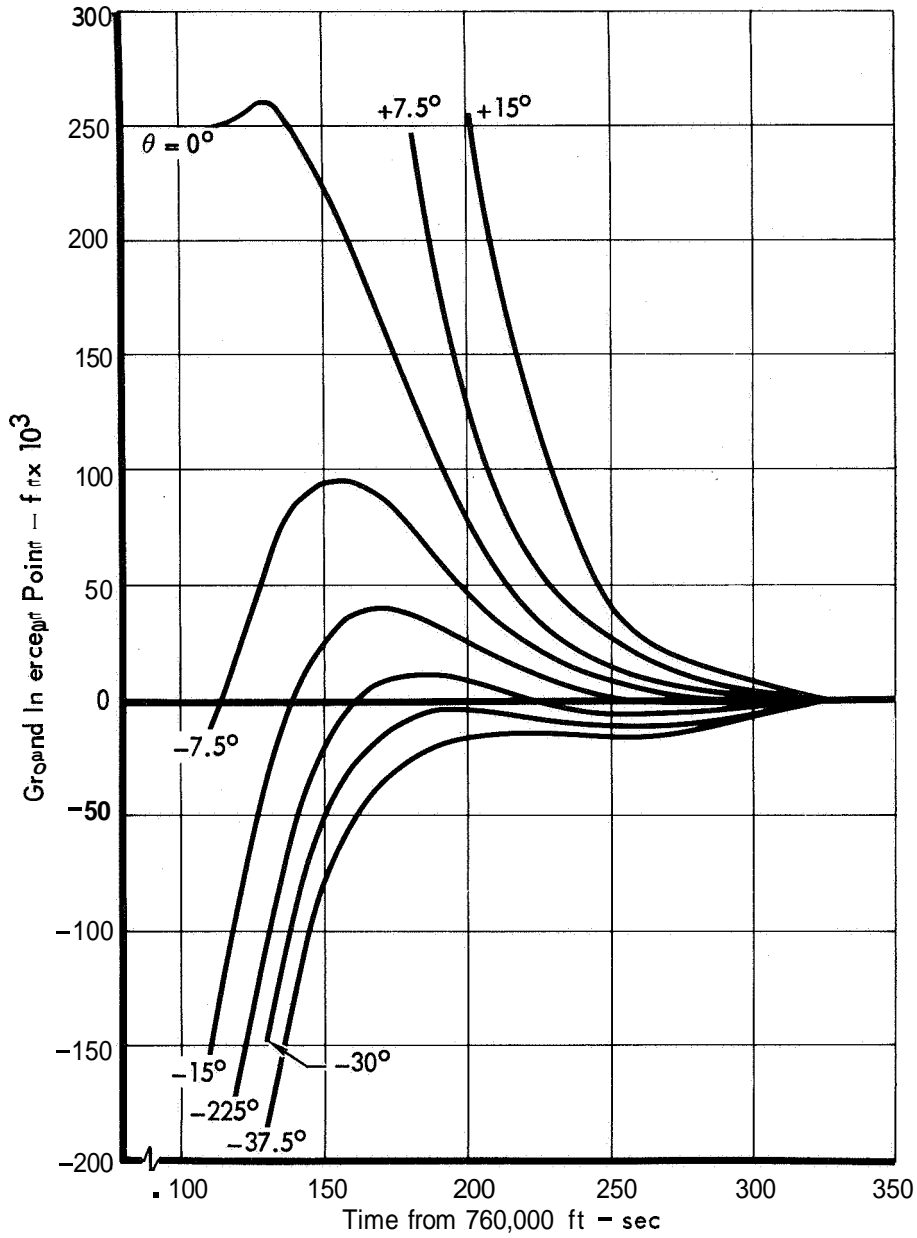
Figure 2.2-5, 2.2-6

luxury of having a wide selection of alternatives. The most logical design approach tries for good landing site pictures at 100,000 feet and backs this up with degraded, oblique imagery above 500,000 feet. Detailed surface imaging is procured in the terminal phases of descent as a natural extension of the high altitude optical techniques. This method provides not only good landing site identification and detailed surface images, but also supplies the opportunity to achieve the secondary scientific objectives.

One alternative on this basic approach is to use obliquely viewing cameras. It can be concluded from the look angle shift in Figures 2.2-7, 2.2-8 that offset pointing would improve coverage. For a 60 degree field of view and VM-3 atmosphere, the landing site represented by the ground intercept point zero is always within the field of view because the ground intercept point zero remains between the plus and minus 30 degree curves. This is not the case for smaller fields of view. Note that the negative look angle intercepts are not as distant from the zero ground intercept point as the positive look angle intercepts. A bias or an oblique mounting would allow the camera to view the landing site with a minimum field of view. This offset pointing does, however, complicate terminal imaging as the landing impact point will always fall off to one side of the picture under these near vertical descent conditions.

Two less desirable imaging approaches are also possible. These involve pictures either at very high altitudes before environmental effects become a problem, or at very low altitudes after these effects. The high altitude imaging can observe the landing site, but high magnifications are required to do useful work. With a 0.44 inch vidicon format this means small angular fields which are difficult to point. It is also a practical impossibility to achieve 1 meter ground resolution with this type of system before the onset of communications blackout. Low altitude imaging suffers from inferior coverage (or large distortion and poor resolution with very wide angle optics), poor viewing perspective, and operation during a time of high CBS activity. The vehicle activity, i.e., parachute deployment, Aeroshell separation, and descent engine ignition, can lead to temporary obscurations and large oscillations. Orbiter match and 1 meter resolution is possible here, but additional uncertainties in such quantities as descent engine exhaust gas absorption make it an unattractive candidate. Both the low and very high altitude approaches also, cannot accomplish many of the secondary scientific objectives.

GROUND INTERCEPTS FOR VARIOUS LOOK-ANGLES

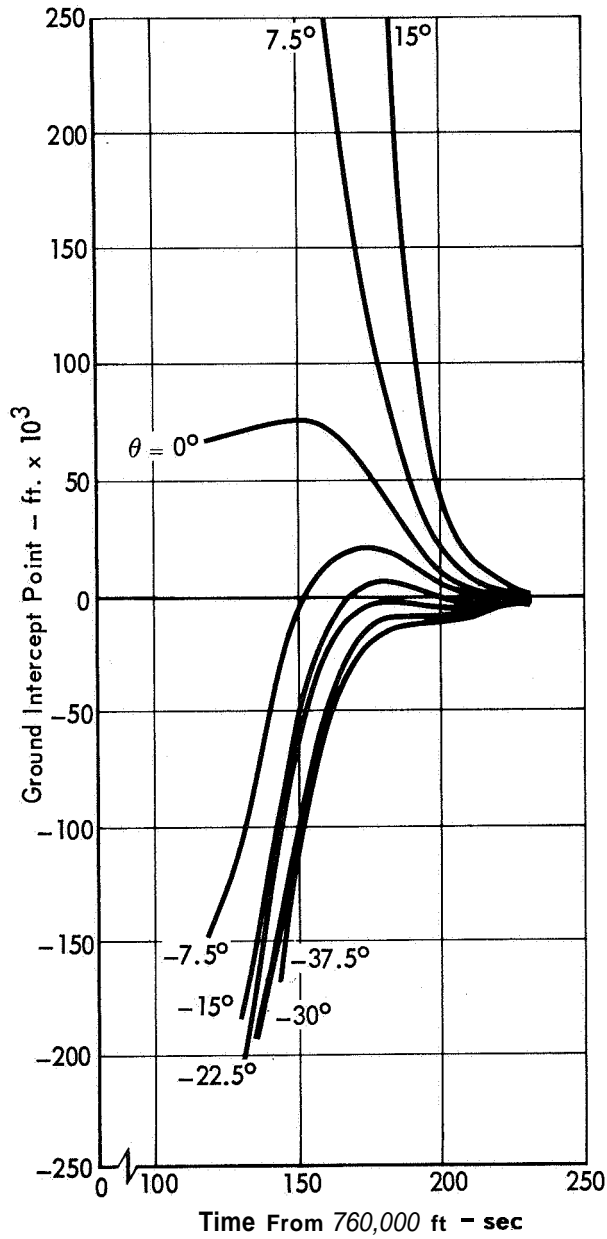


VM-3 Atmosphere
 $V_e = 15,000 \text{ ft-sec}^{-1}$
 $h_e = 760,000 \text{ ft}$
 $M/C_D A = 0.25$
 $\gamma_e = -20 \text{ deg}$

Time from Entry (sec)	Altitude (kft)	Range (kft)
120	200	704
140	142	489
160	109	336
180	89	226
190	80	170
200	74	145
220	60	92
240	50	63
260	38	42
280	26	27
300	15	15
320	5	5

Figure 2.2-7

GROUND INTERCEPTS FOR VARIOUS LOOK-ANGLES



VM-8 Atmosphere
 $V_e = 15,000 \text{ ft-sec}^{-1}$
 $h_e = 760,000 \text{ ft}$
 $M/C_D A = 0.25$
 $\gamma_e = -20 \text{ deg}$

Time from Entry (sec)	Altitude (kft)	Range (kft)
120	190	675
140	106	395
160	47	173
180	29	84
200	17.5	35
220	8	21
240	~ 0	~ 0

Figure 2.2-8

Comparison of Alternatives - The optical parameters of coverage and resolution may be traded off in order to benefit one altitude regime at the expense of another. It is felt that the first concept, i.e., pictures over the total descent profile provides the best balance and highest probability of success. The problems encountered here are also typical of those encountered in any other approach.

a. Flow Field Effects - Optical losses can come from a self-luminous flow field, from small particle scattering, from light absorption, and from a breakup of the optical wavefronts. The first two effects mask and soften the brightness changes which carry detail in the ground scene. Absorption reduces the amount of energy available for image forming, sometimes to the point where picture recording is impossible. Wavefront degradation gives the impression of viewing through a ground glass; everything is washed out.

Work at the Vidya Corporation (reference Vidya Rpt. #37, 26 April 1960 to 26 January 1961) has shown that, even for earth atmospheric densities, luminosity due to the atmospheric gases is down several orders of magnitude from where it could cause problems. Ablation products, on the other hand, always generate detectable luminosity. For example, the first photographic measurements on the Gemini program were directed at recording the luminous wake during reentry. Evaluation of one of the photographs from GT-2 (reference NASA-MSD Houston photo No. 5-65-13171) indicates that the wake brightness was greater than 400 foot lamberts. The atmospheric pressure and temperature conditions at the time the photo was taken are of the same order of magnitude as those encountered during a Martian entry and it is concluded that the GT-2 wake brightness is a conservative approximation for the Martian case,

Ablation products, in addition to being self-luminous, tend to adhere to the television viewing window and scatter and diffuse the light. Figure 2.2-9 shows the magnitude of this effect for typical ablators when the window is illuminated by the sun at an angle θ from the window normal. These numbers are for Earth conditions roughly equivalent to that of Mars and graphically illustrate the magnitude of the problem. In all cases, except that of teflon, luminance numbers can run up as high as a few thousand foot lamberts. Teflon cannot be used because of the problems it introduces in other phases of the design. Adhering particles can also attenuate light by absorption. This absorption forces a shift in the sensing characteristics of the television. When Automatic Gain Control (AGC) is available, the exposure time for each picture can be increased to compensate for the light loss. This compensation is limited, however, for soon the motion effects begin

LIGHT SCATTERING FROM A WINDOW CONTAMINATED BY ABLATION DEPOSITION PRODUCTS

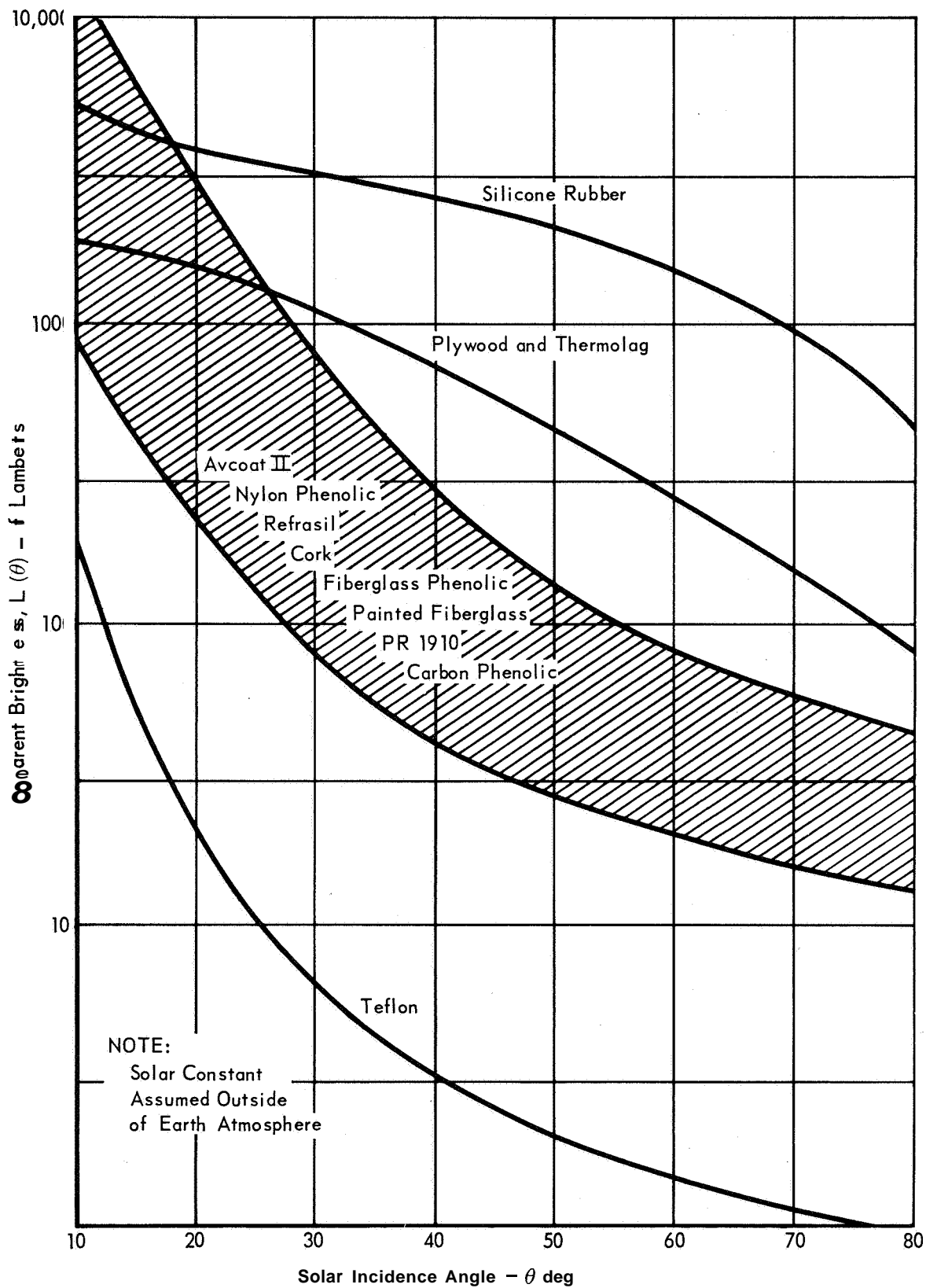


Figure 2.2-9

to become noticeable as image smear. Exposure time cannot usefully be increased beyond this point. When AGC is not used the limited dynamic range of the vidicon tube introduces an apparent loss of performance. Increasing absorption causes the useful low light signal level to approach the noise level of the tube until eventually the signal is obscured. Only the brightest objects in the scene remain to convey detail and the pictures suffer.

If ablative deposit is severe enough it can change the amplitude and phase characteristics of the incoming light waves. A coarse, random distribution of particles or roughening of the window surface will break up the order in the light bundle and destroy the image forming capability.

A quantitative estimate of each of these effects is presented in Figure 2.2-10. Optical resolution for a ground scene 200,000 feet away is evaluated as a function of background luminance and window transmittance. The field of view is 50 degrees and the inherent contrast ratio of the object scene is assumed to be 10:1.

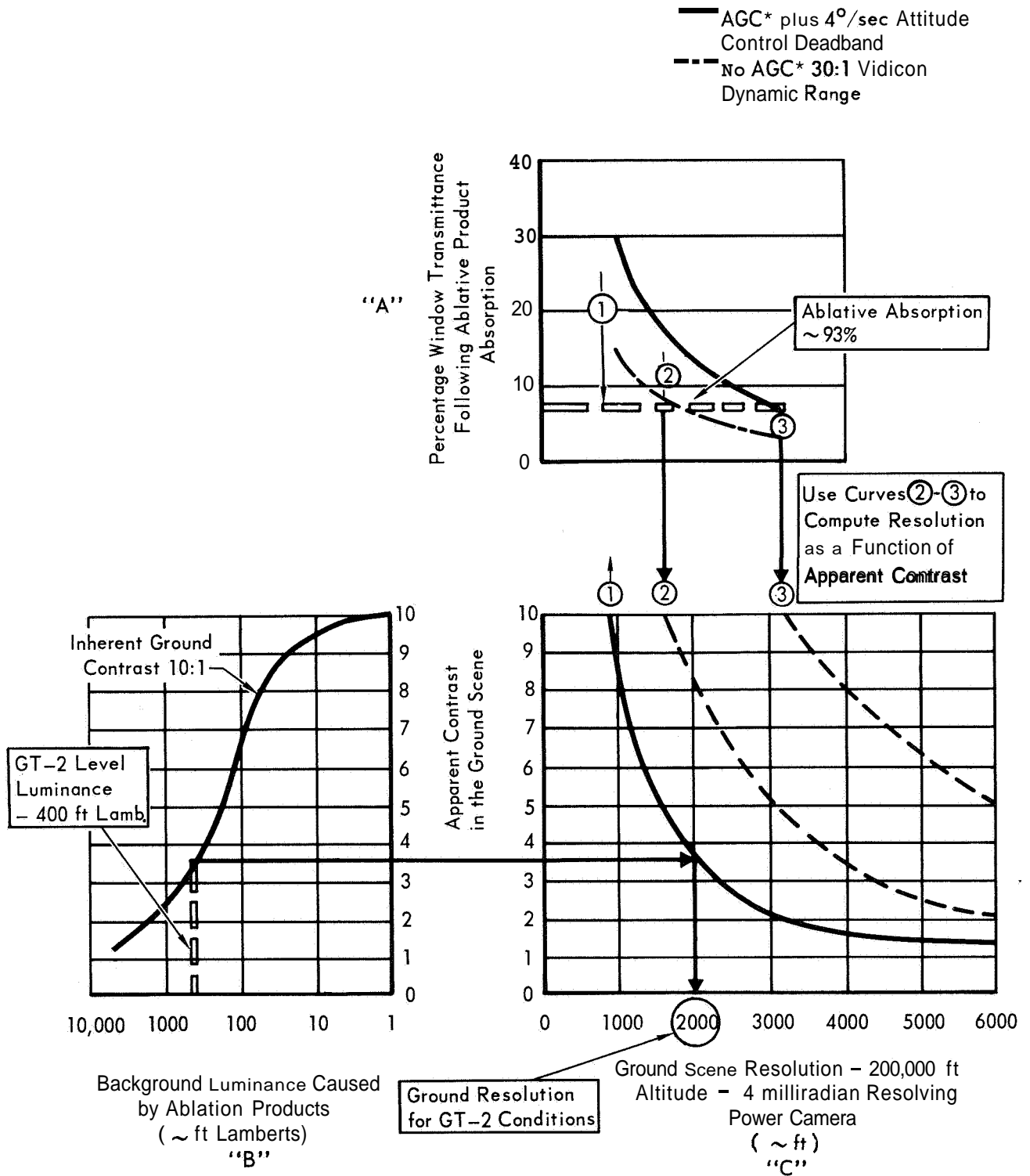
Figure 2.2-10A indicates how ablation product absorption restricts window transmittance. At the onset of ablation reduced transmittance has no influence on optical performance, however, at sufficiently low values of transmittance ground resolution begins to deteriorate. These values are 30 and 15 percent transmittance depending upon whether AGC is used or not used. If AGC is available, image motion is the loss mechanism. With no AGC, exposure reduction accounts for the losses. The magnitude of the optical loss is obtained by projecting the transmittance values down into Figure 2.2-10C. A family of loss curves results, typical of which are those shown for points 1, 2, and 3. The choice of other reference points would lead to a different set of curves in Figure 2.2-10C.

When a veiling background is present, the inherent contrast is reduced and an apparent contrast C_a results (reference Hall, Photographic Considerations for Aerospace, Itek Corp. 1965). For a representative case (2000 foot lamberts highlight, 200 foot lamberts lowlight) this apparent contrast is given as

$$C_a = \frac{2000 \div \text{background luminance}}{200 \div \text{background luminance}}$$

The range of background luminances which satisfy this equation and which could be present during a Martian entry are shown on Figure 2.2-10B. If the apparent contrast is known, then the angular resolution, and consequently the ground resolution of the camera system can be calculated through reference to the signal response curve of the vidicon. The preferred design has the performance shown by the solid curve 1 on Figure 2.2-10C.

METHODS TO COMPUTE GROUND RESOLUTION IN THE CASES OF ABLATIVE ABSORPTION AND LUMINANCE



*AGC - Automatic Gain Control

Figure 2.2-10

To clarify these ideas, consider the examples illustrated on Figure 2.2-10. Figures 2.2-10A and B illustrate the optical degradation produced by 93 percent ablative absorption. In a camera system with no AGC, point 2 projected onto C indicates that ground objects the size of 1600 feet can be detected if they have a contrast ratio of 10 to one or better. Ground resolution (as evaluated by curve 2) decreases with decreasing contrast. If AGC is employed, curve 3 (along with point 3) must be used, and the resulting image smear will limit ground resolution to 3200 feet for 10:1 contrast. A resolution of 6000 feet can be achieved for scene with a contrast ratio of 5:1.

Figures 2.2-10B and C are used to compute the effect of GT-2 luminance levels. The 400 foot lambert values, together with a 10:1 inherent contrast, and the no absorption curve 1 of graph C determine a ground resolution value of 2000 feet.

A series of laboratory tests were conducted to investigate these ablative optical effects. The test setup, with the heat flux levels and materials studied is shown in Figure 2.2-11. Ablative deposition from these tests on quartz window samples is illustrated in Figure 2.2-12. To emphasize the magnitude and variation of these test runs, enlarged pictures of views through two of the sample windows are presented. Figure 2.2-13 shows the type of absorption experienced and Figure 2.2-14 indicates the breakup of the outer optical surface.

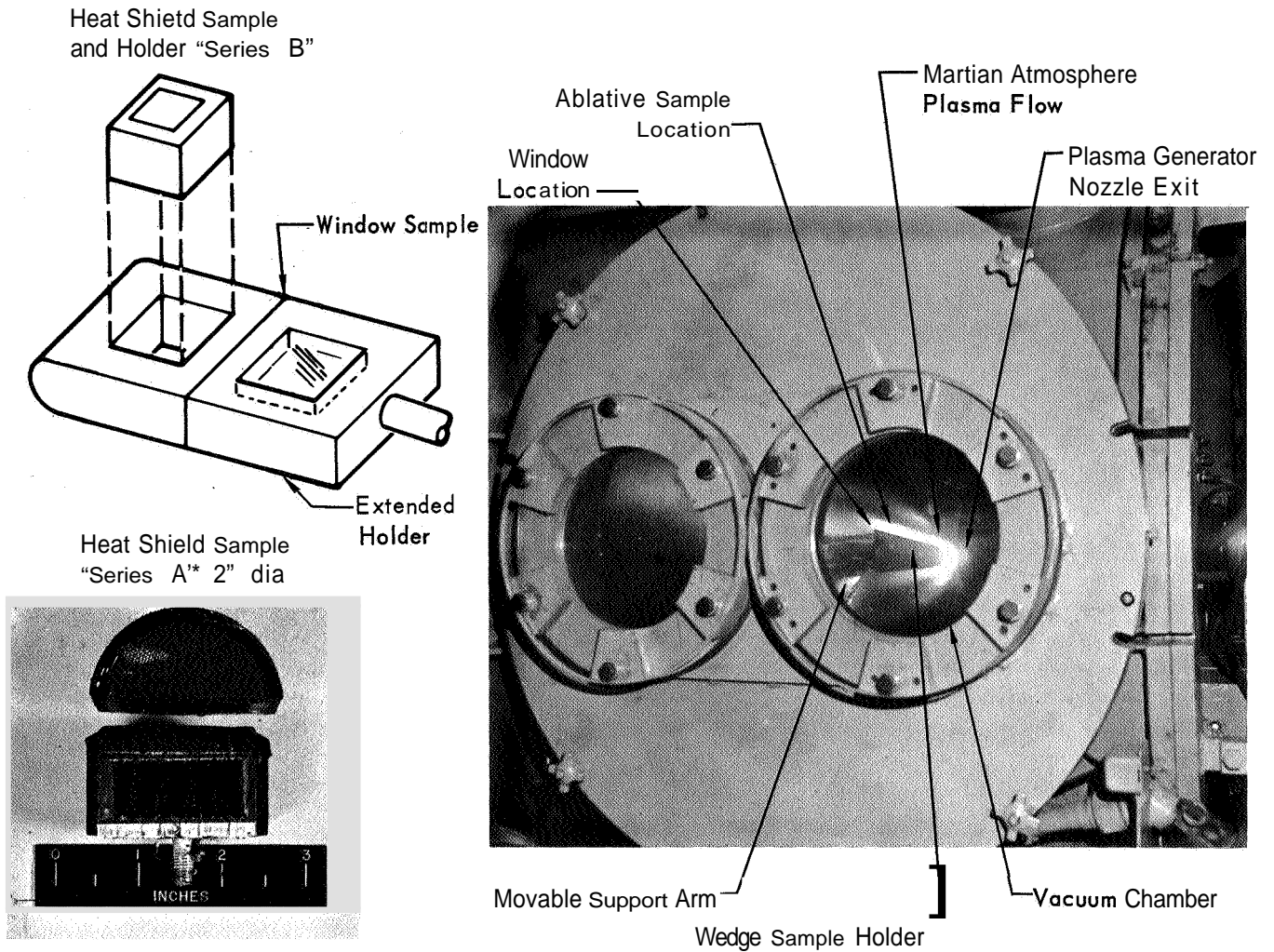
b. Nose Cap Selection - It can be seen from the previous discussion that even the conservative GT-2 calculations violate the basic objective of achieving a ground resolution of at least 1000 feet. The conclusion is that ablative products can seriously restrict television performance and have the potential to negate it completely. Any design employing a completely ablative nose cap risks this loss. A totally non-ablative nose cap is unfeasible because of its weight. As a compromise between these alternatives, the window has been located close to the roll axis, and a non-ablative nose cap is provided for Aeroshell areas forward of the window.

c. Camera Compartment Heating - Heat transmission into the instrument compartment is quite effective as the back surface of optical window will reach temperatures as high as 600°C. The alternative methods of heat protection that have been considered are:

- a. Provide a window that is capable of absorbing high thermal pulses without overheating.
- b. Use recessed cavity and separated flow techniques.
- c. Provide active cooling.
- d. Provide no protection and accept the resulting image degradation.

KEY FOR LABORATORY ABLATIVE DEPOSITION TESTS

A. EXPERIMENTAL TEST SETUP



B. EXPERIMENTAL RESULTS

RUN NO.	FLUX LEVEL	MATERIAL TYPE
1-A	12 Btu/ft ² -sec	1004
2-A	12	1030-1
3-A	12	1030-2
5-A	12	NASA 603
6-A	12	S-6
7-A	12	s-10
a-A	12	s-20
9-A	12	S-20T
10-A	15.4	S-20 (High Angle of Attack)
22	12	S-20T (Low Density Honeycomb)
23	15.4	S-20T (Low Density Honeycomb)

Figure 2.2-11

ABLATIVE PRODUCTS DEPOSITION ON TV WINDOW

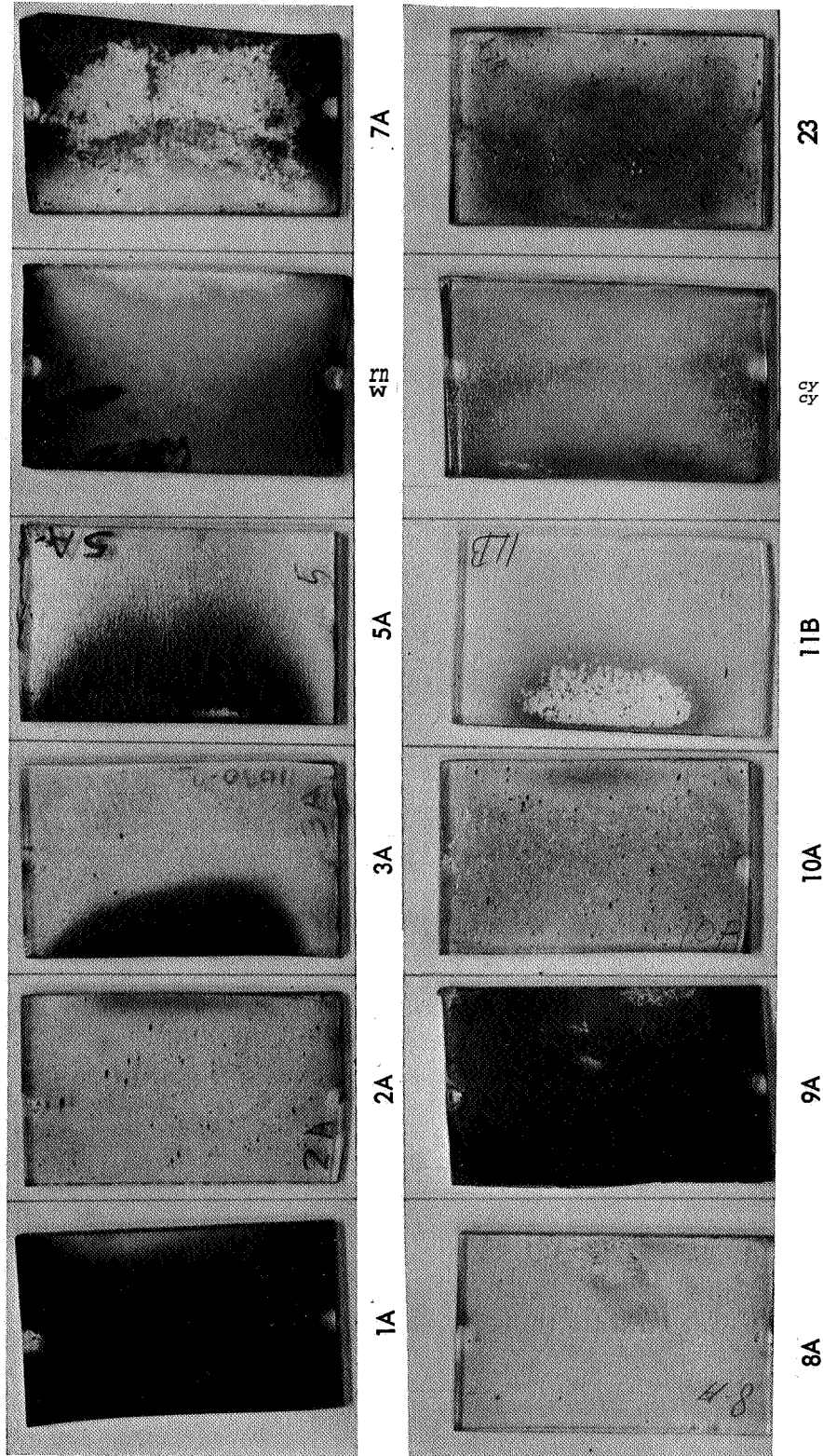


Figure 2.2-12

LOW TRANSMISSION DUE TO ABLATION PRODUCTS DEPOSITION

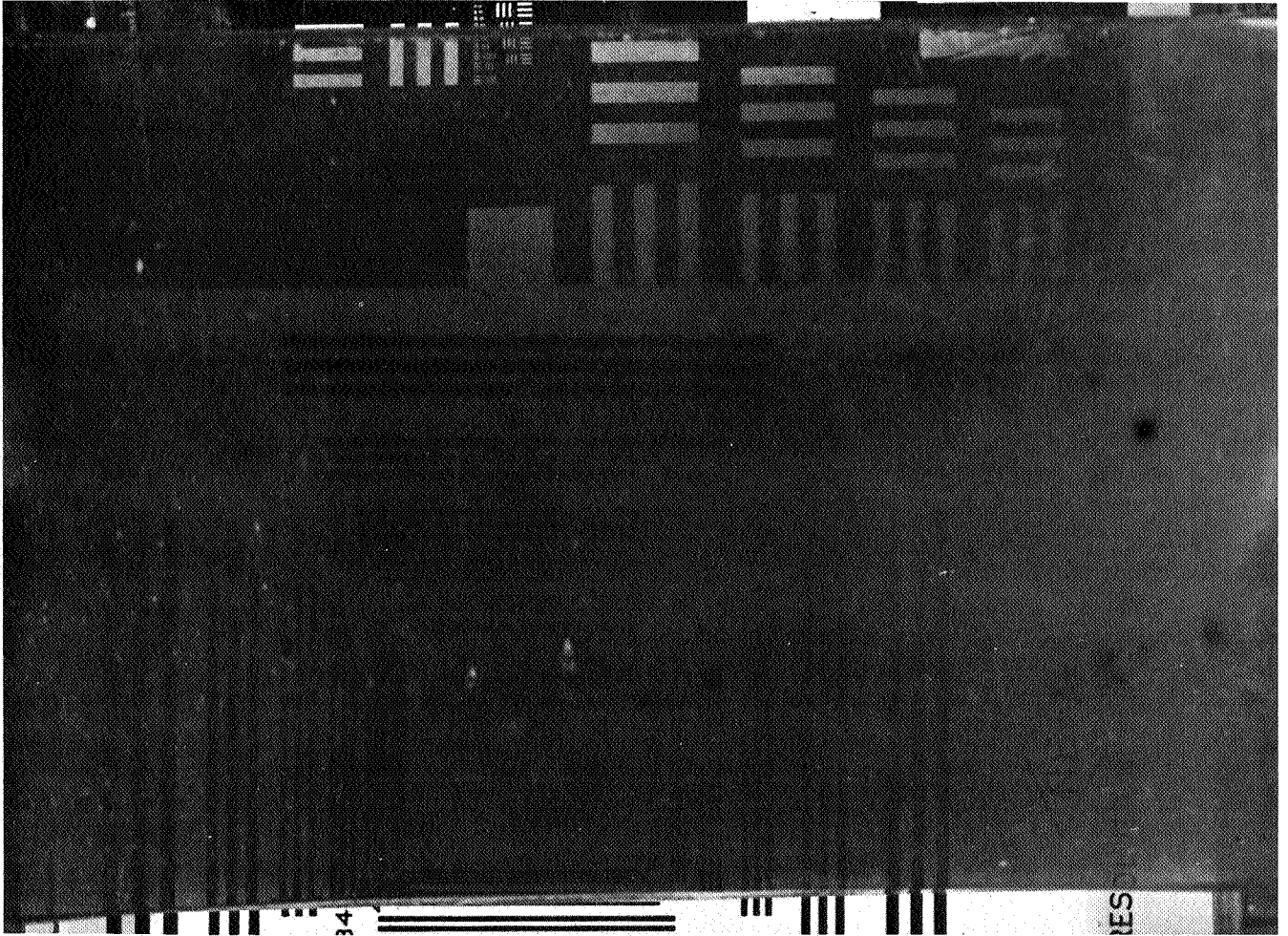


Figure 2.2-13

2-27

DISTORTION DUE TO WINDOW SOFTENING

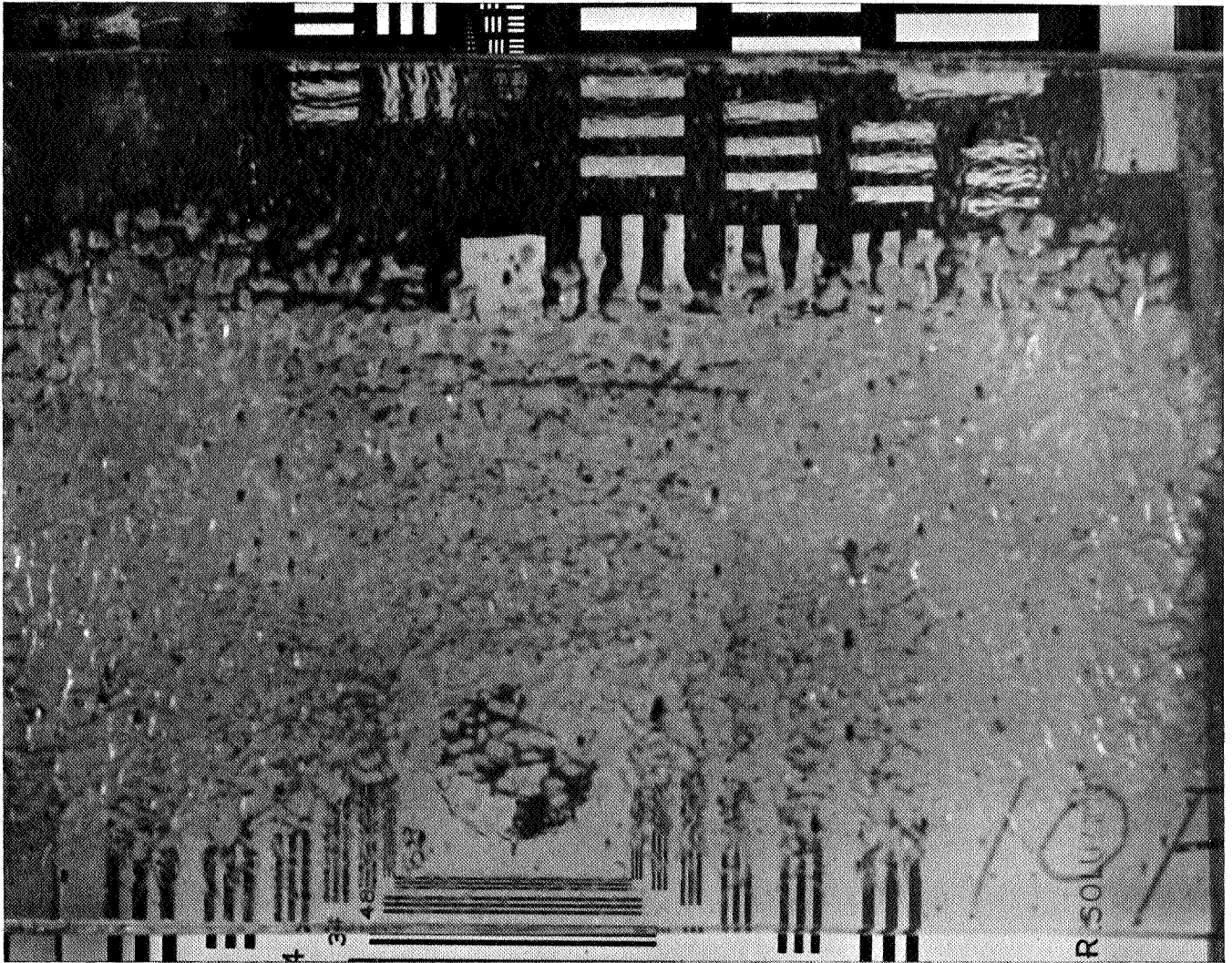


Figure 2.2-14

An investigation of all the factors indicated that the single pane window which is capable of absorbing the thermal pulse is the best choice. This window will become hot enough to generate considerable radiation. Through the use of spectrally selective optical coatings, heat levels can be brought to within acceptable limits. These coatings transmit visible light but totally reflect thermal radiation. They can be placed on the outer surface of the camera optics or on the back of the window surface.

d. Communications Blackout - Another item of major interest relates to the loss of information during communications blackout. The imaging system will be operative during this time and ground scenes will be detected. However, these do not get transferred back to the Orbiter. The extent of blackout depends heavily on the type of atmosphere encountered and the descent technique employed. Limiting values are summarized as follows:

<u>Atmosphere</u>	<u>Entry Angle</u> <u>(degrees)</u>	<u>Velocity</u> <u>(ft/sec)</u>	<u>Blackout Altitude (ft)</u>		<u>Comments</u>
			<u>Start</u>	<u>Finish</u>	
VM-9	-10.4	13,000	462,000	250,000	Earliest Emergence
VM-2	-10.4	13,000	170,500	93,000	Shortest Altitude Interval
VM-8	-20	15,000	167,500	59,000	Latest Emergence
VM-3	-20	15,000	435,000	130,000	Longest Altitude Interval

The alternatives are to obtain useful imagery only at times other than during blackout or to provide data storage during blackout. For five second intervals between images from alternate cameras, data is generated at 50,000 bits/second. It is possible to accumulate 7.5 million bits for a 150 second blackout period. Use of an endless belt tape recorder and transmission of both new and stored information at 100,000 bits/second could be accomplished for about 40 pounds additional weight for recorder, more powerful transmitters and for batteries. This seems a high price to pay for the additional images.

e. Post-Landing Imagery - It is possible to take pictures after touchdown because the camera equipment is available and the high data rate channel is still open as long as the Orbiter is in view. They would provide a real time panoramic survey of the local surroundings. This concept is not included in the selected design due primarily to weight considerations.

Selection of Preferred Approach - The imaging system described in Figure 2.2-15 has been selected as the preferred design concept. It satisfies the constraints and supplies a reliable, comprehensive solution to the imaging problem.

Both cameras start with a five second spacing at 800,000 feet altitude. A contrast enhancement filter is introduced alternately with a clear filter, but out of phase between cameras, in order to secure a balanced spectral sampling with altitude. At 500,000 feet, the ground resolution near the landing site from camera 1 will approximate that of the Orbiter, which has been assumed to be 1000 feet. Framing will continue through blackout. No convenient, reliable method exists to temporarily shut the camera down, and besides, this imagery may be qualitatively valuable in the prediction of the interaction conditions. Communication blackout can end as early as 250,000 feet allowing camera 2 to start a high quality investigation of the site location. Best imagery here will take place below 100,000 feet where ground resolutions of 500 feet are possible.

During parachute deployment and Aeroshell separation, imagery will be degraded by motion or occultated by structure. Image quality will tend to decrease after descent engine ignition at 5,000 feet because of engine plume and vibration effects and more so below 200 feet when defocusing becomes a problem. These angular losses will be offset in part by the decrease in object distance and thus terminal resolutions on the order of inches should be expected from both cameras. Descent imaging is terminated by camera ejection at 90 feet to avoid damaging the impacting SLS.

The performance of the preferred design, including a description of coverage, resolution, and loss of brightness is summarized in Figure 2.2-16. The resolution that is available is plotted as a function of altitude for six specific trajectories, in Figures 2.2-17 through 2.2-22. These figures include examples for four atmosphere models. The main point to note in these figures is the impossibility of keeping the exact landing location in view throughout descent with a narrow field of view. Certainly, imagery of the surrounding area is well-documented and correlated, but continuous observation of the actual site is often lacking, particularly at high resolution. A better definition of the atmosphere or a more sophisticated imaging concept is required to achieve more optimum results.

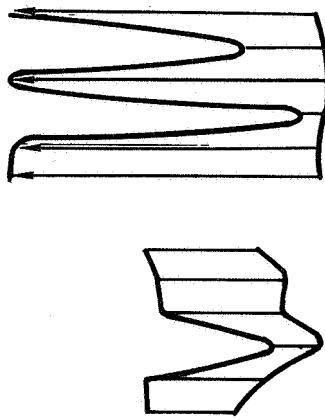
For typical extremes of entry conditions, a VM8 atmosphere and initial entry angle (γ) of -20° and -10.4° , Figure 2.2-23, shows the ground and sky portions of the total field-of-view (FOV) for the 50" FOV and 8" FOV cameras as a function of

PREFERRED DESCENT IMAGING SYSTEM

	CAMERA 1	CAMERA 2
Purpose:	High resolution pictures for very high altitude site identification and detailed surface evaluation in the terminal descent phase.	Wide angular coverage to maintain viewing and establish identification of the landing site at moderate to low altitudes.
Detector:	Slow Scan Vidicon, 200 x 200 line,	0.44 inch format
Optics: Focal Length	3.2 inches	0.5 inches
Field of View	8°	8°
	(Unvignetted)	
Angular Resolution	0.0007 radians	0.004 radians
Focal Ratio	F/1.5	F/1
Sequencing: Exposure Time	10 milliseconds	5 milliseconds
Cycle Time	10 seconds	10 seconds
Phasing	Alternating operation = out of phase firing every other 5 seconds.	
Data: Initiation	First picture taken at 800,000 feet	
Picture Content	240,000 Bits per picture (6 bit amplitude resolution)	
Readout	50,000 Bits per second, continuous for combined system	
Termination	Camera system forcibly removed from CBS at 90 ft Altitude.	
Installation:	CBS impact pad mounting, window on aeroshell 40 in. off the roll axis and pointing parallel to it.	
Thermal Protection:	Single glazing SiO₂ window and non-ablative nose cap extending out to window.	
Special Spectral	One contrast enhancement filter possible in addition to clear.	
Features: AGC	Gain control used to optimize exposure.	

Figure 22- 15

PERFORMANCE CAPABILITIES FOR A DESCENT TELEVISION SYSTEM.



VM-3 (-10.4) 13 kft/sec
 VM-7 (-20°) 15
 VM-7 (-13.6°) 15
 VM-8 (-20°) 13
 VM-9 (-20°) 15
 VM-9 (-10.4) 13

View of Landing Site Lost
 by Narrow Field Camera

VM-3 (-10.4) 13 kft/sec
 VM-7 (-20°) 15
 VM-7 (-13.6°) 15
 VM-8 (-20°) 13
 VM-9 (-20°) 15
 VM-9 (-10.4°) 13

Communications Blackout

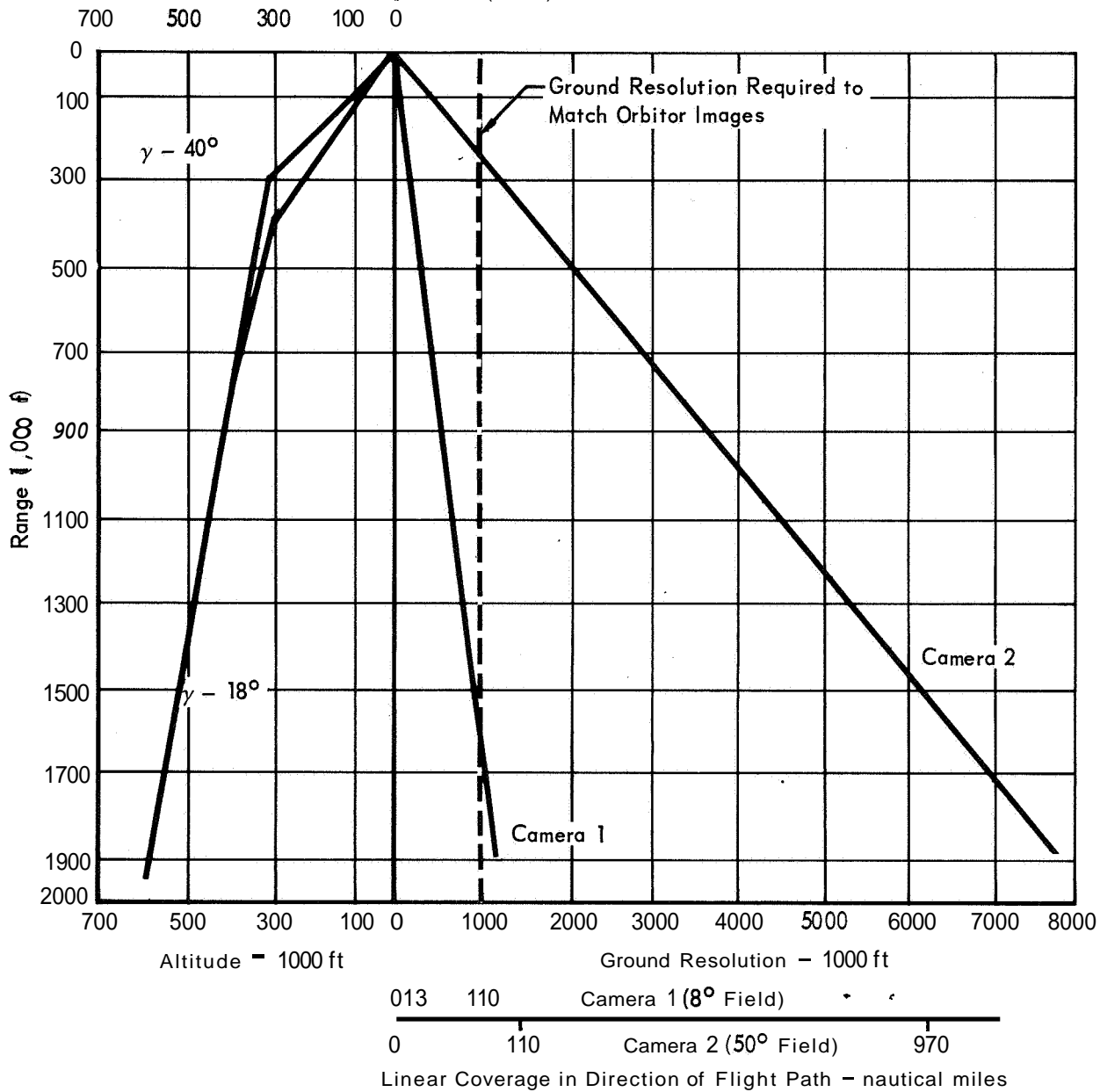


Figure 2.2- 16

DESCENT TV INTERCEPTS

VM-7 Atmosphere
 $\gamma_E = -20 \text{ deg}$
 $h_E = 760,000 \text{ ft}$
 $M_{CDP} = 0.30 \text{ slug ft}^2$
 $V_E = 15,000 \text{ ft sec}$

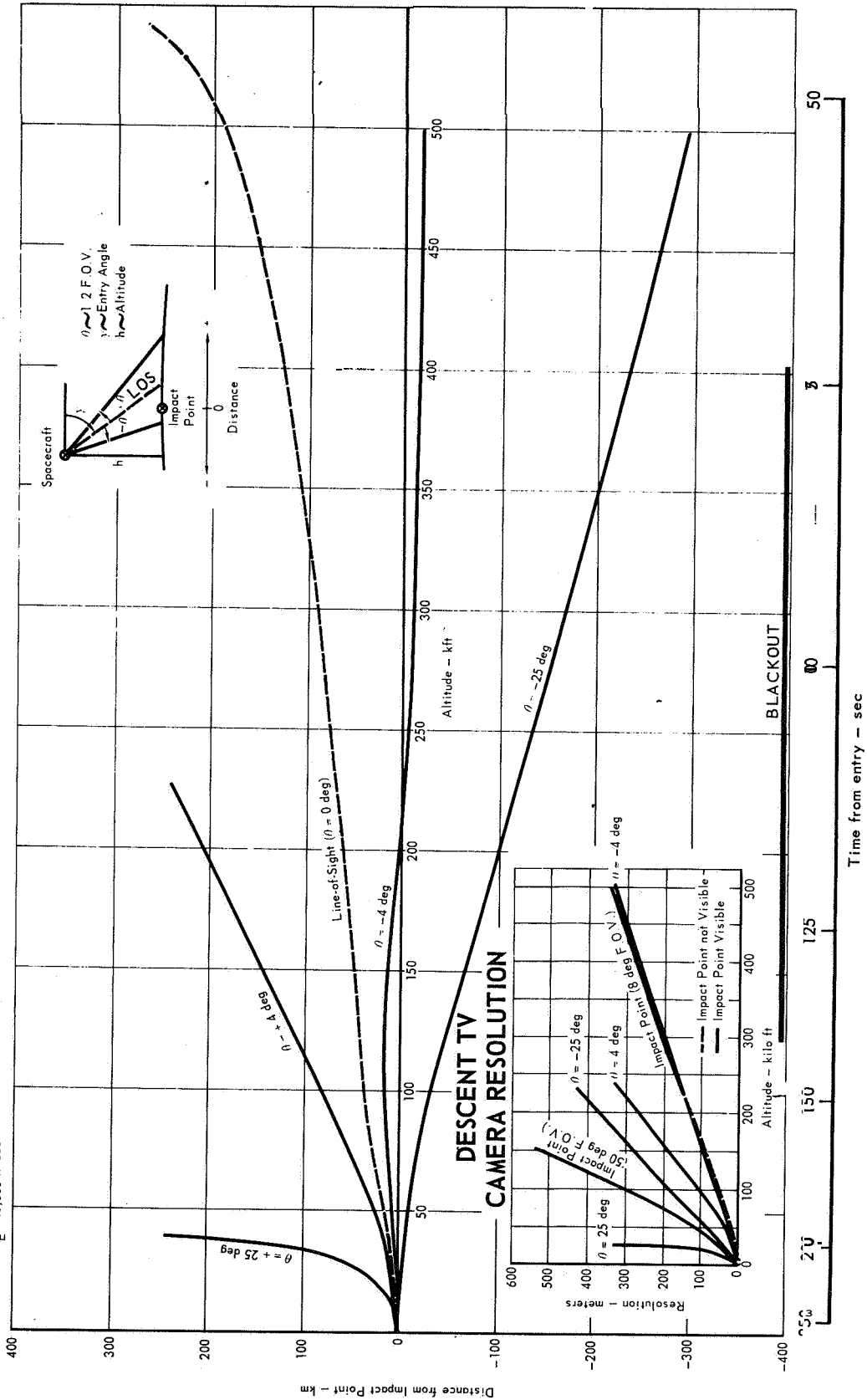


Figure 2.2-17

DESCENT TV INTE C&JHS

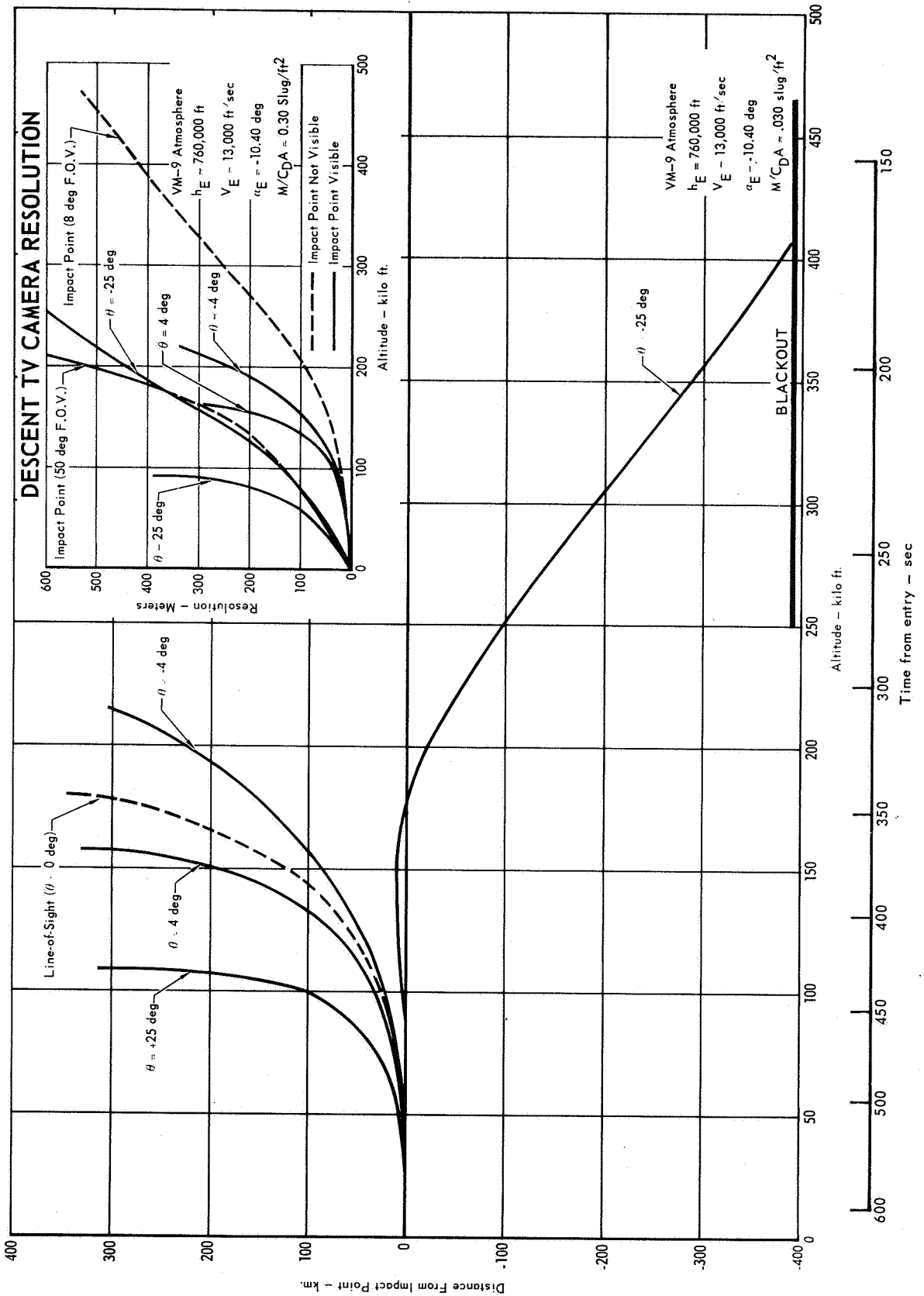


Figure 2.2-18

DESCENT TV INTERCEPTS

$\gamma_E = -20.0$ deg
 $h_E = 760,000$ ft
 $M_{CPA} = 0.30$ slug ft²
 $V_E = 15,000$ ft sec

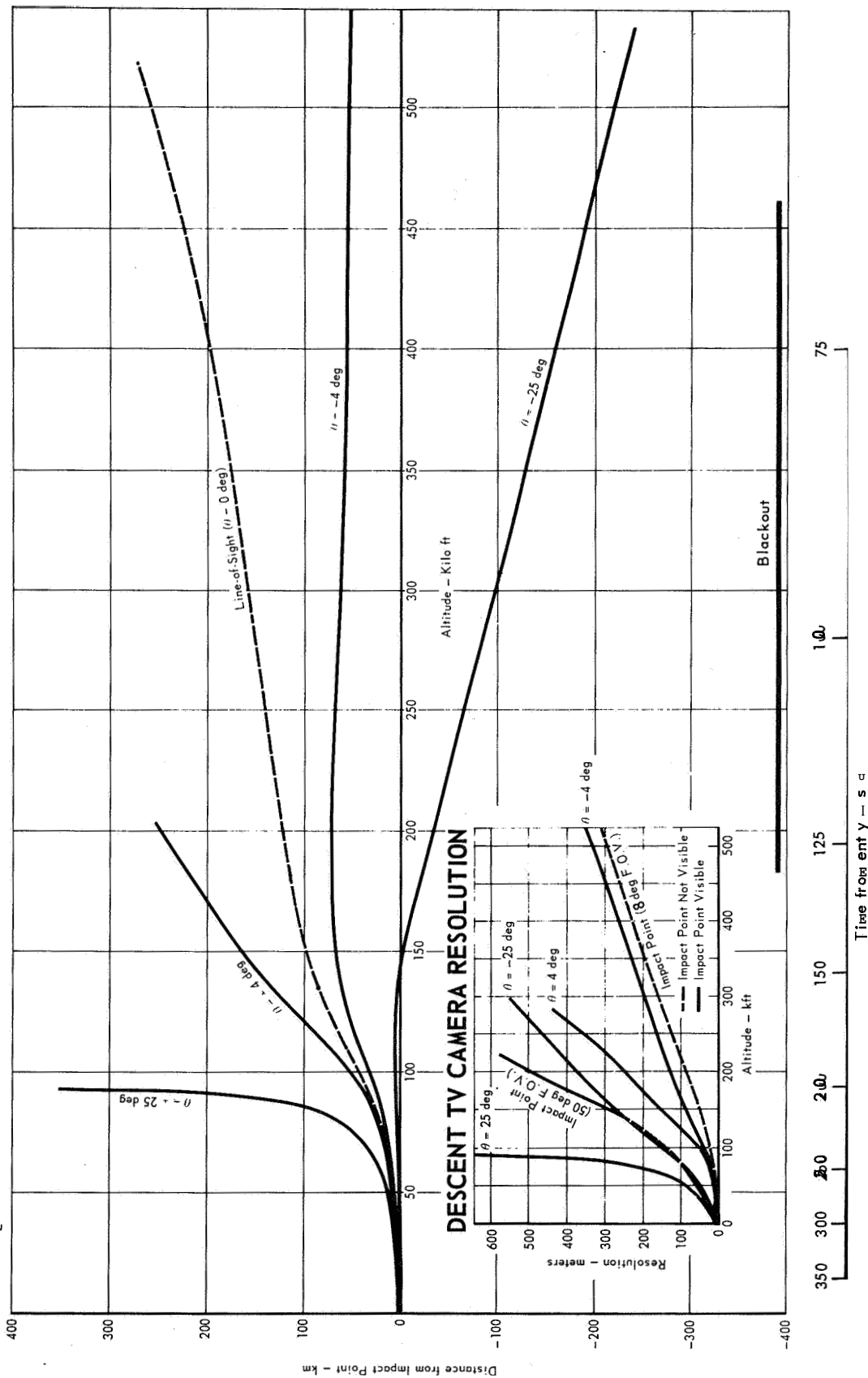


Figure 2.2- 19

DESCENT TV INTERCEPTS

$V_M = 8$ Atmosphere
 $\gamma_E = -10.40$ deg
 $h_E = 760,000$ ft
 $M C_{D_A} = 0.30$ slug ft²
 $V_E = 13,000$ ft/sec

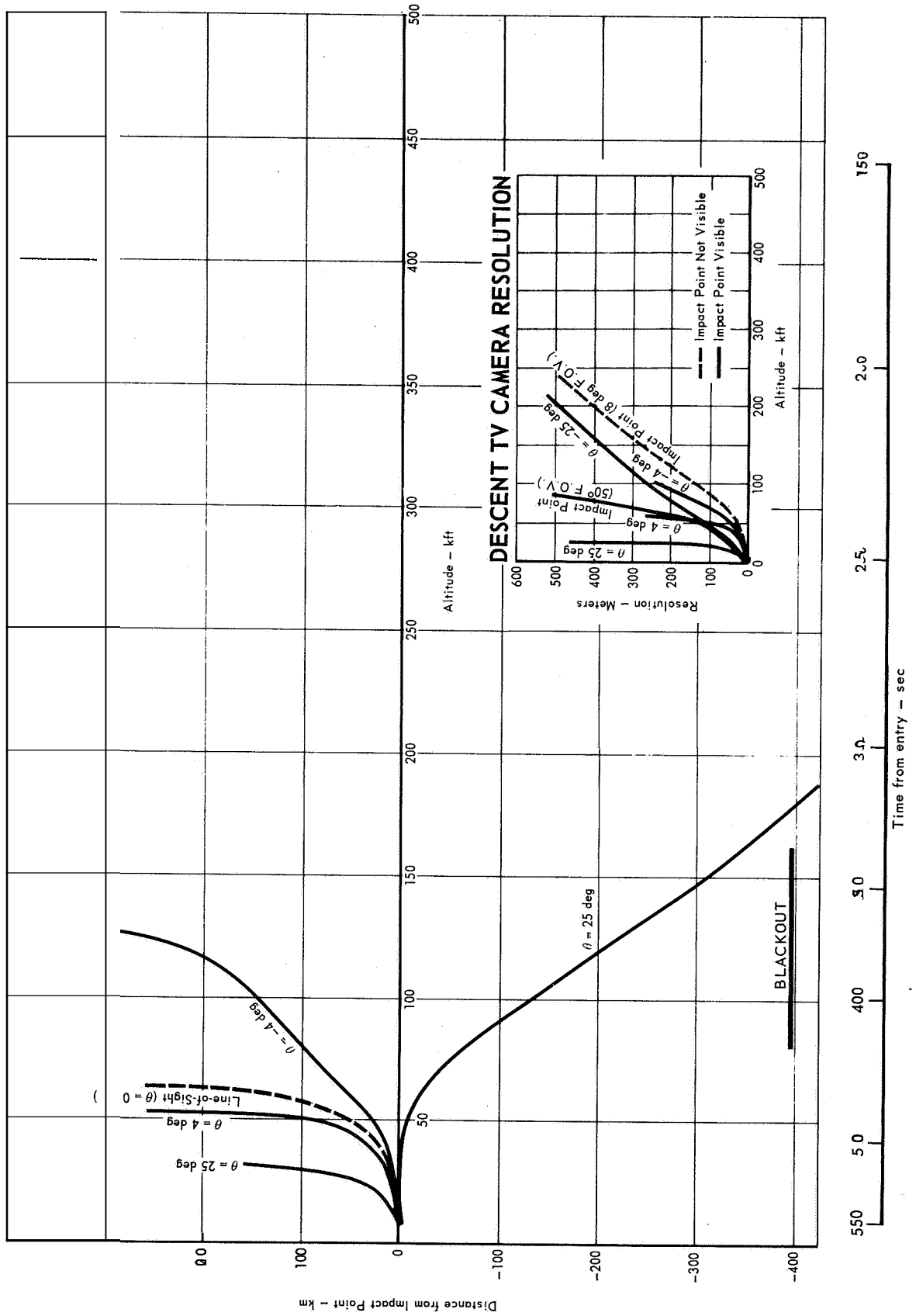


Figure 2.2-20

DESCENT TV INTERCEPTS

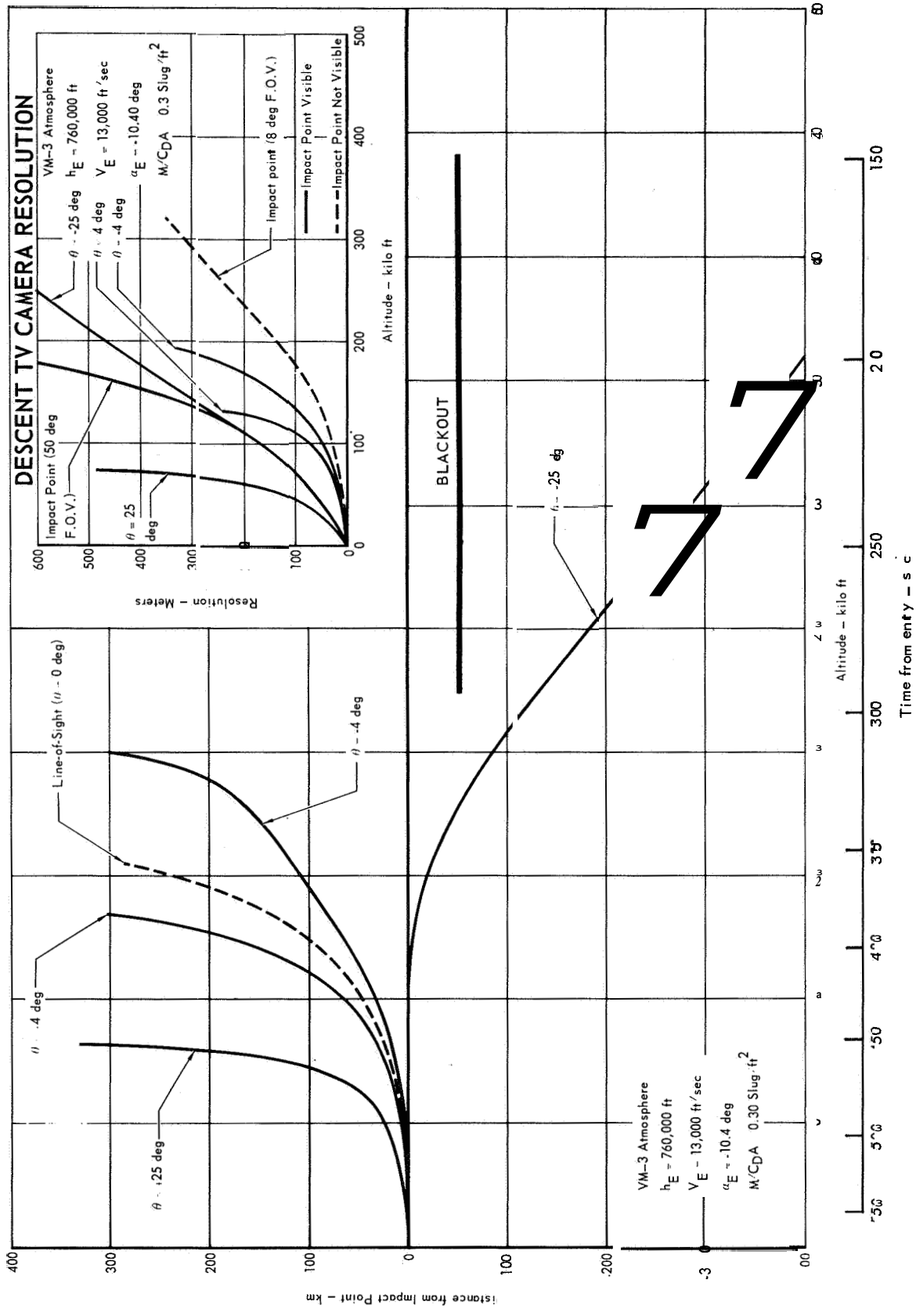


Figure 2.2-21

DESCENT TV INTERCEPTS

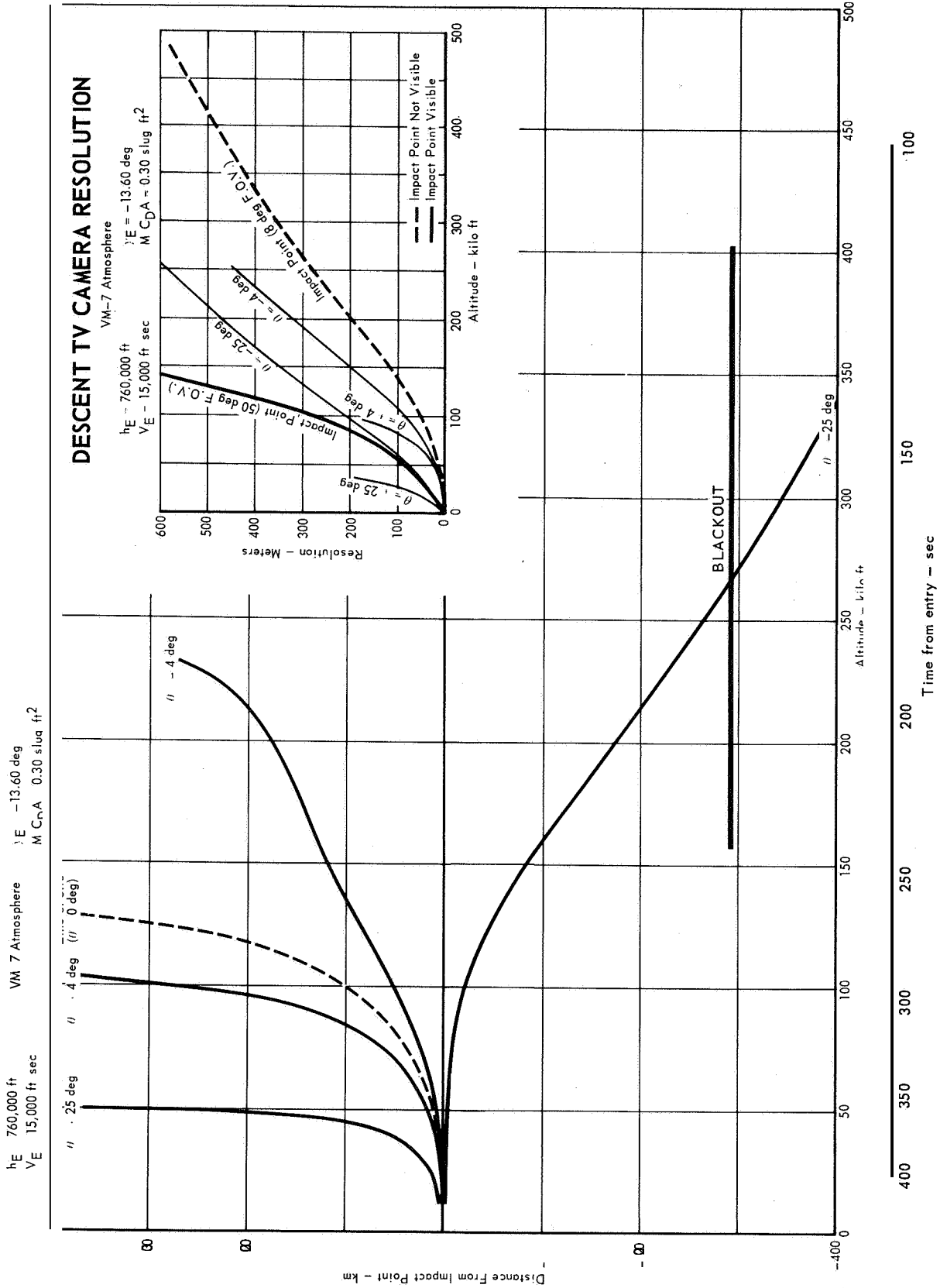


Figure 2.2-22

**GROUND AND SKY COVERAGE DURING ENTRY IMAGING
(ANGLE-OF-ATTACK = 0°)**

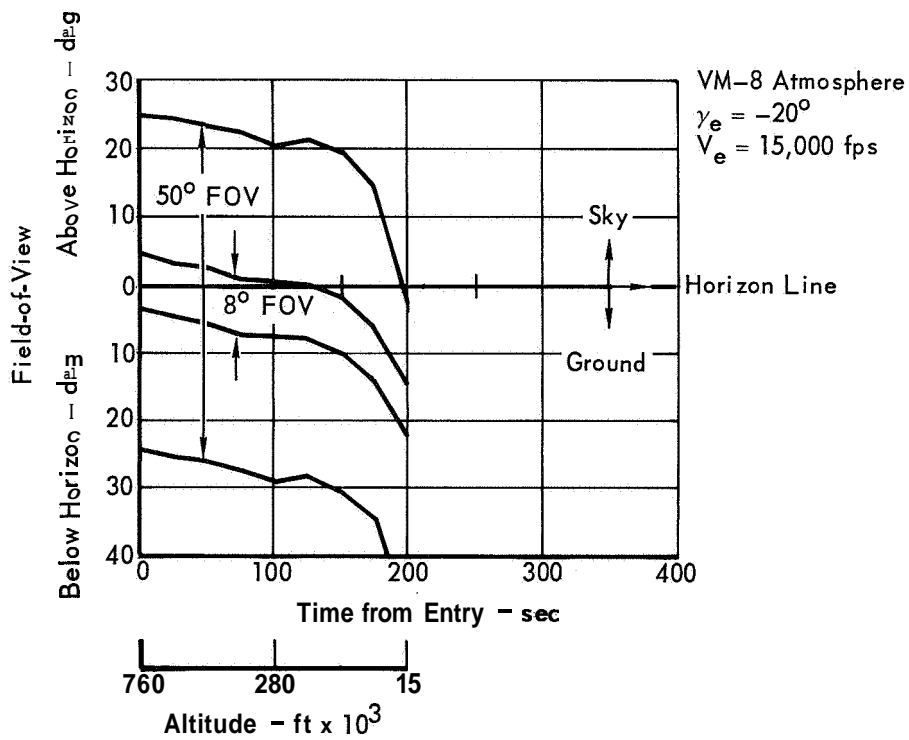
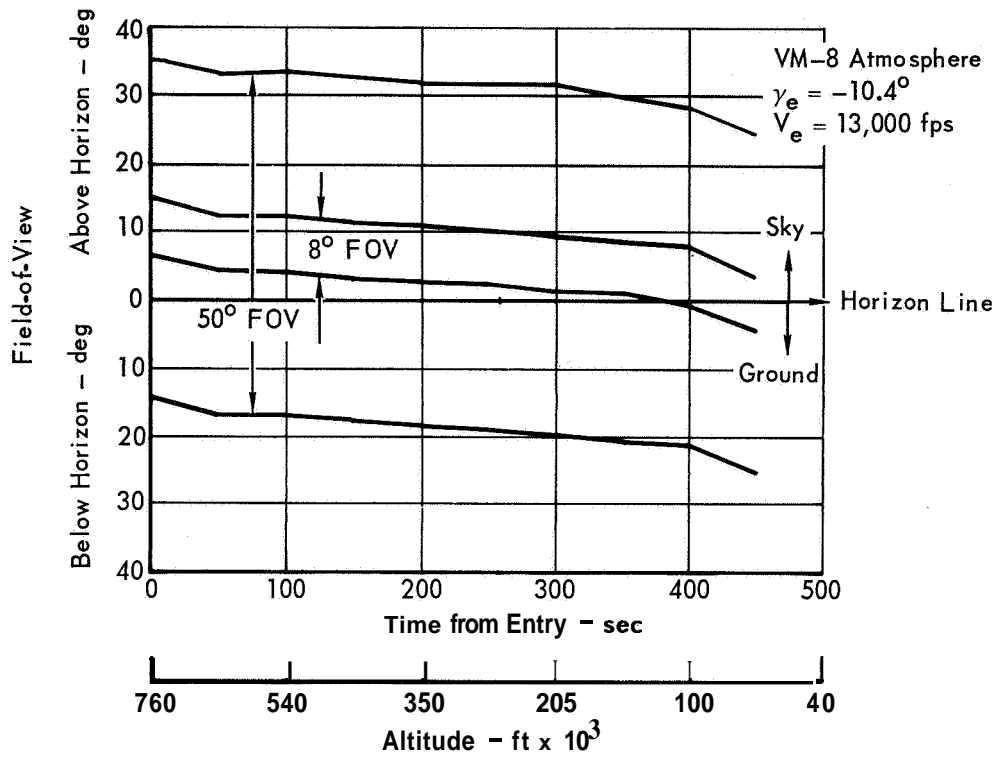


Figure 2.2-23

time from entry and altitude. A VM-8 atmosphere was chosen because it represents a "worst case" situation in which a maximum amount of sky and minimum amount of surface are imaged. Figure 2.2-23, minimum entry angle condition ($\gamma = -10.4^\circ$), shows that the 50" FOV camera images about 50% sky and 50% ground from entry to an altitude of 70,000 feet. The 8° FOV camera images sky only down to 125,000 feet at which point the surface features start to appear in the FOV. The other entry extreme, a maximum entry angle ($\gamma = -20^\circ$) shows that both cameras retain ground features within their FOV's. The wide FOV camera has a 50% sky and 50% ground coverage from entry at 760,000 feet down to about 40,000. At this point ground features start to appear more prominently in the FOV. The narrow FOV camera has extremely good coverage below 520,000 feet.

The preferred design concept directed at landing site identification and detailed surface imaging also offers considerable promise in fulfilling the less prominent informational requirements. In particular, stereoscopic comparisons will be possible on a frame-to-frame basis, especially at the lower altitudes due to the sizeable overlap in coverage. This will greatly improve the information content. Wide angle, two color viewing which includes the Martian limb in the initial frames will provide the basis for photometric and atmospheric attenuation evaluations. Continuous 50 degree coverage over major portions of the trajectory will generate pictures for photogrammetric mosaic to aid in assessing altitude profiles. Thus, all the ingredients are present which provide for completely successful information collection.

SECTION 3

SCIENCE INSTRUMENTS

The analysis, considerations and assumptions used to define the characteristics of the preferred instruments, including investigations of alternate techniques for the ESP measurements are discussed in this section.

Our preferred Entry Package uses the typical instruments as described in the JPL Constraints Document. Additional detail characteristics not defined in the Constraints Document were selected for use in defining the operational sequence and the support subsystems.

Our preferred ESP science instruments include: 1) TV cameras which take photographs every 5 sec from alternate cameras starting at 300 seconds prior to a predicted 800,000 ft altitude, 2) diaphragm capacitance pressure transducers which provide stagnation and base pressure measurements, 3) platinum resistance thermometers (the gas flow over the stagnation temperature sensor is restricted prior to Mach 5 to prevent excessive sensor temperatures), 4) a mass spectrometer with a molecular leak connected to the inlet port, and 5) a tri axis accelerometer with dual range for the longitudinal axis (0 to 30 g and 0 to 5 g) and a single range for the other two axes (± 2 g). An alternate higher-weight-payload which provides an increased measurement capability includes instruments for direct density measurements by gamma backscatter, a facsimile camera for post touchdown imaging (backup to surface lab camera), and an atmospheric composition determination by solar UV and X-ray absorption as listed in Figure 3-1.

	<u>Science Instrument Payloads</u>	
	Selected Science Instruments Payload Weight, lbs	Alternate Science Instrument Payload Weight, lbs
Pressure	2 (2 sensors)	4 (4 sensors)
Temperature	1 (2 sensors)	1 (2 sensors)
Acceleration	2	2
Mass Spectrometer	8	8
Vidicon Cameras	14	14
Backscatter Densitometer		5
Solar Absorption Detector		2
Aerosol Impact Detector		2
Facsimile Camera	—	8
Total	27 lbs	46 lbs

Figure 3-1

3-1

3.1 ATMOSPHERIC PROPERTIES INSTRUMENTS - The time history of the quantities to be measured depends on the entry conditions employed and the atmosphere encountered. Maximum accelerations, pressures and temperatures will occur for the fastest, steepest entry condition which is:

- o $V_E = 15,000 \text{ ft/sec}$

- o $\gamma_E = -20. \text{ degrees}$

Much of the entry will occur at hypersonic Mach numbers where high temperature gas dissociation, ionization, and chemical relaxation phenomena occur. If measurements are made at lower supersonic Mach numbers ($M < 5$), the effects of chemistry on the measurement of gas properties will be reduced. For a Mach number less than 5, the supersonic equations describing the flow about the vehicle will be valid and can be employed to extrapolate measurements made in the flow field to the ambient free stream properties. Contamination from the heat shield which is still hot from the hypersonic entry must be avoided.

The TV window could be completely covered with ablation products deposition which would prevent the TV from obtaining clear views of the surface during the descent phase following peak heating until the Aeroshell is separated. In addition, the atmospheric composition measurement could be affected by the contamination products of the ablating heat shield.

The ceramic heat shield (hardened Fiberfrax) of our preferred design was therefore selected to eliminate contamination due to vehicle outgassing and ablation products and thus significantly improve the quality of data to be gathered. Clear TV views of the surface are obtained during the entire entry and descent and composition measurements free of ablation products are obtained by using the non-ablative heat shield section.

3.1.1 Pressure - The purpose of these instruments is to obtain pressure measurements for use in atmospheric profile reconstructions over the maximum possible portion of the entry. Figure 3.1.1-1 presents a typical stagnation pressure profile and Figure 3.1.1-2 presents a typical free-stream pressure profile for entry into the Martian atmosphere.

The preferred approach is to use two diaphragm capacitance pressure transducers, one located in the stagnation region and the other located in the base region.

3.1.1.1 Constraints - Selection of the pressure measurement technique is constrained by the following:

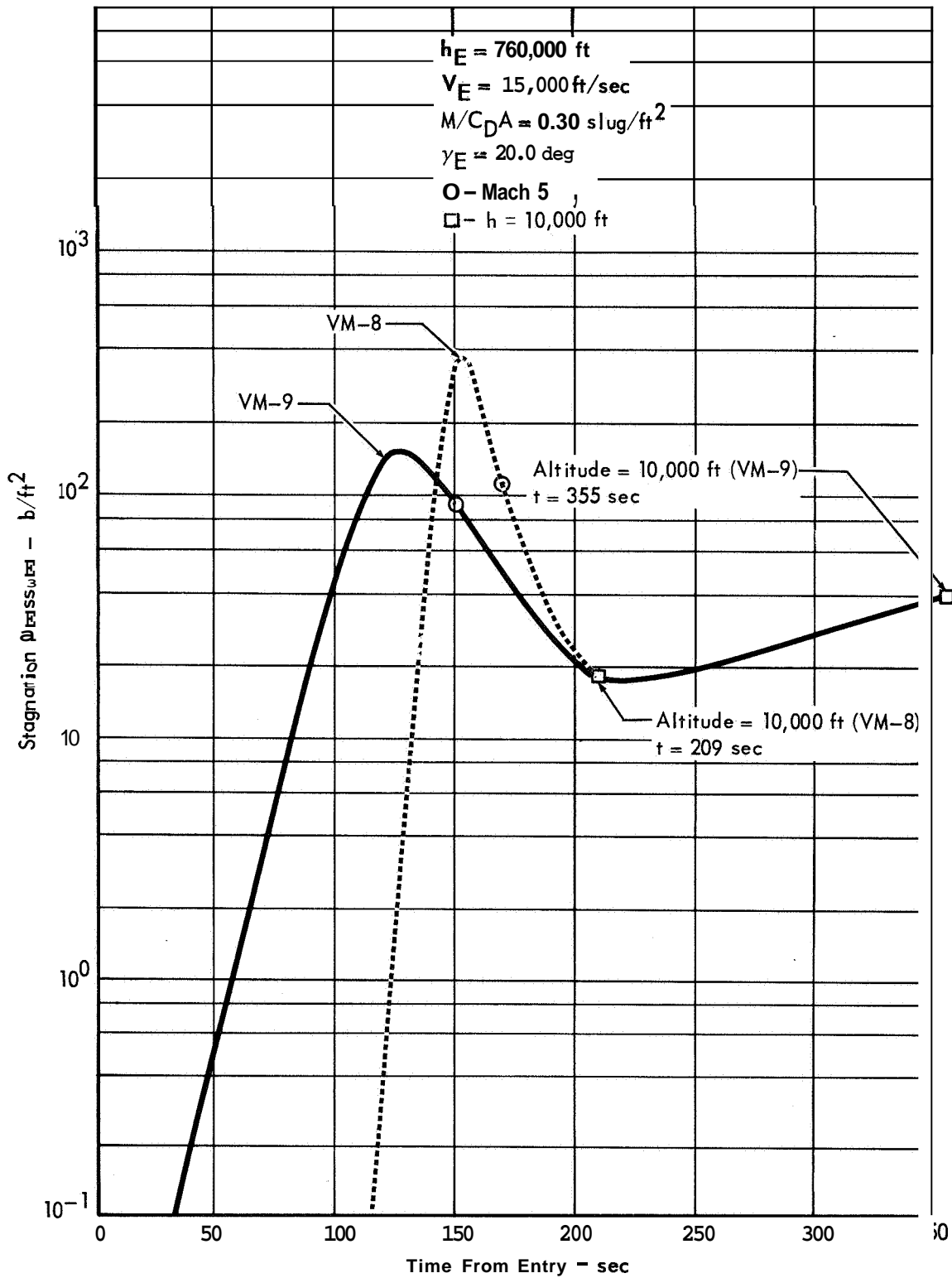


Figure 3.1.1-1

FREE STREAM PRESSURE PROFILES

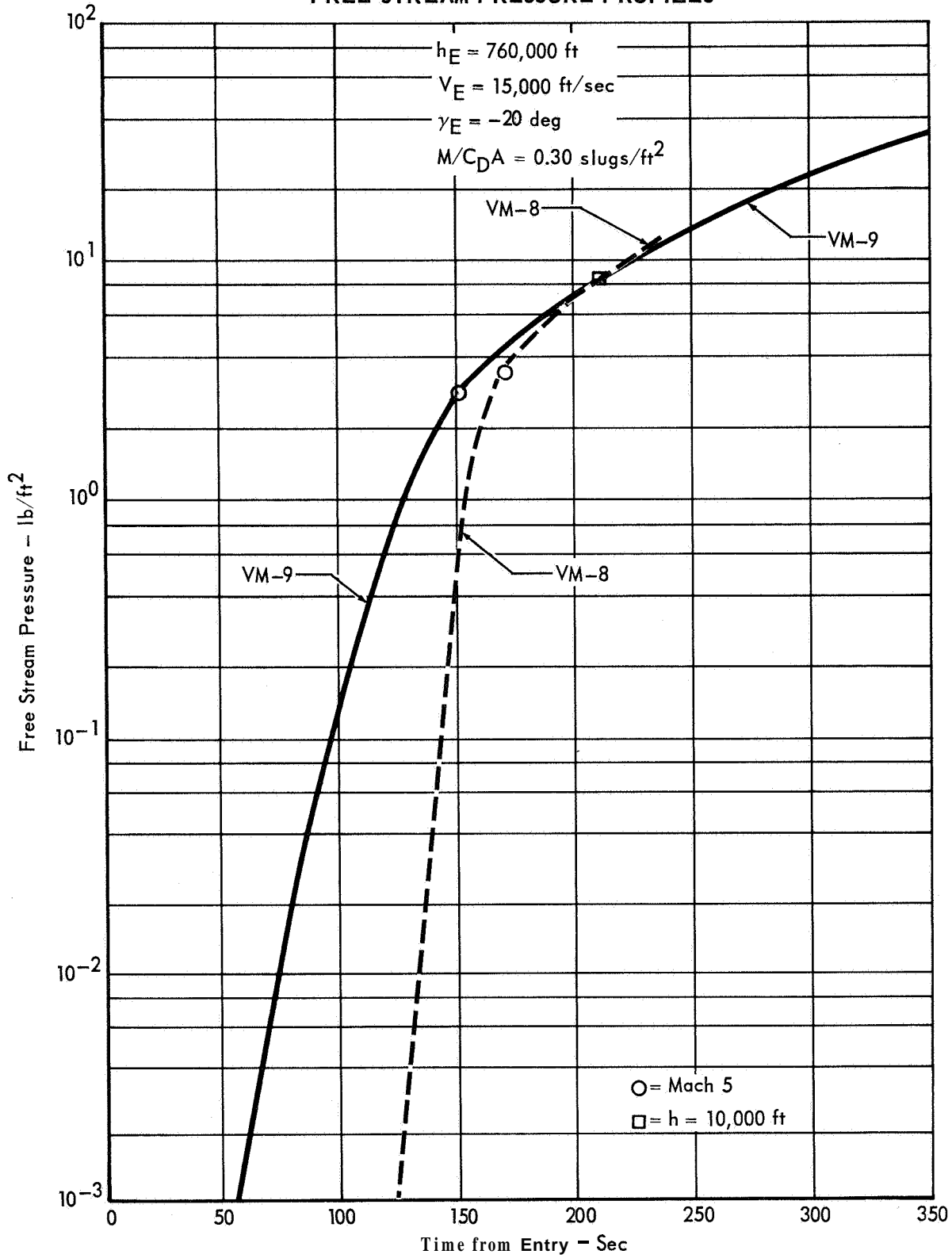


Figure 3.1.1-2

- Measurement technique must not be based on observing temperature phenomena.
- Response time of the instrument must be compatible with pressure profile being measured.
- Acceleration sensitivity must be small.
- Measurements must be made at an area whose pressure coefficient behavior is known so that sensed pressures can be related to free stream pressures.
- Proof pressure must be at least 23 psia to survive the thermal sterilization cycle without performance degradation.
- Knowledge of the atmospheric composition must not be required to permit data interpretation.
- Requirements of interfacing subsystems must be met.
- The maximum stagnation pressure is 375 lbs/ft² (VM-8)

3.1.1.2 Alternatives - Four types of pressure transducers were considered as candidates for making the pressure measurements described above. They were the diaphragm potentiometer type, the diaphragm capacitance type, the thermocouple vacuum gauge type, and the vibrating diaphragm type. Considerations affecting the choice of one instrument over the others were sensitivity to composition and temperature, size, weight, power, and accuracy.

After the transducer type was selected, further alternatives which affect the design of the sensor were considered. They included:

- Location(s) of transducer to obtain the most accurate data over the entire entry profile, especially the subsonic portions.
- Input power level and regulation requirements.
- Output signal characteristics.

3.1.1.3 Comparison - Instrument insensitivity to composition is a prime consideration in the selection of the transducer for obtaining these measurements. This consideration is important because of our lack of knowledge about the Martian atmosphere composition. The selection of an instrument which depends upon a knowledge of composition for accurate data interpretation reduces the probability of obtaining accurate free-stream pressure profiles since two instruments must function properly; the pressure transducer and the composition determination instrument. Of the four transducer candidates listed, both the vibrating diaphragm type and the thermocouple vacuum gauge require composition knowledge for data interpretation.

High temperature sensitivity is another undesirable characteristic. All of the above four candidate instruments have temperature coefficients which are

acceptable for the purposes of this experiment.

The size, weight, and power requirements of all four transducer candidates appear to be compatible with ESP size, weight, and power constraints if minor development efforts are undertaken.

The accuracy requirement can be met by all the transducer candidates except the diaphragm potentiometer type which has increasingly poorer accuracy as full range pressures decrease.

Selection of the transducer leaves the locations of the transducers on the Aeroshell unresolved. Three general areas and combinations thereof are considered. General areas for transducer location are the stagnation region, the wall region near the sphere cone tangency point, and the base region. The stagnation region is a highly desirable location because the pressure coefficient behavior in this region is well known as long as angle-of-attack excursions remain within ± 20 degrees. Pressure obtained from this transducer is related to free-stream pressure by the relation:

$$P_s = C_{P_s} q + P_\infty$$

where P_s = stagnation pressure

C_{P_s} = stagnation pressure coefficient which varies with Mach number and angle of attack

$$q = \frac{\rho V^2}{2} \text{ (dynamic pressure)}$$

P_∞ = free stream pressure

The wall pressure is related to the free-stream pressure by the relation:

$$P_w = C_{P_w} q + P_\infty$$

where P_w = wall pressure

C_{P_w} = wall pressure coefficient which is a function of Mach number and angle of attack

If the stagnation and wall locations were selected as the two choices, a density profile determination can be made which is independent of P_∞ . This would be achieved by subtracting P_w from P_s resulting in the following:

$$P_s - P_w = (C_{P_s} - C_{P_w}) q$$

If we use a differential type transducer for the wall measurement, the $P_s - P_w$ is measured directly, thus reducing the measurement error which would be present if two instruments were used. Thus, we would have a measured data point (ΔP):

$$\Delta P = (C_{P_S} - C_{P_W}) \rho q \quad \text{where} \quad \Delta P = P_S - P_W$$

C_{P_S} and C_{P_W} are known from calibration data so that only q is unknown. A numerical value for q generated by the above relation is then used in the relation:

$$q = \frac{\rho V^2}{2}$$

This provides a density profile determination which is dependent upon knowledge of only q and velocity. Velocity will be obtained from the ESP accelerometer output. However, use of these two instruments, both of which are mounted on the Aeroshell would preclude taking pressure measurements below the Aeroshell separation altitude.

The third region for location of a transducer is the CB base region. This transducer would be mounted on the aft end of the ESP with direct access to the CB base region. This instrument would remain with the CB throughout the entry.

Compatibility with input voltage levels of the Power Subsystem dictates selection of either a 28.5 ± 5 vdc or $5.00 \pm .05$ vdc power level while compatibility with the Telemetry Subsystem requires selection of a 0 to 5 vdc, single-ended output, a 0 to 40 mvdc double-ended output; or a digital output.

3.1.1.4 Selection - The selected approach is two diaphragm capacitance pressure transducers, one located in the stagnation region and the other located in the base region. This arrangement provides coverage over the entire profile with the additional advantage of taking pressure data on the surface of Mars prior to terminating ESP operations.

It is considered desirable to include additional transducers at the sphere-cone tangency point to sense stagnation/wall differential pressure. These transducers would provide data for density profile determination independent of free-stream pressure, and provide backup transducers for the one in the stagnation region.

3.1.2 Direct Density Measurements - One of the most important atmospheric properties is the density and its variation with altitude. It is valuable to the VOYAGER program to incorporate an instrument which will directly measure the density and be independent of results calculated from pressure, temperature, composition and accelerometer results. The preferred instrumentation is a gamma backscattering densitometer.

3.1.2.1 Constraints - The most difficult problem with a direct density measurement is that, during a supersonic entry, a shock wave is built up around the vehicle and there is no direct contact between the vehicle and a sample of the

atmosphere with free stream properties.

3.1.2.2 Alternatives - Instrumentation studies have shown that the use of radiation is a powerful technique for density determination. The types of radiation that could be used are alpha and beta particle radiation, and X-ray or gamma radiation.

3.1.2.3 Comparison - Particle radiation (alpha or beta) is not useful since it is easily stopped. This leaves X-rays or gamma radiation. A conventional X-ray tube requires large amounts of weight and power, and when it is used continuously some means of cooling must be provided. The use of a radioisotope source is therefore indicated. Since high energy gamma radiation requires heavy shielding, a low energy source would be more suitable.

3.1.2.4 Selection - A gamma backscattering densitometer is the only means of obtaining a direct free stream density measurement during supersonic entry. An instrument of this type has been designed by Giannini Controls Corporation for NASA (Contract Number NAS1-5341) and has performed well on upper atmosphere flight tests.

A schematic representation of this instrument is given in Figure 3.1.2-1. A collimated gamma source directs radiation through the heat shield. A collimated detector is arranged so that its cone of acceptance intersects the cone of gamma radiation beyond the shock wave. There are no special windows in the heat shield required for either source or detector. Since the heat shield will scatter as much as 40 percent of the gamma rays out of the beam, it is necessary to continuously monitor the heat shield thickness.

Source - The source used is Gadolinium - 153 (Gd^{153}) which has an average gamma energy of 100 Kev. The source strength is 490 curies. It is mounted on a tantalum collimator and is covered with an ablator to protect it in case of a fireball accident on the launch pad.

Main Detector System - A functional block diagram of the main detector system is given in Figure 3.1.2-2. A tellurium doped sodium iodide scintillation crystal is optically coupled to a photomultiplier tube, whose output pulses are proportional to the energy of the detected gamma rays. The photomultiplier tube used by Giannini is a ruggedized design built to withstand sterilization and a high operating temperature (150°C). The output pulses are amplified and fed into a discriminator which rejects all the pulses outside the energy range of the back-scattered gamma rays (70-80 Kev). These pulses are then integrated, giving a 0-5 vdc analog signal which is proportional to the intensity of the gamma rays detected.

GAMMA BACKSCATTERING DENSITOMETER SCHEMATIC REPRESENTATION

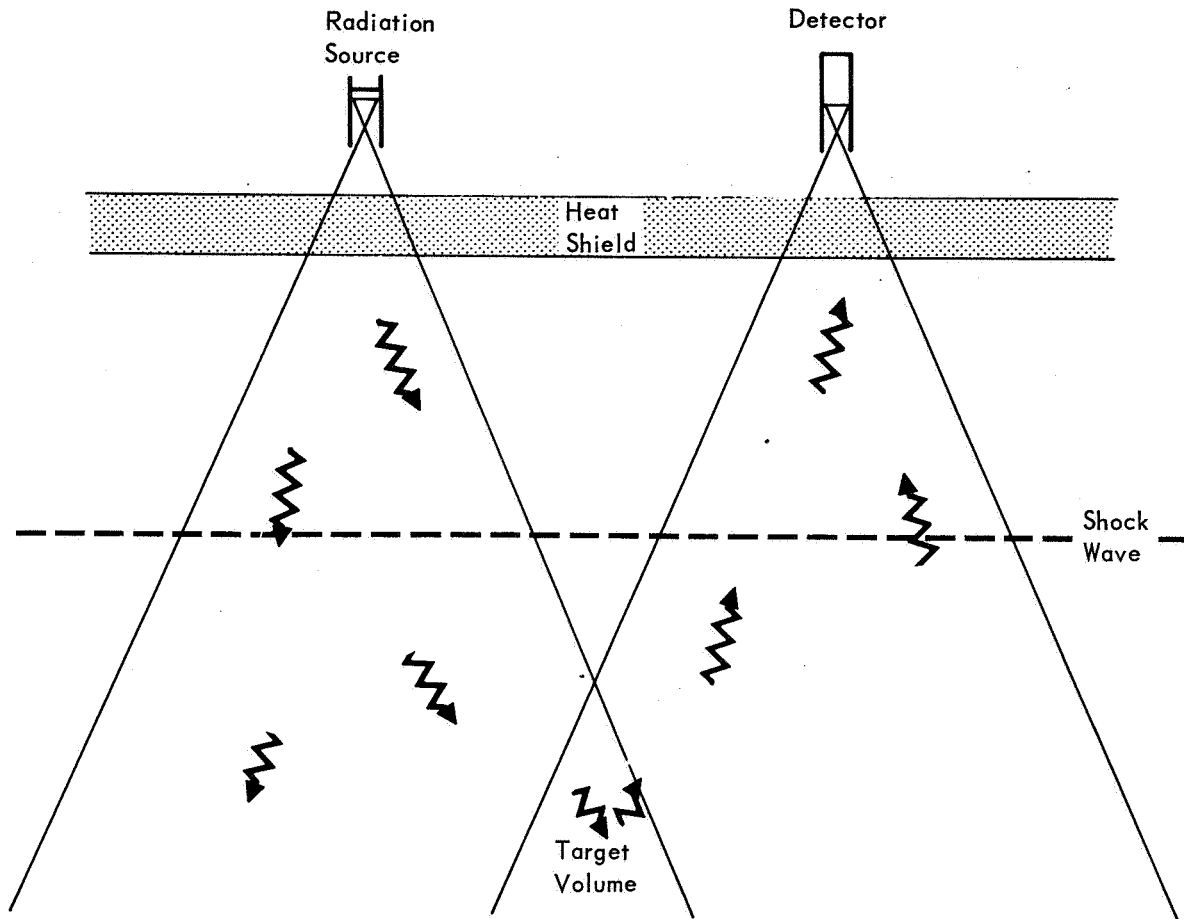


Figure 3.1.2-1

**GAMMA BACKSCATTERING DENSITOMETER
MAIN DETECTOR SYSTEM BLOCK DIAGRAM**

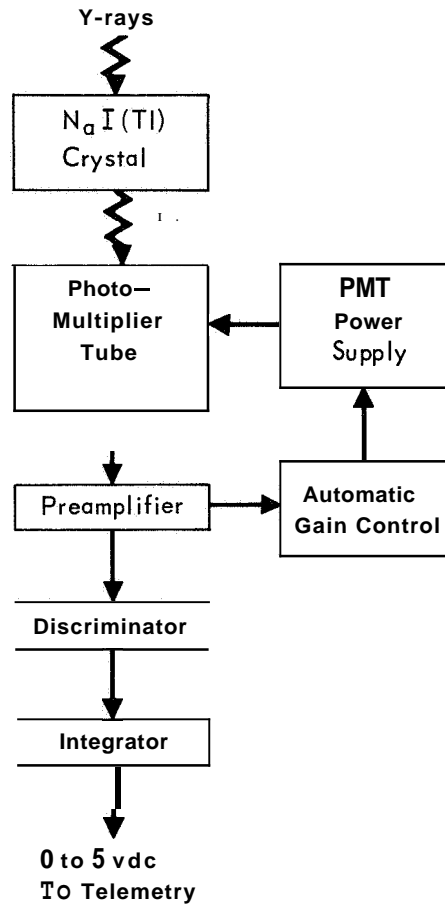


Figure 3.1.2-2

An automatic gain control circuit controls the photomultiplier tube power supply. It uses a small Cesium-137 (Cs137) gamma source (662 Kev) located next to the scintillation crystal for a calibration point.

Ablation Gage System - Gamma backscattering can also be used to monitor the heat shield thickness. A functional block diagram of the ablation gage system is given in Figure 3.1.2-3. A collimated proportional counter is placed next to the main source. Its output is handled in the same manner as the main detection system and the output is a 0-5 Vdc analog signal. A separate Americium-241 (Am^{241}) source is used for the ablation gage near the main detector.

Power Supply - The instrument contains its own regulated power supply. It requires 5 watts at 28.5 ± 5 vdc.

Physical Characteristics - The overall configuration is shown in Figure 3.1.2-4. There are two units, one with the main sources and the passive ablation sensor, and the other with the main detector, active ablation sensor and the remaining electronics. The characteristics are tabulated in Figure 3.1.2-5.

Performance Objectives - In the worst postulated VM model atmosphere the gamma backscattering densitometer should give the density at 100 K ft. to within 10% and to within 5% at the surface of the planet.

Interface Definition - An interface block diagram is given in Figure 3.1.2-6. The instrument requires 5 watts of power from the 28.5 ± 5 vdc power supply. The telemetry subsystem reads the three analog signals once per second from the start of the entry. These go to seven bit analog to digital converters and are telemetered. Since the maximum operating time is 700 sec, the maximum required bit capacity is 14,700 bits.

Reliability and Safety Consideration - The gamma backscattering densitometer offers redundancy for the other entry atmospheric properties experiments. In case of failure of one or both of the ablation gages, the accuracy before separation of the heat shield would be degraded. A failure of the main detector system would result in a complete failure.

Although radiation safety is not a serious problem due to the low energy of the gamma rays, some simple precautions must be taken. The Cs^{137} source, which is 0.1 microcuries, poses no health hazard. The 100 millicurie Am^{241} source is mounted in a capsule. A temporary tantalum shield is used over the collimator during assembly. The main Gd^{153} source requires a 1 cm thick tantalum shield over the collimator during assembly and a 1.5 cm thick lead shield over the part of the heat shield which is adjacent to the main source prior to launch.

**GAMMA BACKSCATTERING DENSITOMETER
ABLATION GAGE BLOCK DIAGRAM**

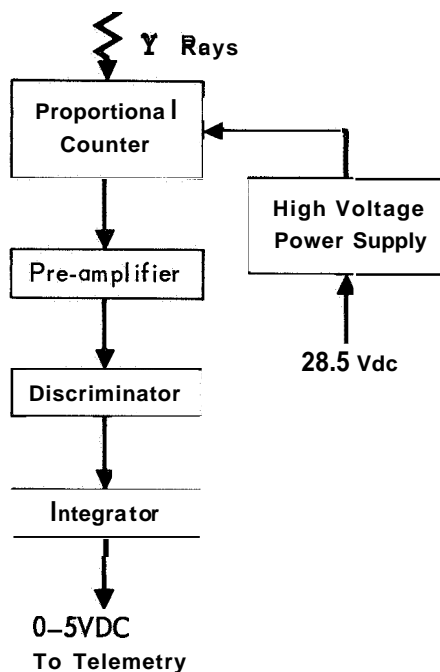


Figure 3.1.2-3

GAMMA BACKSCATTERING DENSITOMETER CONFIGURATION

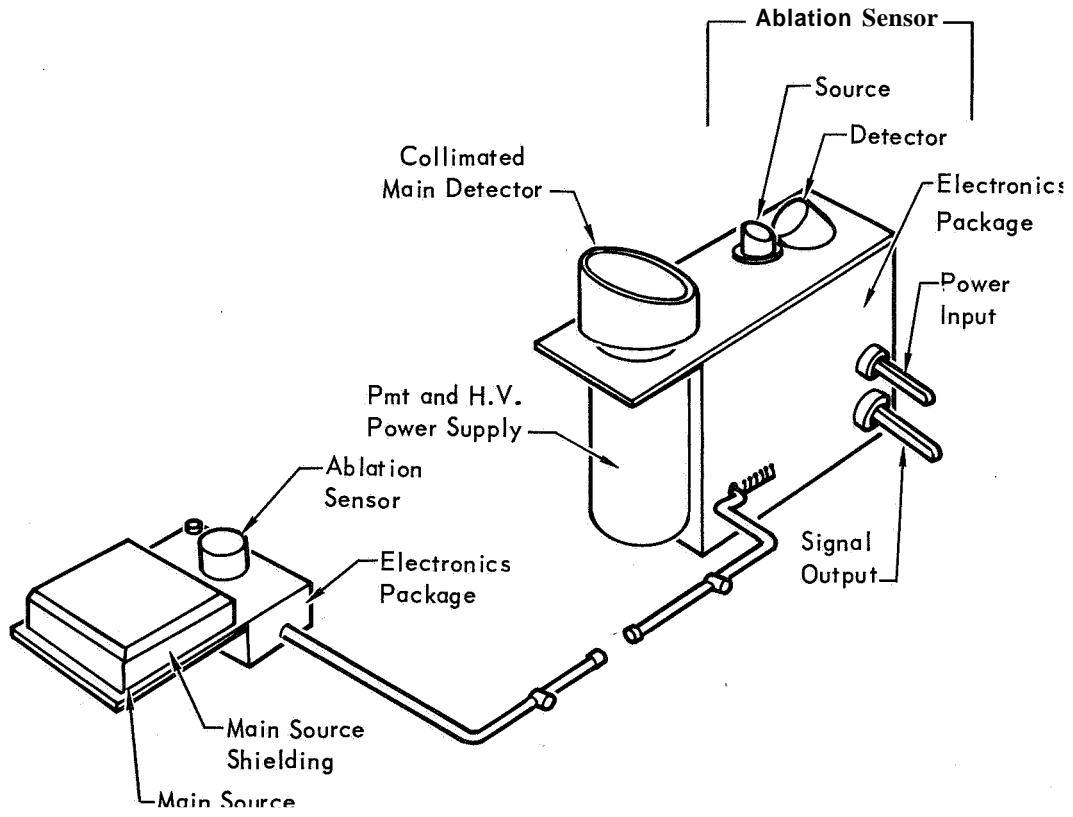


Figure 3.1.2-4

GAMMA BACKSCATTERING DENSITOMETER INTERFACE BLOCK DIAGRAM

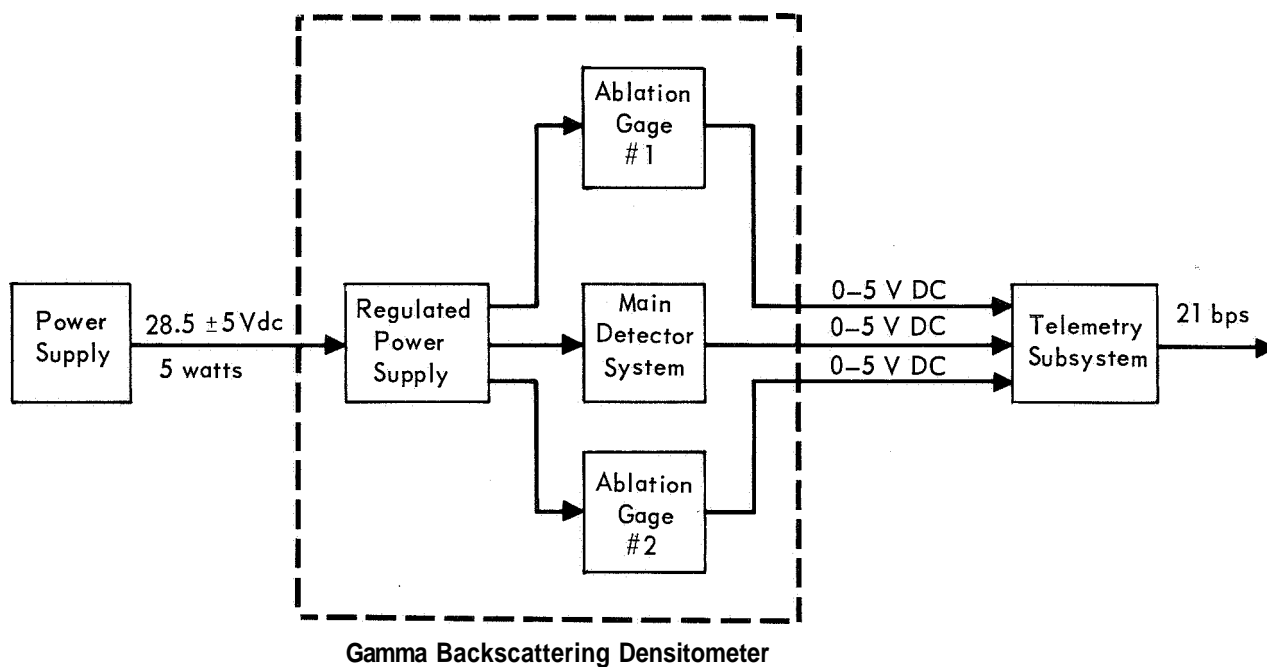


Figure 3.1.2-6

Test Requirements - The following preflight calibration tests must be performed.

- o Obtain count rate versus density relationship with and without heat shield in a vacuum chamber.
- o Repeat with varying thickness of heat shield with ablation gages in place.
- o By means of heavy shielding, measure all direct transmission between the three sources and the three detectors.
- o Using the complete density sensor, measure the multiple scattering effects within the heat shield and shock wave as a function of atmospheric pressure using a simulated shock, vacuum chamber and multilayer heat shield.

Development Requirements - This instrument is very close to present state-of-the-art capabilities. Normal development should produce an instrument with the desired accuracy for the size, weight and power required.

3.1.3 Temperature - Temperature is one of the quantities needed to reconstruct the atmospheric profile. Measurements will be made from an altitude corresponding to Mach 5.0 until ESP operations are terminated some 120 seconds or more after touchdown. Figure 3.1.3-1 presents typical stagnation temperature profiles and Figure 3.1.3-2 presents typical free-stream temperature profiles for a nominal entry into the Martian atmosphere. Total temperature measurement at both the stagnation point and the base region is the selected approach.

3.1.3.1 Constraints - Selection of the temperature measurement technique to achieve the objective listed above is constrained by the following:

- o The sensing elements must be protected from the peak heating loads encountered prior to Mach 5.0 operation.
- o Ablation products must not inhibit flow through the sensor when the valve is opened at Mach 5.0.
- o The CB design excursion allowances on angles of attack must be accommodated without performance degradation.
- o The response time of the instrument must be short enough to permit temperature profile tracking.
- o Access to the atmosphere at a point where the sensed temperature can be related to the free-stream temperature is required.
- o Measurements are required both before and after Aeroshell separation.
- o Interfacing subsystem requirements must be satisfied.
- o The maximum stagnation region temperature is 4500°K (VM-9).

3.1.3.2 Alternatives - The total temperature measurement approach is the method employed for obtaining the desired data. The location of the instruments is the prime consideration. Candidate locations are: the stagnation region, the wall region, the base region, and combinations of these locations.

The total temperature sensor can be designed to tolerate heat loads over the entire profile. However, other considerations may indicate designs which do not have to tolerate such temperature extremes. The sensor flow can be unrestricted during the entire entry resulting in high temperature design requirements, or flow can be inhibited during peak heat portions of the entry to reduce the thermal design requirements.

3.1.3.3 Comparison - Location of the sensor at the stagnation region normal to the pitch-yaw plane permits the flow at zero angle-of-attack to enter the probe directly, and allows the port to be flush with the Aeroshell mold line.

A second possibility for location is on the wall of the aeroshell near the

STAGNATION TEMPERATURE PROFILES

$h_E = 760,000 \text{ ft}$
 $V_E = 15,000 \text{ ft/sec}$
 $\gamma_E = -20 \text{ deg}$
 $M/C_D A = 0.30 \text{ slugs/ft}^2$

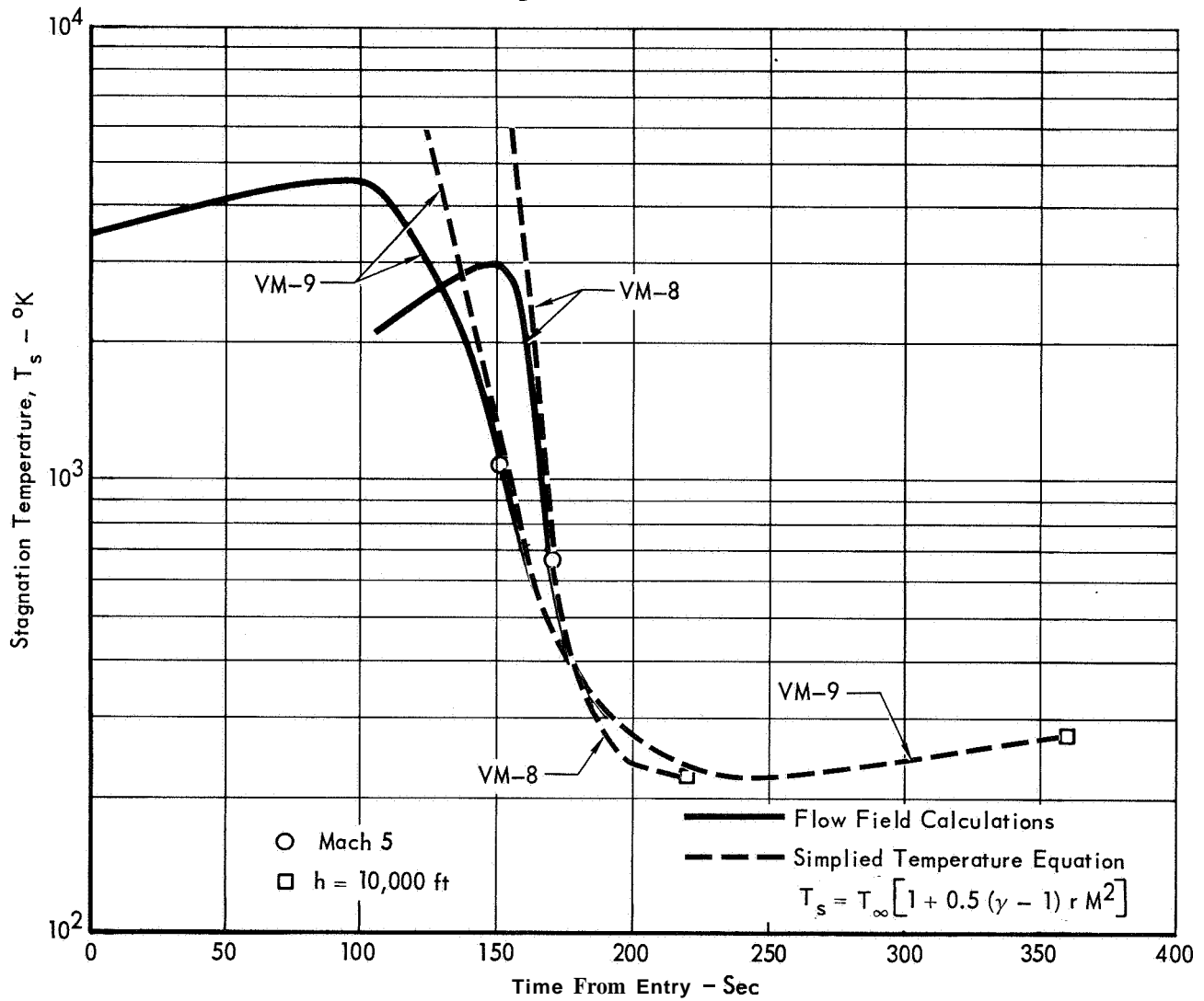


Figure 3.1.3-1

FREE STREAM TEMPERATURE PROFILES

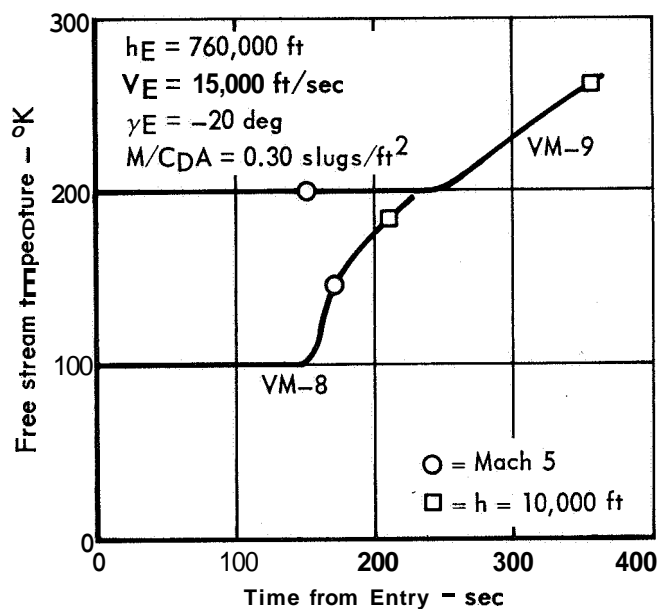


Figure 3.1.3-2

sphere/cone tangency point. Location at this point requires a protruding assembly since flow is more nearly parallel to the aeroshell contour than perpendicular to it. A further disadvantage to this location is that the angle-of-attack excursions coupled with the roll rates will provide gas flow directional changes which are extremely hard to accommodate.

The third location possibility is in the base region of the CB. Location of a sensor here provides one immediately obvious advantage over the other two possibilities: the transducer will be with the ESP throughout its operation rather than being separated with the Aeroshell as will the other two. However, the problems associated with obtaining non-ambiguous data in the base region are numerous. Flow field considerations are much more complex in the base region. Other factors which must be evaluated for use of a temperature transducer located in the base region include:

- o Thermal propulsion effects
- o Parachute effects
- o Flow velocity must be determined for both the CB entry and terminal descent configurations

Temperatures at the stagnation region can approach 4500°K as shown in Figure 3.1.3-1. Design of a temperature transducer that can tolerate these temperatures would require protective coatings for the sensing elements. Any coating on the element serves to increase the response time and for some cases the response time would possibly be increased beyond desirable limits.

3.1.3.4 Selection - The preferred approach is two total temperature probes - one located at the stagnation region and the other located in the base region. Flow through the stagnation point probe will be restricted during the peak heating period. This arrangement provides coverage over the entire entry profile with the additional advantage of making temperature measurements on the surface of Mars, prior to ESP operation termination, by using the base region temperature sensor.

3.1.4 Composition Determination by Mass Spectrometer - The purpose of the ESP composition measurement is to determine atmospheric constituents from an altitude corresponding to Mach 5.0 until ESP operations are terminated a nominal 120 seconds after touchdown. The preferred approach is to use a mass spectrometer obtaining samples from the stagnation region.

3.1.4.1 Constraints - The selection of the instrument for making atmospheric composition measurements is limited to a quadrupole or magnetic sector mass spectrometer. In addition, the atmosphere samples must not be contaminated by heat shield ablation

products.

3.1.4.2 Alternatives - The alternatives for this experiment include alternatives in type of instrument and sampling technique. The mass spectrometer instrument alternatives include the following:

- o quadrupole
- o double - focusing magnetic
- o single - focusing magnetic

The sampling alternatives include:

- o base region sampling port
- o stagnation region sampling port
- o wall region sampling port

17

3.1.4.3 Comparison - The quadrupole and double-focusing magnetic sector instruments have approximately the same weight, power, and size characteristics. The single-focusing magnetic deflection instrument if designed to measure only four or five species, would be significantly lighter and smaller and would require less data transmission. It would, however, be able to measure only the major constituents of the atmosphere.

All of the various types of mass spectrometers offer their own advantages and some have disadvantages which preclude their selection for the Voyager mission. The monopole mass spectrometer for example, is mechanically simpler than the magnetic deflection and quadrupole types and is inherently more rugged. However, the monopole mass filter is a weak-focusing instrument and gives poorer results at the low mass numbers of interest for this atmospheric analysis. The time-of-flight mass spectrometer is mechanically the simplest of all, and unlike the others, has no critical alignment requirements. However, the time-of-flight instrument requires precise timing circuits, the stability of which, for a many-month mission, would be difficult to maintain reliably. Since one of the possible significant constituents of the Martian atmosphere is Argon, all of the instruments share a common problem which is the low pumping capacity of small getter-ion pumps for the noble gases.

Of the various sampling alternatives the stagnation region sampling port in the non-ablative section of the heat shield can most easily meet the requirement of obtaining atmospheric samples uncontaminated by ablation products.

3.1.4.4 Selection - The ESP composition measurement experiment is one in which considerable current development is taking place, and the optimum instrumentation

is not obvious from among the several possible approaches. The quadrupole instrument, represents a conservative choice.

The quadrupole mass spectrometer is a strong focusing type of instrument. It can be designed such that nearly all of the ions of a given mass will pass through the quadrupole filter for a specific range of voltages applied to the electrodes. The quadrupole mass spectrometer can be operated in a continuous sweep or scan mode where it is necessary to sweep the applied voltages and to mark the times corresponding to passage of each mass. It also can be operated in a stepped mode where the applied voltages are stepped in increments corresponding to changes of 1 atomic mass unit. There are no stringent stability or precision requirements on the voltage steps and, because the voltages are stepped the detector current and applied voltages correlation is somewhat simplified for this mode of instrument operation. However, due to time requirements for transient damping it may not be possible to scan the entire mass range of 10 to 60 in 2 seconds in the stepping mode. For the present the quadrupole is assumed to be operated in a continuous scan mode.

The stagnation temperature sensor outlet tube maintains a continuous stream of atmospheric gas flowing from the stagnation point to the base region from Mach 5.0 to Aeroshell separation. Routing of this tube past the mass spectrometer eliminates the need for a separate port and tube for mass spectrometer sampling. By using a separation technique that insures continuous gas flow through the tube after Aeroshell separation, the tube can continue to provide fresh gas samples all the way to touchdown. The relatively large stagnation temperature outlet tube volume and the small pumping capacity of the mass spectrometer ion pump requires that the mass spectrometer inlet be switched to a smaller capillary tube to insure that fresh atmosphere samples are obtained during the short operational period after touchdown. Use of a ceramic nose cap prevents ablation product gases from entering the stagnation region sampling ports throughout the entire entry and descent operations. The option for separate ports for stagnation temperature and pressure sensors and for mass spectrometer sampling free from ablation product interference is thus available for all possible desired stagnation region sampling schemes.

3.1.5 Composition Determination by Absorption Methods - No single technique completely provides atmospheric composition data over a total entry profile as each method is beset with its own limitations. For example, the Argon pumping limitations may severely limit mass spectrometer operations. In this light it is useful to consider absorption spectroscopy as a supplement or alternate to the mass spect-

rometer technique already discussed. The equipment needed to perform the experiment outlined below weighs approximately 2 lbs. and requires less than 1.5 watts of electrical power. The total data output during entry and descent is 6240 bits.

Scientific Objectives and Approach - The scientific objectives of this experiment are:

Principal Objectives:

- o To determine the density and altitude distribution of CO_2 , O_3 , N_2 , and A in the Martian atmosphere.
- o To determine the solar flux of biologically significant ultraviolet radiation reaching the surface.

Additional Objectives:

- o To determine the atmospheric scattering properties (molecular and aerosol), and hence obtain information about the aerosol content and profile.
- o To measure the absolute solar flux at the top of the atmosphere and the atmospheric albedo.

Measurements of the attenuation of solar ultraviolet radiation in three wavelength bands and of solar x-rays in one band can satisfy these objectives. The four bands are chosen so as to permit the maximum of information about the atmosphere consistent with the simplicity of the experiment. The general idea is to measure the solar constant at the top of the Martian atmosphere in each band of interest, then measure the attenuation, if possible to extinction (occurs only in far UV and X-ray measurements, "extinction" being the threshold flux of the sensors), as the optical thickness of the atmosphere increases in the descent to the surface.

Two bands, 2200-3000 Å and 3000-4000 Å, furnish information on molecular density, aerosol content, and ozone, if present, in the atmosphere below 15-25 km. These bands may also detect high altitude aerosol layers. The other two bands, 2-8 Å and 1050-1350 Å (or 1225-1350 Å, or 1425-1480 Å), furnish information on CO_2 number density and total number density in the upper atmosphere.

Upper Atmosphere Measurements: 1050-1350 Å and 2-8 Å Bands - Two model atmospheres VM-7 and VM-8 are considered for purposes of discussion. These were chosen since they represent probable extremes in terms of atmospheric composition and scale height. Both models assume a surface pressure of 5 mb. VM-7 assumes a composition of 20% CO_2 and 80% N_2 with a mean scale height of 14.2 km; VM-8 assumes 100% CO_2 with a scale height of 5 km. VM-8 is therefore considerably closer to current

estimates than is VM-7.

Absorption in the 1050-1350 Å Band - The intensity of radiation is given by

$$\log \frac{I}{I_0} = - \int_0^L \sum_i \sigma_i n_i dx \quad (1)$$

and if σ is independent of path length

$$\log \frac{I}{I_0} = - \sum_i \sigma_i N_i \quad (2)$$

where L = path length, I = intensity of radiation at $x = L$, I_0 = intensity of radiation at $x = 0$, σ = absorption cross section (cm^2), n = number density of molecules (cm^{-3}), and N = number of molecules per unit column (cm^{-2}).

The intensity of solar radiation at altitude z in a planetary atmosphere is given by

$$\log \frac{I}{I_0} = - \int_z^\infty \sum_i \sigma_i n_i dz' \quad (3)$$

and for an isothermal atmosphere this reduces to

$$\log \frac{I}{I_0} = - H \sum_i \sigma_i n_{0i} e^{-z/H} \quad (4)$$

where H is the scale height.

Almost all absorption in the 1050-1350 Å band atmosphere will be by CO_2 . The absorption cross section for CO_2 at 1216 Å is about $7 \times 10^{-20} \text{ cm}^2$ (Reference 1) and this, combined with its number density, provides a total absorption which is orders of magnitude larger than that of any other possible atmospheric constituent. The number of molecules of CO_2 per unit column, calculated from equation 1, that will absorb 10%, 50%, and 90% of the incident solar radiation is:

Percent Absorption	$N (\text{cm}^{-2})$
10	1.5×10^{18}
50	9.9×10^{18}
90	33×10^{18}

The altitude at which N molecules- cm^{-2} will be between the sensor and the Sun depends on the atmospheric structure and on the zenith angle, θ . For zenith angles up to about 75° , N varies as approximately $\sec \theta$. For larger zenith angles

sec θ must be replaced by the Chapman function.

Equations (2) and (4) are derived on the assumption that σ is independent of path length (e.g. pressure). This is a good assumption for the Martian atmosphere because σ is independent of pressure over the entire pressure range (2.7 x 10⁻³ to 133 mb) investigated in Reference 1.

The absorption cross section, σ , and the solar constant are functions of wavelength. However because the solar Lyman- α line contributes most of the energy in the band of interest, σ at 1216 Å serves as a satisfactory approximation. In general, the spectral variation of the solar constant, and the detector efficiency can be taken into account by

$$\sum_{\lambda} I_{\lambda} \Delta\lambda = \sum \epsilon_{\lambda} I_{o_{\lambda}} e^{-\sigma_{\lambda} \int_0^L n(x) dx} \Delta\lambda \quad (5)$$

where ϵ_{λ} = detection efficiency at wavelength λ , $I_{o_{\lambda}}$ = solar constant in wavelength interval $\Delta\lambda$, and $\int_0^L n(x) dx = N$, the number of molecules per cm² between the detector and the Sun.

Absorption in the 2-8 Å Band - The absorption of X-rays is given by:

$$\log \frac{I_x}{I_o} = - \frac{1}{N'} \int_0^L \sum_i \mu_i n_i A_i dz \quad (6)$$

where I_x = intensity of radiation at $z = L$, I_o = intensity of radiation at $z = 0$, L = path length, μ = mass absorption coefficient, n = number of atoms per cm³, A = atomic weight, and N' = Avogadro's number.

If the gas is of uniform composition (complete mixing), (6) can be written

$$\log \frac{I_x}{I_o} = - \bar{\mu} \int_0^L \rho(z) dz \quad (7)$$

where $\bar{\mu} = \frac{\sum \mu_i f_i A_i}{\sum f_i A_i}$, $\rho(z)$ = density in g-cm⁻³ = $\frac{1}{N} \sum n_i A_i$, and f_i = fraction of total number of atoms.

Absorption of solar X-rays in a planetary atmosphere is given by (again, assuming complete mixing)

$$\log \frac{I_x}{I_o} = - \bar{\mu} \int \rho(z) dz = \sum \int \rho_k(z) dz \quad (8)$$

and for an isothermal atmosphere

$$\log \frac{I_x}{I_{0x}} = - \bar{\mu} H \rho_0 e^{-z/H} \quad (9)$$

The actual situation is not quite as simple as outlined because of the variability of the parameters involved in the 2-8 Å range. The mass absorption coefficients of the atomic species concerned vary by about two orders of magnitude; the number of solar photons of a given energy varies by a few too many orders of magnitude depending on the temperature of the emitting regions; and the efficiency of the detector depends upon wavelength. Hence, the actual number of photons transmitted a given distance through a single atomic species is given by

$$\sum_{\lambda} I_{\lambda} \Delta\lambda = \sum_{\lambda} \epsilon_{\lambda} I_{0\lambda} e^{-\mu_{\lambda} \int_0^L \rho(x) dx} \Delta\lambda \quad (10)$$

where ϵ_{λ} = efficiency of detector at wavelength λ , $I_{0\lambda}$ = number of photons per wavelength interval at $x = 0$, and $\Delta\lambda$ = wavelength interval, This equation must be summed over all atomic species.

For purposes of illustration we may take μ at 5.5 Å as representative and assume $I_{0\lambda}$ to be constant.

With these simplifying assumptions, we determine the number of molecules per unit column required for 10%, 50%, and 90% absorption of X-rays in a pure CO₂; and 80% CO₂ 20% N₂; a 50% CO₂ 50% N₂; and a 20% CO₂ 80% N₂ atmosphere. The results are:

NUMBER OF MOLECULES

Percent Absorption	100% CO ₂	80% CO ₂ 20% N ₂	50% CO ₂ 50% N ₂	20% CO ₂ 80% N ₂
10	3.5 x 10 ¹⁸	4.1 x 10 ¹⁸	4.9 x 10 ¹⁸	6.0 x 10 ¹⁸
50	2.3 x 10 ¹⁹	2.7 x 10 ¹⁹	3.2 x 10 ¹⁹	4.0 x 10 ¹⁹
90	7.7 x 10 ¹⁹	9.0 x 10 ¹⁹	1.1 x 10 ²⁰	1.3 x 10 ²⁰

Altitude Range of Measurement - The altitude range of measurement depends upon the surface pressure; it is shifted upward for a given atmospheric structure as surface pressure is increased. In addition, differences in composition, e.g. an increase of N₂, result in an upward shift of the X-ray measurement range with respect to the 1050-1350 Å measurement range. The altitudes at which 10% and 90% absorption occur for the VM-7 and VM-8 atmospheres, and for zenith angle $\theta = 0$ are:

Percent Absorption	<u>VM7</u>	<u>VM8</u>
x-Ray 10	148 km	60 km
90	104 km	45 km
Lyman- α 10	104 km	65 km
90	73 km	49 km

The principal difference between the two atmospheres is in their different scale heights (5 km in the VM8 and 14.2 km mean, 10 km for CO₂, in the VM-7). This is partially offset for the 1050-1350 Å absorption by the smaller amount of CO₂ in the VM7 atmosphere.

The effect of a non-zero zenith angle for the Sun on the altitude at which absorption is a given value is easily evaluated. This effect is given, for an isothermal atmosphere, by

$$z_e - z_v = H \log (\sec \theta) \quad (11)$$

where z_θ = altitude for $\theta = \theta$, and z_v = altitude for $\theta = 0$.

Hence, even for a zenith angle of 75°, the altitude for a given absorption is shifted upward only about 0.6 H or 3 km for the VM8 and 6-8 km for the VM-7 atmosphere.

Data Analysis - This section outlines the analysis of data following the step where the data have been reduced to give percentage absorption vs altitude.

1050-1350 Å - CO₂ is almost certainly the dominant absorber of 1050-1350 Å radiation in the Martian atmosphere. Hence, each data point giving the amount of absorption at a given altitude can be used to calculate directly the number of molecules of CO₂ per unit column between the detector and the Sun by means of equation (5). Two or more data points enable the scale height of CO₂ at these altitudes to be calculated.

2-8 Å - For illustrative purposes, the simplified equation (8) is used here rather than the exact equation (10).

Equation (8), for X-ray absorption, can be written as

$$\log \frac{I_x}{I_{0x}} = -\frac{1}{N'} \sum_k \mu_k N_k A_k$$

where N' = Avogadro's number, A_k = atomic weight, and N_k = number of atoms per unit column of species k . Measurements in the 1050-1350 Å band will give N_C and N_O .

If substitution of these values and the observed X-ray attenuation into the above equation produces equality between both sides, then the atmosphere must be composed

almost entirely of CO_2 . If equality is not obtained, then one or more additional gases are present in appreciable amounts, most probably N_2 and/or A. In this case, substitution of N_C and N_O into the above equation will permit calculation of the sum of the N_2 and A contributions, i.e.,

$$C = \mu_N A_N N_N + \mu_A A_A N_A \quad (12)$$

If, in addition, the total atmospheric density, or mass per unit column (m), is measured independently

$$m = \frac{1}{N_O} (N_C A_C + N_O A_O + N_N A_N + N_A A_A) \quad (13)$$

will be known. Equations (12) and (13) can then be solved for the two unknowns, N_N and N_A , hence determining the numbers of N_2 and A present in the atmosphere at that altitude. Measurements at two or more altitudes permit the scale heights of N_2 and A to be determined.

Possible Substitute Bands for 1050-1350 Å - The type of ablator used for an entry probe may affect the 1050-1350 Å measurements. If the ablator contains an appreciable amount of organic material, atomic hydrogen can be emitted and this will resonantly scatter the solar Lyman- α . For this case, the use of one of two possible substitute bands is desirable. These are: 1225-1350 Å and 1425-1480 Å. The 1225-1350 Å detector is similar to the 1050-1350 Å detector except that a CaF_2 window is used instead of a LiF window for the low wavelength cutoff. The 1425-1480 Å detector is an ion chamber with a sapphire window. The absorption cross section of CO_2 in both the 1225-1350 Å band and the 1425-1480 Å band is about $7 \times 10^{-19} \text{ cm}^2$, or an order or magnitude greater than at the Lyman- α wavelength. For an exponential atmosphere, the altitude z at which absorption is a given percentage is given by

$$z = z_{1216} + 2.3H$$

where z_{1216} = altitude at which Lyman- α absorption is the given percentage.

Hence, all altitudes for CO_2 absorption in the VM-7 atmosphere must be increased by about 23 km and all altitudes in the VM-8 by about 12 km.

The 1425-1480 Å region is a continuum region of solar radiation, and the CO_2 absorption cross section is about the same throughout the region. This simplifies the data analysis; however, the 1225-1350 Å region is one of prominent solar emission lines, the strongest being the O I triplet at 1302.2, 1304.9, and 1306.0 Å and the C II doublet at 1334.5 and 1335.7 Å. In addition, the CO_2 absorption cross section is quite variable in this spectral region. This complicates the data analysis.

There is one final consideration. Fjelbdo et al. (Reference 2) believe that OI may be a major constituent of the Martian atmosphere above about 70 km. The absorption cross section of OI at the OI triplet resonance is about $3 \times 10^{-13} \text{ cm}^2$ (Reference 3). If the temperature of the OI is 100 °K at Fjelbdo's estimate, then it will absorb strongly only at the center of the solar OI lines. A preliminary calculation indicates that although the amount of OI suggested by Fjelbdo et al. would completely absorb radiation at the line centers, absorption over the entire line widths would be less than 5% and hence, less than about 1% of the solar radiation in the entire 1225-1350 Å band. If, on a more detailed analysis, the OI absorption should prove to be measurable, it would provide at least a quantitative measurement of OI. At the same time, it would not compromise the CO₂ measurement because virtually all OI absorption would have occurred before measurable CO₂ absorption commenced.

Lower Atmosphere Measurements: 2200-3000 Å and 3000-4000 Å Bands - The same model atmospheres are considered as those for the upper atmosphere.

- ° 2200 to 3000 Å Band - In this region of the spectrum, the solar radiation is attenuated by: 1) , perhaps ozone absorption, 2) scattering by the molecular atmosphere; and 3) scattering by aerosol particles. These have been discussed in detail in References 4 and 5, and hence the phenomena will only be outlined here. The calculations show that with the Sun at the zenith, the attenuation due to molecular scattering is about 10%, the maximum due to ozone absorption is about 5%, and that due to aerosol scattering is about 15%. For a 70° solar zenith angle, these values change to 25%, 12%, and 40%, respectively. In addition, the scattered radiation comprises about 10% of the direct solar radiation at the planet's surface for the Sun at zenith, and about 50% for an 84° zenith angle. This wavelength band serves to determine the atmospheric ozone content, if large enough to be measurable, and combined with measurements in the 3000-4000 Å band, the molecular and aerosol scattering contributions. The atmospheric aerosol content can be determined once the aerosol scattering contribution is known (References 4 and 5). Additionally, this band serves to delineate the flux of biological importance which reaches the surface.
- ° 3000 to 4000 Å Band - In this band, attenuation is due almost entirely to molecular and aerosol scattering. Details are discussed in References 4 and 5. With the Sun at the zenith, the molecular scattering contribution should be about 3% and that of aerosols 12%. These figures roughly

double for a 70° solar zenith angle. This band, combined with the 2200-3000 Å band, serves to separate the molecular and aerosol scattering contributions to the attenuation.

- o Altitude Range of Measurement - In the 2200-3000 Å band, 10% attenuation will have occurred at a height of about 12-25 km depending upon the solar zenith angle. Therefore, unless there is some unforeseen strong, high-level absorber or scatterer, all data in this channel will be obtained below about 15-25 km. In the 3000-4000 Å 10% attenuation will have occurred at a height of about 14 km.

- o Data Analysis - Data analysis is detailed in References 4 and 5.

Experimental Approach - An important fact is that the hardware for this experiment already exists, and has a proven record of performance in rocket and satellite experiments since 1949.

- o Instrumentation - The experiment package consists of from five to twelve small sensors, (including solar aspect sensors if such are not already on board) and the associated electronics. The exact number of sensors required depends upon the particular mission constraints. If a complete or partial lock onto the Sun can be made during entry, such that the sensors see the Sun throughout the descent, only five sensors are required: one for each band and one solar aspect sensor. If the entry vehicle rotates at least 60 rpm, only five sensors are needed. Any spin rate less than 60 rpm requires additional sensors, at least ten (two in each band), to provide a sufficient amount of data. If there is no solar lock-on and no spin, a minimum of twelve sensors is required: two each in the X-ray and far W bands, three each in the middle and near UV, and two solar aspect sensors. The required equipment for the 12 sensor case is listed below:

<u>Item</u>	<u>Quantity</u>
Soft X-ray Geiger counter 2-8 Å	2
Far W ion chamber 1050-1350 Å	2
Middle UV diode phototube 2200-3000 Å	3
Near UV diode phototube 3000-4000 Å	3
Solar aspect sensor - visible	2

The viewing cone of the soft X-ray and far UV sensors is 2π steradians, for the middle UV and three of the near UV sensors, it is $\pi/2$ steradians, and for the solar aspect sensors it is 2π steradians.

The size, weight and power of the units, including their electronics, are :

<u>Unit</u>	<u>Size (in.)</u>	<u>Weight (oz)</u>	<u>Power (Watts)</u>
Soft X-ray (2)	3	6.4	.05
Far W (2)	2.4	3	0.002
Middle W (3)	3	1.5	0.001
Near W (3)	3	1.5	0.001
Solar Aspect sensors (2)	10	4.	0.56
Electronics	12	<u>15.</u>	0.8
		31.4 Oz.	

All of the above equipment can meet sterilization requirements. The operating temperatures are all less than 50°C.

All sensors are chosen and provided with appropriate amplification to cover their range of measurement adequately. A conservative minimum current of 10^{-11} amperes is established for all the W sensors, with maximum current capability to 10^{-7} being available; small currents can be measured. Each sensor differs in its quantum efficiency. The Geiger counter measures 1 to 10^4 photons/sec (efficiency is 100%), therefore 1 to 10^4 counts/sec. All sensors can be placed independently of their associated electronics, however, the following pointing constraints apply:

- a. At least one of each type of sensor must be placed to have the Sun in view at the time of entry. If the vehicle rolls sensors must be pointed with zenith angles which allow continuous measurement during descent.
- b. The pairs of far UV, X-ray and solar aspect sensors must be placed back to back to establish a viewing cone of 4π steradians for each band as a pair.
- c. The three middle and three near W sensors, having a zenith angle the same as the Sun, must be separated by 120° in the horizontal plane from each other, one reference sensor of each group of three being aligned with the viewing cone axis of one reference solar aspect sensor.
- o All sensors are highly rugged ceramic-metal photosensitive tubes with a proven history in previous rocket and satellite flights. The soft X-ray sensor is a Geiger counter with a 0.005" beryllium window, trans-

mitting the 2–8 Å band, responding to single photons by ion–pair production in the fill gas. It measures the attenuation of solar flux in this band from all atmospheric constituents. The far UV sensor is an ion chamber responding to Lyman- α (1215.7 Å) as the principal solar flux in its passband (1050–1350 Å). It measures solar flux attenuation due to atmospheric CO₂. The middle UV sensor is a solar blind rubidium telluride diode phototube with a vycor window, responding to solar flux in the 2200–3000 Å band. Attenuation in this band is due to O₃ absorption and molecular and aerosol scattering. The near UV Sensor is an extended response solar blind cesium telluride diode phototube with a pyrex window, responding to solar flux in the 3000–4000 Å band. It measures solar flux attenuation due to molecular and aerosol scattering.

- o Control and Data Time Histories - The commands required for instrument operation are simply turn-on after separation and turn-off after touchdown. The total data output is 6240 bits, with a breakdown as follows .
- o Solar Calibration Data - (Prior to entry)
 - (5 samples) x (12 sensors) x (8 bits/sensor) = 480 bits
- o Entry Measurements Data
 - (60 samples) x (12 sensors) x (8 bits/sensor) = 5760 bits
- o All sensors are scanned as closely together as possible during each sampling.
- o Sample Requirements - The prime objective should be to minimize contamination of the atmosphere by either retrorocket or ablator materials during the measurement period.
- o Viewing Requirements - All sensors must have an unobstructed view of the Sun within their viewing cone. Since they are all mounted on their appropriate support structure, placement or integration of the package should be such as to achieve this requirement and this should be regarded as of prime importance to the success of the experiment.
- o Test, Checkout and Development Requirements
 - a. Design/Development Sequence - The sequence is (1) a prototype package is fabricated for optimization of all electrical performance objectives, (2) a simulated environmental test is made to establish accuracy of measurement with change of irradiation source angle, and (3) a final design package is fabricated and tested.

- b. Flight Testing - All hardware to be used on flight vehicles would be subjected to a qualification test. Prior to installation, each unit is checked for functional operation and calibrated.
- c. Integrated System Test - After installation, a pre-sterilization and post-sterilization checkout are made to verify no degradation of performance.
- d. Pre-Launch Test - All electrical circuits are checked.
- e. Post-Launch Monitoring and Pre-Separation Tests - A schedule of monitoring is not required. Checkout of circuits prior to separation will be made to verify operation.
- o Constraints on Capsule Design - No special constraint is imposed other than that the sensors receive a minimum of solar electromagnetic radiation during interplanetary travel.
- o Error Analysis - Proper treatment of this subject requires first the analysis of contamination of the atmosphere from retrorocket and ablator gases. In general, a high accuracy of relative measurements to about 1% is possible. Accuracy of absolute measurements can be expected to be around 20-30%. The 1050-1350 Å band appears most sensitive to ablative contamination (Reference 6) primarily because of the presence of atomic hydrogen in the gas envelope. Measurements here can be conducted in the 1225-1350 Å or 1425-1480 Å regions without an appreciable sacrifice in performance. As an example of how each sensor was affected by gas envelope absorption and emission during entry for the NASA Ames high velocity entry probe, the following results are given:

<u>Spectral Band</u>	<u>Viewing Cone</u>	<u>Absorption</u>	<u>Emission</u>
2-8 Å	100°	unaffected	unaffected
1050-1350 Å	100°	atomic hydrogen from ablator can seriously degrade measurement due to resonance absorption of solar Lyman-α. Band can be shifted to 1425-1480 Å to avoid problem	unaffected in VM8, degraded in VM7 atmosphere due to H, O, N, C, Si emission. Band can be shifted to 1425-1480 Å to avoid problem.
2200-3000 Å	60°	unaffected in altitude range of interest	unaffected in altitude range of interest. Any uncertainty can be minimized by shifting

<u>Spectral Band</u>	<u>Viewing Cone</u>	<u>Absorption</u>	<u>Emission</u>
3300-4000 Å	60°	unaffected in altitude range of interest	bands to 2200-2700 Å, avoiding CO emission, or 2200-2400 Å, avoiding C and CO emission unaffected in altitude range of interest. Any uncertainty can be minimized by shifting band to 3550-3800 Å, avoiding CO and CN emission

The effect of retrorocket gases for the VOYAGER entry would have to be similarly assessed. Unless the source of contaminants can be modified to optimize measuring conditions for the experiments, the experiment can be adapted by appropriate ultraviolet band changes, for example, 1225-1350 Å, 1425-1480 Å, 2200-2400 Å and 3550 Å and 3550-3800 Å, thereby minimizing errors from contaminant absorption and emission. Likewise, there are a number of possible substitute X-ray bands available, such as 8-20 Å and 44-60 Å. The important point is that the experiment is sufficiently flexible to avoid contamination problems under a wide range of conditions.

3.1.6 Acceleration - The purpose of the ESP accelerometer is to measure accelerations along three orthogonal axes &ring the entire entry profile starting with turn-on 300 seconds prior to reaching the entry altitude of 800,000 feet, and terminating at touchdown. Typical calculated acceleration profiles for the roll axis at zero angle-of-attack are shown as Figure 3.1.6-1 and the corresponding acceleration rates of change are presented as Figure 3.1.6-2. The selected instrument is a tri-axis servo force balance accelerometer.

3.1.6.1 Constraints - Selection of an accelerometer is constrained by the following:

- o The instrument must have high accuracy in order to permit accurate density and temperature profile determinations.
- o The maximum acceleration will be 21 g (VM-8) Earth measure.
- o The range and frequency response must be compatible with the acceleration profiles encountered during entry.
- o A digital output is required because the accuracy requirements are more stringent than can be accommodated by the Telemetry Subsystem analog-to-digital converter.
- o The requirements of interfacing subsystems must be met.

3.1.6.2 Alternatives - Two ways of measuring acceleration have been considered.

These are:

- o A tri-axis accelerometer.
- o Three single axis accelerometers.

A study of the typical acceleration profile presented in Figure 3.1.6-1 coupled with a requirement for high accuracy, presents a second set of alternatives - the roll axis accelerometer could be either single range or dual range.

Two basic types of accelerometers are considered - the servo force balance type and the piezoelectric type. Choice of one over the other is dictated primarily by frequency response required.

Other alternatives are input voltage level, location with respect to both CB entry and terminal descent configurations, and Telemetry Subsystem sampling rate.

3.1.6.3 Comparison - The tri-axis unit appears more desirable than the single axis units because:

- o Weight, volume, and power savings can be achieved.
- o A tri-axis unit is procured with the internal axes already aligned, thus simplifying the installation and alignment procedures.
- o All three units can be mounted closer to the c.g. because of the reduced volume.

ACCELERATION PROFILES

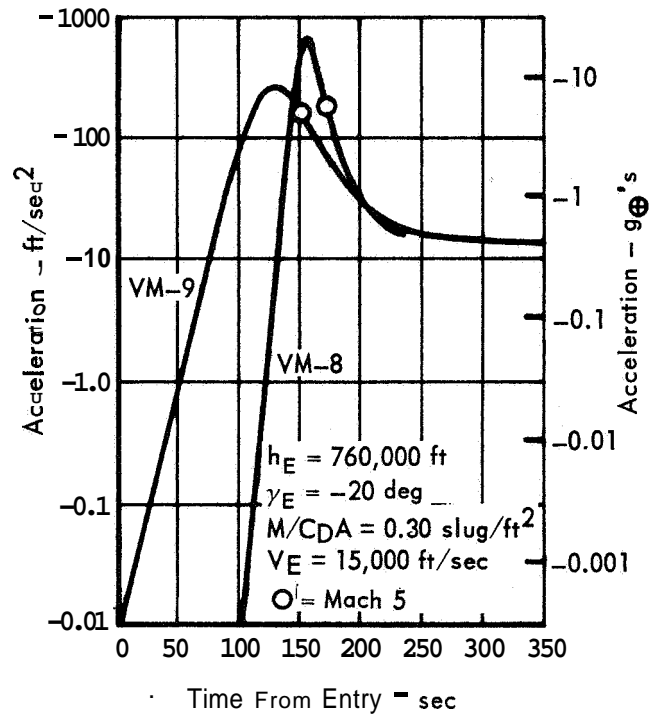


Figure 3.1.6-1

ACCELERATION RATE PROFILES

$h_E = 760,000$ ft
 $\gamma_E = -20$ deg

$M/C_D A = 0.30$ slug/ft²
 $V_E = 15,000$ ft/sec

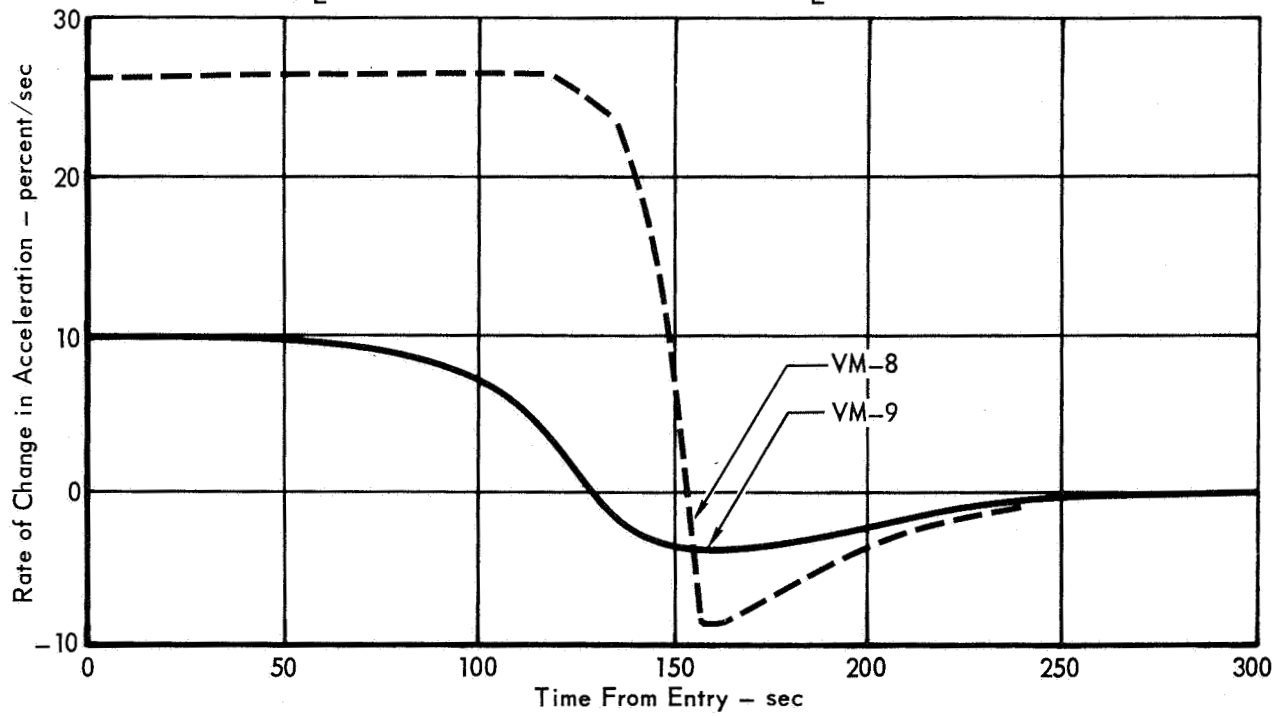


Figure 3.1.6-2

- o Mounting and wiring interfaces are simplified because one connector and one mount will accommodate the instrument rather than three of each.

Figure 3.1.6-1 indicates that accelerations will range from less than $-.01$ ft./sec.² to approximately -700 ft./sec.² during a nominal entry. In order to obtain high accuracy, it may be desirable to use a dual range in the roll axis. A 0 to 30 Earth g range will accommodate any peak but with a 10 bit digital output, the output quantization of the unit is limited to $-.03$ g which means that accelerations might not be detected until more than 100 seconds after the nominal entry height of 800,000 feet is passed. Selection of a second range of 0 to 5 Earth g's would provide a quantization capability of $.005$ g for most of the entry profile. The only addition to the accelerometer is an output circuit change and an automatic range selection circuit. The dual range output is feasible if the accelerometer resolution is $.005$ g or better and this poses no problem.

The acceleration rate as shown in Figure 3.1.6-2 indicates that a servo force balance type is preferred over the piezoelectric type since the piezoelectric types perform rather poorly at very low frequencies.

The power levels available for the accelerometer from the Power Subsystem are 28.5 ± 5 Vdc and $5.00 \pm .05$ Vdc. The 28.525 Vdc voltage level is selected and any other regulation or level changing required will be handled by the accelerometer electronics. Input signals to the Telemetry Subsystem must be digital since the analog-to-digital converter in the Telemetry Subsystem does not have a long enough word length to accommodate the accelerometer accuracy requirements.

The desirable location for the accelerometer is at the c.g. of the CB. However, two items prevent this from being possible for this accelerometer:

The c.g. is inside the SL and an ESP/SL interface is not allowed.

During the entry, there will be many c.g. shifts. The most prominent ones are:

- o Parachute deployment, and
- o Aeroshell separation.

Therefore, the accelerometer location selected is in the CB just ahead of the SL and on the roll axis.

Referring again to Figure 3.1.6-2, it can be seen that the acceleration rate changes a maximum of 26.5 percent per second from its previous reading in the case of entry into the VM8 atmosphere. Therefore, it appears that a sampling rate of 2 per second would be an adequate choice. Lower sampling rates will not track the acceleration profile very well, and while higher sample rates would provide data improvements proportional to the increased Telemetry Subsystem costs, the costs

are too high to accommodate a higher sampling rate.

3.1.6.4 Selection - The preferred approach for the accelerometer is a tri-axis servo force balance accelerometer which provides a 10 bit digital output word for each axis. The roll axis unit will be dual range. The telemetry subsystem sample rate is 2 samples per second on each axis and the input voltage level selected is 28.525 Vdc.

3.1.7 Capsule Bus Sensor Data - The radar altimeter and the guidance and control subsystem process data that describe the dynamics of the Capsule Bus. These data may be used to augment Entry Science Package measurements.

3.1.7.1 Radar Altimeter - The range altimeter, which is part of the Landing Radar subsystem, consists of an electronics package, with an integral dipole secondary antenna mounted on the main ground plane, a primary conical monopole antenna which is part of the Aeroshell nose cap, and an interconnecting RF cable. The altimeter provides altitude measurements from 200,000 ft. to 50 ft. by pulse-radar ranging techniques. This data which is sent to the TCM subsystem at a 1 sample per second rate for telemetering back to Earth, consists of 14 bit binary coded digital words. These provide altitude correlation for entry science atmospheric measurements and for TV imaging. Additional data on backscattering cross section of the surface can be derived from radar return signal strength. Transmitter forward and reflected power is measured and will provide some information on the electrical properties of the plasma sheath.

3.1.7.2 Inertial Sensor Data - The Guidance and Control Subsystem (GCS) includes the Inertial Measuring Unit (IMU) and the digital Guidance and Control Computer (GCC). The IMU contains three orthogonal rate integrating gyroscopes that sense attitude rotations, and a Z-axis accelerometer. These inertial sensors are pulse rebalanced so that their outputs are pulse trains. Each gyro output pulse represents an incremental rotation of the Capsule Bus about one of its body axes. The accelerometer output is a pulse train in which one pulse represents a small change in capsule velocity along the Z-axis. All four sensor signals go to the GCC for processing into attitude and thrust control commands. Several computed quantities are sampled and telemetered. These telemetered data are: body rate about each of three axes, three attitude errors measured with respect to a computed reference frame, and Z-axis acceleration. The direct inertial sensor outputs are not telemetered. Typical formats and ranges of the telemetered data words are listed in Figure 3.1. 7-1. These words are telemetered at a rate of 91 bits per second. GCS status data requires a rate of 35 bits per second, which added to the data rate,

GCS SENSOR DATA TELEMETERED DURING ENTRY

SIGNAL	COMPUTATION RATE Hz	TELEMETRY FORMAT	QUANTIZATION PER BIT	SAMPLE FREQUENCY SAMPLE/SECOND	BIT RATE (BITS PER SECOND)
Roll Attitude Error	200	6 Bits + Sign	0.15 deg	1	7
Pitch Attitude Error	200	6 Bits + Sign	0.15 deg	1	7
Yaw Attitude Error	200	6 Bits + Sign	0.15 deg	1	7
Roll Body Rate	200	6 Bits + Sign	1 deg/sec	1	7
Pitch Body Rate	200	6 Bits + Sign	1 deg/sec	2	14
Yaw Body Rate	200	6 Bits + Sign	1 deg/sec	2	14
Z-Axis Acceleration	25	7 Bits	5 ft/sec ²	5	35

Figure 3.1.7-1

makes a total GCS bit rate of 126 **bits per** second, and occupies 21 percent of the total CB telemetry channel capacity. **Any** significant increase in the use of GCS data over that listed in Figure 3.1.7-1 would have to be accommodated by the ESP telemetry channel.

3.2 ENTRY TV - Emphasis has been given to matching the specified detectors with the resolution and coverage requirements through the proper choice of optics, and to package the system in a form compatible with the CB. The preferred instrumentation is a slow scan vidicon similar to those used on Rangers 3, 4 and 5.

3.2.1 Constraints - The instrument description for the entry science experiment is the Phase B Constraints Document (JPL Rpt PD 606-4) specified dual vidicons with 200 x 200 picture elements, 6 bit amplitude sensitivity, a 0.44 inch format, camera axis parallel to the capsule roll axis, and resolution matched to the Orbiter down to 1 meter per line pair. Each television frame will contain at least 240,000 bits of data 200 by 200 elements at 6 bits/element.

3.2.2 Alternatives - Three types of instruments initially seem suitable for entry imagery. These are: conventional photographic cameras with on-board film processing and electro-optical film readout similar to that used on Lunar Orbiter, conventional vidicon TV, and slow scan vidicon TV.

3.2.3 Comparison - The photographic electro-optical conversion technique can be eliminated immediately on the basis that the equipment would weigh more than 100 lbs, be complex, and have an access time on the order of minutes. Photographic emulsions must be shielded from radiation during the interplanetary transit.

Conventional fast readout vidicons retain their charge pattern for no longer than 0.2 seconds. To readout the desired 240,000 bits of data in this short length of time requires a telemetry channel with a capacity of 1.2 million bits/second, or buffer storage, neither of which is practicable.

The slow scan vidicon has an internal storage time of 20 seconds, and can fulfill all instrumentation requirements. In normal operation these tubes can be exposed in a few milliseconds, read out in 2 to 5 seconds, erased in another 5 seconds, and be ready to recycle. Two of these cameras used in an alternating sequence with 10 second cycle time, provides a system that is compatible with both the 50,000 bit/second telemetry channel and the operational imaging requirements. RCA has developed a suitable antimony-sulfide-oxy-sulfide (ASOS) vidicon photoconductor which can be sterilized without photocathode deterioration (reference JPL Space Program Summary 37-43, Vol. IV, pages 273 and 264.)

Figure 3.2-1 lists the physical and performance characteristics of eight vidicon cameras that have been used on previous space programs.

3.2.4 Selection - The preferred design is a slow scan vidicon, and is most similar to those used on Rangers 3, 4, and 5. The Ranger units correlate especially well with the weight (14 pounds), power (20 watts), and volume (700 cubic inches) called

VIDICON CAMERAS USED ON PREVIOUS SPACE PROGRAMS

CAMERA NAME	NIMBUS AVCS	APT	TIROS	RANGER(F)	RANGER (P)	RANGER (3,4,5)	OAO	MILITARY I
Type of Vidicon	1" Vidicon Electromagnetic Deflection and Focus - ASOS	1" Vidicon Electro-Magnetic Deflection and Focus - ASOS	0.5" Vidicon Electromagnetic Deflection and Focus - ASOS	1" Vidicon ASOS, E - M Deflection and Focus	1" Vidicon ASOS, E - M Deflection and Focus	1" Vidicon ASOS Electrostatic Deflection and Focus	1" Vidicon ASOS Electrostatic Deflection and Focus	0.5" Vidicon ASOS E-M Deflection and Focus
Resolution (T V Lines)	800 Horiz. 600 Vert.	700 Horiz. 550 - 600 Vert.	400 Horiz. 350 Vert.	700 Horiz. 700 Vert.	200 Horiz. 200 Vert.	200 Horiz. 150 Vert.	350 Horiz. 300 Vert.	400 Horiz. 350 Vert.
Frame Time (Seconds)	6.5	200	2.0	2.56	0.2	10.0	1	2.0
Bandwidth (K C)	60.0	16	62.5	200.0	200.0	2.0	60.0	62.5
Dynamic Range	*0.40 to 0.004 (Ft Cand. Sec)	0.7 to 0.01 (Ft Cand. Sec)	1.0 to .01 (Ft Cand. Sec)	0.68 to .004 (Ft. Cand. Sec.)	0.27 to .003 (Ft. Cand. Sec)	.3 to .01 (Ft Cand. Sec)	2nd to 7th Magnitude Star	1.0 to .01 (Ft Cand. Sec)
Signal/Noise (DB) (Peak Signal) (Peak to Peak Noise)	30	17	34	30	29	23	29	34
Erase and Prepare Time (Seconds)	26	8	28/8	2.56	0.64	3	0	126/14
Repetition Rate(Seconds)	91	208	30/10	5.12	0.84	13	Cont Read	128
Residual Image(Per Cent)	5	5	2/10	3	10	10	N/A	2
Highlight Brightness (Ft Lamberts)	11,800	11,800	8,500	650/2700	650/2700	2,400	2nd Magnitude Star	8,500
Lens Focal Length (MM) and Aperture	17 MM F/4 to F/16 (Variable Iris)	5.7 MM F/2 - F/11 **	5MM F/1.5	25MM/76MM F/1, F/2	25MM/76MM F/1, F/2	40 Inches F/5.6	76MM F/0.87	5MM F/1.5
Exposure Time (MilliSeconds)	40	40	1.5	5	2	20	No Shutter	1.5
Active Lines	833	800	500	1150	300	200	350	500
Image Format (Inches)	0.44 x 0.44	0.44 X 0.44	0.25 X 0.25	0.44 X 0.44	0.11 X 0.11	0.44 X 0.44	0.44 X 0.44	0.25 X 0.25
Horiz Line Time (MilliSeconds)	7.5 MS	250 MS	4.0 MS	2.22 MS	0.666 MS	50 MS	2.86 MS	4.0 MS
Weight per Camera (lb)	9.1	10.23	6.5(3 lb Lens)	6.9	6.1	(No Lens or Shutter)	12.5(Lens=4lb)	6.5
Sensor Ass	6.8	9.75	3.9	7.8	7.0	Camera & Control = 6.0	8.5	3.9
Electronics	2.3	19.98	3.9	2.7	2.7		21.0	3.9
Controls	18.2		14.3	17.4	16.6			14.3
Total								
Power per Camera(Watts)	19.0		9.4	21.0	22.8			9.4
Camera	2.0		2.2	9.7	9.7			2.2
Controls	21.0	18.0	11.6	30.7	32.5	5.2	9.0	11.6
Volume (Cu in)								
Sensor Ass	135	215	139	93	87	Power Mod = 72	175	139
Electronics	156	312	112	350	350	Camera Elec=199	385	112
Controls	104	0	86	91	91	Total	0	86
Total	400	527	337	534	528		560	337

* Exclusive of Auto Iris Control (Regulated Power Input).

** Adjustable

Figure 3.2-1

out by the Constraints Document. The VOYAGER optics, packaging, and programming will differ from that used on Ranger but not so much as to appreciably change the basic design concept.

3.2.4.1 Operational Considerations - An investigation of the lighting conditions shows that on the average 200-2000 foot lamberts can be expected from the Martian surface. This follows from a 5600 foot candle maximum illumination, a 0.05-0.35 albedo range, and early morning and late afternoon imaging. Referencing these numbers to a 0.01 foot candle seconds limiting phototube sensitivity and a conservative optical filter transmission of 0.4, gives optical focal ratios around $f/1$ or $f/2$ and exposure times of 5-10 milliseconds. Section 2.2 defines the resolution and coverage required to meet the mission objectives. These requirements can be fulfilled by selecting focal lengths which provide fields on the order of 8° and 50° and angular resolving powers of 0.0007 radians and 0.004 radians, respectively. These numbers in turn define rate stabilization tolerances as shown as Figure 3.2-2.

In order to minimize losses due to image motion it is necessary to:

- a. Keep exposure times as short as possible, use enhancement filters to optimize visual contrast, employ Automatic Gain Control (optical and electronic), and cycle rapidly. This approach counteracts variations in brightness, image smear, and momentary losses in imagery.

3.2.4.2 Installation - This equipment will be mounted close to the Aeroshell in a fixed position. The necessity to get the optics close to the window in order to minimize the window size places a serious constraint on attempts at any other mounting location. This is particularly true when one considers that the window location on the Aeroshell is determined in part by the thermal conditions at the peak decelerations and in part by the type of nose cap design. The second positioning consideration relates to integration with the Aeroshell structure, the descent engine nozzles, and the descent radar. Finally consideration must be given to a structural arrangement that is stable and rigid during imagery, but easily removable before impact to prevent its interfering with the crushable attenuator.

3.2.4.3 Thermal Protection - Temperatures greater than 20°C measured from a reference ambient pose serious operational problems. Therefore the TV must be packaged in a radiantly reflective shell that is thermally isolated from external heat sources or sinks. Radiative heat inputs through the optical entrance pupil can be minimized by the use of infrared reflective but visual transmitting, inter-

TV RESOLUTION
EFFECT OF DESCENT IMAGERY, EXPOSURE
AND STABILIZATION ON RESOLUTION

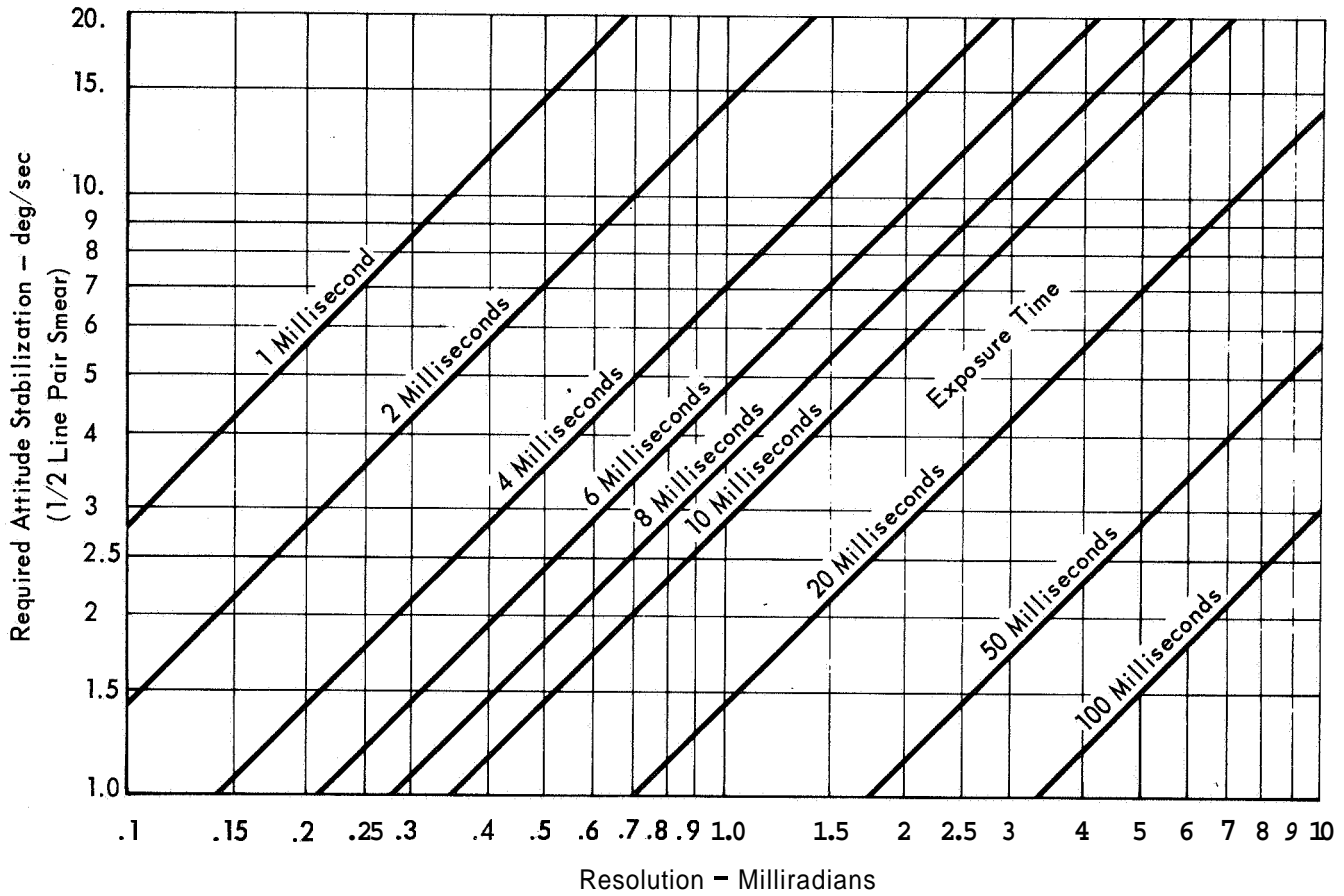


Figure 3.2-2

ference coatings.

3.2.4.4 Utilization - The system must be warmed up, calibrated, turned on, cycled, correlated, and shutdown. The best way to implement this process is to secure a good baseline checkout of the system, noting bias levels, synchronization, stability, and internal temperatures, just prior to release from the Orbiter and while a favorable environment still exists. Warmup should be long enough to eliminate any transient phenomena. At the start of the imaging run, a constant check of critical voltages and temperatures should be made so that any abnormalities in performance can be detected and corrected. This correction could be as serious as instrument shutdown during flight or as simple as a renormalization of the data during the image reconstruction phase. In addition, the CB attitude control system must be monitored continuously during this phase to insure image correlation. Cycle rates are determined by the image overlap requirements. The two cameras could cycle simultaneously thus providing a tight correlation between the two types of pictures. Because of the uncertainties of the environment, it is felt that an alternating sequence gives a better pictorial profile with altitude and maximizes the number of useful images. A constant cycle rate should be used because it is the most direct, reliable technique and at the same time produces some data redundancy at camera separation from the CB.

3.2.4.5 Testing - Camera testing after sterilization offers several alternatives. A highly desirable one is to generate a picture of a test pattern. This gives a check on the optical as well as the electro-mechanical performance of the design. However, to avoid contamination of the optical surfaces from outgassing produced by sterilization, the surface must be protected by coverings and baffles. These opaque elements stay in place until the sterilization canister is separated from the CB prior to entry. To provide an optical test requires;

- a. a collimator built-in as part of the television system,
- b. an external, laboratory collimator projecting through a window in the sterilization canister, or
- c. extensive qualification testing of the television subsystem before CB sterilization; only electro-mechanical testing following it.

Approach (a) is impractical and unreliable. Method (b) is very good, but requires special canister design. Approach (c) is the best compromise.

REFERENCES

1. Watanabe, K., M. Zelikoff, and E.C.Y. Inn, Absorption Coefficients of Several Atmospheric Gases. AFCRL Technical Report 53-23, dated June 1953.
2. Fjelbdo, G., W. C. Fjelbdo, and V. R. Eshleman, "Models for the Atmosphere of Mars based on the Mariner 4 Occultation Experiment," J. Geophys. Res., 71, 2307-2316 (1966).
3. Morse, F. A., and F. Kaufman, "Determination of Ground State O, N, and H by Light Absorption and Measurements of Oscillator Strengths," J. Chem Phys., 42, 1785-1790 (1965).
4. Proposal to Determine Martian Atmospheric Properties Through Solar Ultraviolet and X-Ray Attenuation Measurements. Douglas Report No. SM-5200SP, dated Mar. 1966.
5. Sirounian, V., Ultraviolet Radiation in the Martian Atmosphere., Douglas Report DAC-59033, dated Feb. 1967.
6. Mukherjee, N. R. and H. G. Gross, Effects of Flight Dynamics and the Gas Envelope of an Entry Probe on Solar UV and X-Ray Measurements in the Martian Atmosphere, Douglas Report DAC-60628, dated April 1967.

SECTION 4
ENTRY SCIENCE PACKAGE - SUPPORTING SUBSYSTEMS

4.1 ELECTRICAL POWER - The Electrical Power Subsystem must meet the electrical power requirements of the Entry Science Package (ESP) and minimize its electrical interface with the Capsule Bus and Surface Laboratory. The electrical power requirements of the Entry Science Package equipment are shown in Figure 4.4-1. The power subsystem must provide 223 watt hours of electrical energy and a peak power level of about 345 watts. Power is provided from a sterilizable, sealed, silver zinc battery during descent to the surface of Mars. This battery is float charged during cruise and provides power for equipment operation when FSC power is not available.

The power sources considered for the Entry Science Package, the selected source, the status of development of this source, methods of storage during cruise, and constraints imposed on terminal Flight Capsule sterilization by its use are discussed in the following paragraphs. In addition, this section discusses alternate methods of providing power source redundancy for the ESP, the power grounding concept, and compares the preferred approach of providing unregulated power from the battery to the ESP equipment with providing central power regulation within the power subsystem.

4.1.1 Power Source Selection - Candidate power sources for providing the electrical power and energy requirements of the Entry Science Package include the following:

- a. Sealed AgZn Battery
- b. Automatically Activated AgZn Battery
- c. Hydrazine Powered Turbine Alternator
- d. Silver Cadmium Battery
- e. Nickel Cadmium Battery

The estimated characteristics of these energy sources sized to meet the ESP requirements are shown in Figure 4.4-2. The sealed silver zinc battery was selected because of its high energy density, low volume and because it results in a minimum power interface between the Capsule Bus and Entry Science Package.

The most attractive alternate to the sealed silver zinc battery is the automatically activated battery. The short operating time and high discharge rate requirement makes the use of this device very attractive. Operation of the

ENTRY SCIENCE PACKAGE ELECTRICAL POWER REQUIREMENTS

EQUIPMENT	CRUISE-WATTS	MARS DESCENT		TOTAL ENERGY
		WATTS	TIME (min)	
Radio		270	27	121.5
Telemetry	2	2	450	15
		1.7	27	0.77
Instrumentation	3	3	450	22.5
		7	27	3.15
Data Storage		8	27	3.6
Descent Vidicons		20	27	9.0
Pressure Transducers		1	27	0.45
Accelerometers		2	27	0.9
Temperature Probes		0.2	27	0.09
Mass Spectrometer		7	27	3.15
Power Switching & Logic Unit	2	2	450	15
Battery Charger	5			
Electrical Heater	3	3	450	22.5
Line Losses (6%)	09	19.5		12.3
Total	15.9	346.4		229.91

Figure 4.4-1

COMPARISON OF POWER SOURCES FOR ENTRY SCIENCE PACKAGE

POWER SOURCE PARAMETER	MANUALLY ACTIVATED AgZn BATTERY	AUTOMATICALLY ACTIVATED AgZn BATTERY	SILVER CADMIUM BATTERY	NICKEL CADMIUM BATTERY	HYDRAZINE POWERED TURBINE ALTERNATOR*
Watt Hours/ Pound	15-20	10-15	12-15	8-10	11 ▲
Watt Hours/Cu In.	1.5	1.0	1.5	1.3	1.0
Voltage Regulation	1.25 to 1.86 volts/cell	1.25 to 1.6 volts/cell	0.9 to 1.4 volts/cell	1.0 to 1.4 volts/cell	28V DC +1%
Storage Life	1 Yr	3 Yr	2 Yr	5 Yr	> 1 Yr
Heat Sterilizable	Yes	Yes	Yes	Yes	Yes
Surface Contamination	No	No	No	No	Yes
Power Available During FSC Midcourse Corrections	Yes	No Derive from capsule bus	Yes	Yes	No Derive from capsule bus

*Selected System

▲Includes fixed weight fuel & tankage

Figure 4.4-2

Entry Science Package equipment during cruise periods when Flight Spacecraft power is not available to the Flight Capsule makes either a manually activated system necessary in the Entry Science Package, or requires that the Capsule Bus main power distribution bus provide power to the Entry Science Package. The latter requirement is not considered to be consistent with the constraint of making the Flight Capsule elements (CB, ESP, SL) mutually independent and self-supporting to the maximum extent practical.

Silver-Zinc Battery Development - Review of development work on sealed, sterilizable, long wet life, AgZn batteries indicates that significant advances have been made in this technology. The design and performance parameters used for sizing the Entry Science Package battery are conservatively estimated on the basis of accomplishments of three battery development programs. These are: (1) a program conducted by the Electric Storage Battery Company to develop a battery using an organic separator material, (2) a program conducted by the Eagle Picher Company to develop a battery using an organic separator material, and (3) a program conducted by the Douglas Astropower Laboratory of the McDonnell Douglas Corporation to develop a battery using an inorganic separator material. All of these development programs have shown promising results. Cells of all three types have been heat sterilized at 135°C for approximately one VOYAGER sterilization time period and given satisfactory performance afterward. The design parameters of the cells which were subjected to heat sterilization testing are shown in Figure 4.4-3. A summary of the heat sterilization and wet stand tests is shown in Figure 4.4-4. Polarization curves for these cells are shown in Figure 4.4-5 along with polarization curves of Douglas Astropower cells utilizing new separator materials, DE(F), giving significantly higher performance capability. Testing of cells using these separators is now in process at Douglas Astropower Laboratory. These test results, provide evidence of the ability to sterilize AgZn batteries. The ESP battery must be capable of discharging almost completely at the 0.6 hour rate (C/0.6) which will require the use of a thin plate battery. Silver zinc batteries with plate thicknesses on the order of 10 mils or less have been used in other applications. Recent work by the Electric Storage Battery Company on a 9 ampere hour cell capable of being discharged at the one hour rate, indicates that a battery of this type can be made sterilizable. This battery uses a new separator material which is different than the material used in the cells of Figure 4.4-4. It is expected

DESIGN PARAMETERS OF STERILIZABLE CELLS TESTED

MANUFACTURER DESIGN PARAMETERS	ESB MODEL 334	EAGLE PICHER	DOUGLAS ASTROPOWER
Capacity	40 amp hr	8 amp hr	2 amp hr
Separator	5-RA1-116	4 Parnion -307	Inorganic - Z (8)
Cell Case	Polyphenylene oxide	Polypropolene	Polyphenylene oxide
Type of cell	Sealed	Sealed - pressure relief	Sealed
Battery Case	-	Magnesium-sealed	-
Cells/Battery	-	6	-
No. of Cells Tested	7	12	16
Operating Temp	80°F	75°F	77°F

Figure 4.4-3

SUMMARY OF STERILIZABLE AgZn CELL AND BATTERY TESTS

MANUFACTURER PERFORMANCE	ESB MODEL 334	EAGLE PICHER CO		DOUGLAS ASTROPOWER
		BATTERY NO. 1	BATTERY NO. 2	
Sterilization Environment	135°C-120 hr-1 cycle	145°C-36 hr-3 cycles		145°C-36 hr-3 cycles
Wet Stand Time	-	10 months	10 months	5 months-4 cells, 3 months-4 cells, 2 months-4 cells, 1 month-4 cells
Wet Stand Condition	-	Discharged	Charged	Charged
Discharge Rate	4 hr rate to 13 v/cell then 8 hr rate to 13 v/cell	4 hr rate to 1.25 v/cell	4 hr rate to 1.25 v/cell	7 hr rate for 1 hr then 2.7 hr rote to 1.0 v/cell
Energy Density	31.5 wh/lb	30 wh/lb	38 wh/lb	20.5 wh/lb*
Cycle Life Following Wet Stand (100%Depth)	-	2	16	2+

*Projected for optimized battery design

Figure 4.4-4

PLATEAU VOLTAGE OF STERILIZABLE AgZn CELLS

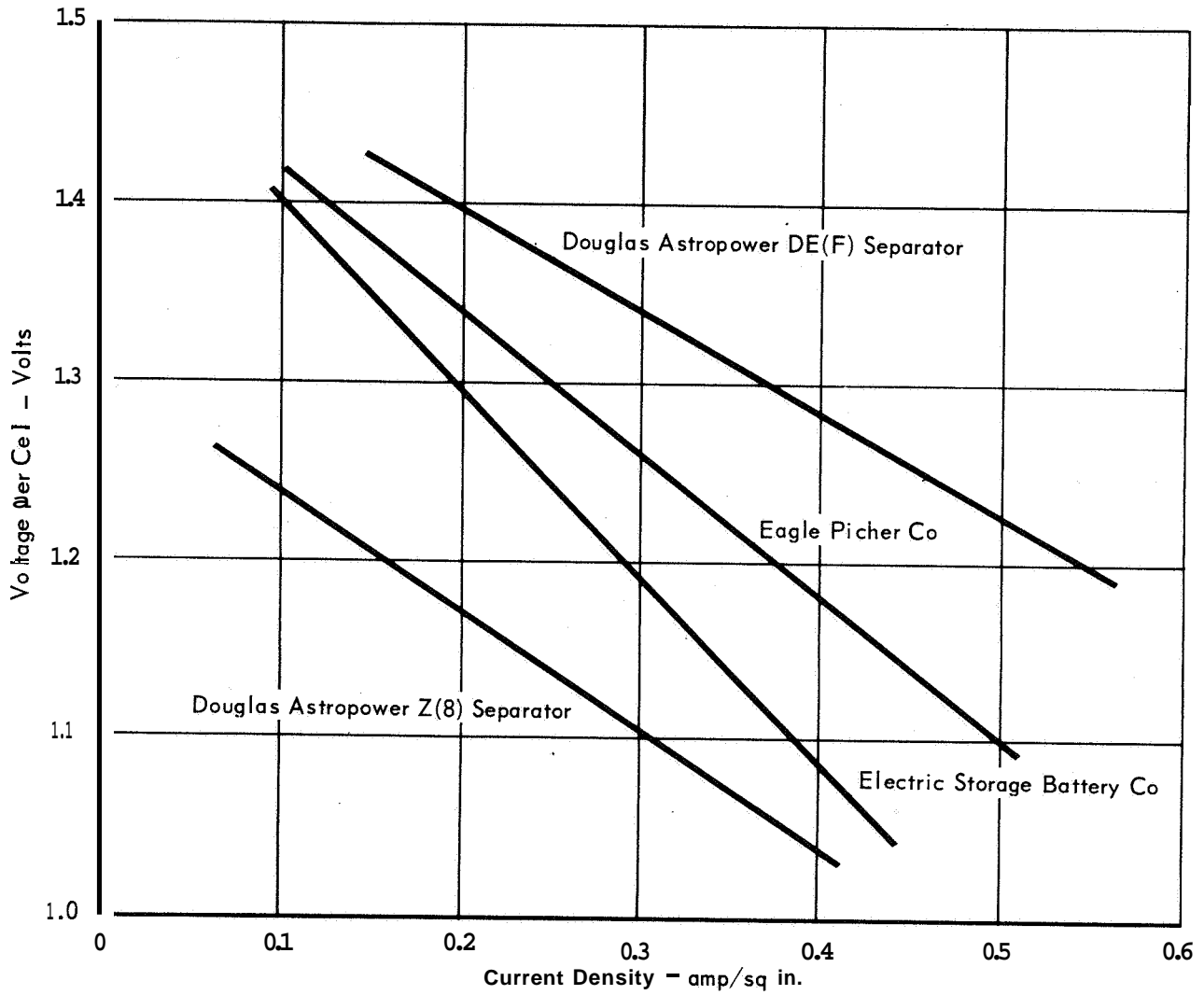


Figure 4.4-5

that a battery energy density of 15 to 20 watt hours per pound can be achieved in this type of battery. A conservative figure of 15 watt hours per pound was assumed for the purpose of the subsystem design.

Constraints on Terminal Flight Capsule Sterilization - The baseline Electrical Power Subsystem design described in Part G, Section 7.0 points out that charge/discharge cycling of the battery prior to heat sterilization is not presently planned. This is due to the limitations on the cell being developed by the Electric Storage Battery Company. It is possible that use of the battery prior to sterilization might result in zinc metal remaining in the negative plate after complete discharge causing excessive hydrogen formation and consequent overpressure of the cells. This limitation is considered to be a major restriction on the sterilization and pre-launch operation, because no battery performance checks are possible prior to terminal Flight Capsule heat sterilization. Discovery that the battery does not give satisfactory performance after sterilization would require that the entire Flight Capsule be subjected to a second cycle of terminal heat sterilization with a new battery. Work performed on the Eagle Picher battery by the General Electric Company demonstrated that this battery can survive the heat sterilization after charge/discharge cycling. Depending on future developments in this area, this restriction may be removed at a later time, however the present design concept is constrained to assure battery sterilization prior to formation charge.

An alternate approach to sealed AgZn battery wet heat sterilization is to be investigated by the McDonnell Douglas Corporation under contract NAS8-21114 to the NASA Marshall Space Flight Center. The objective of this work is to demonstrate dry heat sterilization of the battery pack, and filling and sealing of the cells in a sterile environment. This concept may offer an alternative to wet heat sterilization although presently the approach does not meet the constraints of JPL SE003BB002-2A21. The use of this approach would require cooling of the battery during Flight Capsule terminal heat sterilization and decontamination of the battery case by ETO.

Only the equivalent of one cycle (120 hours) of heat sterilization at the type approval test temperature of 135°C or above has been demonstrated. The capability of these systems to survive longer periods at the type approval temperature is not known at this time and will require further testing. It is presently planned for the flight batteries to be installed at the launch facility

prior to Flight Capsule terminal sterilization, and the design of the Capsule Bus will allow easy access to the battery locations. Failure of any Flight Capsule equipment during or after terminal heat sterilization which necessitates a second heat sterilization cycle, may also require battery replacement depending upon what further battery development and testing indicates.

Battery Storage During Cruise - Selection of the preferred approach to battery storage during the cruise phase of the mission requires additional wet stand testing on AgZn cells. Eagle Picher cells assembled into 6 cell batteries and tested by the General Electric Company (Eagle Picher Batteries of Figure 4.4-4) survived 10 month wet stand period after sterilization and then were cycled. The battery stored in a discharged condition yielded 98% of its initial capacity after the wet stand period, and has survived 11 additional cycles to date. The battery stored in a charged condition, after replacing the capacity loss, delivered 75% of its initial capacity after the wet stand period but failed to accept a charge after the second discharge. Analysis of the cell indicates that failure was due to dehydration of the electrolyte caused by loss of hermetic seal. Increased electrolyte concentration is believed to have resulted in accelerated oxidation of the separator. These tests indicate that a battery of this construction, on long wet stand in a discharged condition, has a high probability of survival. Testing is considered desirable, however, to compare cell degradation in a charged open circuit condition, discharged condition, and stand on float charge.

Maintaining the battery on continuous charge during cruise was selected as the preferred approach for the following reasons:

- a. It is a lighter weight approach than open circuit charged stand since the battery need not be oversized to allow a 4 to 12 percent per month expected loss of capacity.
- b. It is preferred over standing in a discharged condition, since the battery is independent of the battery charger, insofar as partial mission success is concerned.
- c. Internal power must be provided within the Entry Science Package during periods when FSC power is not available for cruise commutator operation.
- d. The power dissipated in the battery charger serves the same purpose as electrical heaters.

4.1.2 Battery Charger Selection - A two step float charge method of battery charging was selected based upon work performed by the Goddard Space Flight Center, using this type of charger in tests of long cycle life AgZn batteries. This type

of charger appears to offer a reduction in the cell degradation processes of zinc dendrite penetration of the cell separators and silver migration through the separators.

4.1.3 Interfaces - The electrical power subsystem has interfaces with all other subsystems in the Entry Science Package, an interface with the Capsule Bus, and an interface with the Surface Laboratory in the baseline design concept.

The trade studies required to properly design these interfaces are the following:

- a. Alternate methods of providing a redundant power source for the Entry Science Package.
- b. Alternate approaches to providing power to the ESP electronics equipment (unregulated battery voltage, regulated DC power, regulated AC power) which results in a minimum weight approach with acceptable probability of partial as well as total mission success.
- c. Comparison of providing power to the ESP equipment from the CB versus the use of the ESP battery.
- d. Alternate approaches to the design of a primary power ground reference system.

Capsule Bus Main Battery Redundancy - The two approaches considered for providing redundant battery capacity to the ESP are (1) providing this redundancy from the Surface Laboratory and (2) providing this redundancy within the ESP. The first approach is the preferred approach. Standardization of the ESP is not affected as later missions will utilize a long term power source with secondary batteries, and projected later mission requirements indicate that sufficient power and energy should be available from the Surface Laboratory to act as a backup for the ESP battery during descent. The factors considered in selecting the preferred approach are shown in Figure 4.4-6.

Use of Capsule Bus Power by the ESP - Two approaches were considered for providing power to the ESP. These are (1) integrating the ESP Electrical Power Subsystem with the Capsule Bus Electrical Power Subsystem such that the Capsule Bus main battery provides the requirements of the ESP, and (2) the selected approach of having a separate battery in the ESP. The selected approach resulted from the requirement to make the vehicles independent to the maximum extent practical. The factors considered in the comparison are shown in Figure 4.4-7.

COMPARISON OF APPROACHES FOR PROVIDING REDUNDANT POWER TO THE ESP

DESIGN APPROACH COMPARISON FACTORS	1. REDUNDANT BATTERY IN ESP	2. REDUNDANT POWER FROM SL *	SELECTION
1973 Voyager Capsule Systems Constraints and Requirements Document	Requires independence of vehicles to the maximum extent practical.	Primary power sources are independent. Redundant mode power from SL is considered to be within document constraints.	Approach 1
2. Reliability (Probability of ESP Electrical Power Subsystem mission success)	0.9942	0.9923	Approach 2
4. Interface Complexity	Requires 33 pounds of batteries and battery chargers in the ESP. ESP Interconnections • FSC power • Commands	Requires only 16.5 pounds of battery and battery charger in the ESP. ESP Interconnections • FSC power • Commands • Backup SL power	Approach 1

* Selected Approach — because of light saving.

Figure 4.4-6

COMPARISON OF APPROACHES FOR PROVIDING ESP POWER

DESIGN APPROACHES COMPARISON FACTORS	1. SEPARATE CAPSULE BUS AND ENTRY SCIENCE PACKAGE BATTERIES*	2. CAPSULE BUS BATTERY ONLY - ESP NEEDS MET BY CAPSULE BUS	SELECTION
1. 1973 Voyager Capsule Systems Constraints and Requirements Document	Requires independence of vehicle to the maximum extent practical.	Makes ESP dependent upon CB power subsystem	Approach 1
2. Flight Capsule Reliability (Probability of total electrical power subsystem mission success)	0.9576	0.9535	Approach 2
3. Flight Capsule Weight	Combined CB and ESP electrical power subsystem requires 64 pound battery in CB and 16.5 pounds of battery plus battery charger in ESP	CB electrical power subsystem capable of meeting ESP needs require 72.6 pound main battery.	Approach 3
4. Interface Complexity	ESP Interconnections <ul style="list-style-type: none"> • FSC power • Commands • Backup SL power 	ESP Interconnections <ul style="list-style-type: none"> • CB power 	Approach 4

* Selected Approach - By consideration, since CB power source makes ESP dependent upon CB operations

Figure 4.4-7

Primary Power Ground Reference - Three approaches to the design of a ground reference system were considered. These are discussed, along with the trade-offs involved, in Volume 11, Part B, paragraph 5.6. The preferred design uses a dc-dc converter/regulator (located in the Adapter) to provide regulation of the raw dc power obtained from the Spacecraft, and to provide isolation between the Spacecraft and Flight Capsule electrical/electronic systems. In addition, the preferred concept requires that the Flight Capsule's primary power return circuit be referenced to ground by a single connection to the Surface Laboratory's central ground point (CGP).

4.1.4 Power Distribution - Alternate approaches to distributing power to the Entry Science Package equipment during descent are (1) provision of unregulated power from the main battery to the ESP equipment with a voltage regulator of 23.5 to 33.5 volts dc, (2) use of a central regulator in the power subsystem providing an output voltage regulated to within 1%, (3) use of a central inverter in the power subsystem providing a square wave ac output with voltage regulation in the range of 1%, and (4) use of a central power supply in the power subsystem to provide the particular outputs required by the ESP equipment. The primary advantage of the first approach, which was selected, is that no catastrophic failure mode exists which can terminate the entire mission. In this concept the telecommunication and experiment equipment contain power supplies to provide the precise voltage required. An additional advantage of the approach is that it provides maximum flexibility, in that design modification to subsystems can be managed within the equipment and do not affect the power subsystem design.

The use of a central regulator within the power subsystem approach requires the use of block redundancy. This redundancy does not eliminate the possibility of a failure of the redundant regulator because it is subjected to the same environmental conditions as the primary regulator. Also this technique does not eliminate the need for transformer coupled power supplies in the Entry Science Package equipment, which are necessary for signal and power ground isolation as well as for conversion to voltage levels required for subsystem equipment operation. It does, however, in some cases eliminate the need for regulation in the ESP equipment. The overall weight of this approach does not indicate a reduction over the selected approach. This approach is not considered as attractive as alternate 3.

Approach 3 is the most attractive alternate to the selected approach. Here the use of a central inverter in the power subsystem does eliminate the need for

inversion in the equipment power supplies and some weight saving may be afforded. An exact weight comparison requires detailed knowledge of the outputs required from the equipment power supplies which are not known at this time. This concept does require block redundancy and switching to replace the primary inverter in the event of a failure. In addition, the short rise and fall time of the square wave creates a broad spectrum of interference which is difficult to remove from susceptible circuits.

Approach 4 is not considered attractive. Circuit redundancy within the power supply would be used instead of block redundancy which would result in complex switching. The wiring weight is increased because of multiple voltage distribution. Considerable integration is required to preclude subsystem design from including superfluous vs power conditioning and to require early, accurate definitions of all subsystem power requirements. Any deficiency of the early definitions, yields an inadequate or delayed power conditioner design due to the inflexibility of the method after completion of the hardware design.

The approach of placing the conversion and regulation equipment required into the ESP power using equipment was selected because it does not create a single failure possibility which can result in complete loss of ESP data, and it provides flexibility in allowing design modification to be managed within the subsystem and experiment equipment.

4.2 TELECOMMUNICATIONS - The ESP telecommunications design was dominated by two factors, multipath and entry ionization. The analyses of these two factors are difficult because of the large uncertainties in the Martian environment, and the wide range of orbits and entry trajectories which must be accommodated.

To resolve these questions we examined the entire spectrum of orbits/entry trajectories/atmospheres, candidate modulations, antenna patterns, data storage - retransmission techniques, ablator effects upon the wake ionization and diversity transmission approaches. Figure 4.2-1 is a summary of the computer programs, tests and simulations which were employed to solve the Martian entry telecommunications questions. Our design provides a maximum return of entry data within the design requirements and constraints.

The solutions derived for the multipath and entry ionization questions indicated that a significant increase in low frequency science data retrieval probabilities could be achieved by cross-strapping the Capsule Bus and ESP packages prior to transmission. This cross-strapping is achieved with minimum interference to the ESP.

4.2.1 Propagation Analysis - The capsule link propagation analysis is based upon a 340-400 MHz relay link to the spacecraft.

The frequency range-from 150 to 500 MHz was investigated in detail. Frequencies below 150 MHz were excluded because of galactic noise and antenna size limitations. Frequencies above 500 MHz were excluded because of the higher space loss incurred when the antenna beamwidths must be held constant. The results of the study indicated that the total vehicle weight was minimized at a 350 MHz transmission frequency. The two specific frequencies for the preferred design are required to be 60 MHz apart in order to minimize the equipment complexity in the spacecraft, see Paragraph 5.5.3. 400 MHz was chosen to be compatible with the space research and telemetry bands, and 60 MHz below it, 340 MHz.

A relay, rather than a direct to Earth link was chosen primarily because the necessary high gain steerable antenna for a direct link is not compatible with the entry geometry.

The heart of the propagation analysis is the design control table, Figure 4.2-2. The transmitter power, forty watts, is a design parameter which must be adjusted to provide an adequate signal margin under the most severe propagation conditions. The transmitting circuit losses are an engineering estimate based upon the cable routing within the vehicle configuration. The transmitting antenna gain and design space loss are predicated upon the allowable envelope of Spacecraft/Capsule

PROPAGATION COMPUTER PROGRAMS AND SIMULATIONS

REFERENCE PARAGRAPH	COMPUTER PROGRAM	TEST/SIMULATION	DESCRIPTION
4.2.1.1	Echo		Computation of all of the geometric parameters required for the multipath problem
4.2.1.1	LS2 to LS8		Solutions to the complex statistical functions necessary to evaluate FSK in a multipath environment
4.2.1.1		Bit sync simulation	Simulation of the multipath environmental effects upon candidate bit synchronizer designs
4.2.1.2	KAIF		Chemical equilibrium program for hot gas mixtures*
4.2.1.2	-		Mixing and diffusion program for any gases*
4.2.1.2	-		Ray trace program - electromagnetic profile*
4.2.1.2		Test	Sulfur hexafluoride seeding tests with an RF plasma generator
4.2.1.2	T-684		Pointed cone - aerodynamics
4.2.1.2	T-785		Shear layer - aerodynamics
4.2.1.2	T-299		Method of characteristics - aerodynamics
4.2.1.2	T-805		Entropy layer patch - aerodynamics
4.2.1.2	T-687		Charring ablation program - thermodynamics
	T-689		Laminar boundary layer with mass addition - thermodynamics
	T-666		Chemical equilibrium composition of gas - thermodynamics
4.2.4		Test	Antenna pattern Pattern Development Tests

*Plasma Programs

Figure 4.2-1

TELECOMMUNICATION DESIGN CONTROL TABLE

ITEM NUMBER	PARAMETER	VALUE	TOLERANCE (dB)	SOURCE
1	Transmitter Power (40 W)	46.0 dBm	+ 0.5 -0.5	▲
2	Transmitting Circuit Loss	-0.5 dB	+ 0.2 -0.3	◆
3	Transmitting Antenna Gain	5.1 dB	+0.5 - -0.5	4.2.1.1 and 4.2.4
4	Transmitting Antenna Pointing Loss	Included in Line 5.	-	-
5	Space Loss (f = 400 MHz, R = 10,000 km)	-164.5 dB	-	4.2.1.1
6	Polarization Loss	0.0 dB	+ 0.0 -0.5	4.2.4
7	Receiving Antenna Gain	9.9 dB	+ 0.0 -3.0	4.2.1.1 and 4.2.4
8	Receiving Antenna Pointing Loss	Included in Line 7	-	-
9	Receiving Circuit Loss	-1.0 dB	+ 0.2 -0.2	◆
10	Net Circuit Loss	-151.0 dB	+ 0.9 -4.5	Sum Lines 2 through 9
11	Total Received Power	-105.0 dBm	+1.4 -5.0	Sum Lines 1 & 10
12	N_o ($T_s = 555^{+25}_{-80}$ °K)	-171.2 dBm/Hz	+ 0.2 -0.7	4.2.3
13	Bit Rate (55,860bps)	47.5 dB-bps	-	4.2.2
14	Required E/ N_o	13.6 dB	-	4.2.1.2
15	Threshold Power	-110.2 dBm	+ 0.2 -0.7	Sum Lines 12 through 14
16	Margin	5.2 dB	+ 2.1 -5.2	Lines 11 Minus Line 15

▲ Design Variable ◆ Engineering Judgement

Figure 4.2-2

positions at the time of entry. The derivation of this envelope is given in the first part of the multipath analysis. The transmitting antenna gain figure includes the efficiency of the candidate antenna, reference Paragraph 5.5.4. Polarization loss in the left hand circularly polarized antenna subsystem is principally due to the "loss" of circularity off-axis. The degree of off-axis look angle required is given in the first part of the multipath analysis, while the antenna ellipticity is discussed in the antenna analysis section.

The receiving antenna design gain is based upon the allowable envelope of spacecraft - capsule look angle variations, discussed in the multipath section, together with the envelope of orbit orientations with respect to the sun and Canopus discussed in Paragraph 4.2.4. The gain includes the receiving antenna efficiency. The receiving circuit loss, as was the transmitting circuit loss, is an estimation based upon the vehicle configuration. The noise temperature analysis is given in Paragraph 4.2.3.

The ESP rate of 55,860 bps is derived from formatting the instrumentation requirements given in Figure 4.2-3. The formatting techniques and trades are presented in Paragraph 4.2.2, while the actual formats are given in the Entry Science Package Telemetry Subsystem functional description, Volume IV, Part G, Section 4.

The sum of the adverse tolerances is 5.3dB, thus with a power margin to just overcome the adverse tolerances, a "threshold" signal energy to noise density ratio of 13.4 decibels is established. From the bit error histories illustrated in Paragraph 4.2.1.1 this signal level would result in an average probability of bit error of 5.2×10^{-4} for the preferred design in the worst case atmosphere-trajectory.

4.2.1.1 Multipath Analysis - The Capsule to Spacecraft communications link will be corrupted by an "indirect" transmission path reflected off the surface of the planet. This analysis is concerned with identifying the degree of this interference. The problem is divided into three parts; geometry, modulation, and effects. The geometric consideration identifies those parameters which are concerned with the direct and indirect path lengths, antenna look angles, entry trajectories, reflectivity models, etc. The modulation consideration identifies the gross effects of multipath upon

ENTRY SCIENCE PACKAGE INSTRUMENTATION LIST

PARAMETER NUMBER	PARAMETERS	RANGE	TYPE	ACCURACY	SAMPLES/SECOND					
					LAUNCH & CRUISE	PREPARATION CHECKOUT	DE-ORBIT	ENTRY	TERMINAL DESCENT	
RE1-2	Radio Subsystem									
RE3-4	Transmitter Power (2)	25° to 150°F	HL	3%		.05		.05	.05	
RE5-6	Crystal Temperature (2)		LL	3%		.05		.05	.05	
RE7-8	Transmitter Frequency (2)		HL	3%		.05				
RE9-10	Modulator Verification		HL	3%		.05				
RE11	Oscillator Drive (2)		HL	3%		.05				
	Antenna Reverse Power		HL	3%		.05				
DE1	Telemetry Subsystem									
DE2	Oscillator Temperature	25° to 150°F	LL	3%		.01		.01	.01	
DE3	Telemetry Mode		D	4 bits		.01		.01	.01	
DE4	Vehicle Time		D	10 bits		.01		.01	.01	
DE5	DC Power	15-35 vdc	HL	3%		.01		.01	.01	
DE6-8	Slaved to Reference Frequency		BL			.01		.01	.01	
DE9-11	ADC Linearity Voltages (3)		HL	3%		.01		.01	.01	
DE12	Low Level Amp Linearity Voltages (3)		LL	3%		.01		.01	.01	
DE13-16	Transducer Voltage Source		LL	3%		.01		.01	.01	
DE14-16	Cruise Commutator DC Power	15-35 vdc	HL	3%		.01		.01	.01	
	Cruise Commutator ADC Linearity Voltages (3)	0-5	HL	3%		.01		.01	.01	
DE17-19	Cruise Commutator Low Level Amp Linearity Voltages (3)	0-4 mv	LL	3%		.01		.01	.01	
DE20	Cruise Commutator Mode		D	4 bits		.01		.01	.01	
DE21-23	ADC Linearity Voltages (3)	0-5 v	HL	3%		.01		.01	.01	
DE24-26	Low Level Amp Linearity Voltages (3)	0-40 mv	LL	3%		.01		.01	.01	
DE27	Telemetry Memory Readout									
DE28	Data Storage Temperature		LL	3%		.01		.01	.01	
TE1-8	Thermal Control									
	Structure Temperatures (8)	-150° to 500°F	LL	3%		.01		.01	.01	
EE1	Electrical Power									
EE2	Battery Voltage	15-38 vdc	HL	1%		.01		.01	.01	
	Battery Temperature	0° to 120°F	LL	3%		.01		.01	.01	

Figure 4.2-3

EE4 EE5 EE6	Battery Current Transfer Switch Operation Redundant Battery Sw Operation	0 to 6 amps	LL BL BL	1%	.001 .001 .01	.01 .01 .01	.01 .01 .01	.01 .01 .01
VS1-2	Television	CHARACTERISTICS						
VE3	Frame No.	2 Camera Alternate						
VE4-5	IRIS Setting (2)	Frames from 800 kft to						
VE6	Filter Position	Touchdown. 200 Elements/ Line, 200 Lines/Frame,						
VE7	Camera No.	Cameras Alternate Com- plete Frames, 6 bits/ Element						
VE8-9	Vidicon Temp (2)	≤ Engineering Status	D	6 bits	1/FR	1/FR	1/FR	1/FR
VE10-11	Lens Assy Temp (2)	≤ Engineering Status	D	6 bits	1/FR	1/FR	1/FR	1/FR
VE12	Electronics Temp	≤ Engineering Status	D	2 bits	1/FR	1/FR	1/FR	1/FR
VE13-14	Target Voltage (2)	≤ Engineering Status	BL		.1	.1	.1	.1
VE15-16	Erase Lamp Status (2)	≤ Engineering Status	LL		.1	.1	.1	.1
VE17	Light Level	≤ Engineering Status	LL		.1	.1	.1	.1
PE1	Descent Atmosphere Properties		HL		1.0	1.0	1.0	1.0
PE2	Stagnation Temperature		HL		1/5	1/5	1/5	1/5
PE3	Stagnation Pressure		HL		1/30	1/30	1/30	1/30
PE4	Base Temperature		LL		1/30	1/30	1/30	1/30
PE5	Base Pressure		HL		1/30	1/30	1/30	1/30
PE6	X-Axis Accelerometer		D	10 bits	1/30	1/30	1/30	1/30
PE7	Y-Axis Accelerometer		D	10 bits	1/30	1/30	1/30	1/30
PE8	Z-Axis Accelerometer		D	10 bits	1/30	1/30	1/30	1/30
PE9	Z-Axis Range Mass Spectrometer	50-8 Bit Words per 2 sec Scan, Readout in 8 sec. No Readout During Scan, 10 sec Cycle	BL D	8 bits	1/30 1 scan	1/30	1/30	1/30
PE10	Pressure Trans Temp	Engineering Status	LL	7 bits	1/30	1/30	1/30	1/30
PE11	Mass Spectrometer Bt	Engineering Status	HL	7 bits	1/30	1/30	1/30	1/30
PE12	Mass Spectrometer RF Voltage	Engineering Status	HL	7 bits	1/30	1/30	1/30	1/30
PE13	Mass Spectrometer Diode Temperature	Engineering Status	HL	7 bits	1/30	1/30	1/30	1/30
PE14	Mass Spectrometer Pump Pressure	Engineering Status	HL	7 bits	1/30	1/30	1/30	1/30
PE15	Mass Spectrometer Filament No.	0-27 v Engg Status	HL	2 bits	1/30	1/30	1/30	1/30
PE16	Mass Spectrometer Ion Chamber Temp	Engineering Status	HL	7 bits	1/30	1/30	1/30	1/30
PE17	Mass Spectrometer Detector Range	Engineering Status	HL	7 bits	1/30	1/30	1/30	1/30

Memory content verification - Readout entire memory on command.

HL - Single ended high level 0 to 5 volts

LL - Double ended low level 0 to 40 millivolts

D - Digital
BL - Bilevel

4-18-2

various modulation schemes, i.e., coherent vs noncoherent, wideband vs narrowband, diversity, etc. The final part of the analysis combines the previous sections to provide bit error "histories" during entry.

The results of this analysis indicate that, (1) multipath is most severe in the period near the end of plasma blackout and (2) a noncoherent wideband 2FSK frequency diversity system will provide the best performance in the Martian multipath entry environment.

Geometric Considerations - The entry geometry problem appears at first to be undimensional and unbounded. The major trajectory parameters are orbit size, de-orbit anomaly, de-orbit delta velocity, de-orbit deflection angle, atmosphere, entry angle and attitude. In order to bound the problem thirty-four trajectory cases have been examined for the period from de-orbit thrust to 100 kilofeet. These cases range over de-orbit anomalies from 170 to 300 degrees, entry angles of -20 and -14 degrees, and both large (4400 X 23400 km) and small (4900 X 13400 km) orbits. The envelope of these cases is given in Figure 4.2-4. A ten degree angle uncertainty is added to give the required antenna pattern. Assuming a gaussian shaped pattern; the optimal pattern would be squinted 25' off the roll axis. However, roll control is not available during entry, thus the pattern must be symmetrical about the roll axis. In order to provide an adequate effective radiated power (gain x transmitter power) at the extreme view angles where the gaussian antenna pattern gain is low, the "on-axis" gain provides a range capability greater than that experienced on any trajectory. This range is designated the "design range" and is 10^4 km for a symmetrical pattern about the roll axis.

The relative Spacecraft position at the time of capsule entry as "seen" from the Capsule is shown in Figure 4.2-5. Superimposing the pattern requirement from Figure 4.2-5; and allowing both a $\pm 20^\circ$ entry attitude tolerance and a 3 decibel entry range tolerance, an envelope of "allowable" spacecraft positions may be computed. This is given in Figure 4.2-6. A second boundary is the trailing horizon limit. This is computed by assuming that the relative Spacecraft/Capsule lead angle is constant during entry, and assures that the Spacecraft will not fall below 34' of the trailing horizon.

From the envelope of allowable Spacecraft/Capsule positions (and the entry trajectory constraints discussed in Volume II - Part B - Section 2.3.), two bounding cases are chosen; the first at 313' S/C anomaly, 9° F/C lead for VM-9, and the second at 300' S/C anomaly, 27° F/C lead for VM-8.

DESCENT TRAJECTORY GEOMETRY — EFFECTS ON CB ANTENNA PATTERN SHAPE

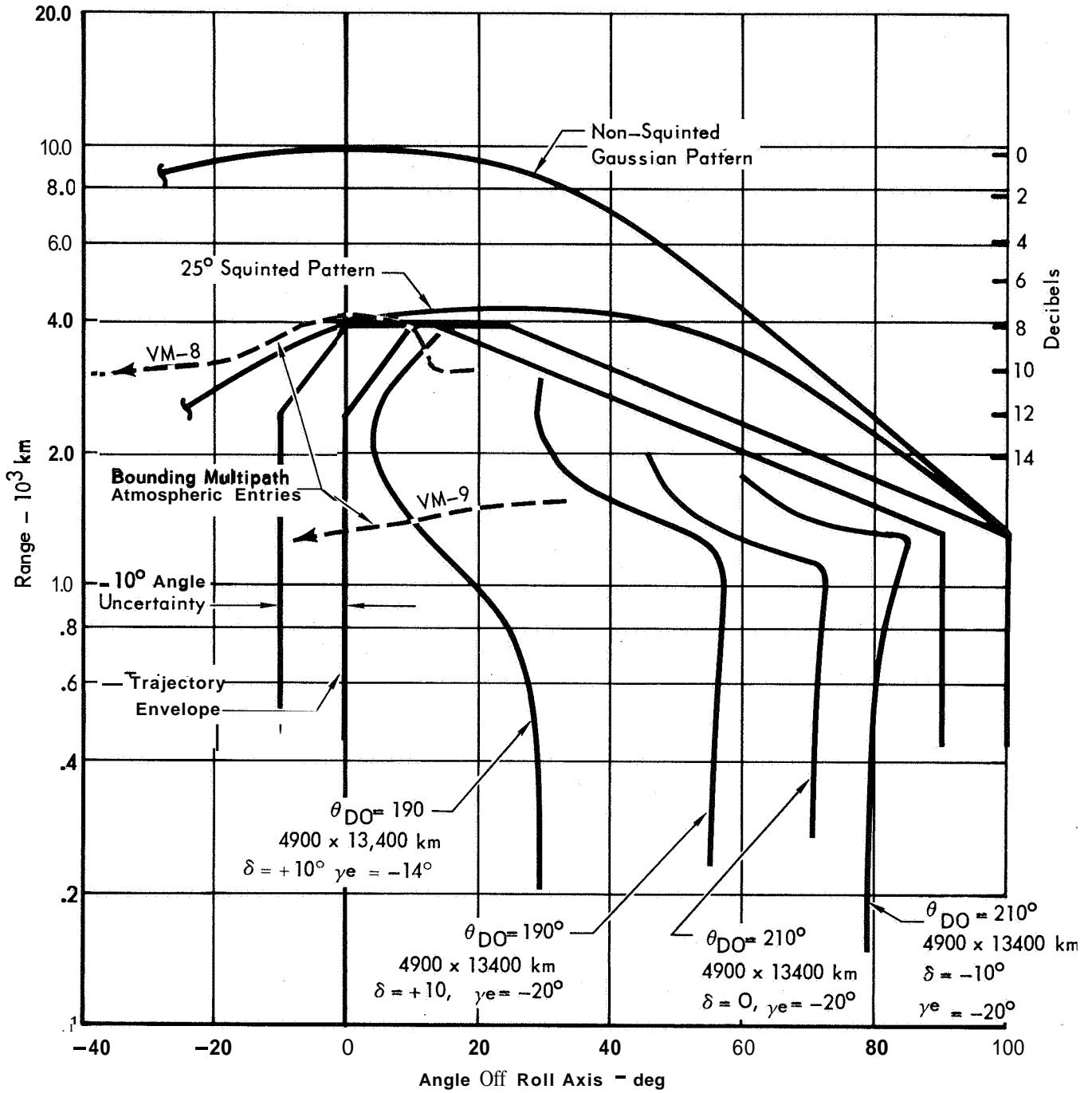


Figure 4.2-4

ANTENNA PATTERN LIMITS

- 3dB Range Margin
- ± 20° Attitude Margin
- Situation at Entry

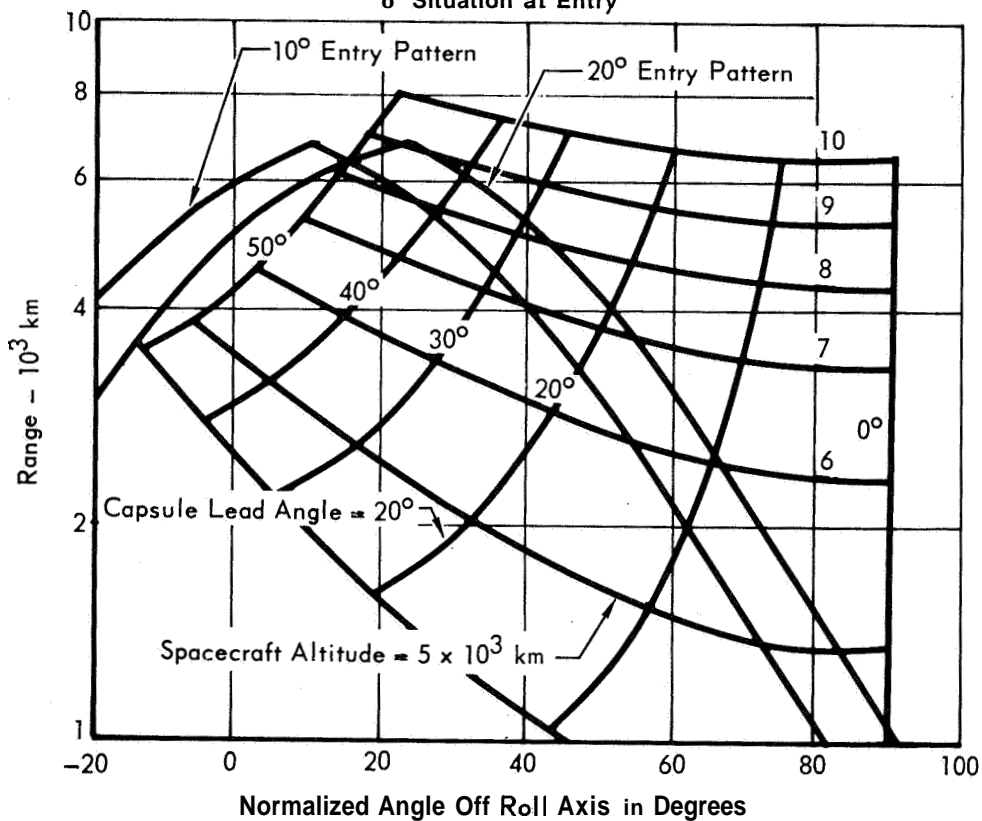


Figure 4.2-5

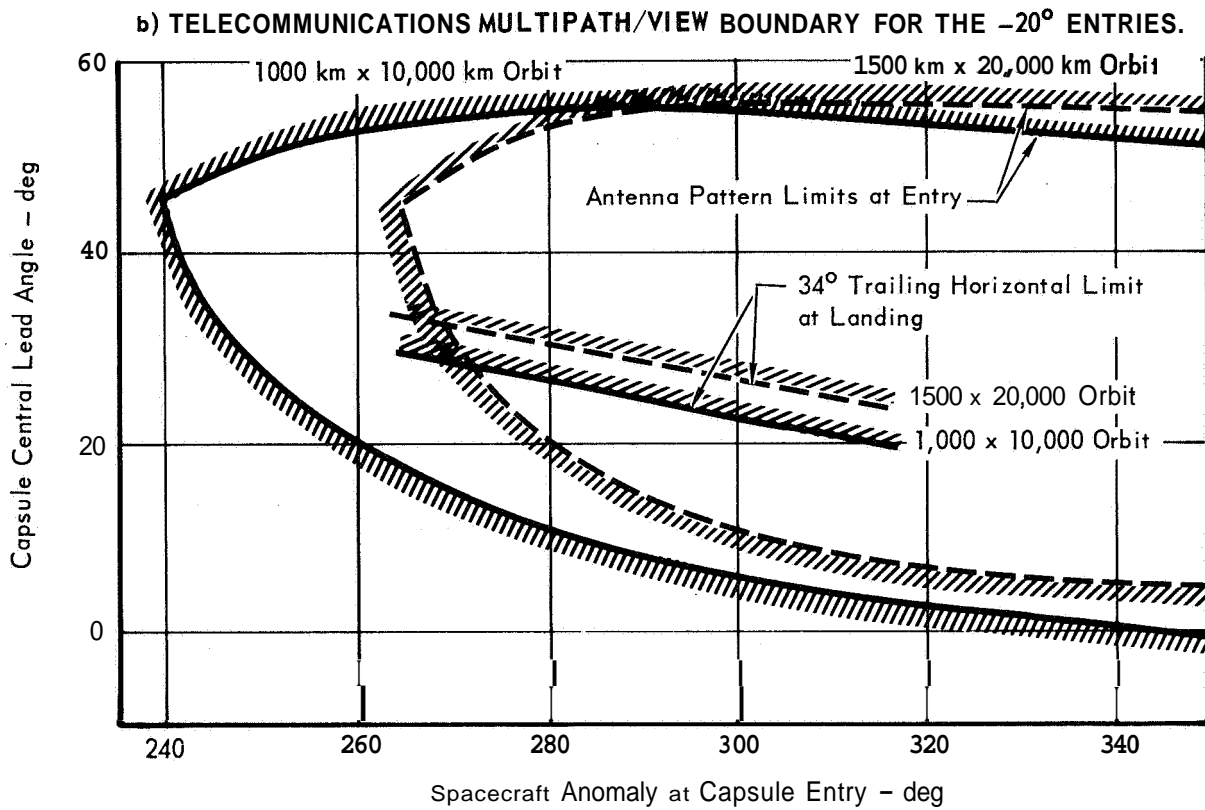


Figure 4.2-6

Measurements of Mars in 1965 (see References 4.2-2 and 3) have indicated that the average power reflectivity is 3 to 10% ($\rho = .17$ to $.32$) at 10 to 20° latitude. However, one measurement produced a reflectivity of 13% ($\rho = .36$) and greater values would certainly have been measured if greater resolution were available. In these measurements, a pure sine wave was transmitted at S-band, but because of rotational Doppler the echo spanned a frequency of 7.6 kHz. Most of the reflected power was contained in a band of only 450 Hz, corresponding to reflections from a disk about 250 miles wide. The Arecibo measurements (Reference 4.2-3) noted that there is a tendency for high values of radar reflectivity to be associated with the dark region on Mars.

The measurements substantiate a reflectivity assumption of $\rho = 0.3$ at normal incidence, i.e., poor ground. From the Arecibo measurements it is evident that there is a probability of about 0.05 of experiencing a mean reflectivity of approximately 0.4 over an extended area (greater than 250 miles wide). Assuming that this reflectivity is equally probable at any latitude, there is a significant probability (0.05) that the Capsule relay will operate over this area for essentially its entire descent.

The Arecibo measurements give a mean square reflectivity (ρ^2) of 0.06 with a variance of about 0.03, assuming a normal distribution of reflectivity. If the same ratio of variance to mean square applies to the higher mean square of 0.13, then the variance would be 0.06. This would yield the following probabilities of experiencing a given reflectivity in the "worst-case" reflectivity zones.

<u>ρ^2</u>	<u>ρ</u>	<u>P(ρ)</u>
.13	.36	.5
.19	.44	.2

The fact that most power was reflected in a band of 450 Hz implies that a reflection with a specular component can be expected. As pointed out by RCA, Reference 4.2-4, surface roughness cannot be ignored and results in a Rayleigh-distributed scatter reflection component. Hence the reflection can, in general, be expected to consist of a specular plus scatter component.

Given the bounding orbits, the antenna characteristics, and the surface reflection coefficients, the direct (D) to indirect (J) path geometry ratios may be defined. The D/J ratio is the summation of the delta free space loss (A FS), the delta antenna gains (A AG) and the surface reflectivity (A RC). Figure 4.2-7 gives the bounding D/J histories. Note that the most severe multipath (lowest D/J) occurs immediately

GEOMETRY ADVANTAGE HISTORY

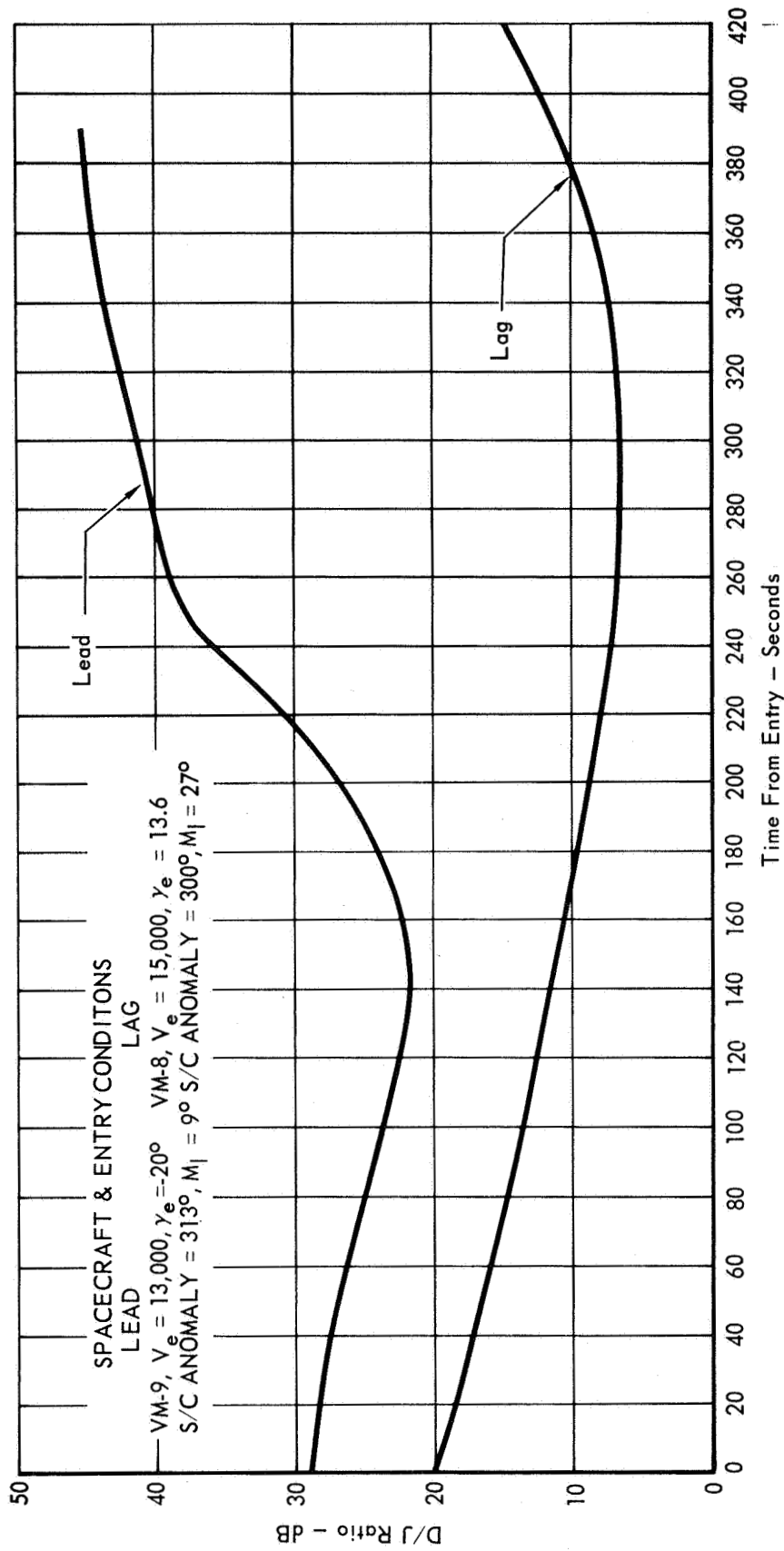


Figure 4.2-7

after plasma blackout. This is the period when the most significant entry package data occurs, and where the spacecraft borne bit synchronizer must reacquire synchronization. This is also the time during which the blacked out delayed storage bits are transmitted.

Modulation Selection - Several modulation techniques were considered for use on the Entry Science Package relay link. Noncoherent FSK operating with a wideband nontracking receiver was selected because of its simplicity and predictable performance in a multipath environment.

Five basic judgements were made in the selection of a modulation technique for the capsule bus link, as follows:

- a. Coherent or non-coherent modulation
- b. Wideband or narrow-band tracking receiver
- c. Choice of specific modulation technique
- d. Bit synchronization techniques
- e. Use of diversity

Coherent modulation techniques are approximately 2 to 3 dB more efficient than non-coherent in a non-fading environment. However, several other factors negate this efficiency advantage in a multipath environment.

The most critical period of operation for the link will be immediately after termination of radio black-out during entry. At this time, the strength of the interfering signal received via planet reflection will be strongest due to a disadvantageous attitude of the capsule. At the same time the receiver must acquire frequency and time synchronization with the signal. The reflection will be offset 3 to 5 kHz in frequency. As it is likely that the reflected signal will contain a strong specular component, there is a possibility that a phase-lock receiver would acquire the reflection instead of the direct signal. It is conceivable that anti-interference lock circuits could be designed, but these circuits would add an objectionable amount of complexity and might interfere with the acquisition of the direct signal.

In summary, phase coherent methods such as PSK and PSK/PM have been ruled out because of the possibility of locking to a strong reflection signal at the critical instant of acquisition after black-out ends. A non-frequency tracking receiver is preferred for reliability and rapidity of acquisition at this critical time. Hence non-coherent FSK or MFSK is preferred. The battery weight savings for 4 FSK is offset by the additional weight of oscillators. In addition, the receiver would be more complex with a different bit sync regeneration method required. For an M greater

than 4, weight savings diminish further. Hence the preference for the more simple and reliable method indicates binary FSK as the best choice.

The bit synchronizer must recover a timing signal, from either the data signal itself or some separate part of the signal designed specifically for this purpose, and use this timing signal as a reference in the data channel of the synchronizer.

In the situation where a signal is corrupted by both thermal noise and multipath interference the thermal noise affects the signal in the same manner as it would in the absence of multipath. The multipath signal can be considered to be additional noise which is partially coherent with the signal. In the VOYAGER situation the multipath signal and the desired signal seen at the detector output have virtually identical frequencies (generally much less than 1 Hz separation), but a random phase relationship. Therefore, the approach is to distinguish between the two on the basis of phase rather than frequency. This is accomplished by the use of a gate analogous to a range gate in radar applications.

An experimental investigation was performed to determine the effects of multipath interference on bit synchronizer performance. The laboratory system was of a hybrid nature in that the effects of the multipath environment on an envelope detected 2-level, frequency shift keyed (FSK), split-phase signal were simulated by digital computer. By means of digital to analog conversion the video output of the digital computer was passed into bit synchronization equipment for processing. The bit synchronization equipment in this study consisted of a commercially available general purpose bit synchronizer and a special purpose bit synchronizer, designed to give superior performance in the multipath environment as discussed in the previous paragraph.

Preliminary results of this simulation are shown in Figure 4.2-8 together with a theoretical analysis of that noise environment from Reference 4.2-5. The figure presents theoretical curves discussed in the Effects of Multipath Interference paragraph, as well as the measured error rate curves for the cases where a noisy signal feeds both the data channel and the timing circuits and where a noisy signal feeds the data channel with the timing information derived from an identically filtered clean signal.

Three types of diversity are applicable to the relay link; polarization, time and frequency. Space diversity is not applicable because the differential Doppler wavelength is excessive. Polarization diversity is not useful because the two signals are dependent and the statistics of the signals are not identical, see Reference 4.2-4.

MULTIPATH SIMULATION DATA

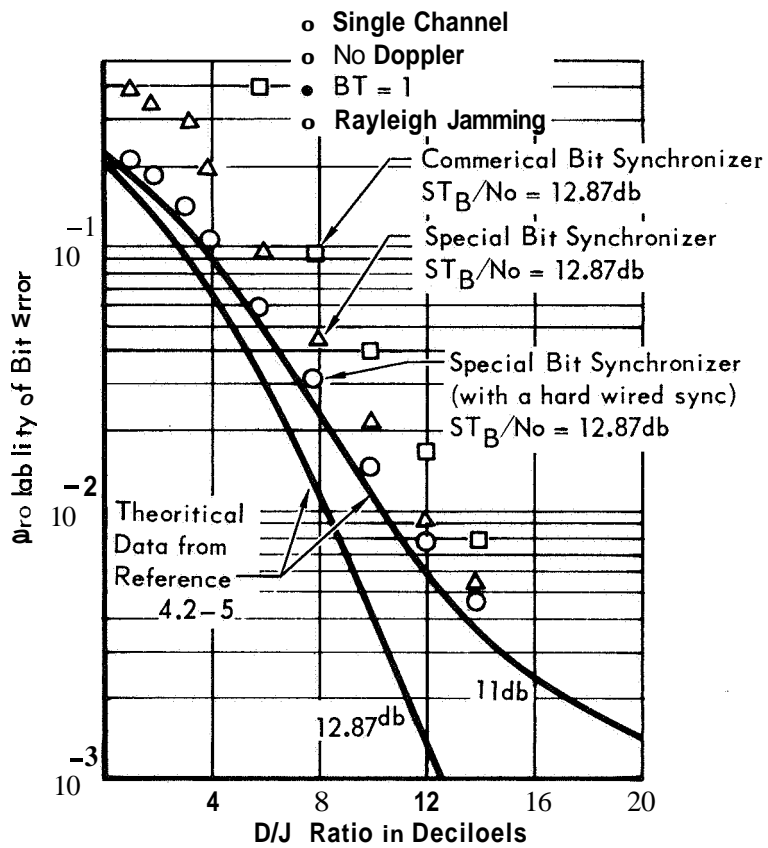


Figure 4.2-8

Polarization selectivity will be useful, but this would require a priori knowledge of the reflection coefficient history. This knowledge is not available, particularly due to the wide range of possible atmospheres.

Time diversity is not employed per se, as a long time delay is being employed to combat the entry ionization blackout. In order to use this plasma delay as an effective diversity system, the real time bits must be stored and combined with the delayed bits prior to bit detection. Due to the long time delay inherent in the plasma blackout and the associated differential Doppler, effective use of time diversity is not possible. A non-optimum usage of the dual delay storage is practical however. Since each bit is transmitted 3 times, except those absorbed during blackout, the times between these transmissions (50 sec and 100 sec) are sufficiently long that fading can be considered independent. After bit decoding on the ground, the 3 bits corresponding to a given information bit may be extracted and a majority decision rule may be used, thus decreasing the resultant effective error probability

Frequency diversity is an appealing consideration, particularly since an "extra" transmitter also adds to the reliability of the link in addition to combatting multipath interference.

Effect of Multipath Interference - The first section of the multipath analysis identified the character of the geometry problem, and described how bounds were drawn about it. The second section discussed the factors significant in the selection of a modulation technique. A non-coherent FSK system was chosen. This section serves to identify the specific effects of the multipath geometry upon the candidate modulation system, and finally to formulate bit error histories.

Three approaches have been taken to identify the effect of the multipath interference upon the modulation; they are compared in Figure 4.2-9. The first approach is a purely signal strength approach and is adequately documented in References 4.2-4 and 4.2-6. A serious disadvantage to the signal-strength-only analysis is a lack of direct feeling for the error history, and an in-depth description of the influence of the interference upon the modulation technique.

The second approach is an extension of the techniques of References 4.2-7 and 4.2-8 and is documented in Reference 4.2-9. The significant character of the Martian multipath environment may be termed fast fading which results in intersymbol interference. The rate of fading of the indirect path is classically slow relative to a bit period, however the differential path length is great, thus the received indirect path signal may change bit state "independent" of the received direct path signal.

A COMPARISON OF APPROACHES

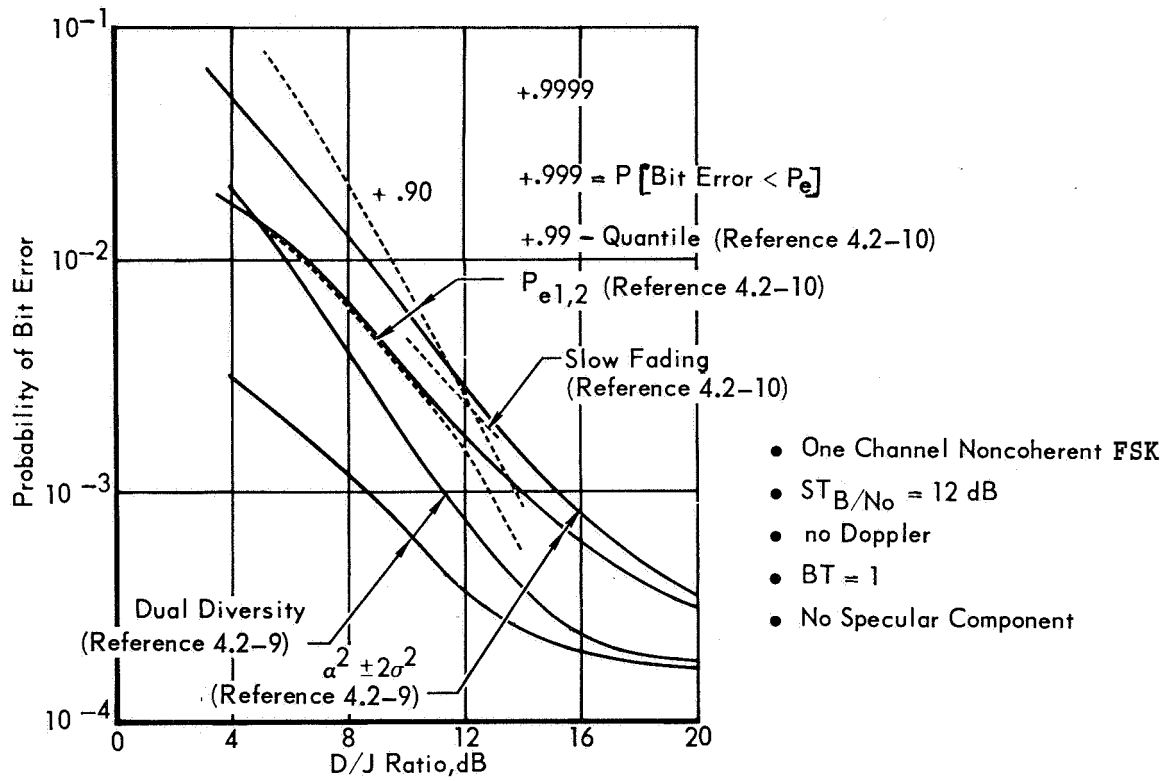


Figure 4.2-9

The third, and most sophisticated approach, is documented in Reference 4.2-10. Two channel models are studied. The first assumes that the delay in the indirect path length relative to the data bit is small so that, except for producing a phase variation, such a delay can be ignored, i.e., a mark-mark situation (P_{e1}). The second model assumes the delay in the indirect path length relative to the data rate is greater than one bit so that it is reasonable to assume the direct and reflected path transmissions are uncorrelated, i.e., a mark-space situation (P_{e2}). Evaluation of the performance for both channel models bounds the performance of the real channel for the total time that the relay is in operation.

Figures 4.2-10 and 4.2-11 combine the D/J histories developed in the geometry section with the bit error degradations of this section and result in a bit error history.

It is seen that the use of diversity "gains" approximately 25% of total battery power. The required transmitter in the frequency diversity case is then 4 dB less than the non-diversity counterpart to achieve the same error rate.

BIT ERROR HISTORY

SPACECRAFT & ENTRY CONDITIONS
 VM-8, $V_c = 15,000$ fps, $\gamma_e = -13.6^\circ$,
 FSC Anomaly 300, $M_1 = 27^\circ$

LEGEND:
 - - - Mark-Space Interference
 ——— Mark-Mark Interference

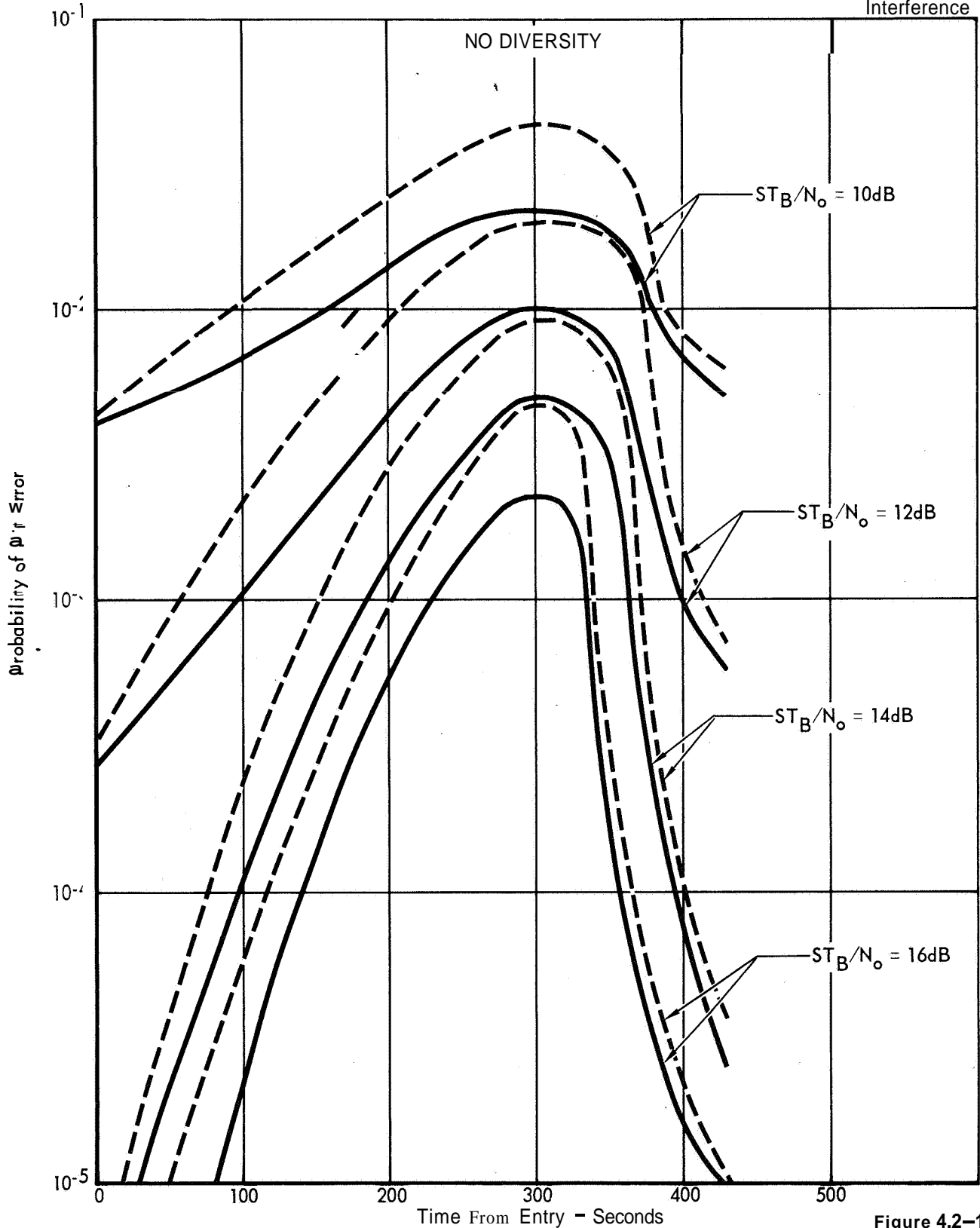


Figure 4.2-10

BIT ERROR HISTORY

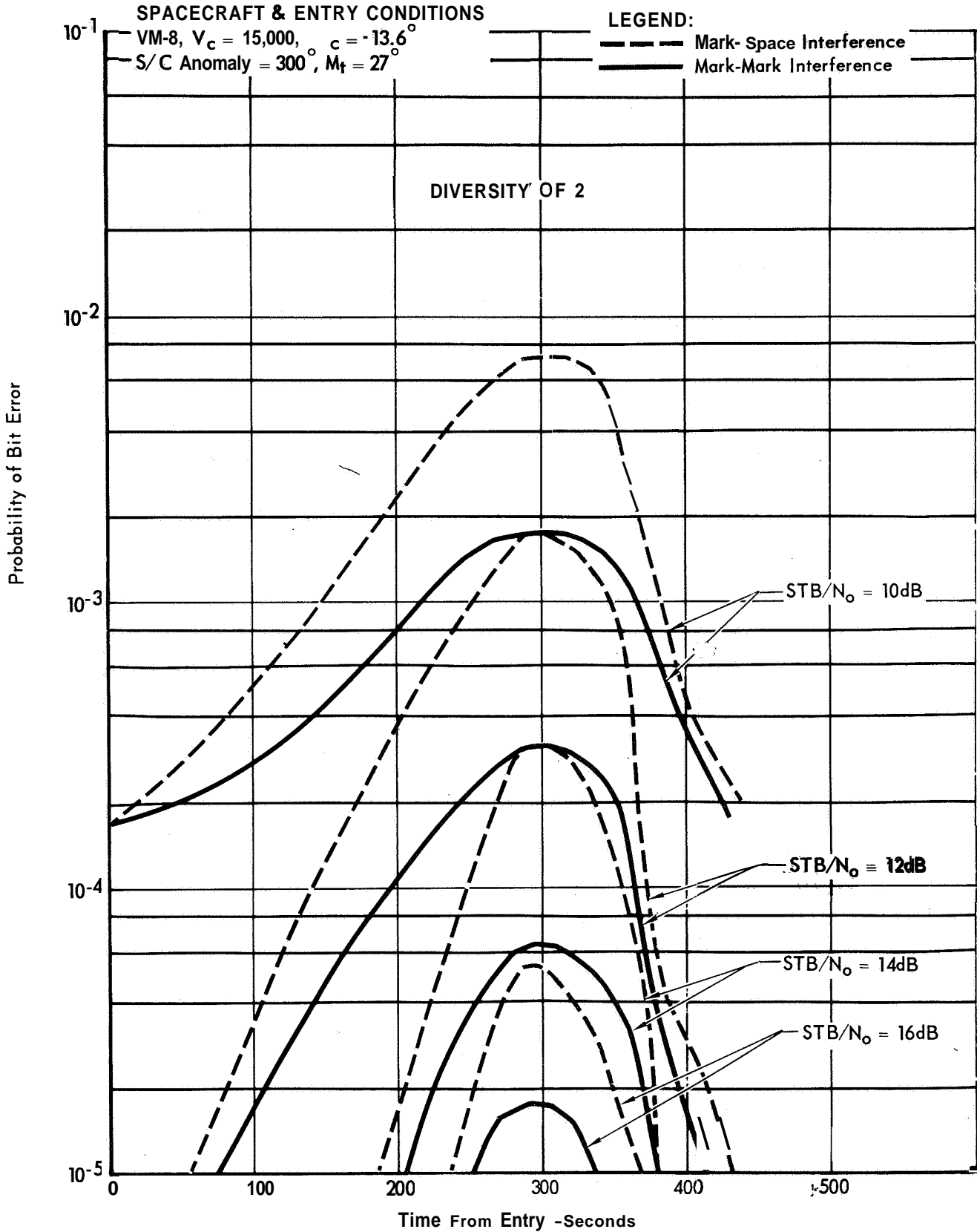


Figure 4.2- 11

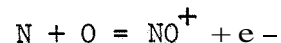
4.2.1.2 Entry Ionization Analysis - The first phase of a detailed blackout analysis for Martian entry has been performed, in which the pertinent parameters affecting the flow field prediction and the resulting telecommunication degradation have been examined. The analysis included predictions of blackout conditions due to atmospheric gases for the model atmospheres, a worst case sample calculation accounting for the effect of ablation gases, and an estimate of the cost to minimize the blackout times.

Conclusions drawn from this Phase B VOYAGER study on entry blackout are:

- a. The maximum blackout time is less than 150 seconds; the minimum time from end of blackout to impact (without terminal propulsion) is more than 60 seconds.
- b. Atmospheric gases in the model atmospheres which contain nitrogen will ionize easily and cause atmospheric blackout; atmospheres devoid of nitrogen will only cause short blackout periods and then only for fast steep entries.
- c. Ablation products will cause blackout for velocities and altitudes where blackout does not exist due to the atmospheric gases and worsen the blackout caused by atmospheric gases. The metallic elements in the heat shield material cause the high ablation gas ionization levels.
- d. An S-band telemetry system will have much shorter blackout times than a VHF system.
- e. Seeding with sulphur hexafluoride in a quantity of less than one percent can cut the ablation ionization fifty percent.

Martian Atmospheric Blackout - Maximum blackout duration exists between the time of shock formation and the time the vehicle velocity drops below a velocity in the vicinity of 10,000 fps. The actual times of beginning and ending blackout depend upon the transmitting frequency and the atmospheric composition, which are analyzed in this section.

The 100%CO₂ of model atmospheres VM-2 and VM-8 do not ionize as easily as air, and thus blackout is not as probable for those atmospheres. In air, ionization is principally due to the reaction.



This same reaction exists for Martian atmosphere models in which nitrogen and oxygen are present. But the other model atmospheres depend primarily on the ionizing reactions involving CO⁺ and O⁺, which require more energy than NO⁺ to form; consequently, the plasma sheath is quite tenuous for these atmospheres.

The ionization in the wake region is found by expanding the Capsule Bus electron concentration from the stagnation density to the free stream density. This is the frozen far wake approximation.

Since the collision frequencies are low, the plasma for blunt body entry vehicles is a high pass filter to the transmission waves from the entry vehicle.

Effects of Ablation Products on Wake Conditions - The effect of ablation gases upon the wake ionization is an important consideration for a plasma blackout analysis. The analysis presented here is based on the maximum heating condition - the steep entry into the VM-3 atmosphere listed in Figure 4.2-12 because this presents the trajectory-atmosphere condition for the greatest heating rate. The factors in this analysis are:

- a. The heating rate distribution and the resulting total ablation mass loss rate for a typical silicone elastomer ablator.
- b. The shock shape and inviscid flow properties on the heat shield.
- c. The boundary layer temperature ablation mass fraction, and the equilibrium ion concentrated profiles.
- d. The shear layer location and its density and temperature profiles.
- e. The electron concentration in the wake resulting from the boundary layer and shear layer conditions.

The VOYAGER antenna system is mounted on the base of the vehicle. In this position, the antenna experiences minimum heating. The transmitted signals are directed into the wake, where they are less likely to be blacked out, as the flow field geometry, Figure 4.2-12 illustrates. The boundary layer gases, which contain the ablation products, expand rapidly as they pass the base of the vehicle and feed the shear layer. It is in the shear layer that ablation products interfere with communications.

The first step in the analysis was to calculate heating and ablation rates. For the GE ESM 1004X preferred ablator, peak heating and peak ablation occurs at an altitude of 200,000 feet and a velocity of 23,000 ft/sec; ablation occurs for about 80 seconds, ceasing at an altitude of about 110,000 feet. All the candidate

WORST CASE CALCULATION CONSIDERATIONS

Entry Conditions

Atmosphere VM-3
 Velocity 15,000 ft/sec
 Angle -20
 Altitude 800,000 ft

Trajectory Point

Time 120 seconds
 Altitude 200,000 ft
 Velocity 13,000 ft/sec

FLOW FIELD GEOMETRY

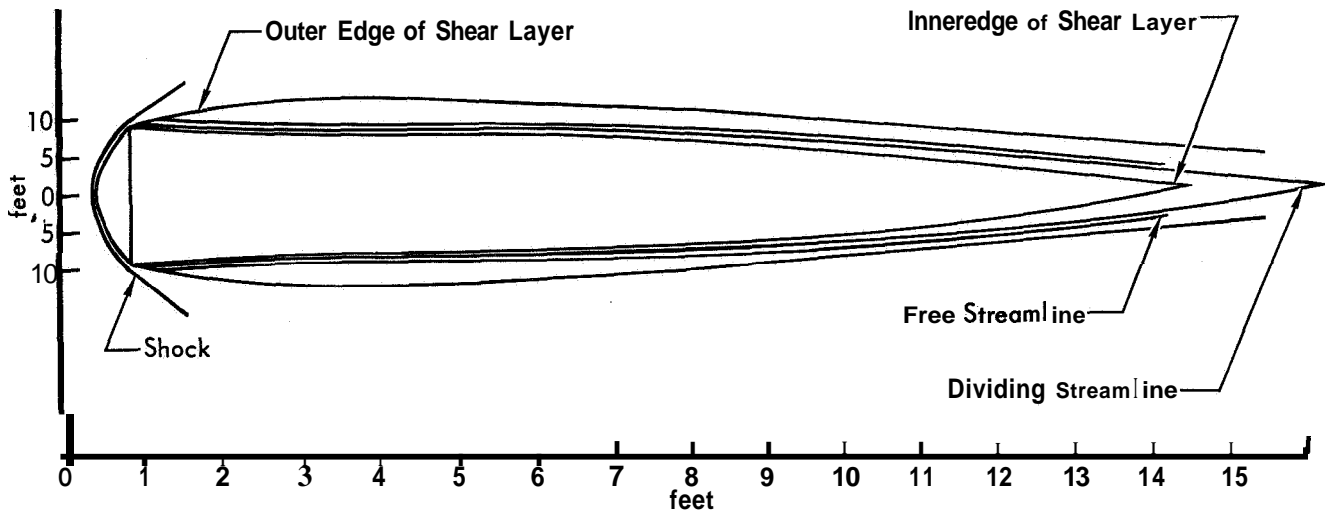


Figure 4.2-12

4-3s

ablator materials are composed of a silicone elastomer base; so the heating rate distribution, calculated by Eckert's reference enthalpy method, and the ablation rates, by a McDonnell computer program for the GE ablator are considered typical.

The second step was to calculate the inviscid flow field by a stream tube method (Reference 4.2-11). The shock shape was taken as a spherical bow shock merging into a conical shock. At the base of the vehicle, the entropy layer gases generated by the spherical shock are merged with the boundary layer. The inviscid flow properties are constant and equal to the properties of a ~~VM3~~ atmosphere across a conical oblique shock.

Step three was to employ the ablation rate data and the inviscid flow properties to calculate the boundary layer characteristics. The boundary layer properties were calculated for a mixture of ablation and atmospheric gas. Near the wall the ablation concentration and temperature vary widely and approach the inviscid flow conditions about 1.0 inch from the wall.

From the temperature, mass fraction, and pressure the multicomponent equilibrium composition profiles were calculated for some 70 gas species. The composition of the ablation gas was calculated from non-charred (virgin) material compositions taking into account the data on preferential elements loss from MDC S-3 material tests (Reference 4.2-12). The non-charred material and the ablation gas composition for the MDC S-3 and GE ablators are derived from tests presented in Figure 4.2-13. The aluminum in the GE material determined the electron concentration in the boundary layer as seen from the figure for the conditions used.

The fourth step in the wake flow field analysis was to determine the gas properties in the shear layer. The location of the shear layer was determined by the method of characteristics.

The expansion was made from the inviscid flow properties (which were constant from the boundary layer edge to the shock) to a wake base pressure of two lbs. per square foot (which was estimated from experimental data on other blunt shapes). The calculated free streamline where the pressure equals the base pressure was used as a reference condition in the shear layer analysis.

The shear layer properties were calculated by the method of Dennison and Baum (Reference 4.2-13). The effect of the recirculating flow was neglected by limiting the boundary layer gases to the shear layer above the dividing streamline. Thus, all the boundary layer gases passed directly into the neck of the wake. The profiles of temperature and density at different stations along the dividing streamline are shown in Figure 4.2-14. The figure shows that neither the density nor the

ABLATOR CONFIGURATION

(% By Weight)

ELEMENT	MDC S-3 MATERIAL		G.E. MATERIAL	
	VIRGIN	ABLATOR GAS	VIRGIN	ABLATOR GAS (EST.)
Silicon	26.82	19,355	37.6	26.65
Carbon	25.63	50.57 1	286	40.64
Hydrogen	5.80	14,705	7.12	19.9
Oxygen	34.802	11.296	23.92	8.55
Magnesium	0.5 4	.473	-	-
Boron	0.2	0.142	-	-
Aluminum	0.56	0.74	2.76	4.26
Potassium	1.14	0.768	-	-
Calcium	0.058	0.01 7	-	-
Titanium	4.23	1.933	-	-

BOUNDARY LAYER IONIZATION PROFILES GE ABLATOR

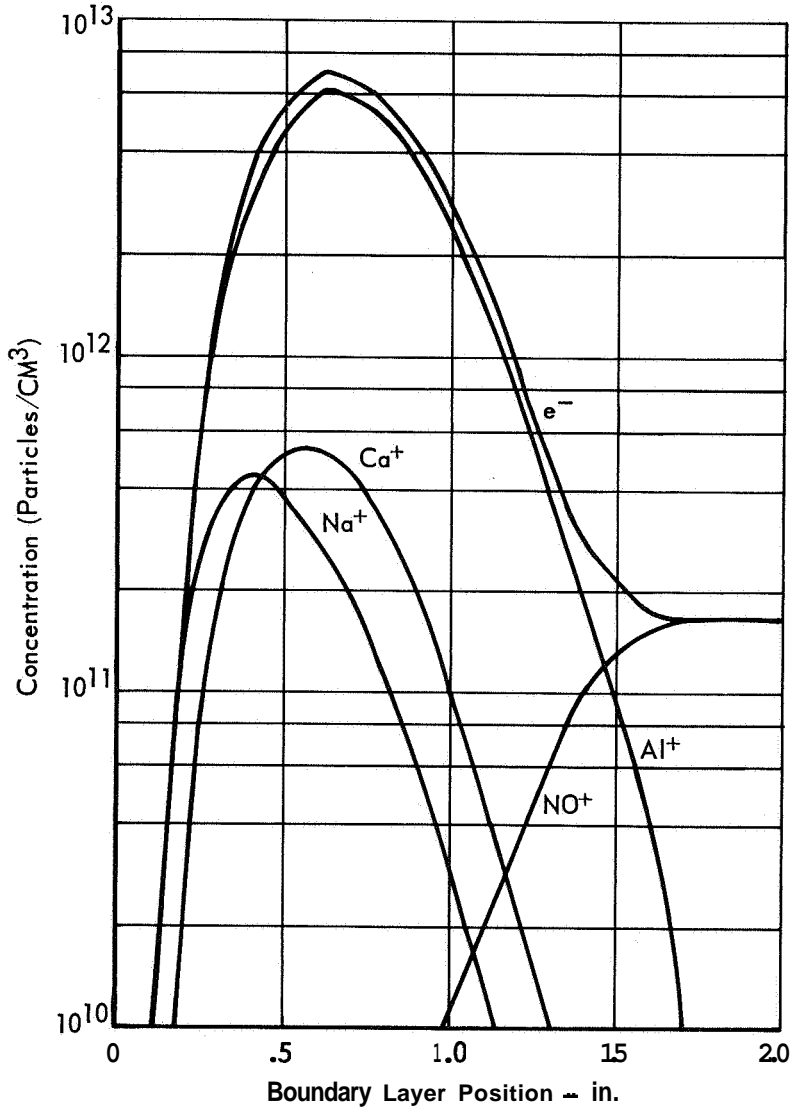
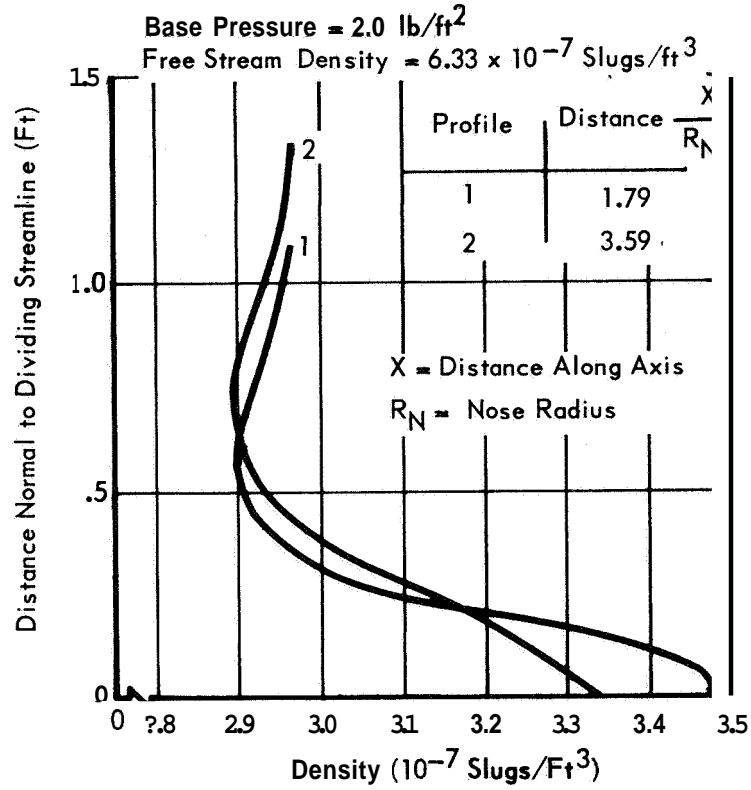


Figure 4.2-13

VOYAGER SHEAR LAYER DENSITY PROFILES



VOYAGER SHEAR LAYER TEMPERATURE PROFILES

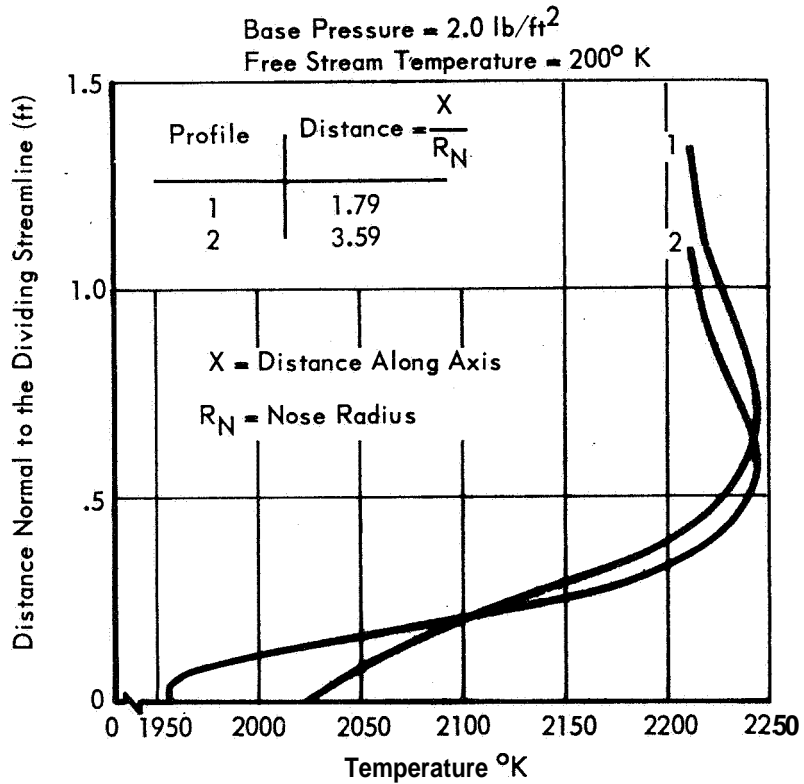


Figure 4.2- 14

temperature varies appreciably across the shear layer.

The final step was to calculate the plasma properties in the wake. The characteristic reaction lengths indicate that the aluminum recombination reaction in the wake is frozen, because it requires a three body mechanism. On the other hand, the nitric oxide ion, because it is a two body recombination mechanism, is almost in equilibrium. This calculation also shows that equilibrium is a good assumption for the boundary layer.

Since the reaction rate of the principal ion source is frozen, the ionization levels decrease as they pass through the wake due to expansion and diffusion. Figure 4.2-15 gives electron concentration profiles in the boundary layer and at several positions in the wake. The peak electron concentration decreases from 9×10^{12} electrons per cm^3 at the capsule base to 3×10^{11} in the neck of the wake. Neglecting the effects of the ablation gases and higher recombination rates for the NO^+ ion, the atmospheric ion concentration minimum is only about 7×10^9 electrons per cm^3 .

This detailed wake electron concentration calculation shows that the ablation gases cause a minimum plasma frequency of 4.9 GHz which will cause blackout and frequencies below C-band. Neglecting the effect of ablation gases the minimum plasma frequency is only 750 MHz, causing VHF but not S-band blackout. From this calculation it is seen that the frozen far wake approximation predicts a slightly higher plasma frequency (1250 MHz) for the atmospheric gases. The effect of ablation is sufficient to cause blackout for conditions which are not normally blacked out for atmospheric gases, e.g. for worst case trajectory-atmosphere investigated the ablation products increase the electron density from 1.7×10^{11} e/cm, to 7×10^{12} e/cm³.

Alleviation - When the ablation products cause the blackout a promising technique for reducing the electron concentration in the VOYAGER wake is the use of seedants. For effectiveness, they must be delivered to the wake regions of highest electron concentration. When the blackout is due to atmospheric gases, the inviscid flow contains the peak electron concentrations and seedants are not effective in reducing this ionization.

Experiments were performed to determine the effect of various chemical seedants in reducing electron concentration. Water and sulphur hexafluoride were each evaluated in a radio frequency generated CO_2 plasma. The experiment shows that seeding with less than 1.0 percent of sulphur hexafluoride (SF_6) reduces the electron concentration by 40 percent. Further increasing the amount of seedant does not significantly reduce the electron concentration.

PLASMA PROFILES IN THE WAKE

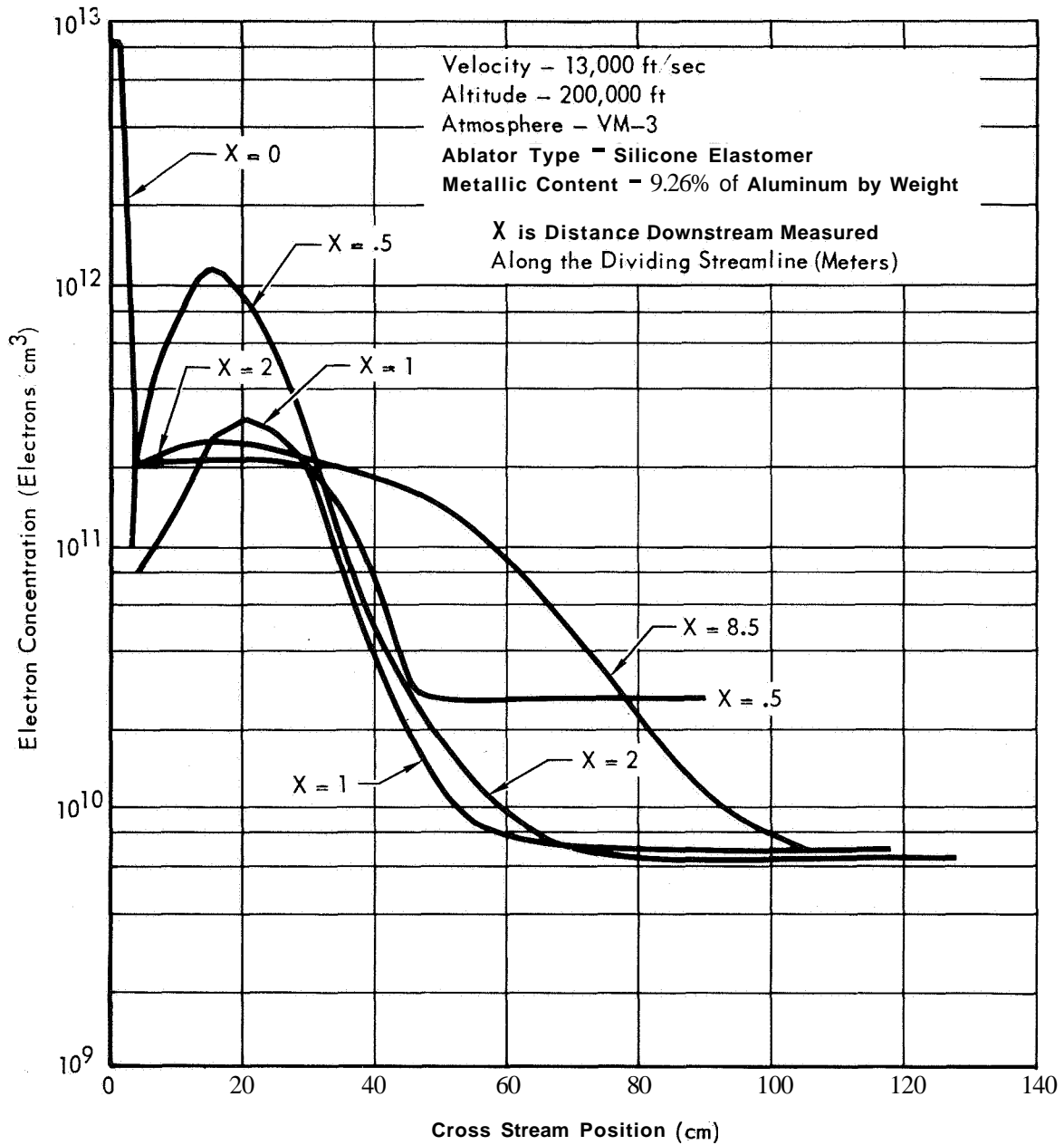


Figure 4.2-15

Sulphur hexafluoride attacks free electrons. This reaction is fast so that the seedant would be effective in reducing the electron concentration on the VOYAGER wake even though the combination reactions are frozen. If only a **small** reduction in electron concentration is needed to restore communications, seeding can be effective in creating a window through the plasma.

Summary - During the descent stages of the VOYAGER mission, the communications between the ESP and the S/C will be blacked out for a significant time. The blackout time depends on the Martian atmospheric composition, the initial trajectory conditions, the transmission frequency, and the heat shield material used. A blackout time is predicted for each of the 10 atmospheres, for each of the four limiting entry trajectories under the following assumptions:

- o Blackout will begin under worst case conditions at the altitude where viscous heating begins in the boundary layer of the shock.
- o Blackout will typically end by the time the entry vehicle slows to 10,000 fps.

These assumptions give a worst case estimation of the blackout time, tabulated in Figure 4.2-16. The post blackout time is also shown, during which the communications system must re-transmit the blackout data prior to impact. (This time is assumed for the case with no terminal deceleration).

The maximum blackout time is 145.9 seconds, thus the maximum interleaving delay must be at least 145.9 seconds. (See Section 4.2.2.1). The minimum post blackout view time is 67 seconds, thus if a 145.9 second delay were used, all of the data would not be played back for this trajectory. A "tap" is employed then at a maximum of 67 seconds, i.e. a "second" delayed data bitstream is required to insure that **all** of the blacked out data is played back.

It would also be advantageous to "minimize" the tap length to achieve an order of time diversity during the worst case multipath condition, i.e., post blackout. In other words, the multipath time may be said to "reduce" the post blackout time. The minimum tap length is set by the 27.2 second blackout condition, however, a maximal delay playback of 145.9 seconds would "miss" this point. The design (rounding off) maximum delay is then 150 seconds with a 50 second tap. The combined effect of the atmospheric and ablation gases causes a blackout in each model atmosphere. The time delay design will allow all data to be received at least one time during the entry mode.

BLACKOUT COMPUTATIONS (FROM TRAJECTORIES)

TRAJECTORY IDENTIFICATION	(i) TIME FIRST BEGIN DECREASE VELOCITY	(ii) TIME AT 10 Kfps (SEC)	(iii) TIME OF IMPACT (SEC)	(iv) (i - ii) B.O. TIME (SEC)	(v) (ii - iii) POST B.O. TIME (NO TERMINAL DECELERATION) (SEC)
1. VM-1, 15,000 fps, -20°, 0.3	69.2	139	280	69.8	141
2. VM-1, 15,000 fps, -13.6°, 0.3	109.0	226	444	117.0	218
3. VM-1, 13,000 fps, -20°, 0.3	77.8	144	286	66.2	142
4. VM-1, 13,000 fps, -10.4°, 0.3	163.1	309	553	145.9	244
5. VM-2, 15,000 fps, -20°, 0.3	124.7	152	248.5	27.3	96.5
6. VM-2, 15,000 fps, -13.6°, 0.3	221.4	283	446	61.6	163
7. VM-2, 13,000 fps, -20°, 0.3	136.9	163	255	26.1	92
8. VM-2, 13,000 fps, -10.4°, 0.3	330.4	407	587	76.6	180
9. VM-3, 15,000 fps, -20°, 0.3	66.0	133	310	67.0	177
10. VM-3, 15,000 fps, -13.6°, 0.3	104.3	217	466	112.7	249
11. VM-3, 13,000 fps, -20°, 0.3	74.3	140	316	65.7	176
12. VM-3, 13,000 fps, -10.4°, 0.3	154.9	295	573	140.1	278
13. VM-4, 15,000 fps, -20°, 0.3	121.7	150	269	18.3	119
14. VM-4, 15,000 fps, -13.6°, 0.3	213.8	285	461	71.2	176
15. VM-4, 13,000 fps, -20°, 0.3	133.8	161	277	27.2	116
16. VM-4, 13,000 fps, -10.4°, 0.3	319.3	403	599	83.7	196
17. VM-5, 15,000 fps, -20°, 0.3	61.6	129	343	67.4	214
18. VM-5, 15,000 fps, -13.6°, 0.3	96.2	209	493	112.8	284
19. VM-5, 13,000 fps, -20°, 0.3	69.7	136	348	66.3	212
20. VM-5, 13,000 fps, -10.4°, 0.3	144.0	283	595	139.0	312
21. VM-6, 15,000 fps, -20°, 0.3	112.6	149	302	36.4	153
22. VM-6, 15,000 fps, -13.6°, 0.3	193.2	262	482	68.8	220
23. VM-6, 13,000 fps, -20°, 0.3	124.3	157	308.8	32.7	151.8
24. VM-6, 13,000 fps, -10.4°, 0.3	289.5	372	615	82.5	243
25. VM-7, 15,000 fps, -20°, 0.3	72.6	140	257	67.4	117
26. VM-7, 15,000 fps, -13.6°, 0.3	115.0	234	429	119.0	195
27. VM-7, 13,000 fps, -20°, 0.3	81.6	144	260	62.4	116
28. VM-7, 13,000 fps, -10.4°, 0.3	164.9	307	541	142.1	234
29. VM-8, 15,000 fps, -20°, 0.3	125.4	153	220	27.6	67
30. VM-8, 15,000 fps, -13.6°, 0.3	222.8	288	435	65.2	147
31. VM-8, 13,000 fps, -20°, 0.3	137.7	163	236	25.3	73
32. VM-8, 13,000 fps, -10.4°, 0.3	332.2	412	580	71.8	168
33. VM-9, 15,000 fps, -20°, 0.3	60.2	125	385	64.8	260
34. VM-9, 15,000 fps, -13.6°, 0.3	93.8	200	528	106.2	328
35. VM-9, 13,000 fps, -20°, 0.3	67.9	132	392	64.1	260
36. VM-9, 13,000 fps, -10.4°, 0.3	140.1	272	630	131.9	358
37. VM-10, 15,000 fps, -20°, 0.3	103.8	140	345.8	36.2	205.8
38. VM-10, 15,000 fps, -13.6°, 0.3	173.1	250	515	76.9	265
39. VM-10, 13,000 fps, -20°, 0.3	115.0	150	353	35.0	203
40. VM-10, 13,000 fps, -10.4°, 0.3	259.3	355	641	95.7	286

Figure 4.2- 16

4.2.2 Telemetry Subsystem - The most significant analysis of the telemetry subsystem design is presented in this section including commutation, data format, reliability analysis, and instrumentation.

4.2.2.1 Commutation - The Commutator portion of the telemetry subsystem involves data sampling (digital, analog and bi-level) and analog to digital conversion. This section presents a summary of the alternate multiplexing techniques considered for use in the ESP telemetry subsystem, and the analysis used to optimize the gate treeing. As used in this section the term, multiplexing, includes the functional operations of gating and channel sequencing (programming).

Both whole number and modified pulse-width analog converters were considered. The whole number converter was chosen for reasons of both data source interface and multiplexer programmer simplicity.

The basic multiplexer configurations were compared in a trade study to determine the best configuration for the ESP telemetry subsystem. Multiplexer configurations similar to previous Mariner telecommunications systems are characterized as "hardwired" configurations in this study. The alternate configuration studied is the stored-program configuration which uses electrically alterable memory for multiplexer programming. The multiplexer configurations are insensitive to the type of whole-number converter chosen, so the converter design is not a parameter of the study.

Since there are numerous ways of mechanizing each type of configuration, attempts to optimize each configuration were made during the study to achieve maximum trade-off effectiveness. Accomplishing this goal required detailed analyses of analog and digital circuit devices and memory techniques. The device evaluation indicated that bipolar integrated circuits (IC's) should be used for all digital applications and hybrid or MOSFET IC's for analog (linear) circuits. The storage devices trade study concluded that core or plated-wire memories are preferred for medium-size storage applications such as the stored programmer memory.

Multiplexer Configuration Trade Study - Criteria used to compare the hardwire and stored-program multiplexers included reliability, physical, versatility, and program management considerations. The failure rate in percent per 1000 hours is used as the measure of reliability in this trade study. Because of its direct effect on the mission probability of success, reliability was assigned the highest relative weighting value of 0.4.

Physical considerations included weight, power requirements and the number of

wires required to cross the CB/ESP interface; their relative importance is reflected in an assigned weighting value of **0.3**. The methodology employed to compute a single value for system performance including the multiple considerations was as follows:

- (1) Compute a relative performance value in terms of: (a) weight, (b) power and (c) interface wires.
- (2) Average the three performance values computed in (1) above to achieve a single value.

Versatility was assigned a value weight of 0.2; the two basic considerations were system ability to accept design changes with minimum hardware modification and limited re-programming prior to separation from the S/C.

Program management considerations such as cost and development risk are important but not considered applicable to this trade study since neither system appears to have an advantage over the other.

A summary chart for the multiplexer configuration trade study is presented in Figure 4.2-17. The stored-program multiplexer configuration is selected from the trade study results.

Multiplexer Techniques Trade Study - Since the multiplexer configuration trade study resulted in the selection of the stored-program configuration for the baseline system, only the multiplexer trade study for the hardwired configuration is summarized, with the major emphasis placed on the stored program Configuration.

Hardwired Multiplexer - Three multiplexing techniques were evaluated for the hardwired configuration: ring counter, matrix programming and interlaced tube. The ring counter and matrix programming techniques have been used in past and present systems. The interlaced tube programming method, a relatively new technique, is described in the next section.

Criteria used for hardwired multiplexer evaluation, in order of decreasing importance, are reliability, physical parameters (size, weight, power, etc.), performance and flexibility. The trade study indicated that the matrix programmer was best in all categories except performance, where the interlaced tube method provides a somewhat better sample efficiency. The ring counter method ranked lowest in all categories. The matrix programmer was selected for use with the hardwired system.

Stored Program Multiplexer - In the stored-program configuration the multiplexer programmer is a stored program sequencing unit. As a result of an

ESP TRADE STUDY SUMMARY, MULTIPLEXER SELECTION (EP ALTERNATE 3b)

Functional and Technical Design Requirements: Sampling, ADC and Data Interleaving	MATRIX OF DESIGN APPROACHES		Selected Approach: No. 2
	1 - Hardwire	2 - Stored Program	
Trade Considerations Reliability Weight = 0.4	.34 λ (%/1000 hrs) = 11.01	.4 λ (%/1000 hrs) = 9.42	2 - 1
Physical Considerations Weight = 0.3	.28 Number of Wires = 4 Weight = 3. lbs Power = 4.4 w	.21 Number of Wires = 11 Weight = 4.2 lbs Power = 3.4w	1 - 2
Versatility Weight = 0.2	.16 ● Reprogramming involves hardware modifications. ● No in-flight programming possible	.2 ● Some software reprogramming possible. ● Some in-flight programming possible.	2 - 1
Total	0.78	0.81	

Figure 4.2- 17

4-4s

optimization study, random-select FET analog gates were selected for **use** with the stored-program Sequencing. Therefore, the difference between the techniques discussed below is confined to memory and channel address logic. The three programming techniques evaluated for the stored-program telemetry configuration are multiple access, table look-up and interlaced tube.

Multiple-Access Program - The multiple-access programming technique has been used predominately in stored-program decommutator stations and recently has been adopted for the Titan III and Poseidon PCM telemetry systems. The technique is easily implemented and efficient in core utilization. The multiple-access terminology is derived from the need to access memory two or more times for all subcommutation frames (i.e., first-level subframes required two memory accesses; second-level sub-subframes required three memory accesses, etc.).

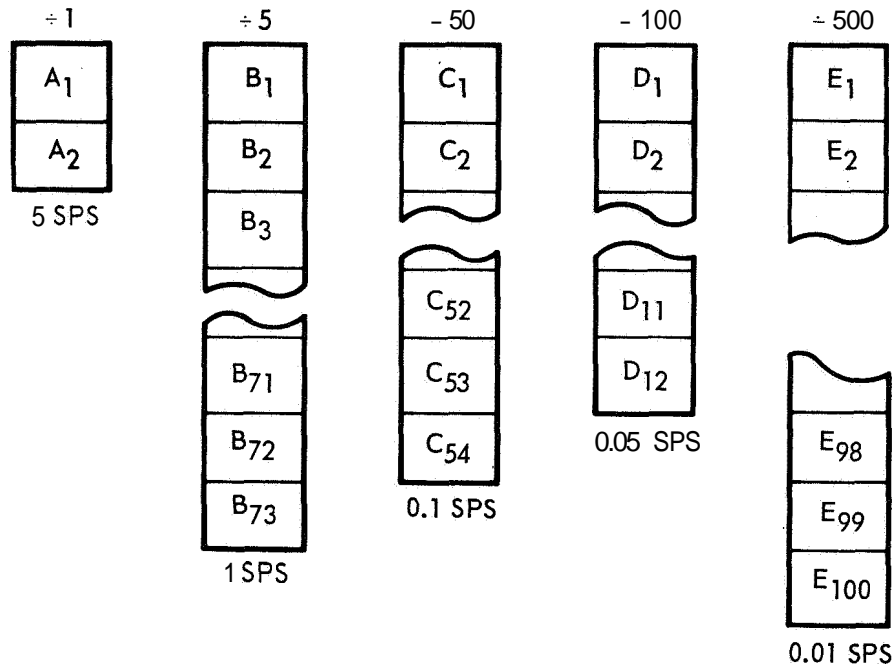
One additional flag bit per memory word is required to indicate when the content represents a subframe memory location rather than a channel address. A special memory-position index number is used at the end of each frame to reset the subframe instruction in the appropriate higher-level frame. Some scratch pad is required for storage of the pointers for each rate group. Core memory programming is easily accomplished by listing channel addresses and index number in order of sequence and sampling frequency.

Look-Up Table Program - In terms of logic operations, the look-up table program technique is the simplest form of stored program sequencing but it requires large memory capacity. Programming is achieved simply by listing all channel addresses in order of major frame sequencing, repeating channel numbers as required until the major frame is complete.

Storage capacity is determined by the length of the major frame which is the product of the maximum frame lengths within each commutation level, assuming that all frames within a given subcommutation level are even multiples of the longest frame within that level. If this condition is not met, it will be necessary to take the product of all frame lengths within the multiplexing pattern. Under such conditions, the major frame length can exceed the time duration of the lowest rate subframe. In any case, memory required to satisfy the ESP multiplexing is extremely large using this technique.

Interlaced Tube Program - The interlaced tube programming technique is similar to the multiple-access programming technique described above since it also requires scratchpad and special index instructions. Figure 4.2-18 is an example of an arbitrary multiplexing format produced by the interlaced tube.

INTERLACED TUBE FORMAT EXAMPLE



$$S_{mf} = 9000 \text{ Samples/Major Frame}$$

$$S_{pf} = \frac{S_{mf}}{500} = 18 \text{ Samples/Prime Frame}$$

$$\text{Sample Rate} = 18 \times 5 = 90 \text{ SPS}$$

Frame No. 1	A ₁ , A ₂ , B ₁ , B ₂ , B ₃ , B ₄ , B ₅ , B ₆ , B ₇ , B ₈ , B ₉ , B ₁₀ , B ₁₁ , B ₁₂ , B ₁₃ , B ₁₄ , B ₁₅ , B ₁₆
Frame No. 2	A ₁ , A ₂ , B ₁₇ , B ₁₈ , B ₁₉ , B ₂₀ , B ₂₁ , B ₂₂ , B ₂₃ , B ₂₄ , B ₂₅ , B ₂₆ , B ₂₇ , B ₂₈ , B ₂₉ , B ₃₀ , B ₃₁ , B ₃₂
Frame No. 5	A ₁ , A ₂ , B ₆₅ , B ₆₆ , B ₆₇ , B ₆₈ , B ₆₉ , B ₇₀ , B ₇₁ , B ₇₂ , B ₇₃ , C ₁ , C ₂ , C ₃ , C ₄ , C ₅ , C ₆ , C ₇
Frame No. 6	A ₁ , A ₂ , B ₁ , B ₂ , B ₃ , B ₄ , B ₅ , B ₆ , B ₇ , B ₈ , B ₉ , B ₁₀ , B ₁₁ , B ₁₂ , B ₁₃ , B ₁₄ , B ₁₅ , B ₁₆
Frame No. 500	A ₁ , A ₂ , B ₆₅ , B ₆₆ , B ₆₇ , B ₆₈ , B ₆₉ , B ₇₀ , B ₇₁ , B ₇₂ , B ₇₃ , E ₉₄ , E ₉₅ , E ₉₆ , E ₉₇ , E ₉₈ , E ₉₉ , E ₁₀₀

Figure 4.2-18

The construction simplicity of these formats is clear. For purposes of this description, a major frame represents the total number of samples required to sequence through all data sources and a prime frame is the least number of samples required before a data source is repeated (determined by the highest sampling frequency within the data ensemble).

The interlaced-tube format is constructed by first listing all measurements in groups (tubes) of descending sampling frequency as shown in Figure 4.2.-18. The number of major frame samples, S_{mf} , is determined by:

$$r_{\max}$$

where: r = sampling rate of a given rate group.

N_r = number of samples in the r^{th} rate group, and
 r_{\min} = lowest sampling frequency.
 r_{\max} = highest sampling frequency..

The number of prime frame samples, S_{pf} , is:

$$S_{pf} = S_{mf} \frac{r_{\min}}{r_{\max}}$$

The system sample rate in sps is, of course, $S_{pf} (r_{\max})$. If the prime frame is not an integer number of samples, spare channels must be added in any desired combination to meet this requirement. Although this constraint is similar to other multiplexing techniques, it should be noted that the interlaced-tube procedure generally requires fewer spares, resulting in greater sampling efficiency. Under no condition will it result in reduced efficiency over the other techniques considered.

The channel sequence format produced by the tube method shown in Figure 4.2-18 is generated as follows:

During the first prime frame, the two 5-sps plus the first sixteen 1-sps channels are sampled. During the second prime frame, the two 5-sps plus pins 17 and 32 of the 1-sps channels are sampled. During the fifth minor frame, the two 5-sps and last nine pins of the 1-sps plus the first seven pins of the 0.1-sps channels are sampled. The next five prime frames will be identical to the above sequence except that pins 8 through 14 of the 0.1-sps tube will be sampled during the tenth frame. This procedure

continues until the five-hundredth prime frame; at this time the last seven pins of the 0.01-sps tube are finally sampled. The sequence then repeats.

Stored-Program Trade - The results of the Stored-Program trade study are presented in Figure 4.2-19. The criteria used in the evaluation are physical parameters, reliability, flexibility, and performance. Reliability is weighted the heaviest, followed by physical parameters (power and weight), performance and flexibility in that order. The weighting factors used were 0.4, 0.3, and 0.2 and 0.1 respectively.

Due to inefficient memory utilization, the look-up table programming technique suffers in both physical parameter and reliability grading. Although the identical logic algorithm can be used for both interlaced-tube and multiple-access techniques, multiple-access does require a few more words in storage (this difference is too small to be observed in the grading numbers).

Because all addresses associated with the higher sampling rate groups are repeated many times in the look-up table memory, programming of software changes become considerably more difficult than with the other techniques. Programming for the multiple-access techniques is slightly more complicated because of the extra jump instructions required and can become considerably more complicated if super-commutation (cross-strapping) is required. Performance is confined to the improved sampling efficiency of the interlaced tube. Look-up table is given a higher ranking than multiple-access since it is possible to program the look-up table with a tube format; however, programming would be further complicated.

Interlaced-tube programming is selected for the stored-program configuration since it is ranked highest under all criteria.

Commutator Reliability Considerations - Detailed reliability analysis of a commutator design concept was conducted, Reference 4.2-14 and methods determined by which the reliability can be maximized. The methods consist of incorporation of a combination of multi-channel cooperative and circuit block redundancies. Analysis results are directly applicable to the VOYAGER commutator design concept.

The basis for the analysis was elimination of critical single point failures, improvement of fail-safe design features and maximization of total and partial probability of successful commutator operation.

A generic PCM commutator and encoder design is shown in Figure 4.2-20

TRADE STUDY SUMMARY, HYBRID MULTIPLEXER

CRITERIA	MATRIX OF DESIGN APPROACHES			SELECTION 2
	NO. 1 LOOK-UP TABLE	NO. 2 INTERLACED TUBE	NO. 3 MULTIPLE ACCESS	
Physical Weight - 0.3	Power, 11.5 Watts Weight, 10 lb .05	Power, 2.4 Watts Weight, 1.5 lb .3 .4	Power, 2.4 Watts Weight, 1.5 lb .3 .4	2-3-1
Reliability Index Weight = 0.4	19 .27	28 28	28	2-3-1
Flexibility Weight - 0.1	Maximum number of software modification to accommodate single measurement change. .02	Simplest to change .2	Easy to change. More difficult programming required if cross-strapping is used. .09	2-3-1
Performance Weight - 0.2	Low sample efficiency unless tube format used. .15	Good sample efficiency .2	Low sample efficiency .1	2-1-3
Total Grading	0.49	1.0	0.89	

Figure 4.2-19

GENERIC PCM COMMUTATOR AND ENCODER BLOCK DIAGRAM

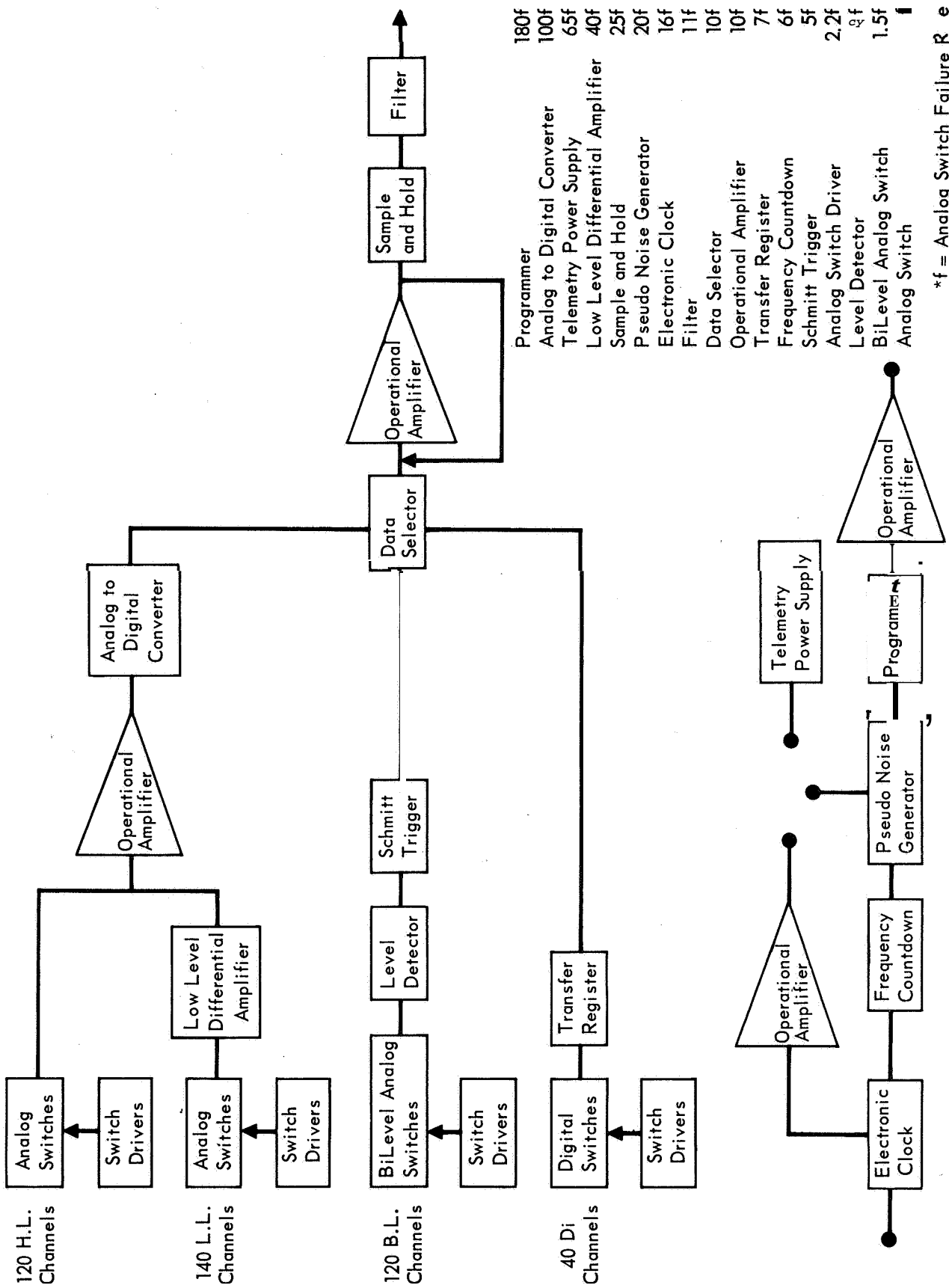


Figure 4-2-20

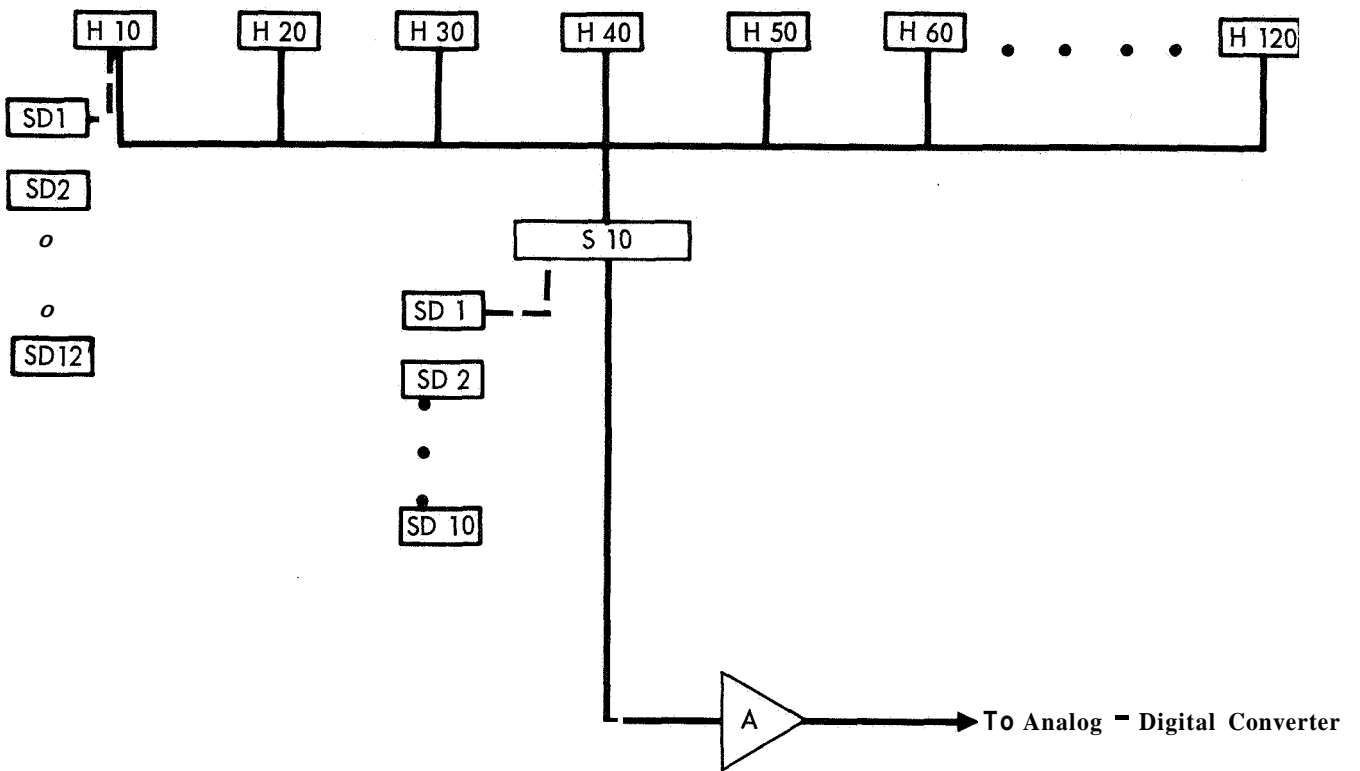
which contains the basic elements for operation and handling of High Level (HL), Low Level (LL), BiLevel (BL) and Digital (D) groups of input data signals. The generic design assumes a standard time division multiplexing method of sampling and gathering input data signals for presentation to a transmitter modulator. All data switches were assumed to be Junction Field Effect Transistors (JFET).

In the analysis, the 120 HL analog data channel group was analyzed and designed as shown in Figure 4.2-21. The reliability of this design was estimated for retrieval of total data, a subgroup (deck) of data and for an individual data channel. A detailed reliability analysis of the generic design was conducted to optimize the design reliability and is shown in Figure 4.2-22, which is the optimum arrangement of data channels which inherently contains multi-channel cooperative redundancy and maximized probability of partial data retrieval. The basis for the analysis and analysis results are as follows: The basic JFET data switch was assigned a failure rate (f). All other elements were assigned an effective failure rate expressed as some multiple of (f). Different data channel arrangements were analyzed and the comparative reliability was estimated for each arrangement. Results are shown in Figure 4.2-23.

Limited circuit block redundancy was added in the most critical switching decks, namely decks F5, T5 and S5 in that order as shown in Figure 4.2-24. This addition optimizes total data retrieval probability at minimum expense of part increases.

The reliability of a PCM Commutator data channel group has been maximized by incorporation of multi-channel-cooperative and limited block redundancy and is the recommended design approach for the telemetry commutator. The multi-channel cooperative redundancy feature essentially decentralizes the first level of analog data switches for optimum reliability and data switch independence in event of any switch failure. Further decentralization from that shown in Figure 4.2-24 however reduces probability of partial and total data channel retrieval for the 120 data channels considered.

HIGH LEVEL ANALOG SIGNAL GROUP



Notes:

1. H10 - First Level Switch Deck (Subgroup) containing 10 Analog Switches.
2. S10 - Second Level Switch Deck containing 10 Analog Switches.
3. SD1 (Switch Driver) Drives all switches in Subgroup H10.
4. Another SD1 drives the first position switch in Deck S10.

Figure 4.2-21

OPTIMIZED CHANNEL ARRANGEMENT
 (120 CHANNELS SPLIT INTO 4 INDEPENDENT GROUPINGS, 5 CHANNELS/SUBGROUP)

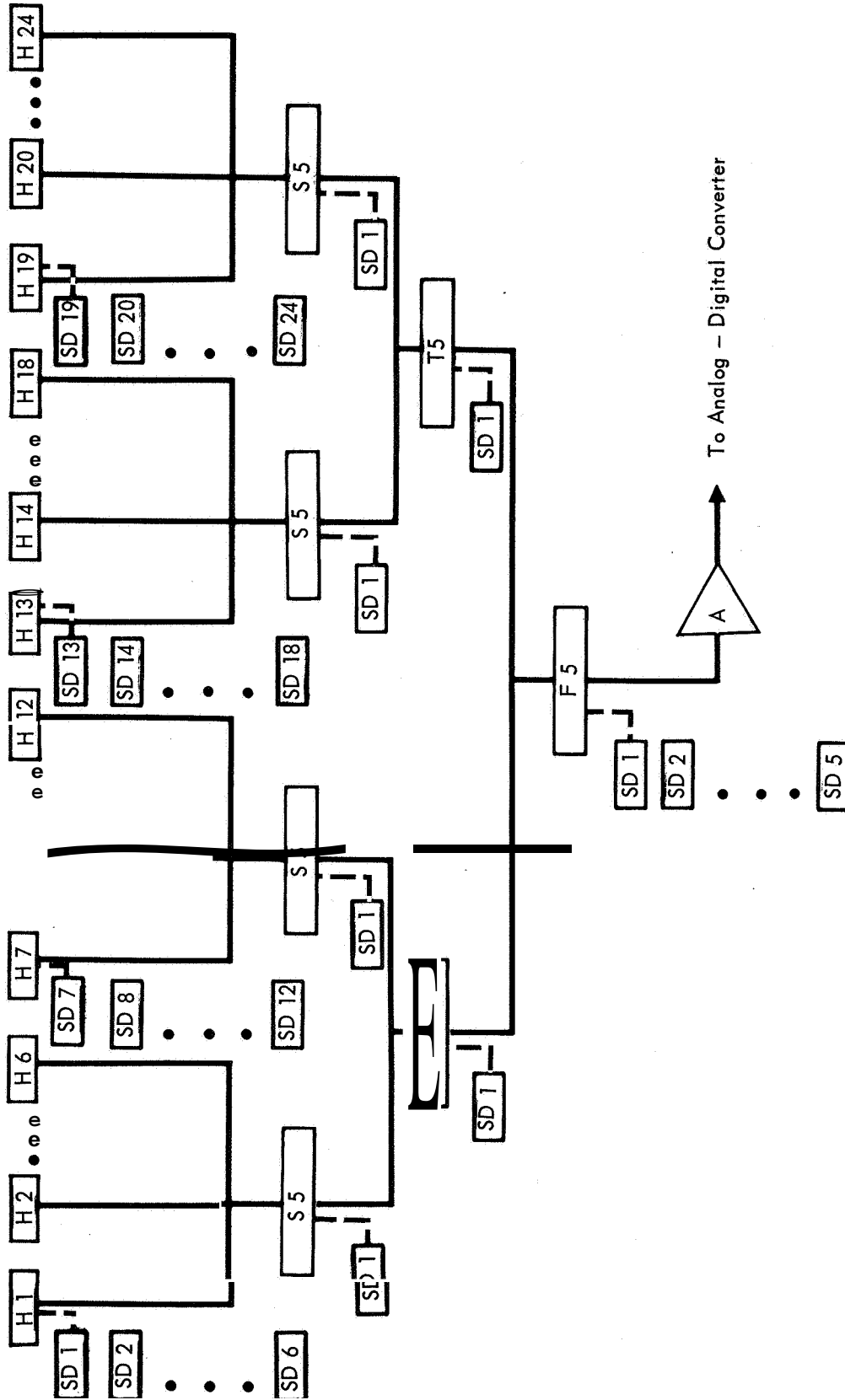


Figure 4.2-22

HIGH LEVEL ANALOG DATA GROUP RELIABILITY SUMMARY

GENERIC DESIGN	GROUP	SUBGROUP	CHANNEL	REMARKS
10 Channels/Subgroup	235f	204f	78f	First level data group divided into independent halves First level data group divided into independent fourths Redundant F5 and T5 analog switches switch drivers and programmer sequencers Redundant S5 analog switches, switch drivers and programmer sequencers
6 Channels/Subgroup	248f	201f	91f	
15 Channels/Subgroup	245f	221f	82f	
8 Channels/Subgroup	238f	201f	82f	
12 Channels/Subgroup	237f	210f	78f	
10 Channels/Subgroup	264f	148f	68f	
5 Channels/Subgroup	315f	107f/5 Channels	60f	
5 Channels/Subgroup	271f	214f/10 Channels	34f	
5 Channels/Subgroup	<235f	65f/5 Channels	<34f	
5 Channels/Subgroup	<235f	130f/10 Channels	<34f	
5 Channels/Subgroup	<235f	< 65f/5 Channels	<34f	
5 Channels/Subgroup	<235f	< 130f/10 Channels	<34f	

NOTE: 1. (f) Values for the last three design configurations are cumulative and represent the optimum design approach.

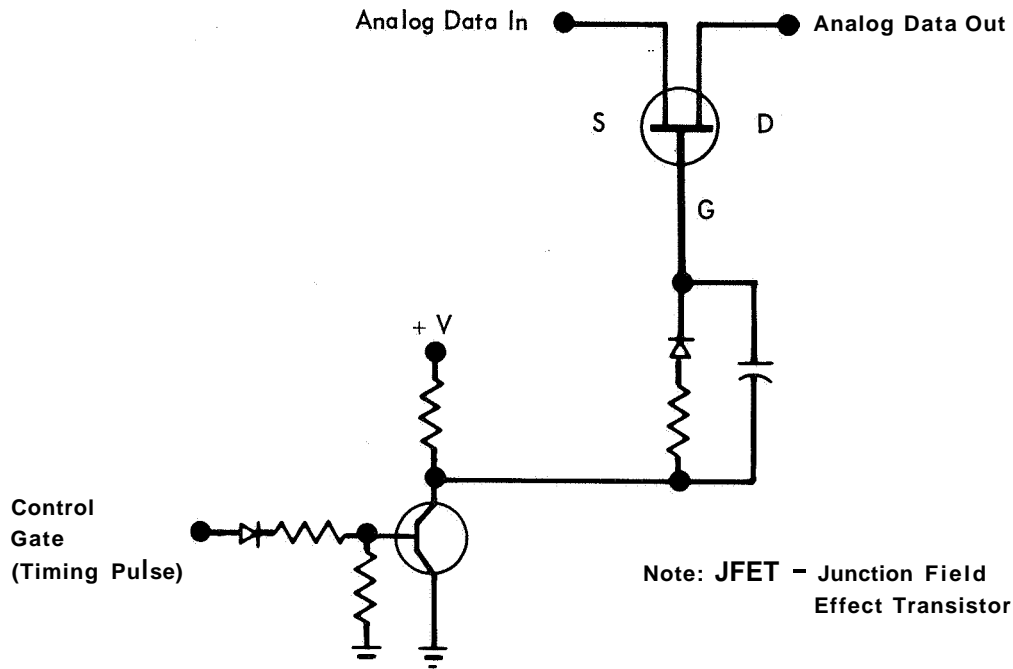
2. As the (f) values are decreased, the reliability is increased exponentially.

3. 1f is equivalent to an analog switch failure rate.

Figure 4.2-23

COMPARISON OF BASIC AND REDUNDANT CIRCUITRY

(a) JFET ANALOG SWITCH AND SWITCH DRIVER



(b) REDUNDANT JFET ANALOG SWITCHES AND REDUNDANT SWITCH DRIVERS

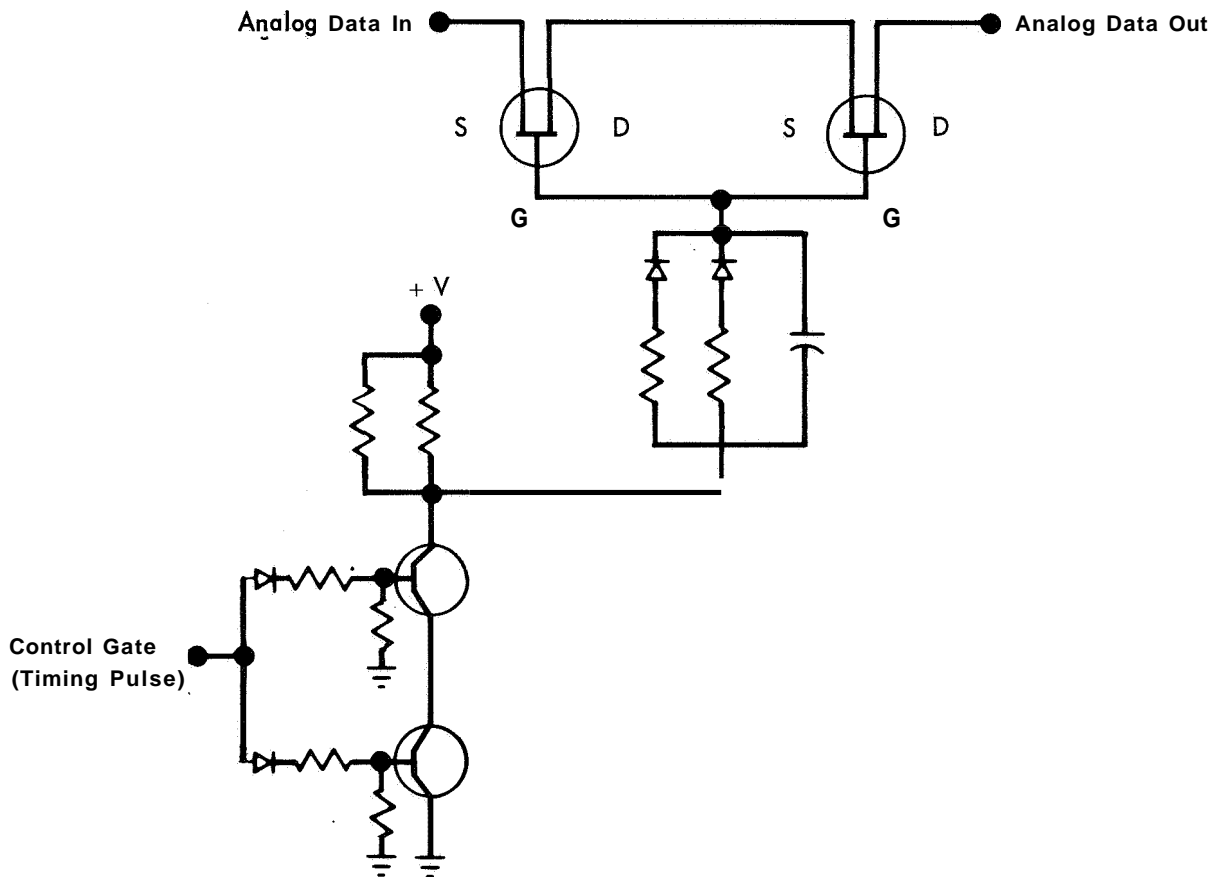


Figure 4.2-24

4.2.2.2 Instrumentation - The term "Instrumentation Equipment" is used to designate the engineering measurement portion of the ESP telemetry system, where the engineering data signals are sensed and conditioned to **outputs** compatible with the PCM encoders. This equipment consists of temperature sensors, signal conditioners and an associated power supply. Specific feasible equipment that can fulfill the ESP instrumentation requirements are reviewed.

Temperature Measurements - Preliminary requirements for 21 ESP temperature measurements have been established. The required temperature ranges are from a low of -150°F to a high of 500°F in four separate ranges as follows:

<u>o</u>	<u>Temperature Range</u>	<u>No. Measurements</u>
	25 to 150°F	4
	0 to 120°F	1
	-50 to 200°F	8
	-150 to 500°F	<u>8</u>
		21

All the temperature monitoring points are located on equipment, components, or structures and require surface type temperature sensors that can be attached to a variety of surface contours. Thermistors, platinum resistance thermometers and thermocouples are likely candidates. Platinum resistance thermometers in a conventional Wheatstone bridge arrangement are the preferred choice and were selected for the following reasons:

- a. Superior R-T characteristics for wide temperature span. (Typical span is -436°F to 1000°F).
- b. Excellent stability of calibration. (The interpolation instrument that is used from -182.97°C to 630.5°C on the International Temperature Scale is the platinum resistance thermometer).
- c. Higher output voltage than thermocouples.
- d. Output, voltage/degree, exactly as desired over wide temperature limits. (This is achieved by adjusting excitation current or bridge design).
- e. Reference junction not required.
- f. Ease of calibration. (Only a small number of calibration points are required).

Alternate bridge designs were also investigated. These were the full bridge, the half bridge, and the Mariner C single ended configuration (Ref. Figure 4.2-25). The full bridge method is preferred because common mode noise signals backed up by the lead wires are rejected by the differential amplifier in the low level commutator and

TEMPERATURE MEASUREMENT METHODS

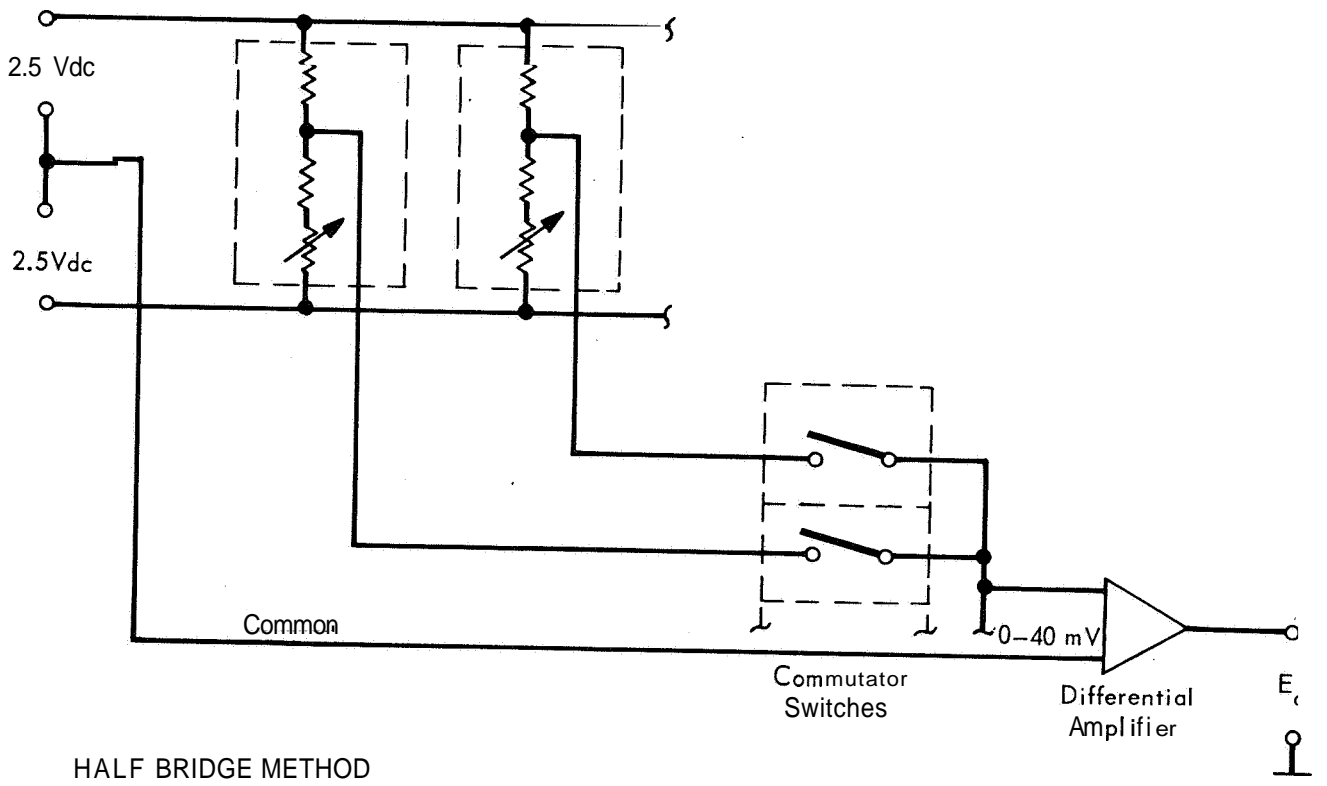
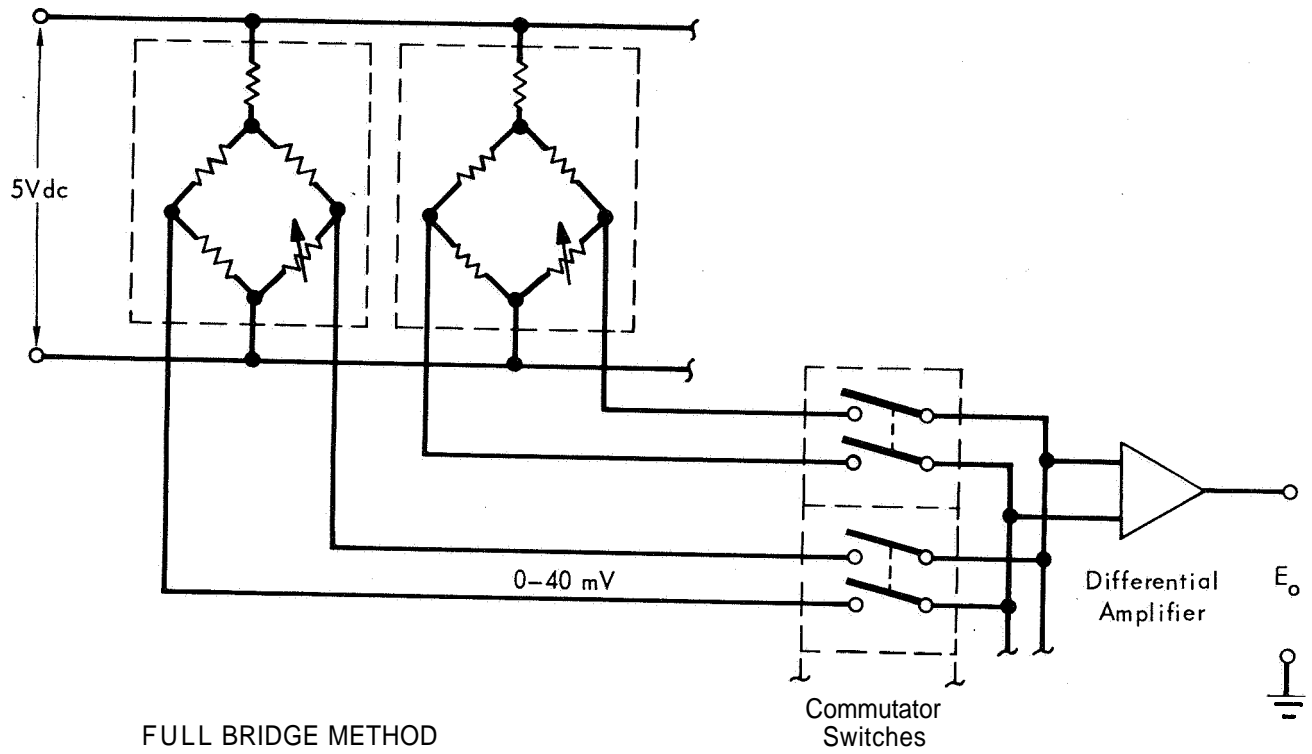


Figure 4.2-25

4-5%

lead wire voltage drop errors are minimized.

Computer calculations for a bridge design for a typical ESP temperature range were contributed by Rosemount Engineering Company and appear in Figure 4.2-26. The main consideration in designing the bridge is to provide minimum power consumption and linear 0-40 mV output using a sensing element R_o value as high as practical without introducing self-heating error. Power consumption is under 4 mW for all range sensors. The bridge completion resistors are low temperature coefficient wire wound, 5 ppm/C°, and result in negligible temperature coefficient error for the ranges involved.

Signal Conditioners - The ESP signal conditioning required includes dc current and voltage monitors.

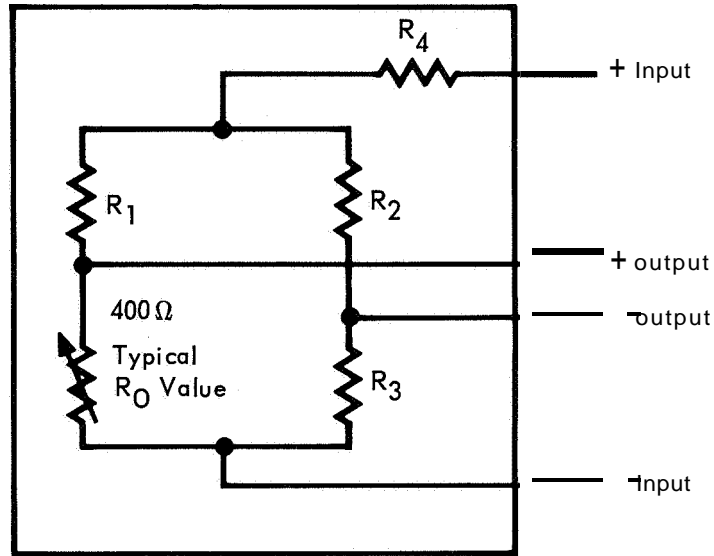
- o Current Monitoring - Two dc current measurements, ranges 0-2A and 0-6A, are now required in the ESP power subsystem. The two methods considered for monitoring dc current were calibrated shunts with amplification by the telemetry low level dc amplifier and individual magnetic amplifiers for each measurement. The shunt method results in a savings in weight and overall power consumption. The disadvantage is poor accuracy near the zero point. To a lesser degree, this is also true of the magnetic amplifiers. Shunt monitoring is capable of meeting the accuracy requirement and will be used for the battery load current measurement. A magnetic amplifier type circuit will be used for the battery charge current measurement where greater accuracy near the zero point and circuit isolation is required. The weight and power savings of using a shunt in this instance as compared to an individual magnetic amplifier is approximately 6 oz. and 0.5 watts.

- o Voltage Monitoring - Three expanded scale dc voltage measurements are now required in the ESP. The circuits needed to perform these voltage measurements utilize operational amplifiers that are well known to the industry and have been used by McDonnell in many previous aerospace applications.

4.2.3 Radio Subsystem - The most important radio subsystem trade areas are discussed in this section.

4.2.3.1 Transmitter Power Amplifier Design - Two types of 45 watt transmitters were considered. One uses an all solid-state power amplifier containing 4 transistors and hybrid combiners; the other uses a single one cavity vacuum tube (ML-2789) amplifier. The results of a trade study Figure 4.2-27 show that the most significant differences exist in the relative simplicity and reliability.

TEMPERATURE SENSOR CALCULATIONS



Schematic Diagram

TEMPERATURE RANGE	BRIDGE RESISTANCE VALUES IN OHMS				POWER REQ.	TEMPERATURE COEFFICIENT EFFECTS
	R ₃	R ₂	R ₄	R ₁		
-50° to +200°	300	9,361	7,500	10,201	1.99 MW	6.08×10^{-7} Volts

Input Required: 5 Volts

Output: 0-40 MV

Figure 4.2-26

ENTRY SCIENCE PACKAGE RF POWER AMPLIFIER CONFIGURATION

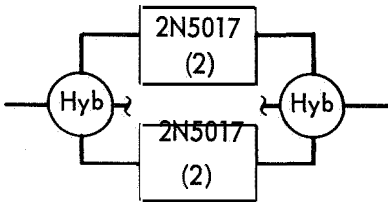
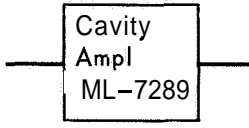
FUNCTIONAL & OPERATIONAL DESIGN REQUIREMENTS	TRANSISTOR DESIGN	VACUUMTUBE DESIGN	SELECTION	
Amplify 400 MHz or 340 MHz RF to Obtain 50 Watt Output			1	
Trade Considerations	Simplicity a. Amplifier b. Power Supply	Complex Simple	Simple Complex	2 1
	RF Drive Required	15 w	5 w	2
	Efficiency a. Amplifier b. Power Supply	60% 90%	52% 80%	1 1
	Weight Size	18 lb 30 cu in.	1.3 lb 35 cu in.	2 1
	Reliability (Including Power Supply)	More Reliable	Less Reliable	1

Figure 4.2-27

The use of the hybrid technique in the four-transistor amplifier permits conservative derating of each transistor and better thermal distribution. Tests of a breadboard model of this transmitter, including the hybrid combiners, show a 0.1 dB variation in unbalanced power over a temperature range of -16 to +100°C.

The other principal factor associated with simplicity and reliability, is the difference in dc voltage levels required. The transistor amplifier power supply is of relatively simple design and provides a regulated 28 volt output. On the other hand, the vacuum tube amplifier must utilize high voltage diodes and high voltage transformers to develop the 1000 volts required. This design is subject to higher stress and possible failure due to voltage breakdown and corona discharge.

4.2.3.2 Antenna Configuration - It is desired to operate one of the two transmitters in the CB and ESP within the exclusive 399.9 to 402 MHz band to simplify the frequency allocation problem. Assuming that a single antenna is shared by two transmitters (one from the CB and one from the ESP) separated by 1.3 MHz at 400 MHz and specifying a diplexer loss of 0.5 dB, the unloaded Q of the diplexer resonators would be 7200. Such a requirement is impractical in diplexer design for space applications. Using separate antennas sufficient isolation can be provided. The isolation requirement between antennas is based on the assumption that the maximum allowable interference signal level is approximately -30 dB from the desired signal. The required antenna isolation, I_{at} is

$$I_{at} = 30 - I_{CB} + 10 \log \frac{P_{ESP}}{P_{CB}}, \text{ or}$$

$$I_{at} = 30 - I_{ESP} - 10 \log \frac{P_{ESP}}{P_{CB}}, \text{ whichever is greater}$$

Where I_{CB} = dB isolation of CB transmitter = 20 dB

I_{ESP} = dB isolation of ESP transmitter = 0 dB

P_{ESP} = ESP transmitter power in watts = 40 watts

P_{CB} = CB transmitter power in watts = 5 watts

Therefore, the isolation between antennas shall be 20 dB minimum. However, when isolators are used in the transmitters, 10 dB isolation between antennas should be sufficient. This isolation requirement is met by employing opposite sense polarization on the CB and ESP antennas. For this reason, separate antennas for the CB and ESP were chosen for the preferred system.

4.2.3.3 Receiver System Noise Temperature - The receiving noise temperature used in the Link Power Budget is 555°, + 25°, -80°K. This derivation is summarized herein.

Antenna Noise Temperature - The antenna temperature is determined by noise sources within the beam of the spacecraft relay link receiving antenna. The principal sources are galactic noise and Martian surface radiation.

The worst case occurs when the beam is completely filled by the planet. This may occur under certain trajectory and landing site conditions. Therefore, the worst case of 283°K is used for the link calculations.

For the quiet sun conditions in 1973-75, the average incremental received noise is estimated at 2°K. Solar noise is thus ignored. During the 1977-79 noisy sun years this will not be the case, Reference 4.2-15, and solar noise will be a factor.

Receiver Noise Temperature - The receiver RF preamp utilizes a state-of-art, low noise silicon transistor, with a noise figure of less than 3 dB. (290°K)

Receiving System Noise Temperature - A line plus diplexer loss of 1.5 dB between the antenna and preamplifier input is predicted. Assuming an ambient temperature of 50°C, and an antenna temperature of 283°C, the receiving system noise temperature is 555°K. The tolerances were estimated based on previous experience.

4.2.3.4 Receiver Diversity Combining Method - The ESP S/C communications link employs frequency diversity to combat multipath degradation. The two diversity channels must be properly combined in order to realize the diversity improvement. The combiner may be either a pre-detection or post-detection device.

Pre-detection combining is more complex than post-detection combining because the received signals must be multiplied by a signal which is a function of the received signals. This necessitates complex measurement circuitry, e.g. differential phase cancellation. Furthermore, theory predicts (Reference 4.2-16) that an equal gain square-law post-detection combiner is essentially optimum for this environment.

4.2.3.5 ESP-CB Signal Compatibility - Since the ESP and CB carriers are separated by 1.3 MHz, and the ESP receiver input bandwidth is greater than 4 MHz (because of stability requirement in filter design), it is unavoidable that the ESP and CB radio signals can simultaneously enter the ESP receiver front end and mixer. The significant cross products are, however, outside the IF band and therefore no cross talk between CB and ESP signals will be detected.

4.2.3.6 Receiver Gain Stability Requirement - Since equal gain dual frequency diversity is employed, the effect of gain variations between the two receivers was briefly investigated.

From Lindsey's work (Reference 4.2-16), the difference between the single channel (zero receiver gain in one channel) and dual-channel (both receivers with equal gain) links is approximately 4 dB. This is based on a bit error probability

of 10^{-3} when the signal-to-interference ratio is 9 dB. The interference is pure Rayleigh (diffuse).

An analysis based on a simplified non-fading model predicted a loss in link performance of 0.3 dB when the differential receiver gain is 3 dB. These receiver mismatch margins are within the capabilities of the baseline design.

4.2.3.7 Receiver IF/LO Configuration - Two IF channels are required in the ESP receiver due to the frequency diversity requirement. The preferred configuration selects a common local oscillator frequency such that it lies midway between the two operating frequencies. This configuration offers the following advantages:

- o Identical IF amplifiers are used for both receivers which would facilitate gain matching between the two diversity receivers.
- o Identical LO/IF design reduces cost.
- o Standard 30 MHz IF frequency simplifies test equipment set-up and test procedure.

In this configuration, one receiver is operating on the image frequency of the other. Consequently interferences would occur if no preselectors are used. The frequency diplexer, however, serves as a means of channeling the diversity signal power from the antenna into the diversity receivers as well as providing frequency isolation. The diplexer can provide at least 60 dB isolation between channels, which is more than sufficient to avoid interchannel crosstalk.

4.2.4 Antenna Subsystem Analysis - To optimize the relay link design, antennas at each end of the link are required which not only provide adequate coverage but also optimize the gain. In this section, the antenna coverage requirements for the ESP transmitting and receiving antennas are developed from the geometry of the relay link. The rationale for the selection of specific designs is included.

4.2.4.1 ESP Antenna Subsystem - The ESP antenna subsystem must provide radiation pattern coverage only during the entry and terminal descent phases of the mission. This paragraph discusses the pattern requirements and the results of a radiation pattern study undertaken to determine antenna configuration.

Requirements - The radiation pattern coverage requirements are determined by the view angles and the range from the CB to FSC during the mission phase of intercept. If all possible de-orbit and entry conditions are considered, a large variation of FSC/CB geometry results. This geometry is constrained by the multipath considerations as discussed in Section 4.2.1.1. In that analysis thirty-four possible descent trajectories have been analyzed to determine the view angles and range from CB to FSC at the time of entry. Four typical trajectories, shown in Figure 4.2-4

indicate that the view angle at this time can be as large as 60 degrees from the negative roll axis. This requires that the antenna provide at least 160 degrees of coverage, assuming a ± 20 degree attitude uncertainty, because the CB is not roll stabilized.

In the multipath analysis a gaussian shaped pattern was selected because shaping the pattern at angles greater than 50 degrees off the roll axis is desirable to make the antenna gain in the direct path greater than that in the indirect path. The gaussian pattern, shown in Figure 4.2-4 is centered on the roll axis to provide the required coverage. In this analysis, two multipath limiting entry trajectories were analyzed in detail. The antenna coverage requirements during entry have been derived from these trajectories.

The view angles change rapidly during entry and become as large as 50 degrees off the roll axis at landing for the worst case trajectory. For the VM8 worst-case trajectory at the time of parachute deployment, the CB to FSC view angle is less than 14 degrees off the roll axis. The CB roll axis will be nearly aligned with the local vertical during this phase except for high wind gust conditions. However, the view angle in the VM9 worse case trajectory is 12 degrees from the roll axis at this time and the gaussian pattern provides 15 dB of "range" margin at this angle. A wind gust would effectively shift the pattern, and considering the "range" margin available, a large angular rotation of the pattern could be tolerated.

Antenna Pattern Study - The analysis presented in Section 4.2.1.1 made use of antenna pattern shaping to mitigate the effects of multipath radiation from the ESP transmitting antenna. A broad pattern with sharp rolloff outside the required beamwidth is desired. The pattern was assumed gaussian, centered on the -Z axis of the CB, with a 90" beamwidth in all planes containing the -Z axis. It was shown that such a pattern did satisfy the multipath constraints. The gaussian pattern also provides adequate coverage when variations of CB attitude are considered. Therefore, a test program has been conducted to achieve the desired pattern with a realizable antenna. The test program goals were to identify the antenna which best meets the following requirements:

- o Circular polarization
- o Low axial ratio within the beamwidth
- o 90" beamwidth
- o Approximate gaussian pattern
- o Low backlobes

- o Approximately 20% bandwidth

Three major types of antennas were investigated; conical spirals, flat equiangular spirals and cavity backed Archimedes spirals. Testing was at one-third scale, with various configurations of each antenna type considered. The general results may be summarized as follows:

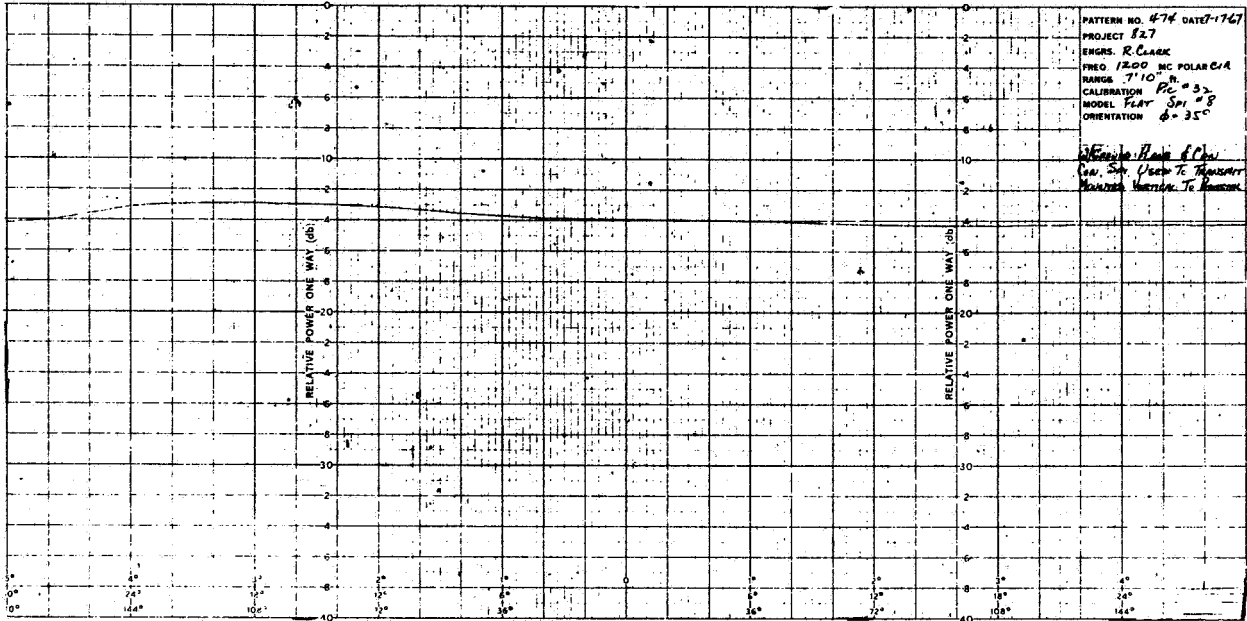
- o The conical spiral which satisfies the pattern requirements is too large at UHF for realistic installation.
- o The flat equiangular spiral of reasonable dimensions provides an axial ratio which is too large.
- o An Archimedes spiral mounted above a cavity (some separation between cavity and spiral) provided the best total radiation characteristics.

Figure 4.2-28 presents the measured pattern of the Archimedes spiral, with the analytical gaussian pattern shown for comparison. Also shown is a conic section at 55° off axis, showing a variation of approximately 1.5 dB. This coverage satisfies the ESP transmitting antenna requirements.

Pertinent characteristics of the antenna selected are as follows:

- o Beamwidth = 95°
- o Gain at 70° off axis = 7.5 dB below maximum
- o Rolloff between 70° and 90° = 0.73 dB per degree
- o On axis axial ratio = <1 dB
- o Backlobe level. = >26 dB below maximum

**ENTRY SCIENCE PACKAGE TRANSMITTING ANTENNA
CONIC SECTION 55° OFF AXIS
(1/3 SCALE MODEL)**



**RADIATION PATTERN
(1/3 SCALE MODEL)**

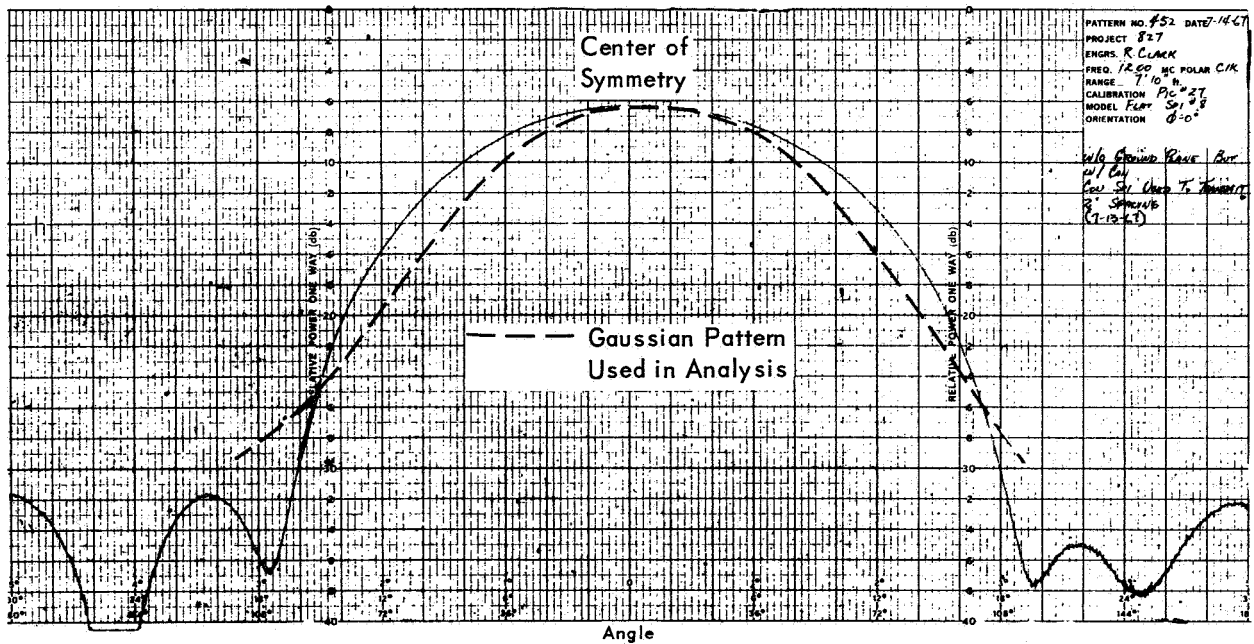


Figure 4.2-28

4.2.4.2 Spacecraft Antenna

Antenna Requirements - Pattern coverage requirements for the FSC mounted ESP receiving antenna are governed by FSC attitude, possible CB dynamics after separation, and landing site selection. Antenna gain requirements are constrained by other link gains and losses in order to limit the ESP Radio Subsystem power consumption and weight. The antenna pattern is required to be at least 50" x 45" based on the above. Maximum possible gain for such coverage is 12.7 dB, less efficiency effects.

Analysis - The ESP receiving antenna subsystem must maintain pattern coverage to the CB during the period from entry until landing. The relative FSC/CB dynamics during this period are dependent on the Martian atmospheric properties, the selected CB attitude and velocity, and the choice of de-orbit conditions. The line of sight referenced to the FSC coordinates is dependent on the above, the choice of landing site (morning or evening), and the calendar date since the FSC is fixed in attitude with respect to the Sun and Canopus lines-of-sight. The bounds for clock and cone angles from FSC to CB, during the interval from entry until landing, are shown in Figures 4.2-29 and -30. The first figure applies to a landing near the morning terminator, and the second applies to landing near the evening terminator. The most dynamic entry occurs under the following conditions; VM-9 atmosphere, entry velocity of 15,000 fps, entry angle, -13.6° , FSC anomaly, 312° , CB anomaly 318° . The clock and cone angle requirements were established by computing the line of sight variation between the FSC and CB for thirty-four cases of deorbit-to-entry dynamics and then placing the dynamic entry cases on the above. For a landing near the morning terminator, Figure 4.2-29 shows a requirement for pattern coverage of approximately 65" x 10° , to include all possible entry cases. The most dynamic single case requires coverage of approximately 45" x 10° . When the effects of FSC attitude uncertainty and possible out of plane entry are included, the most dynamic case requirements become approximately 50° x 45". An evening terminator landing requires the same magnitude of coverage, but in a completely different sector of the FSC coordinate system. If both the morning and evening terminator landings are covered by a single fixed pattern, the required coverage is approximately 200° x 45° . The maximum possible gain of 200° x 45" pattern is 6.0 dB. The maximum gain from a 50" x 45" pattern is 12.7 dB. If the FSC mounted antenna is pointed on the basis of selected landing site, the higher gain pattern may be employed.

**ENTRY SCIENCE PACKAGE RECEIVING ANTENNA VIEW ANGLE REQUIREMENTS
LANDING NEAR MORNING TERMINATOR
(20 MARCH 1974)**

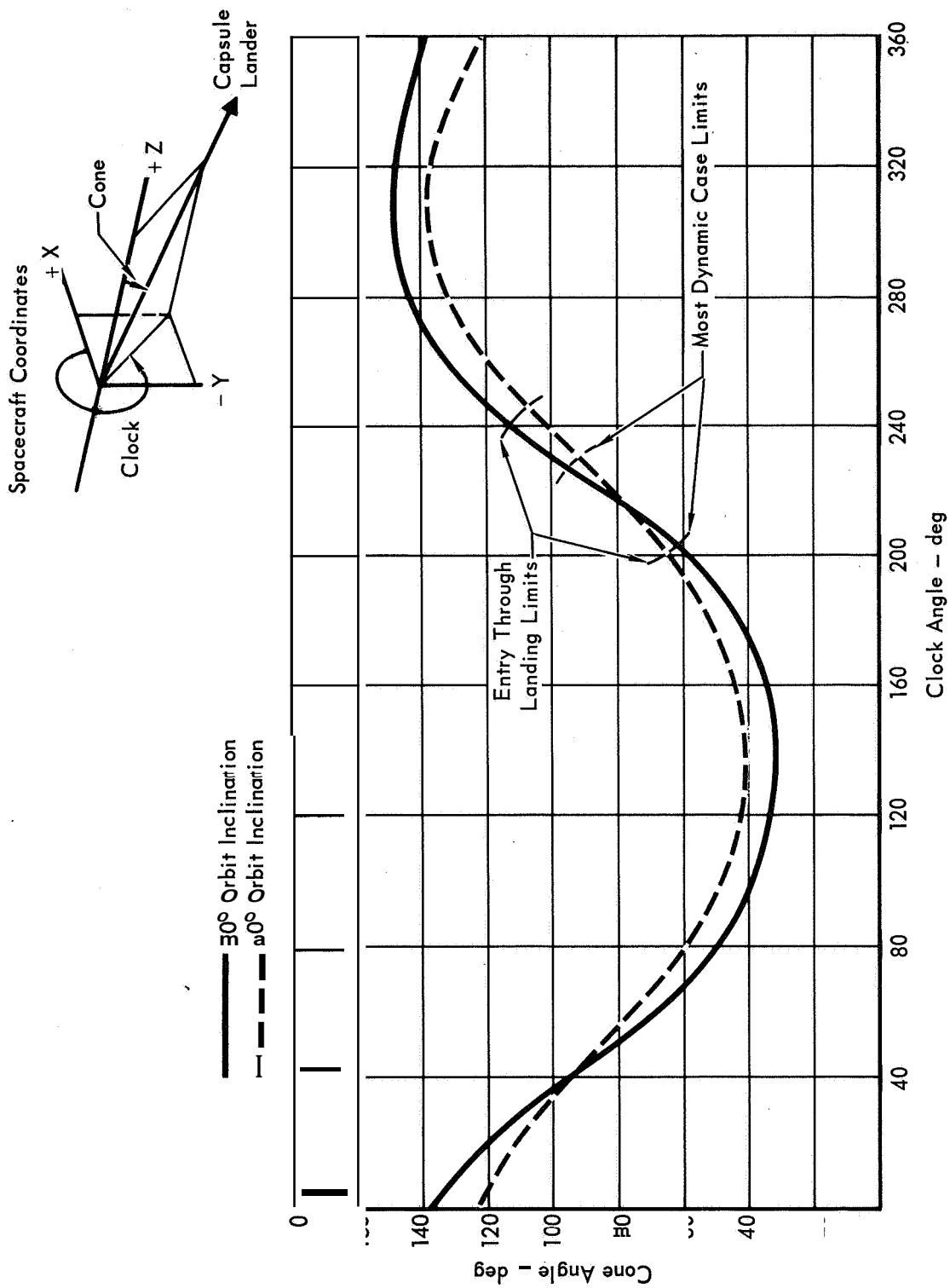
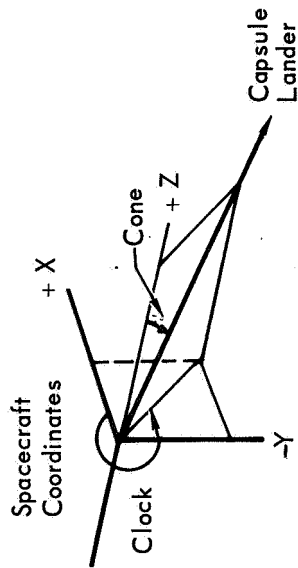


Figure 4.2-29

**ENTRY SCIENCE PACKAGE RECEIVING ANTENNA VIEW ANGLE REQUIREMENTS
LANDING NEAR EVENING TERMINATOR
(3 FEBRUARY 1974)**



30° Orbital Inclination

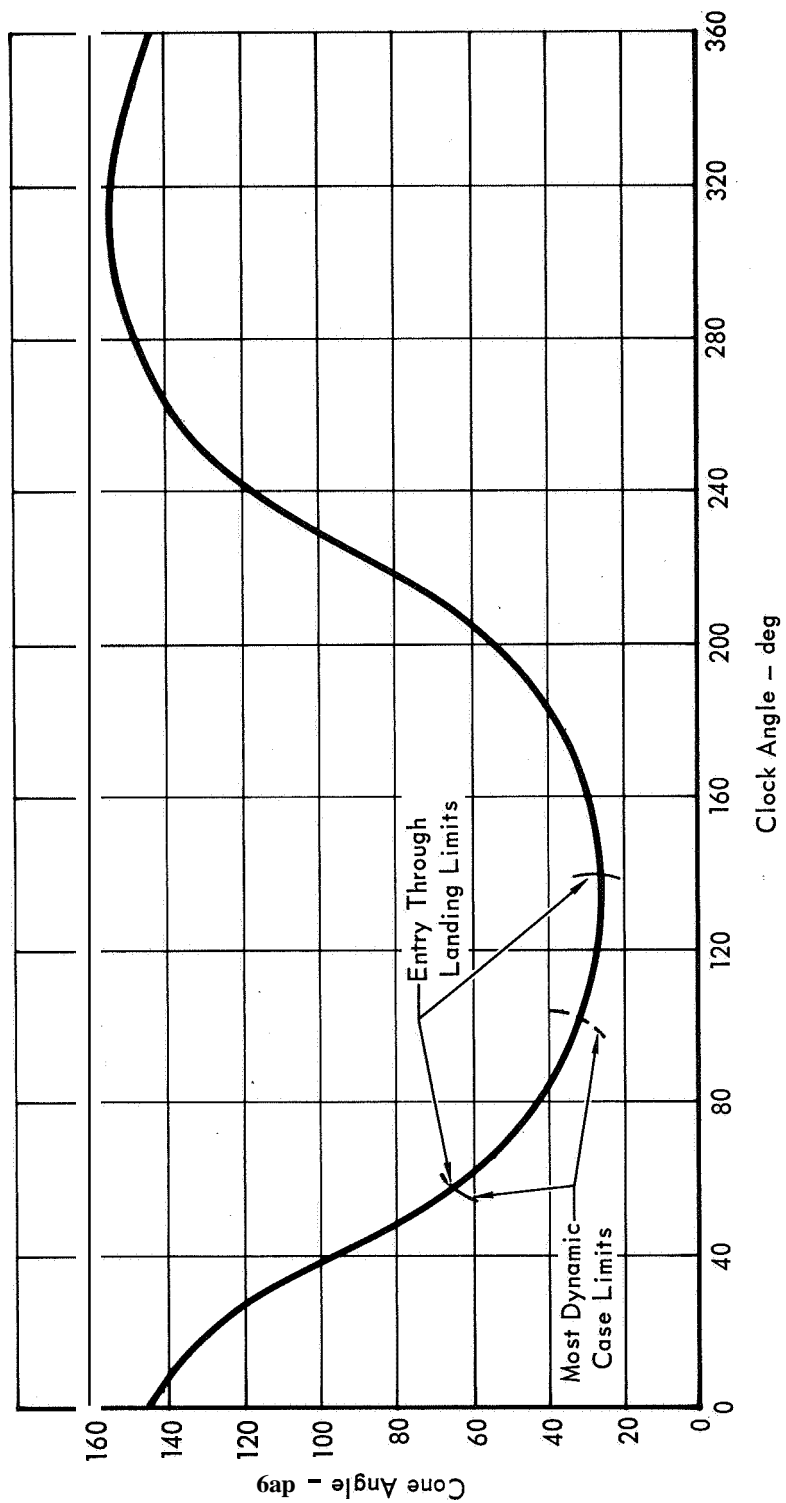


Figure 4.2-30

All line of sight cases considered are approximately perpendicular to a FSC coordinate radius vector described by a cone angle of 50 degrees and a clock angle of 320 degrees. Thus, an antenna with a pattern perpendicular to the above radius vector may be rotated about the vector to provide coverage for all cases. If mechanical rotation is not employed, coverage must be obtained through the use of a lower gain antenna pattern, or antenna switching. Any method employed must use circular polarization due to variations in the relative attitudes of the CB and FSC. Also, the required coverage precludes the use of a fixed ESP receiving antenna located within the capsule adapter.

Alternatives - Two basic approaches are considered for satisfying the FSC mounted ESP receiving antenna coverage requirements: first, employ a fixed 200' x 45° pattern; and second, employ a steerable 50° x 45" pattern. Two implementations of the steerable pattern are considered. Figure 4.2-31 summarizes the pertinent features of each approach, using antenna configurations which provide the closest approximation to the desired patterns.

Selection - As shown, all approaches employ antennas mounted on the FSC. This placement is the only possible choice for the body mounted switched array, considering the FSC geometry and the required line-of-sight variation. Mast mounted antennas attached to the FSC may be deployed before CB separation, providing time for telemetry monitoring and backup commands in case of malfunction. A mast mounted antenna stowed in the capsule adapter could not be deployed until after CB separation, with the attendant time delay in status verification.

The RF switched array pattern coverage is limited to two discrete sectors. More complete coverage requires more antennas and switches. Either mast mounted approach provides total coverage of 360' in one plane. Therefore, mast mounted antennas are selected.

The rotating mast implementation provides a gain advantage of greater than 7 dB, reducing ESP Radio Subsystem power and weight requirements. This advantage offsets the increased mast erection mechanism complexity. Also, as discussed in Volume II, Part B, the FSC mounted antenna for the Capsule Bus antenna subsystem must be mounted on a mast. Both subsystems may employ a common mast, since the coverage requirements overlap. The selected approach is, therefore, the FSC mounted antenna which may be pointed to accommodate a morning or evening terminator landing. A helix mounted as shown in Figure 4.2-32 provides the coverage required.

COMPARISON OF CANDIDATES FOR ESP RECEIVING ANTENNA

CANDIDATE APPROACHES

	1	2	3
Implementation	Two antennas mounted on Flight Spacecraft body. RF switches activate selected antenna for morning or evening landing	Single antenna mounted on mast extending from Flight Spacecraft. No mast rotation.	Single antenna mounted on mast extending from Flight Spacecraft. Mast rotated to point antenna for morning or evening landing.
Pattern Coverage, Gain	90° x 90° Instantaneous Maximum gain, 7.15 dB.	360° x 45° Maximum gain, 4.15 dB	55° x 55° Maximum gain, 11.0 dB
Complexity	Mechanically simple, but constrains other structure to provide clear field of view. Requires RF switches and non real time commands.	Requires mast extension mechanism.	Requires mast extension mechanism. Mast rotation requires non real time command. RF switches not desirable. Mast extension improves field of view capabilities.
Configuration	Two crossed slot antennas	Single bicone	H _π I x
Size, Weight	2400 cu in, 3 lb plus RF switches.	1430 cu in, 3 lb plus mast and mechanism	2620 cu in, 1 lb plus mast and mechanism

Figure 4.2-31

**ENTRY SCIENCE
RECEIVING ANTENNA ORIENTATION**

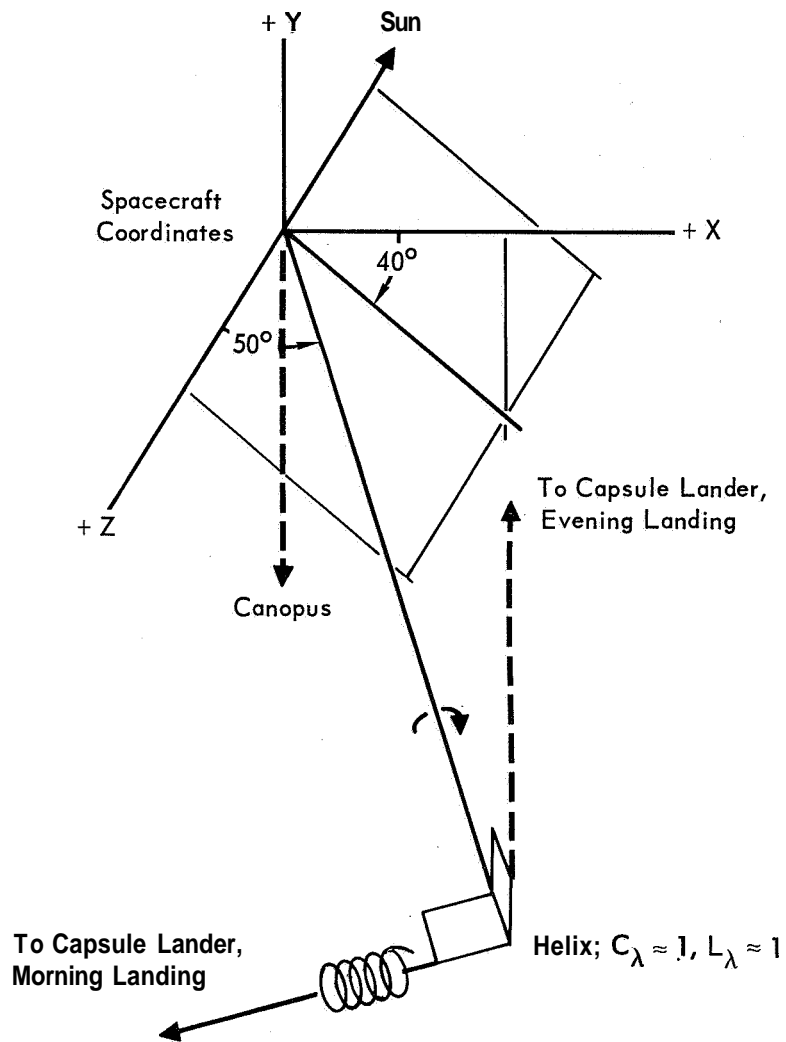


Figure 4.2-32

4.2.5 Data Storage Subsystem - Storage is required in the Entry Science Package telecommunications system because of shock induced ionization blackout. The duration of this blackout period will be a maximum of 150 seconds. (See Section 4.2.1.2).

4.2.5.1 Configuration Trade - Two storage configurations were considered. One utilized external commands from the Capsule Bus Sequencer and Timer or external sensors (such as an accelerometer) to steer the input data to a data store immediately prior to blackout. The store is read out after blackout prior to touchdown, with the stored data interleaved or multiplexed with real time data. This same configuration was recommended for a hard landing probe (Reference 4.2-17). In this application an extremely short time period between end of blackout and landing was anticipated. After blackout, stored data was transmitted at a faster rate than it was accumulated with the quantity of real time data reduced to accommodate the stored data transmission.

For VOYAGER, the time between end of blackout and touchdown will be greater than the blackout period. Furthermore, the real time data rate requirement after blackout does not decrease (Section 4.2.2). A simpler (than the referenced) delay storage implementation has been selected. While reliability was the major consideration of this analysis, the availability of redundant bits obtained by transmitting the stored data throughout the entire operation (separation to touchdown) can provide additional protection against multipath interference. The fading correlation between two points in time separated by the delay store time (150 seconds) is normally expected to be quite small (see Section 4.2.1.1). Therefore, redundant bits may be identified on the ground and used in connection with additional redundant bits obtained via the Capsule Bus (Section 4.2.6) to implement a majority decision algorithm in the Mission Dependent Equipment (MDE).

The baseline configuration incorporates a dual delay storage which includes the Capsule Bus interconnection as recommended in Section 4.2.6.

4.2.5.2 Functional & Technical Requirements - The ESP Storage Subsystem requires 50 second and 150 second storage devices operating as delay lines. Required performance and characteristics are listed below:

- o Input data NRZ data at a bit rate of 910 bps
- o Output data - NRZ data
 - Input data delayed 50 seconds
 - Input data delayed 150 seconds

- o Input and both outputs must be synchronized on a bit by bit basis
- o Total storage requirements ----- 150 seconds x 910 bps
-136,500 bits
- o Delay Time Tolerance - No tolerance can be allowed, i.e, - the storage capacity must be invariant for all conditions (variation of memory parameters with time, temperature, etc.)
- o Meet environmental requirements including sterilization temperature and radiation.
- o Weight, volume and power should be minimized without compromising reliability.
- o The chosen storage devices should be state-of-the art, preferably with flight proven history.

Candidate Storage Devices - Because of the large requirement of 136,500 bits of storage, semiconductor devices are not considered. Although many storage techniques have large packing factors (resulting in low weight and volume) the only techniques at development status are magnetic core memories, plated wire memories and magnetic tape memories. The magnetic core memories may be organized as 2, 3 or 2-1/2 dimensional. The magnetic tape memories may be coplanar (reel to reel), coaxial (reel to reel) or endless loop.

- o Magnetic Core Memories - Magnetic core memories consist of individual discrete toroidal magnetic cores strung on conductive wires to form planar arrays. The wires threading the cores supply the selection of the desired core as well as the capability for writing into and reading out of the particular core.

There are three major core memory organization arrangements and are referred to as 2D, 3D, and 2-1/2D. The first of these, the 2D memory, is characterized by the simplest conductor threading pattern. A pair of orthogonal wire sets are threaded through the cores so that a core encloses every crossing point of the wires. These wire sets are commonly referred to as the X and Y wires. The 2D memory is also known as a word organized memory since all of the bits in a single word are included in a single row of cores within the core plane. Thus all memory is included in the X and Y dimension, giving rise to the 2D (for 2-dimensional) designation. All of the selection logic is supplied by the associated electronic circuitry and thus the 2D memory requires more electronics than the other two types. The advantage of the 2D system lies in its comparatively high operating speed. This is brought about by the minimization of the inductive and capacitive

effects since only the minimum of two conductors per core is necessary. Also, speed is advantageously affected by the higher, noncoincident drive currents that are utilized.

The 3D memory is characterized by a larger number of conductors threading each core and is distinctively different from the 2D memory in that each bit in a particular word lies within a separate core plane of X, Y dimension. The number of bits required in the data word then dictates the number of planes required in the Z axis direction. Hence, the designation of 3D or 3-dimensional organization is appropriate.

The 2-1/2D organization attempts to combine the best features of both the 2D and 3D memories. Essentially the 2-1/2D uses a coincident current read which is similar to the 3D and a linear select write system found in the 2D memory. The coincident current read provides a level of logic decoding within the core matrix itself, thus reducing cost of external electronic decoding, while the linear select write provides high drive currents for fast core switching. In addition, the word capacity is normally doubled by the expedient of doubling the number of core planes with only a small increase in the associated electronics. This is accomplished by the use of a phasing technique for one dimension of drive current.

The selection of a particular type of core memory is based on volume, weight and power vs total bit capacity. The 3D memory is the best choice as it requires much less power and weight than the other two organizations.

- o Magnetic Tape Recorders - Tape recorders are a well known storage media in spacecraft applications. The amount of storage required for this application calls for an endless-loop type of recorder.
- o Plated Wire Memories - A more recent development than the magnetic core memory is the plated wire memory. The basic memory element consists of an elemental segment of plated magnetic material surrounding a conductive wire. A continuous wire plating process results in a continuum of these memory elements along the length of the wire. During the manufacturing process, a polarizing magnetic field is established so that the magnetic domains are lined up circumferentially around the wire substrate. Thus, the magnetic film may be easily magnetized in either rotative direction circumferentially, but not so easily along the length of the wire.

The plated wires are arranged in parallel in a single plane; another set of parallel wires, without a magnetic coating, are interwoven orthogonally. Information is read into the magnetic film by applying currents of proper direction and

amplitude to the orthogonal wire sets. Readout is accomplished by applying current to only the noncoated wire, while the coated wire provides the second function of acting as an output sense winding. The memory plane is thus similar to a 2D word organized memory utilizing magnetic cores.

- o Comparison of the Three Candidate Storage Devices - Figure 4.2-33 presents a summary of the parameters associated with each memory type considering the requirements listed under functional and technical requirements. Based on these requirements magnetic cores have been chosen for this application. Both the 3D core and plated wire memories are ideally matched to the delay storage requirements of synchronous read and write operation and a non-variant and predictable delay line. The endless loop magnetic tape cannot meet these requirements due to the jitter characteristics. A disadvantage of the plated wire memory is its sensitivity to shock and vibration that would tend to disqualify it from space applications at this time, pending further development.

CANDIDATE STORAGE DEVICES

MEMORY TYPE	SIZE (cu in)	WEIGHT (lb)	POWER (watts)	PROBLEMS OF MEETING PHYSICAL ENVIRONMENT	ABILITY TO WITHSTAND STERILIZATION	CHOICE
3D Core Storage	400	6	10	Space Qualified	No Problems Foreseen	1
Plated Wire Storage	300	4	5	Not Space Qualified (Still Under Development)	Status Unknown	2
Endless Loop Tape Storage	500	7	2	Space Qualified	Tape and Lubrication Materials Under Development	3

Figure 4.2-33

4.2.6 Interconnection with Capsule Bus - The Entry Science Package and the Capsule Bus are operated simultaneously during the last 10 minutes prior to touchdown, encompassing the critical entry and landing phases. A significant gain in reliability can be achieved by transmitting in parallel the narrow band (non TV) ESP data over the CB link during this period. Therefore, the CB link has been sized to accommodate this additional data (Vol. II) in order to take advantage of this functional redundancy for the ESP low rate experiments. Another reason for interconnection of the CB and ESP data links is that additional protection against multipath interference is provided during the period when it is most severe (Section 4.2.1.1). Since corresponding bits from the two links may be compared on the ground, when disagreement occurs, the link with the strongest received signal at the spacecraft (as indicated by telemetered AGC voltages) may be selected. Furthermore, additional redundant bits transmitted in non-real time via entry storage may be available. A majority decision logic may then be implemented on the ground to generate the correct bit stream. The data path through the CB link allows operational flexibility for the start-up of the ESP link. This may be useful since the low rate ESP data is significant from the start of entry mode, while entry television may not be required until much lower altitudes are reached.

A trade study was performed on several integrated CB/ESP telemetry subsystem configurations. These are summarized in the following paragraphs.

4.2.6.1 Design Approaches - Three alternate CB/ESP telemetry signal-flow configurations were considered. The first configuration assumes no common interface between the CB and ESP telemetry subsystems (Alternate 1); an abbreviated flow diagram of this configuration is depicted in Figure 4.2-34. Characteristics of this configuration are as follows:

- o CB standardization is assured.
- o Failure in one system cannot degrade performance of the other nor is there mutual assistance.
- o Duplication of entry data storage systems, clocks, multiplexer programmers and data compressors impose physical penalties and possibly cost penalties as well.
- o Pre-assembly checkout is simpler in terms of support hardware.
- o No multipath improvement is provided.

The second configuration (Alternate 2) provides for partial integration of the CB and ESP telemetry subsystems; a simplified block diagram of this configuration is presented in Figure 4.2-35. It should be noted that the telemetry

SIMPLIFIED CB/EP DHS CONFIGURATION (ALTERNATE 1)

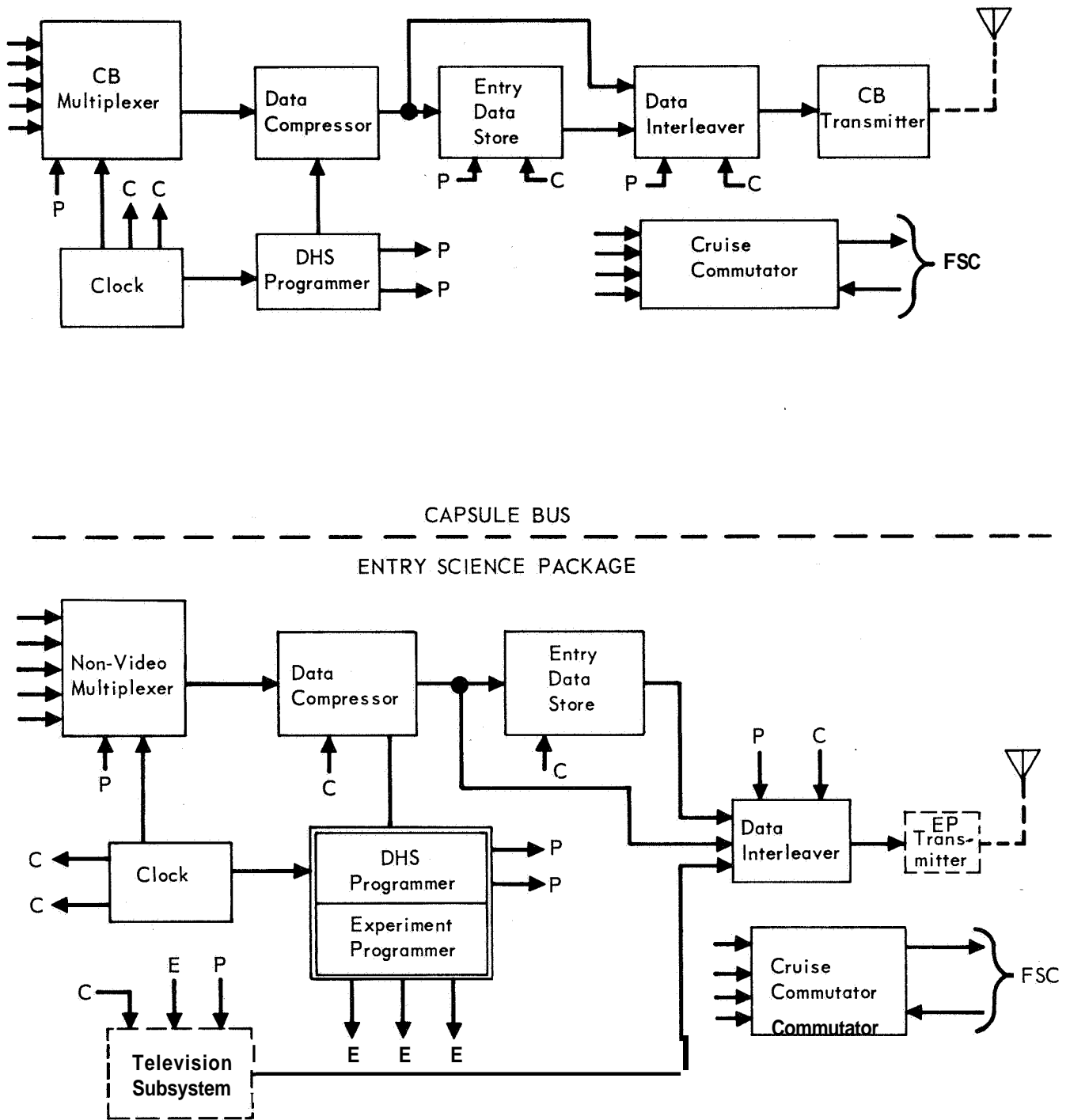


Figure 4.2-34

SIMPLIFIED CB/EP DHS CONFIGURATION (ALTERNATE 2)

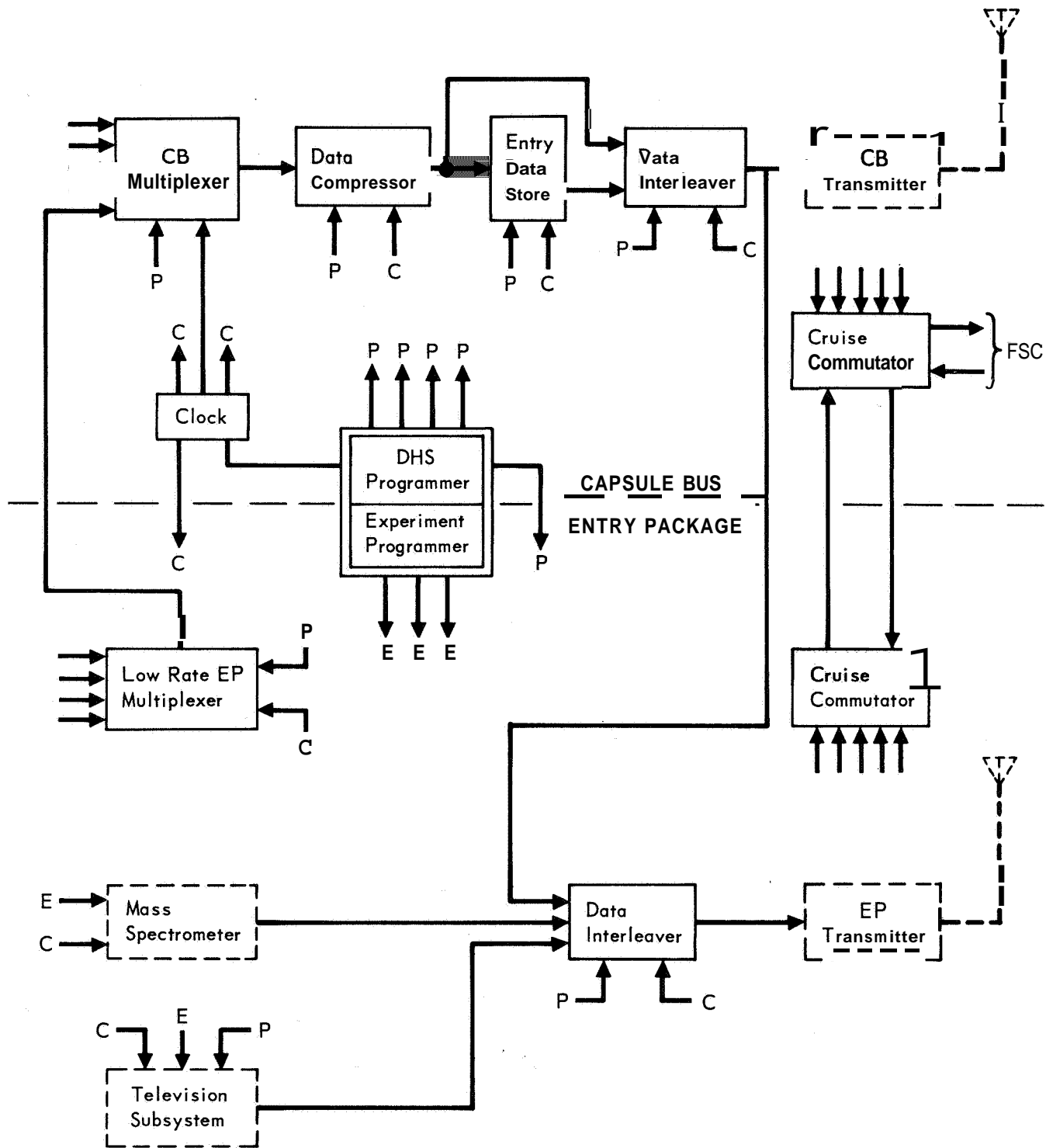


Figure 4.2-35

programmer has not been assigned to either the CB or ESP. Either a single, common programmer located in the CB or dual programmers with sync provided by the CB unit, could be used.

Characteristics of Alternate 2 are as follows:

- o All low-rate ESP data and CB data are transmitted over independent communication links, thereby minimizing multipath degradation.
- o A single entry data storage unit is required.
- o No ESP telemetry interface is required with the spacecraft.
- o Several single-point failure modes can occur, resulting in simultaneous loss of CB and low-rate ESP data.
- o CB standardization is reduced.
- o Pre-assembly checkout may require supplying the ESP manufacturer with an external clock and programmer.

The third configuration (Alternate 3) provides a higher degree of integration than Alternate 2: a simplified block diagram of this configuration is presented in Figure 4.2-36. Again, the telemetry subsystem programmer has not been assigned to either the CB or ESP. Characteristics of the Alternate 3 configuration are as follows:

- o Low-rate ESP and CB data are transmitted over independent communication links, thereby minimizing multipath degradation.
- o A single entry data storage unit is required; failure of this unit may result in loss of all blackout data.
- o No ESP telemetry interface is required with the Spacecraft.
- o Maximum number of alternate paths for CB and low-rate ESP data are attained.
- o CB standardization is reduced.
- o Pre-assembly checkout may require supplying the ESP manufacturer with an external clock and programmer.
- o Single-point failure modes resulting in loss of both real-time CB and low-rate ESP data are minimized.

4.2.6.2 Selection Criteria - Criteria used to evaluate the alternate configurations are: probability of mission success, subsystem performance, versatility and program management aspects. The weighting associated with each of these four criteria is presented in the following paragraphs.

Mission success for the CB/ESP telemetry subsystem can be defined in terms of the percentage of total data expected that can be successfully acquired,

SIMPLIFIED CB/EP DHS CONFIGURATION (ALTERNATE 3)

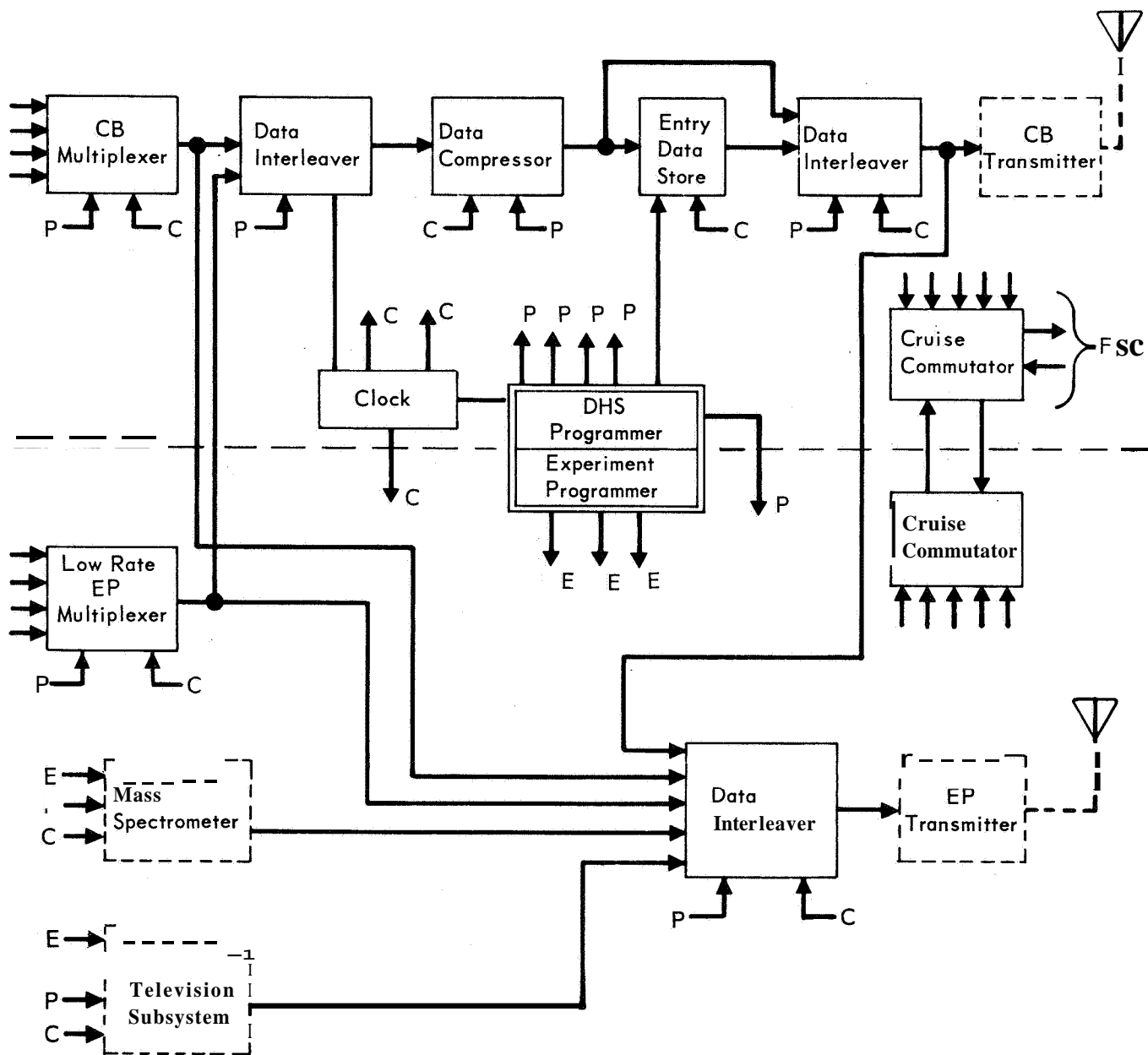


Figure 4.2-36

processed and delivered to the transmitters or **Spacecraft** support system. Of the many factors which can affect mission success, reliability was considered the most significant and was assigned a weighting coefficient of 0.45. (Reliability considerations include probability of component survival, graceful degradation capabilities and alternate functional path availability.)

The most important factors in subsystem performance include weight, power and data transmission rate requirements. These factors were assigned a combined weighting coefficient of 0.3.

The major versatility design considerations include the ease of accommodating changing requirements (both intra-mission and inter-mission), and the ability to assist other subsystems in performance of their assigned tasks. The versatility criterion was assigned a weighting coefficient of 0.15.

Program management considerations were limited primarily to cost and development risk comparisons. Because all candidate configurations use existing state-of-the-art techniques and circuitry, the development risk comparison is based on CB/ESP interface complexity. Program management considerations were assigned the lowest weighting coefficient of 0.1.

4.2.6.3 Evaluation - The reliability of the candidate configurations is based on the probability that a specified quantity and type of data can be successfully delivered to a user subsystem. This probability is determined using the results of detailed analyses of the candidate systems. In the evaluation the CB engineering data was weighted highest, 0.4. ESP low rate measurements were rated slightly less important (0.3) than the CB data because some atmospheric data can be obtained by the CB and SLS. Although the entry television data is significant, it is rated less important (0.2) than the CB engineering data and ESP low rate measurements. The lowest weighting coefficient was assigned to mass spectrometer data (0.1) because the SLS may provide some back-up capability for this experiment.

The reliability analysis indicates that the alternate functional path configurations do not offer the highest probability of successful data acquisition. However, the integrated systems provide better graceful degradation characteristics, resulting in higher overall reliability evaluation, since probability of successful data acquisition and graceful degradation were weighted equally in the evaluation.

A summary of the weight, power and data transmission requirements of each candidate configuration is presented in Figure 4.2-37. By assigning relative value weightings to each of these parameters, a composite value for subsystem performance was derived. The assigned values are 0.4, 0.4 and 0.2 for weight, power and

CB/EP DHS PHYSICAL CHARACTERISTICS TRADE STUDY

DHS PHYSICAL CHARACTERISTICS	MATRIX OF DESIGN APPROACHES					
	Alternate 1	Alternate 2 Common Programmer	Alternate 2 Dual Programmer	Alternate 3 Common Programmer	Alternate 3 Dual Programmer	
Power Requirement Weighting = 0.4	0.32 12.7 W	11.0 W	13.6 W	10.3 W	13.4 W	
Weight - 0.25	0.20 22.2 lb	18.0 lb	22.0 lb	20.1 lb	24.3 lb	
Inherent Redundancy Weighting = 0.45	0	0.5	0.6	0.9	1.0	
Transmission Rates CB Low Rate Weight = 0.05	0.04 119 bps	105 bps	105 bps	112 bps	112 bps	
CB High Rate Weight = 0.05	0.05 1428 bps	1575 bps	1575 bps	1568 bps	1568 bps	
EP Weight = 0.1	0.1 51K bps	54K bps	54K bps	53,424 bps	53,424 bps	
Total Value	0.71	0.91	0.78	0.96	0.85	

Figure 4.2-37

transmission requirements, respectively. Included in the weight considerations is the inherent redundancy which minimizes the need for more weight to eliminate single-point failures.

Versatility has been provided in all of the candidate configurations by a stored program control which permits limited modification during flight. The more complex systems have greater versatility because the multiple path capability results in a greater chance to find and initiate, by command, alternate data paths in the event of an in-flight pre-separation failure.

Perhaps the most important versatility aspect provided in the interlaced CB/ESP System is the reduction of RF multi-path interference through use of frequency diversity techniques.

Cost differences between configurations should be slight. None of the candidate configurations involve high risk items. However, the more complex systems may be slightly more expensive to produce and have a somewhat greater possibility of schedule slippage.

The comparative evaluation of candidate configurations is summarized in the comparison matrix of Figure 4.2-38. This table indicates that Alternate 3 is the preferred configuration.

4.2.6.4 Selected Configuration - Alternate 3 was selected as the baseline functional configuration on the basis of the results summarized in the comparison matrix of Figure 4.2-38. The use of a common programmer located in the Capsule Bus or separate programmers for the CB and ESP were considered. Separate programmers for the CB and ESP, with CB programmer sync provided to the ESP unit, were selected because of the greater reliability provided and fewer interfaces required. Fewer interfaces facilitate the standardization of the CB for future missions in which the ESP is not included. These factors outweigh the small increase in power (3.1W) and weight (4.2 lb.) relative to the total CB/ESP power-weight requirements.

The baseline system includes an entry data store in the ESP in addition to the entry data store in the Capsule Bus. Thus an alternate path for data accumulated during blackout is provided, (see Section 4.2.1.2), and loss of blackout data due to catastrophic failure of an entry data store is precluded. Dual time delay storage is used in the baseline system instead of the single delay assumed in the trade study. However, the validity and conclusions of the trade study are unaffected.

CB/ESP TELEMETRY COMPARISON MATRIX

FUNCTIONAL AND TECHNICAL DESIGN REQUIREMENTS	MATRIX OF DESIGN APPROACHES			SELECTION	
	ALTERNATE 1	ALTERNATE 2	ALTERNATE 0		
Accepts signals from Engineering and scientific sensing devices; samples, processes and formats data for transmission.	<p>Autonomous Systems</p>	<p>Partially Integrated Systems</p>	<p>Fully Integrated System</p>	<p>Selected</p> <p>Alternate 0</p>	
	Reliability	0.50	0.76	0.95	3-2-1
	System Performance	0.71	0.78	0.85	3-2-1
	Versatility	0.10	0.13	0.15	3-2-1
	Management	0.10	0.085	0.075	1-2-3
	0.69	0.85	0.975		

Legend: I - Interleaver, M - Multiplexer, S - Storage

Figure 4.2-38

4.2.6.5 Interleaving - Figure 4.2-39 shows the equipment required to interleave the CBS and ESP data. The purpose of this analysis is to determine what type(s) of data interleaving will be most satisfactory from a synchronization viewpoint.

Three types of interleaving will be considered: frame, word, and bit interleaving. Frame interleaving uses the simplest logic at the receiver to de-interleave the data stream, requiring only the sensing of the frame sync word in consecutive bits to steer the data frame to the correct location for decoding. It will normally require storage prior to interleaving.

Bit interleaving does not require storage prior to interleaving, but the de-interleaving logic is generally more complex. The "one-one" case is degenerate, i.e., the de-interleaving logic is trivial; but the general case of n bits of one bit stream to m bits of the other requires the search for the respective frame sync words to take place over non-consecutive bits of the data stream. Given that at least one of the frame sync words is in the decommutation shift register, the shift register length, L, is defined between

$$(x/n - 1)(m + n) + n \leq L \leq \left\lceil \frac{x}{n} \right\rceil (m + n) \\ \text{for } (x/n \geq y/m)$$

(where x is the sync word length in n data stream and y is the m sync word), to guarantee a long enough shift register to find either sync word.

Word interleaving requires some storage but not nearly as much as frame interleaving. The logic requirements for de-interleaving are much the same as for bit interleaving; frame sync search must always examine non-consecutive bits of the data stream.

Interleavers 3 and 4 of Figure 4.2-39 are designated bit interleavers because the data is in the ratio 1:1:1; in fact, the data streams are identical except for relative timing delays. Interleavers 1 and 2 are also the bit type because there will be simpler logic in the interleaver than for the word or frame type. Interleaver 5 is shown as a frame interleaver because the relative data rates of the three data streams is $(a = c)/b \approx 1/200$, which would cause the shift register lengths (and associated logic) for either the bit or word types to be excessive.

The designation, frame interleaver, covers several variations. One variation is to have definite locations within the television frame for data from data streams a and c. A second approach is to identify data from all streams with adequate address bits for de-interleaving purposes. Still another approach is to interleave complete frames of data from each bit stream. The first approach would

TELECOMMUNICATIONS EQUIPMENTS - DESCENT PHASES

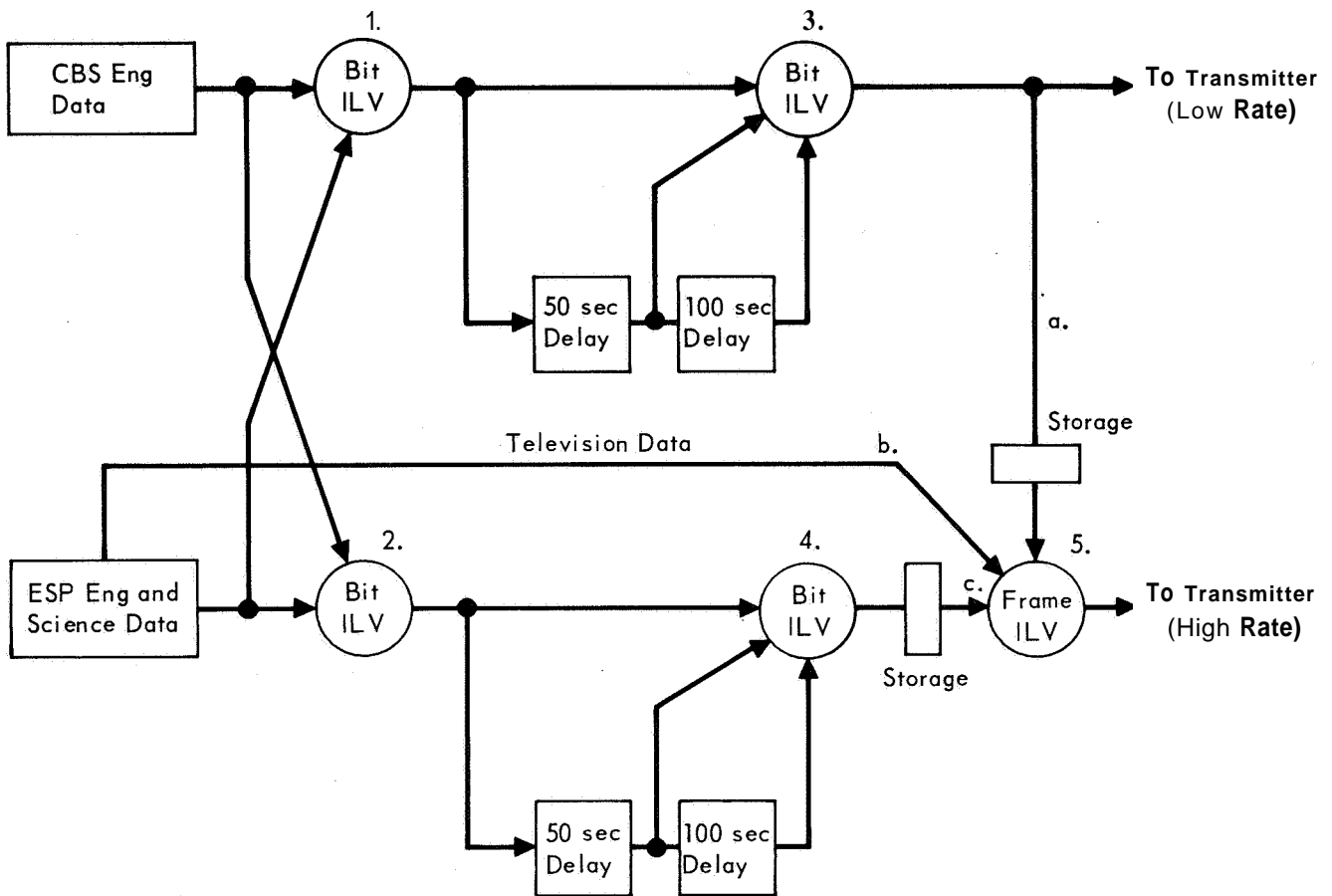


Figure 4.2-39

not add any bits to the data stream (and therefore does not increase the transmission rate), but will be inflexible to future changes in the system. The second will provide great flexibility for the future at the cost of the address bits, but will not create any problems on frame sync or timing, as the third approach will.

4.2.7 Use of Data Compression - We have studied the feasibility of using data compression both to reduce required communication rates by eliminating useless or redundant data and to enhance subsystem performance by providing a higher tolerance to the effects of uncertain environmental factors. The results of both the redundancy reduction and "aliasing" compression studies indicate that data compression is useful for all the experiments, strictly from a compression viewpoint. Moreover, most of the compression algorithms considered have familiar circuit implementations which are easy to integrate into the data system. But readin-readout power requirements due to the high data rate will be excessive. Therefore, data compression is not included in the ESP baseline design.

Constraints - To evaluate data compression feasibility for the VOYAGER mission, several constraints concerning system operation and mission duration were considered:

- a. The maximum data entry occurs when entering VM9 at graze (600 second Entry - 60 second Terminal Descent).
- b. The minimum data entry occurs when entering VM8 at -20° (230 second Entry - 50 second Terminal Descent).
- c. The Entry Television starts operations at 800,000 feet.
- d. Transmission rates of compressed data were calculated after allowing for possible estimation errors on the amount of compressed data (10% allowance).
- e. Compression ratios calculations include forced outputs used for "confidence measurements".

Introduction - Specific data compression methods can be classified either as destructive or nondestructive. The destructive (or user-oriented) type of data compression is so named because a time history of the data cannot be reconstructed, whereas the nondestructive (or source-oriented) type allows reconstruction.

Parameter extraction is almost synonymous with destructive data compression. The information (in the communications sense) is defined using irreversible transformations. Adaptive sampling means that the data channels are sampled at a rate commensurate with the information they convey. Redundancy reduction is equivalent to adaptive sampling except that the data is sampled at a uniform rate but only those samples which are significant are transmitted. Encoding techniques attempt to reduce the data by naming the data elements differently. Adaptive sampling,

redundancy reduction, and encoding all make a time reconstruction possible, and so, are classed as nondestructive techniques (See Figure 4.2-40)

Under each of these classifications are several techniques which have been thoroughly tested by simulations in the laboratory.

From a compression viewpoint, each data output should be matched to several of the more likely candidate techniques as in Reference 4.2-17. The comparison criteria - expected compression, implementation complexity, and buffer reductions - give enough information to choose the best compression algorithm for each experiment, as illustrated in the following examples.

Entry Television - The assumed purpose of the Entry Television (or Descent Imaging) experiment is to obtain pictures of Mars to identify gross properties of the atmosphere and detailed information about the landing site. The candidate television system studied has a 200 lines/frame, 200 elements/line, 6 bits/element (24×10^4 bits/frame) data presentation. It also alternates frames between wide field images and narrow field images. The wide field images help locate the landing site location in Orbiter TV pictures, while the narrow field images give detailed information about the terrain.

The candidate compression techniques are: Robert's Modulation; First-Order Interpolator; and Elastic Encoder. For descriptions of these data compression techniques, see Reference 4.2-18. Figure 4.2-41, the Trade Study Summary Sheet, shows that the Elastic Encoder is the best compression approach, with a computed compression ratio of 8.0:1.

Mass Spectrometer - The purpose of the Mass Spectrometer experiment is to identify the atmospheric composition as a function of altitude. The instrument has an ionization chamber for the gas sample. The ionized gas is focused into a beam and is directed by a varying electrostatic field onto a sensor. Different ions are successively steered onto the sensor as the field changes. The sensor current is proportional to the amount of constituent in the atmosphere; the time the current peak occurs identifies the constituents. These two items are important and will always be transmitted.

As indicated on the Trade Study Summary on Figure 4.2-42, the best candidate technique is the "Unusual Event" method (computed compression ratio = 2.5:1). The present sampling scheme, which is termed the "Periodically Sampled Output" method, is the only other candidate approach.

"Aliasing" Compression - "Aliasing" data compression would not be used to reduce communication rates, but to enhance system performance by guarding against

CLASSIFICATION OF DATA COMPRESSION METHODS

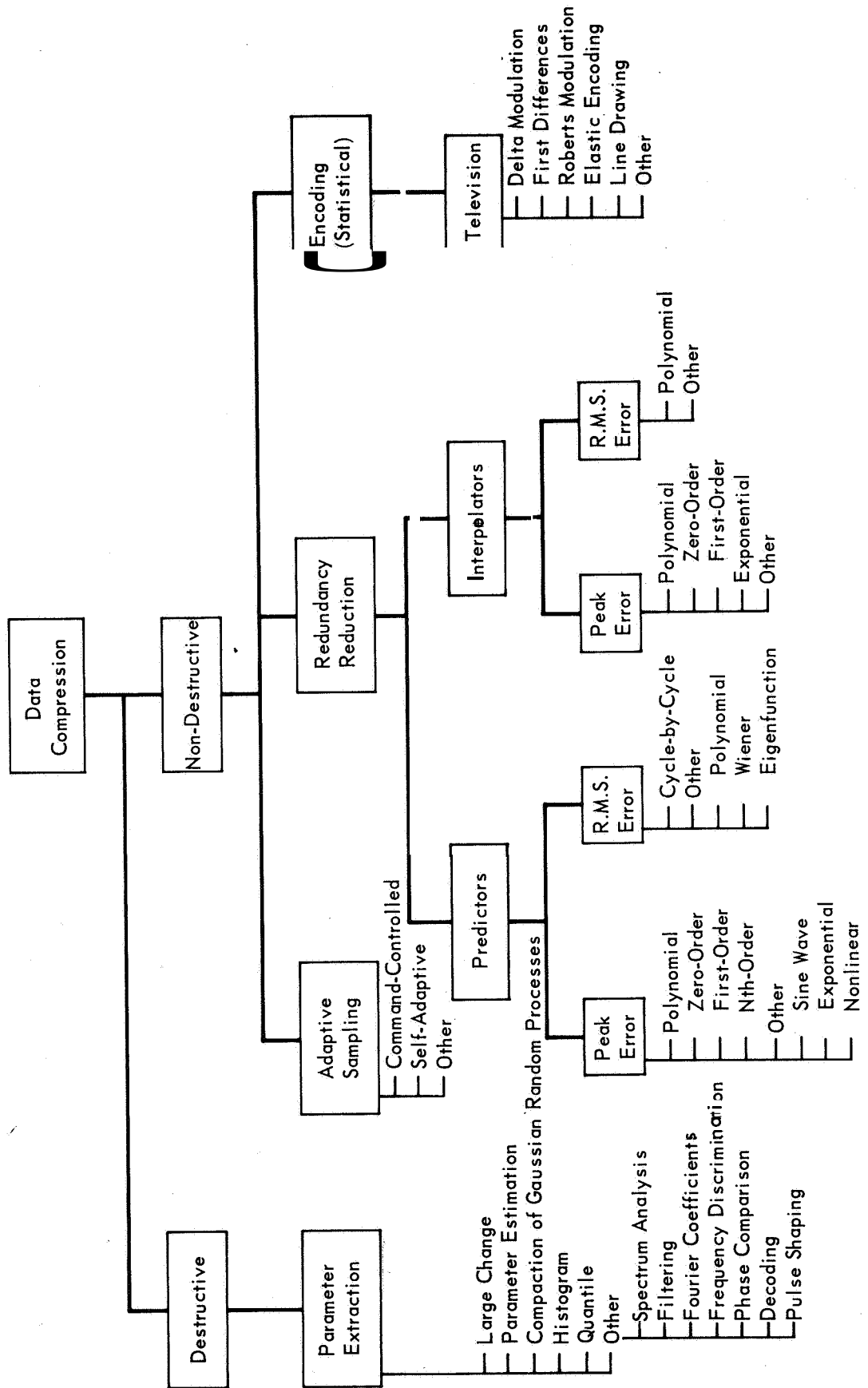


Figure 4.2-40

DATA COMPRESSION FEASIBILITY - ENTRY TELEVISION

FUNCTIONAL AND TECHNICAL DESIGN REQUIREMENTS	MATRIX OF DESIGN APPROACHES			SELECTION
	#1 ROBERT'S MODULATION	#2 FIRST-ORDER INTERPOLATOR	#3 ELASTIC ENCODER	
<ul style="list-style-type: none"> ● Transmit convention (200 x 200 x 6) PCM picture with no loss of fidelity or "information". ● Wide field and narrow field images shall portray landing site location, landing site terrain, and atmospheric conditions. 	<p>Description: Robert's Modulation encodes each picture element of a normal television picture to 3 bits. Then noise is added at the transmitter and synchronously removed at the receiver. Such an operation effectively serves to more finely quantize the data than the 3 bit encoding indicates would be the case.</p>	<p>Description: The data, a normal television picture, contains many gradual tone changes and only a few entirely new elements. This method will process the gradual data with a high compression ratio resulting, but will transmit the original elements where they are entirely different from their neighbors.</p>	<p>Description: The data essentially has two tonal variation frequencies and each is treated separately by this method, which is conceptually complex but physically simple. The picture intensity is more important in regions of gradual transition, while exact location of sudden changes is more important. This method preserves the picture by preserving these things.</p>	Selected Approach #3
Trade Considerations	20:1	4.29:1	8.0:1	3-2-1
Expected Compression				
Implementation Complexity	<ul style="list-style-type: none"> ● Noise generators at transmitter and receiver must be synchronized. ● Quantized to 3 bits in tapered levels. ● No "Scratchpad" or Logic Memory required. 	<ul style="list-style-type: none"> ● Arithmetic logic (multiplication and division) ● Absolute timing information furnished. ● 31 bit Logic Memory ● 49 bit "Scratchpad" Memory. 	<ul style="list-style-type: none"> ● Complex circuit (2 filters, low frequency quantized to 5 bits, high frequency quantized to 3). ● 8 bit "Scratchpad" Memory. 	1-3-2
Buffer Considerations	<ul style="list-style-type: none"> ● Transmission rate cut from 51,408 bps to 26,208 bps. ● Buffer size remains at 1,000 bits. 	<ul style="list-style-type: none"> ● Transmission rate cut to 14,000 bps ● Buffer sized to allow short term compression of 3.42 for 10 seconds, increased to 16,000 bits. ● Tolerate permanent compression of 3.9. 	<ul style="list-style-type: none"> ● Transmission rate cut to 8,000 bps. ● Buffer, sized to allow short term compression of 6.0, increased to 10,000 bits. ● Tolerate permanent compression of 7:17. 	3-2-1

Figure 4.2-41

DATA COMPRESSION FEASIBILITY - MASS SPECTROMETER

FUNCTIONAL AND TECHNICAL DESIGN REQUIREMENTS	MATRIX OF DESIGN APPROACHES		SELECTION
	#1 UNUSUAL EVENT	#2 PERIODICALLY SAMPLED (UNCOMPRESSED)	
<ul style="list-style-type: none"> ● Measure atmospheric composition from data to aid calculation of corresponding gas properties and aerodynamic coefficient corrections and to aid understanding aerodynamics of chosel vehicle configuration. ● Range, Mass Numbers 0 to 60 ● Accuracy $\pm 2\%$ of average molecular weight in atmosphere. 	<p>Description: This data is normally composed of current spikes (identifying the ions present) interspersed with long periods of data inactivity. The "Unusual Event" Method ignores all data inactively, but carefully inspects the spikes to determine the spike magnitude and exact time of occurrence.</p>	<p>Description: The current spikes occur at regular intervals normally, but many of the intervals will be vacant each scan. This method, by sampling each possible location, transmits much data which is useless to the ground observer.</p>	Selected Approach #1
Trade Considerations			
Expected Compressions	2.5:1	1.0:1	1-2
Implementation Complexity	<ul style="list-style-type: none"> ● Peak detector detects and records peak voltage. ● Sampling circuit triggered by peak detector gives timing information. 	<ul style="list-style-type: none"> ● Sampling commutated at regular intervals. 	Z-1
Buffer Considerations	<ul style="list-style-type: none"> ■ Buffer memory is 800 bits, allowing short term compression of 2.0 for 5 minutes. ● Tolerate permanent compression of 2.31 when transmitted at 1,040 bpm (17.33 bps). 	<ul style="list-style-type: none"> ● No Buffer memory required. ● Transmission rate is 2,400 bpm (40 bps) 	1-2

Figure 4.2-42

aliasing errors. Aliasing occurs whenever a channel is sampled at less than twice the highest frequency present in the channel, thus causing the channels frequency spectra to overlap. False output waveforms will be returned if aliasing is present. System design and operation can be described as follows:

A typical instrumentation list defines the sample rate requirements based on expected vehicle performance in an assumed environment. If these sample rate requirements are underestimated, significant measurement errors may be introduced; on the other hand, if the sample rate requirements are adequate, sampling at higher rates would result in unnecessary data transmission.

In the ESP TM, multiplexer sampling rates would be increased to about ten times the required rate. The data compressor will accept this data, separate those samples which would have been provided by a lower-speed multiplexer, and output them without modification. In addition, an appropriate compression algorithm (probably a First-Order Interpolator) will be applied to the remaining samples. If the original sample rate requirements are adequate, the compressor will produce no additional samples of excessively active channels for subsequent transmission. By increasing the communication link capability about 10%, the data compressor output frame format would include all required data samples, followed by an additional 10% of compressed data samples.

For example, if the required sample rate were 100 sps, the compressor output would be 110 sps (the first 100 time slots being the required samples and the last 10 containing any excess samples produced by the compression algorithm). Thus, if the highest per channel sample rate required were 1 sps, at least ten channels could be adaptively increased to 2 sps; similarly one channel could be sampled at 10 sps. If the excessive activity duration is limited or the channel activity is not too excessive, even greater adaptivity can be expected.

Summary - Data compression generally is useful because it allows more "information" to be transmitted with the same number of bits, or allows the same "information" to be transmitted in a smaller number of bits. This study illustrates the second possibility because there are a definite number of baseline experiments to be performed. However, the way is open, after employing data compression on these experiments, to increase the amount of "information" from these experiments to add other experiments up to the original transmission rates.

The earlier studies indicated that data compression will require a slightly larger memory, but will gain 16 dB of additional margin. Also, the calculated data compressor failure rate will be about 2,81%/1000 hours, based on the parts count for existing ground data compressors capable of performing similar operation.

Obviously, this reliability figure can vary as a function of the compressed data store (buffer) capacity, but the compressor is not likely to become a poor risk item. If the multiplexer is designed to operate at both the required sample rates and an order of magnitude faster, the data compressor could be by-passed by ground command any time prior to CB separation.

Conclusions - Data compression is beneficial on the ESP for both tasks from a compression viewpoint. It will eliminate redundant data and it will provide a tolerance to the environmental unpredictability. It is not included in the base-line system because it is not flight proven and because the high data rates on the ESP will make the readin-readout power consumption in the logic memory (core) excessive.

REFERENCES

SECTION 4.2

- 4.2-1 Private Communication with D. Schweizer, Department 613-1 of SRS Philco-Ford at LARS, Cape Kennedy.
- 4.2-2 R. M. Goldstein and W. F. Gillmore, "Radar Observations of Mars", *Science*, Vol. 141, pp 1171-1172, 20 Sept. 1963.
- 4.2-3 R. B. Dyce, "Recent Arecibo Observations of Mars and Jupiter," *Radio Science*, Vol. 69D, pp 1628-1629, December 1965.
- 4.2-4 Selected Studies of VHF/UHF Communications for Planetary (Mars/Venus) Relay Links, Final Report, prepared by Astro-Electronics Division, Defense Electronic Products, Radio Corporation of America, Princeton, New Jersey, under Contract No. NAS 2-3772, AED R-3091; January 15, 1967.
- 4.2-5 G. Schroeder, "Noncoherent Binary FSK in Slow Fading," McDonnell Douglas Corp; I.O.M. 413-AT-70820, August 10, 1967.
- 4.2-6 A. B. Glenn and G. Lieberman, "Effect of Propagation Fading and Antenna Fluctuations on Communication Systems in a Jamming Environment," *IRE Transactions on Communications Systems*, March 1962.
- 4.2-7 G. L. Turin, "Error Probabilities for Binary Symmetric Ideal Reception Through Nonselective Slow Fading and Noise." *Proc. of IRE*, September 1958.
- 4.2-8 W. C. Lindsey, "Error Probabilities for Ricean Fading Multichannel Reception of Binary and N-ary Signals," *IEEE Transactions on Information Theory*, October 1964, pp 339-350.
- 4.2-9 C. A. Hinrichs, "Martian Entry Fading," McDonnell Douglas Corp., VN-11.2.1-4 (DELS), April 29, 1967.
- 4.2-10 L. Schuchman, "Wideband Detection of MFSK Transmission in a Two-Path/Multipath Channel," *Philco Ford TM 119*, July 14, 1967.
- 4.2-11 J. C. South, "Program Description of Appropriate Solution for Supersonic Flow Past Blunt Bodies with Sharp Sonic Corners," *Langley Working Paper NWF-240*, July 12, 1966.
- 4.2-12 C. D. Joerger, H. J. Fivel, G. G. Grose, J. F. Fox, "The Effect of Ablative Products on Gemini Reentry Communications," Final Report Contract No. NASw-1209, April 1966.
- 4.2-13 M. R. Denison and E. Baum, "Compressible Free Sheer Layer with Finite Initial Thickness," *AIAA Journal*, February 1963.

- 4.2-14 VOYAGER Technical Memo 4.1-19 (LQ), dated 5 July 1967
- 4.2-15 "A Feasibility Study of an Experiment for Determining the Properties of the Mars Atmosphere," Vol. III, Book 1, AVCO Corporation, September 1, 1966.
- 4.2-16 W. C. Lindsey, "Error Probabilities for Ricean Multichannel Reception of Binary and N-ary Signals," IEEE Transactions of Information Theory, October 1964.
- 4.2-17 VOYAGER Note VN 11.2.1-37 (LM), "Application of Data Compression to VOYAGER Experiments," July 19, 1967.
- 4.2-18 VOYAGER Note VN 11.2.1-3 (L), "Data Compression Techniques," April 20, 1967.

4.3 STRUCTURAL/MECHANICAL SUBSYSTEM - In selecting the configuration for the structural/mechanical subsystem, the philosophy of keeping the design simple, utilizing flight demonstrated practices, and selecting designs which are within the state-of-the-art and adaptable to familiar analyses was followed. The constraints and requirements imposed on this subsystem do not pose unusual design problems. The most challenging problems were the stagnation point port and the mounting for the entry television cameras. For mounting the accelerometer, an existing major structural element which is rigid and possesses a convenient machined surface was utilized.

A typical torque box type of structure was selected for the ESP equipment container. Pin-jointed members which provide ease of installation and minimum thermal paths were selected to support the UHF antenna. The similarity of functional location requirements indicated locating the base region port near the UHF antenna; therefore, the mounting provisions for the port tube were incorporated into the antenna support bracket.

Entry Television Camera Mounting - The location of the camera container requires that it be ejected prior to impact. To reduce the probability of recontacting the Capsule after its release, ejection to the side away from the Capsule Lander is indicated. The use of springs to supply the ejection force for the separation of the container was considered, but the pyrotechnic thruster is lighter and easier to install and was therefore selected. The compression struts provide adjustment capability and dynamic stability necessary to provide and maintain camera alignment.

Stagnation Point Port - The design of the fitting which provides the port at the stagnation point is determined to a great extent by the thermal protection system selected. The constraints and requirements which affect the selection of the thermal protection system are:

- o Stagnation point temperature of **2300°F**
- o Limiting the temperature of the compartment behind the apex fitting to **325°F**
- o No contaminants in gas samples for mass spectrometer

Ablative-type thermal protection systems could not be used because of their inherent characteristic of releasing contaminants. Teflon-coated and ceramic-coated structures were considered but they, too, give off products which could contaminate the gas samples. The use of a metal-surfaced thermal protection system was indicated. The material selected is beryllium because of its high melting point, high heat capacity at elevated temperatures, low density, and strength characteristics. A single fitting incorporating the necessary ports fulfills the structural and non-contaminating inlet requirements. Thermal protection for the compartment is provided

by utilizing the fitting as a heat sink.

4.4 PACKAGING AND CABLING - Studies were conducted on materials and components, fabrication, assembly and installation techniques to determine the most effective packaging and cabling for the Entry Science Package. These studies are summarized in the following paragraphs.

4.4.1 Cable Studies - Efficient cabling interconnection requires integration with the structure, equipment form factors, and equipment installation. The preferred wire and harnessing techniques provide the necessary integration with a reliable lightweight design. Figure 4.4-1 lists the various materials and techniques studied, and indicates the preferred approach. The preferred wire is MIL-W-8138 1/1 (7 mil) "Kapton" wire in round bundles. Sleeving is applied in areas where abrasion may occur and wire terminations are potted to provide environmental sealing and wire support.

4.4.2 Connector Studies - The cabling study was complemented by an evaluation of connectors. In some cases alternate cabling techniques were discarded because a reliable connector was not available. Figure 4.4-2 lists the connectors studied, summarizes the characteristics and parameters of each connector, and notes the selection for standardization of interconnects. The preferred MIL-C-38999 connector is circular, employs rear entry crimp contacts, has a quarter turn bayonet coupling, is environmentally sealed and has provision for potting.

4.4.3 Equipment Packaging - In assessing various approaches to packaging of the ESP equipment, several considerations dominated. These were: (A) recognition that some elements were constrained to specific locations while others could be grouped, (B) that weight and volume were to be minimized, (C) that simplicity, accessibility and ease of deletion be maximized.

The form factor evaluation considered those science and support items which could be grouped and treated as one assembly. The techniques evaluated for equipment packaging consisted of standardized subassemblies, structurally integrated subassemblies and black box elements. The standardized subassembly was discarded on the basis of the random form factors essential to certain items (for example, the long mass spectrometer with its small cross sectional area). The structurally integrated subassembly concept was considered too complex for the limited-use application of the Entry Science Package. The black box approach, in which each assembly is fabricated as a separate device for the intended installation, was selected. The volumes required by subassemblies are constrained to specified physical dimensions to ensure integration with the other subassemblies, permit adequate mounting


CABLE STUDY SUMMARY


MATERIAL/ TECHNIQUE	ALTERNATES STUDIED	RATIONALE
Wire/Cable Type	<p>Round</p> <p>Flat</p>	<p>Round wire fabricated into round wire bundles allows greater flexibility of circuit design, use of established fabrication, techniques and provides a greater background of development, testing, and experience of use in space flight. Flat cable concepts are limited in development of the basic wire, terminating devices, and fabrication techniques. Flat cable limits circuit design in a vehicle test and/or developmental program.</p>
Wire Specifications	<p>MIL-W-81381/1 (7 mil) Kapton</p> <p>MIL-W-81381/ (5 mil) Kapton</p> <p>W-16878 type E</p> <p>MIL-W-14433 Kynar</p> <p>Raychem T</p>	<p>Only Kapton and Teflon (TFE) meet the initial constraints of compatibility with ETO and heat sterilization. Kapton 7 mil is selected over 5 mil because of limited test and development on the latter. Kapton is stronger and tougher than Teflon (TFE) and realizes up to 15.5% weight savings, to 12% volume savings, has 267% greater tensile strength, 87% less elongation, and has passed 284% greater cut through load tests.</p>
Connector Wire Termination	<p>Crimp Contacts</p> <p>Solder Contacts</p>	<p>Crimp contacts are considered the most reliable method to terminate wires in multi-pin connectors. Certified crimping tools provide uniform terminations with minimum dependence upon operator technique or capability. Replacement of individual wires and/or damaged contacts is possible without degradation and possible damage to adjacent contacts or replacement of the entire connector.</p>
Wire Bundle Covering	<p>None</p> <p>Sleeving</p> <p>Jacket</p>	<p>No covering external to the individual wires is provided for the interconnecting wiring, thus providing cables of less weight and volume, greater flexibility and ease of modification, and less susceptible to damage during change. Sleeving is provided in local areas where the possibility of abrasion and/or handling degradation may exist.</p>
Wire Termination Sealing	<p>Potting Seal</p> <p>Environmental Grommet Seal</p> <p>Non-environmental Grommet Seal</p>	<p>Potting has been selected to provide environmental sealing on all wire terminating devices. Potting provides excellent sealing without regard to grommet capabilities, is lighter and provides wire support for increased dynamic environmental resistance and handling without the use of heavy, volume consuming accessories.</p>
Multiwire Terminating Devices	<p>Terminal Junction Modules</p> <p>Terminal Str</p>	<p>Terminal junction modules offer large savings in weight and volume. They provide flexibility for multiterminations of from 2 to 8 common terminations without additional weight for bussing and complete utilization of the terminating point wire capacity. The module is provided with grommet wire seals and capability for potting. Terminal identification is incorporated on the modules and they are easily assembled and/or changed.</p>

Preferred Concept

Figure 4.4-1

CONNECTOR CHARACTERISTICS SUMMARY

Connector Series Characteristics	D	RE	126	SR	348	
Vendor Specification	Cannon, Cinch MIL-C-8384B	Deutsch	Amphenol	Bendix	Amphenol MIL-C-81511	Micro MIL-C-C
Size Shape Coupling	Subminiature Rectangular Friction	Subminiature Rectangular Allen Hex Jackscrew	Miniature Rectangular Spring Loaded	Standard Rectangular Friction	Subminiature Circular Bayonet	Subminiature Circular Push-Pull Threaded
Number of Contacts	9 to 50	12 to 100	26 to 91	4 to 57	4 to 85	7 to 61
Wire Term. Contact (Size and Type)	#20 Solder or Crimp	#22 Crimp	#12, 16, 20 Solder	#4, 8, 16, 20 Solder	#22 Crimp	#12, 16
Temperature	-65° F to +300° F	-65° F to +300° F	-85° F to +185° F	-67° F to +257° F	-67° F to +302° F	-85° F to +302° F
Inserts	Diallyl Phthalate Glass Fibre Filled Monobloc, Closed Entry Sockets, Grommet Seal or Potted	Hard Plastic Sockets, Silicone Interface and Rear Seal, Glass with Silicone Interface-Hermetics	Diallyl Phthalate Asbestos Filled, Potted Seal.	Resilient Insert, 16 & 20 Contacts Closed Entry Sockets, Potted Seal.	Retention Disc and Locking Nut Grommet Seal.	Diallyl Silicone Ring and Locking Nut Grommet Seal.
Past Usage	ASSET Mariner		F4			Gemini
Hermetic Class 	Yes	Yes	None	None	Yes	Yes
Advantages	Rear Entry, Shape & Size	High Density, Rear Entry, Space & Weight, Environmental Seal, High Temperature, many Contacts	Rack and Panel	Rack and Panel	High Density, High Temperature	High Density, High Temperature
Disadvantages	Only #20 Gage Contacts, Mounting and Alignment Difficult, Interface Sealing Difficult.	Mounting Only #22 Gage Contacts, Limited Development	Temperature Limitations, Only Solder Terminations, Interface Sealing Difficult, No Hermetic Class.	Solder Limitations, Heavy and Large, Interface Sealing Difficult, No Hermetic Class.	Only #22 Gage Contacts, Limited Development.	Many A Parts

 All Hermetic Classes - Solder Type Only.

 Preferred Connector

Figure 4.4-2

4-102 -/

3	RTK	PT	PV	JC	JT	DBA
10	Deutsch MIL-C-26482	Bendix MIL-C-26482	Cannon NAS 1599	Bendix ZPH-2245-0300-B	Bendix MIL-C-38999	Deutsch NAS 1599
re or	Subminiature Circular Push-Pull Bayonet	Miniature Circular Bayonet	Miniature Circular Bayonet	Miniature Circular Bayonet	Miniature Circular Bayonet	Miniature Circular Threaded, Bayonet or Push-Pull
	7 to 85	1 to 61	3 to 61	2 to 61	3 to 128	3 to 61
22 Crimp	#22 Crimp	#16, #20 Solder or Crimp	#16, #20 Crimp	#16, #20 Solder	#16, 20, 22, 22M Solder or Crimp	#12 thru #20 Crimp
257° F	-67° F to +300° F	-65° F to +257° F	-67° F to +392° F	-67° F to +257° F	-67° F to +302° F (392° F Crimp)	-100° F to +392° F
holote, y" loat- sal	Resilient Silicone Raised "Donut" Pins, Closed Entry Sockets, Silicone Inter- face and Rear Seal, Grommet Seal	Resilient Neoprene, Nut & Grommet, or Potting Seal.	Thermosetting Plastic or Glass, Raised "Donut" Pins, Closed Entry Sockets, Grommet Seal	Silicone Nut & Grommet, or Potting Seal.	Epoxy Resin Gaskets & Inter- face Seals, Silicone Rubber Closed Entry Raised "Donut" Pins, Nut & Grommet, or Potting Seal.	Hard Plastic Sockets, Silicone Pin interface, Grommet Seal Closed Entry Sockets, Raised "Donut" Pins, Silicone Inter- face and Rear Seal, Grommet Seal
t		F-4 ASSET BGRV Mariner Mercury Gemini	BGRV			BGRV
	Yes	Yes	Yes	None	Yes	Yes
ity	High Density, Rear Entry, Environmental Seal, High Temperature	Proven Space Usage	Rear Entry, Environmental Seal, High Temperature	Thermal Sterilization, Extreme Vibra- tion, Stringent Inspection, 32 hrs @ 240° F and Ethylene Oxide Gas	High Density Rear Entry, Space & Weight Low Silhouette, Environmental Seal, High Temperature	Rear Entry, Environmental Seal, High Temperature
mbly	Low Voltage and Dielectric Rating, Limited Development	#22 Gage Contacts not Available	#22 Gage Contacts not Available	Only Solder Terminations, #22 Gage Contacts not Available		#22 Gage Contacts not Available

4-102-2

provisions, and assure routing space for the interconnecting cables. The subassemblies of the Entry Science Package Principal Unit are mounted within a lightweight structurally supported and thermally insulated enclosure.

4.4.4 Internal Packaging - The successful management approach to assure reliable electronic equipment requires selection of equipment suppliers on the basis of proven capability and favoring, insofar as possible, each vendor's particular area of design and production competence. Further, a wide variety of internal packaging concepts have successfully performed in space applications, but none has evolved as an ideal approach; therefore, no single internal packaging concept warrants a preferred approach connotation.

From experience, we know that particular attention must be devoted to internal packaging specifications with special emphasis devoted to those areas where a critical operation or process can degrade the reliability of a given packaging technique. Typically, the following broad approaches are recommended and considered appropriate to VOYAGER designs.

- o **Circuit Board Modules** - Circuit board modules are primarily applicable to integrated circuit modules utilizing either series or parallel gap welding or resistance solder reflow for component interconnection. For both techniques the process must be closely monitored and high level of cleanliness maintained. If welding is employed, weld schedules must be critically established and periodically verified. In either case, the use of single or double sided circuit boards and conformal coating with or without embedment is preferred.
- o **Embedded (Cordwood) Modules** - The use of embedded cordwood modules is applicable to either integrated circuit, discrete component or combinations of these components. This approach can be satisfactorily applied by several techniques. The preferred interconnection method is by welding, either to comb or ribbon interconnects. Critical attention to embedment materials, thermally induced stresses and rigorous process controls are necessary. Satisfactory heat sinking is a design complication requiring attention.
- o **Modular Interconnection of Modules** - Minimization of the use of friction contacts is desired to obtain maximum interconnection reliability. Thus, either fabricated multilayer boards (continuous conductors and risers, or risers welded or conductors) or matrix interconnects are preferred as the modular interconnect technique. Module to board connections can be either welded or wire wrapped. The wire wrap technique has the advantage of easier

module replacement and its disadvantage of requiring more space is mitigated by the requirement to incorporate additional space for a second weld if module replacement is necessary.

- o Radio Frequency Packaging - The preferred approach to packaging radio frequency equipment is to utilize functional elements inserted into a metallic compartmentized chassis. This permits individual module operation for test and the compartments facilitate shielding.

4.5 THERMAL CONTROL - The ESP thermal environment will be maintained within the temperature constraints imposed by the various equipment and instruments by use of a fibrous insulation blanket coated with low emissivity overcoating in conjunction with electric heaters. This thermal control approach is best suited for the ESP, based on consideration of overall system performance, simplicity of operation, container reliability and ease of installation. In addition to the ESP equipment located on the lander, two subsystems located in the nose cap assembly are also considered: the entry TV cameras, and stagnation pressure transducer.

4.5.1 Requirements and Constraints - The thermal control subsystem for the ESP is required to maintain the equipment temperatures within their allowable limits throughout all mission phases. Considering the temperature limitations on the various equipments, the battery temperature requirements are most restrictive. The primary ESP thermal control requirements are summarized in Figure 4.5-1.

4.5.2 Thermal Control Approach - In selecting the thermal control system, two primary opposing factors must be considered:

- a. Provide heat retention during the long cruise phase without excessive heater power or insulation weight.
- b. Prevent overheating from equipment operation, and heating from the base region wake and adjacent Aeroshell structure during entry.

The following table summarizes the matrix of thermal control combinations considered for this application:

<u>Thermal Control Combinations</u>	<u>Passive Element</u>	<u>Active Element</u>
A	Insulation and low emittance surface coatings	None
B	Low emittance surface coating	Heaters

ESP INSTRUMENT THERMAL CONTROL REQUIREMENTS

INSTRUMENT COMPONENT	NON-OPERATING TEMPERATURE LIMITS (°F)	OPERATING TEMPERATURE LIMITS (°F)
<u>ESP Equip. Container</u> Batteries	0 to 60	50 to 120
<u>Entry TV</u> Vidicons	- 4to 140	- 4to 104
<u>Atmospheric Properties Instruments</u> Transducer (pressure)	-328 to 250	-328 to 250

Figure 4.5-1

(Selected) C	Insulation and low emittance surface coatings	Heaters
D	Insulation	Heaters and Change of, Phase Materials
E	Insulation	Semipassive device - e.g. louvers

4.5.3 Thermal Control System Evaluation - The environment external to the ESP Equipment Container is influenced by the Aeroshell, Sterilization Canister and Surface Laboratory temperatures during cruise and entry. During the cruise period the Aeroshell and canister temperatures will be maintained above - 140°F by the Capsule Bus Thermal Control Subsystem. The equipment in the ESP Equipment Container is in a non-operating mode during this period, except for battery charging and cruise telemetry. This provides about six watts of waste heat. The trade-off to determine whether additional electrical heater power is needed was made and the results are shown in Figure 4.5-2. It is evident that the power requirements for no insulation would be excessive considering that only a total of 200 watts is available to the entire capsule during cruise; therefore, the selected combination included heaters with insulation and low emittance gold coatings. To allow some contingency, an insulation thickness of 0.75 inch and heater power of two watts have been selected as the design point which requires 3.5 pounds of insulation for the ESP Equipment Container. The insulation material used here is a low density fiberglass fiber bonded with silicone.

Figure 4.5-2 also shows the insulation-power tradeoff for the entry TV camera electronics subsystem. For this subsystem one inch of insulation (weighing 1.0 lb) coated with a low emittance gold coating and three watts of heater power are selected. The insulation thickness of one inch is also sufficient to maintain the entry-TV camera within 100°F during entry phase. Analysis made in Section 5.4 Part E, Volume II shows that the heating from the camera window exposed to entry heating is 60 BTU/ft², and the resulting temperature rise of the entry TV lens is less than 40°F.

For the stagnation pressure transducer, one inch insulation (weighing 0.4 lb) with a low emittance gold coating was selected. As in the entry TV camera, one inch insulation is sufficient to maintain the transducer within 200°F during entry heating. During entry heating the transducer receive about 50 BTU/ft² of radiation heating from the backface of the beryllium atmospheric measurements probe.

INSULATION-POWER TRADEOFF FOR ESP THERMAL CONTROL

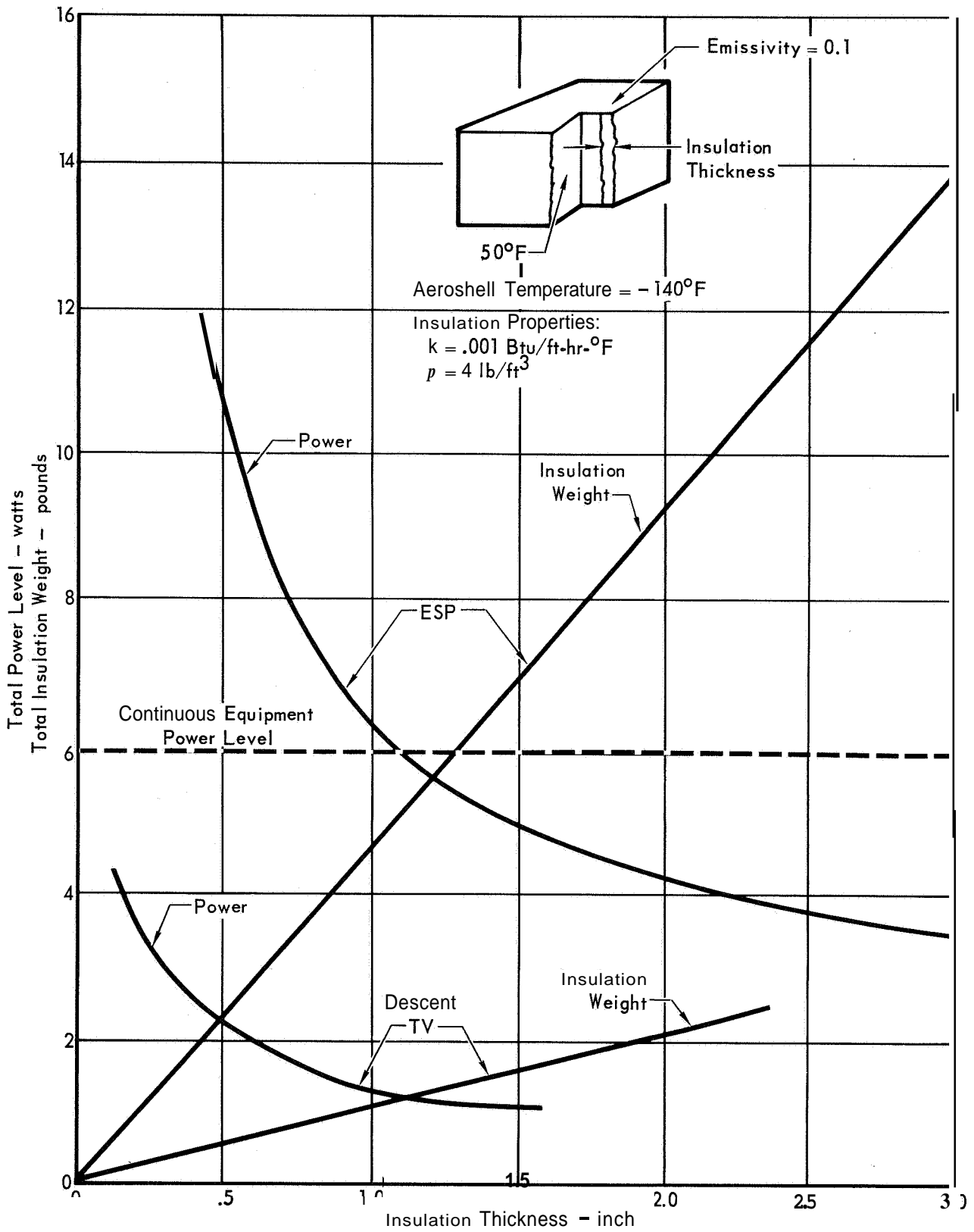


Figure 4.5-2

SECTION 5

CAPSULE BUS/ENTRY SCIENCE INTERFACES

The following paragraphs discuss the alternative designs of the Capsule Bus and Entry Science and their effect on each other. Factors leading to selection of the preferred Entry Science configuration are also presented.

5.1 TRAJECTORIES - Atmospheric reconstruction depends on the measurement accuracy of the entry experiments. If the spread of flight conditions can be narrowed - by reducing the range of atmospheric models or the spread of trajectories - then the operating range of several of the instruments can be reduced. Instruments with a narrower measurement range are more accurate and this will be reflected in the reconstruction of the Capsule trajectory.

At present, the Entry Science Package instrumentation must be designed to cope with a range of atmospheric models and a spread of Capsule trajectories. However, additional data and analysis of the atmosphere prior to the 1973 flight may indicate a narrower band of expected atmospheres. Also, if a narrow band of orbit sizes is defined for the Spacecraft operation, the possible range of Capsule de-orbit entry and landing conditions are reduced. The smaller entry corridor compatible with a narrowed orbit band would reduce the extremes of entry flight; and thus the maximum measurement range for the accelerometers, temperature, and pressure sensors could be reduced, dependent upon the change in the entry corridor.

A third type of flight variation, which is dependent upon the preferred Capsule Bus design, is the deceleration technique. The choice of aerodynamic decelerator, including deployment altitude, will increase or shorten the available flight time, particularly at speeds less than Mach 5. Separation of the Aeroshell terminates the measurement of the stagnation flow characteristics. Ignition of the terminal propulsion also degrades the atmospheric and flight measurements. This interplay of measurement time and trajectory events are dependent on the Capsule Bus design.

One factor which has not been used to restrict the entry trajectory but could be used to enhance the ESP data is the view of the surface as seen by the descent TV. Within the available range of entry angles, the steep angle will permit the high resolution, narrow field of view camera to view more of the area near the landing site. A shallow entry angle will not obtain the higher altitude high resolution camera view of the landing site but its longer flight time does provide the opportunity for more images. The lower resolution camera will obtain a high altitude view from planet limb to a point short of the landing site, depending upon

entry attitude control and accuracy, even for the shallow entry angles. However, consideration of the desired time versus view could well be a secondary factor in the selection of the preferred entry angle as well as entry attitude.

5.2 DE-ORBIT - The success of the Atmospheric Properties Determination Experiment is strongly dependent upon the accuracy of the trajectory reconstruction, which in turn depends upon the precision with which the entry conditions are known.

Since the entry conditions and their uncertainties depend directly upon the de-orbit conditions and their uncertainties, an examination of the implementation of the de-orbit functions would indicate means of minimizing uncertainties in the de-orbit conditions.

5.2.1 Preferred Design and Alternatives - The preferred design and implementation for the Capsule Bus de-orbit phase was described in detail in Part D, Section 4.2; in this section, the alternative designs and implementations are examined.

Preferred Design - The Capsule Bus gyros are caged and spun-up prior to separation from the Flight Spacecraft. When uncaged, the Capsule Bus gyros are not slaved to the Flight Spacecraft gyros, which produces an initial alignment error of magnitude less than or equal to the deadband of the Planetary Vehicle attitude control system (0.5"). This error, however, is removed in the postflight analysis by reduction of the monitored outputs of the FS gyros.

During the approximately 20 minute coast from separation to de-orbit, the Capsule Bus guidance and control computer maintains an attitude reference (a "virtual platform") by Euler angle processing of the strapdown gyro outputs. Attitude is controlled by the reaction control system (RCS) with a 2" deadband.

During de-orbit thrusting, the RCS holds the Capsule attitude against the thrust misalignment torque with an 0.25" deadband. Monitoring of gyro and RCS signals during thrusting determines which side of the yaw and pitch deadbands the Capsule is holding on. Thrust termination is commanded on the integrated output of the body-mounted guidance and control accelerometer. Monitoring the integrated output of this accelerometer determines the "tailoff" velocity increment.

Alternatives and Operational Variations - Alternative mechanizations of the attitude reference function are (1) stable platform and (2) strapdown gyros with simple rate-integration (analog or digital). The stable platform has been eliminated from contention on the basis of weight and reliability. The remaining alternatives were compared on the basis of their error growth rates. Since the simple strapdown system would exceed the design error budget of 0.86" after only 13 minutes, and de-orbit orientation maneuvers are programmed to take 10 minutes,

this approach was also eliminated. The preferred design remains within the specified error limit for up to 29 min of coasting.

Attitude-control alternatives for the period of de-orbit thrusting are the various methods of thrust vector control (TVC): fluid injection, gimballed nozzle, and jet vanes. Fluid injection suffers from weight and complexity, and is eliminated on that basis. Any of the TVC systems cause some interference with the preferred thrust termination method of nozzle blowoff; but, since there are thrust-termination alternatives, this should not be taken as decisive.

Alternative thrust-termination methods are (1) cut off on burn time, computed on the basis of a nominal burning rate history, and (2) motor burnout, achieving the desired entry conditions by varying de-orbit anomaly and attitude.

The preferred mode of de-orbit monitoring begins with monitoring of the Flight Spacecraft gyros, before Capsule Bus separation. Under the priority of communications constraints, however, de-orbit monitoring may have to be limited to the period of retrofire only, or be eliminated entirely.

5.2.2 Effects on Errors at De-Orbit - The de-orbit pointing angle and velocity uncertainties for the various attitude control, thrust termination and de-orbit monitoring alternatives may now be computed. Results of these topic subjects are summarized in Figure 5.2-1.

Attitude Control - The dominant component of the retrofire disturbance is a steady torque, due to thrust misalignment and c.g. offset uncertainties. The oscillatory component, due to asymmetric burning, is negligible. Under such conditions, the TVC systems normally give superior performance to RCS control. Thrust vector control acts as a damped linear system; after an initial lightup transient, the system removes the thrust misalignment error, converging to a steady-state (torque-free) condition in which the thrust vector passes through the Capsule c.g. The residual pointing error is due only to c.g. offset uncertainty. The magnitude of this error is determined by the ratio of the c.g. offset uncertainty and the distance from the c.g. to the effective center of rotation of the thrust vector. For a 3σ c.g. offset uncertainty of 0.26 inches, this error will be 0.27" for a gimballed nozzle TVC, and 0.21° for a jet-vane TVC (using 55 and 71 inches for the distances to the nozzle throat and exit plane, respectively).

RCS attitude control results in oscillatory limit cycle behavior on one side of the deadband. The deadband is 0.25' per axis in pitch and yaw, giving an rms pointing error of 0.35'.

DE-ORBIT ERRORS (3σ) FOR VARIOUS ALTERNATIVES

OBJECTIVE	ALTERNATIVES	ASSOCIATED ERRORS	
		POINTING, DEG	VELOCITY, FT/SEC
Retrofire Termination	ΔV Cutoff *	--	0.4
	Time Cutoff	--	1.5
	Burnout	--	4.0
Attitude Control	Reaction Jets*	0.35	--
	Jet Vanes	0.27	--
	Gimballed Nozzle	0.21	--
De-Orbit Monitoring	From Separation*	0.53	.25
	Retrofire Only	0.73	.25
	No Monitoring	0.77	.47

+Preferred design

Figure 5.2-1

Thrust Termination - For the preferred design, uncertainties in burn history, accelerometer bias and cutoff lags contribute a cutoff error (3 σ) of 24 lb-sec impulse, or less than 0.2 ft/sec for a 4180-lb de-orbit weight.

If cutoff is determined by burn time, a non-nominal burning-rate history can contribute 200 to 400 lb-sec depending upon the nominal burn length. Cutoff-lag uncertainties contribute 21 lb-sec more, for a 35 rssi error of 201 to 401 lb-sec for the time-cutoff method, giving a ΔV uncertainty of 1.5 to 3.1 ft/sec.

If the motor is allowed to burn out, the total impulse will be 172,000 lb-sec \pm 0.3% (3 σ), giving an impulse uncertainty of 516 lb-sec, or 4.0 ft/sec.

De-Orbit Monitoring - Monitoring during retrofire removes the pointing error contribution due to the RCS deadband (0.25 $^\circ$), and the ΔV contribution due to cutoff lags (0.4 ft/sec). Additional pre-separation monitoring removes the initial alignment error due to the FS attitude control deadband (0.5 $^\circ$).

5.2.3 Effects on Errors at Entry - The pointing error and velocity error values of Figure 5.2-1 may be mapped onto errors in entry conditions, using computed sensitivity coefficients. To illustrate the further variation of entry errors with nominal de-orbit conditions, two tables are given (Figures 5.2-2 and 5.2-3), using entry sensitivities for de-orbit anomalies of 180 $^\circ$ and 225 $^\circ$, respectively. For both of these figures the propagation is carried to the nominal entry altitude (800 K ft), rather than to nominal entry time. The arrival time errors in turn lead to large position and velocity errors for all activities which are commanded on an elapsed-time basis.

5.3 AEROSHELL PROPERTIES - The alternatives for science sensor locations depend upon the aerodynamic and other characteristics of the Aeroshell and effect the quality and quantity of science data. The requirements of the science measurements determine the placement of the sensor and the type of heat protection system to be used in the Aeroshell. The following section discusses the alternative Aeroshell design and its influences on ESP science measurements.

5.3.1 Aerodynamic Properties of Capsule for Alternative Measurements

5.3.1.1 Composition and Temperature - The high stagnation point temperatures to be experienced by the extended probe alternative, for stagnation composition and temperature measurement, requires a stagnation point probe extending beyond the local boundary layer thickness but not extending beyond the bow shock distance. This introduces two new problems not discussed previously:

- o Ablation products given off during a major portion of the entry flight phase may interfere with proposed experiments at angle of attack for

ENTRY ERRORS (3σ) FOR VARIOUS DEORBIT ALTERNATIVES
(DE-ORBIT ERRORS PROPAGATED TO ENTRY ALTITUDE)
DE-ORBIT ANOMALY = 180°

OBJECTIVE	ALTERNATIVES	RESULTING ERROR CONTRIBUTIONS				
		VELOCITY (FT./SEC)	FLIGHT PATH ANGLE (DEG)	HEADING (DEG)	CENTRAL ANGLE (DEG)	TIME (SEC)
Retrofire Termination	ΔV cutoff*	0.06	0.03	—	0.08	2.6
	Time cutoff	0.22	0.13	—	0.29	9.7
	Burnout	0.59	0.30	—	0.77	25.8
Attitude Control	Reaction jets*	—	—	0.05	0.02	9.4
	Jet vanes	—	—	0.04	0.01	7.3
	Gimballed nozzle	—	—	0.03	0.01	5.6
De-Orbit Monitoring	From separation*	0.04	0.02	0.07	0.05	14.3
	Retrofire only	0.04	0.02	0.10	0.06	19.7
	No monitoring	0.07	0.04	0.10	0.10	20.9

* Preferred Design

Figure 5.2-2

ENTRY ERRORS (3σ) FOR VARIOUS DE-ORBIT ALTERNATIVES
(DE-ORBIT ERRORS PROPAGATED TO ENTRY ALTITUDE)
DE-ORBIT ANOMALY = 225°

OBJECTIVE	ALTERNATIVES	RESULTING ERROR CONTRIBUTIONS				
		VELOCITY (ft/sec)	FLIGHT PATH ANGLE (deg)	HEADING (deg)	CENTRAL ANGLE (deg)	TIME (sec)
Retrofire Termination	ΔV Cutoff*	0.13	0.01	—	0.03	0.3
	Time Cutoff	.50	.05	—	.10	1.2
	Burnout	1.32	.14	—	.26	3.1
Attitude Control	Reaction Jets*	—	.17	.04	.36	7.0
	Jet Vanes	—	.13	.03	.33	5.4
	Gimballed Nozzle	—	.10	.03	.22	4.2
De-Orbit Monitoring	From Separation*	.08	.25	.07	.55	10.6
	Retrofire Only	.08	.34	.09	.75	14.6
	No Monitoring	.16	.37	.10	.79	15.5

+Preferred Design

Figure 5.2-3

small probe extensions

- o Real gas effects caused by the high temperatures invalidate the perfect gas equation

$$\frac{T_{\text{STAG}}}{T} = 1 + \frac{\gamma-1}{2} \gamma M^2 \quad (1)$$

which relates stagnation point and freestream temperatures.

Composition Sensor - The ablation products will not interfere with the composition sensor as long as the sensor port lies outside the aeroshell boundary layer.

Stagnation Temperature - The relation between stagnation temperature and free stream temperature given by equation (1) is not valid in the high Mach number flight regime. Stagnation point temperature calculated to account for the equilibrium chemistry of the VM atmospheric models has been compared with equation (1) in figure 5.3-1. Agreement is excellent after 150 seconds from entry which corresponds to Mach numbers below 5. Above Mach 5 the two methods differ due to the real gas effects. For the higher Mach number regime the perfect gas relation is unsuitable and the equilibrium chemistry of the gas must be accounted for.

5.3.1.2 Pressure Measurements - Figure 4.3-4 of Part D, Section 4 presented experimental pressure distributions on the preferred VOYAGER configuration. This data shows that the Newtonian pressure prediction at the sphere-cone junction is in error by as much as 30 percent at zero degree angle of attack with closer agreement at increasing angle of attack. As indicated in Section 4.3.1 of Part D, the one strip method of integral relations and correlations of experimental data can be used to better define the pressure levels at the sphere-cone junction as a function of angle of attack, Mach number and Reynolds number.

The extension of the stagnation pressure sensor beyond the aeroshell is permissible as long as its length remains within the shock layer. Figure 5.3-2 presents the shock standoff distance which can be used to define this constraints. Using the data of this figure the maximum sensor length should not exceed approximately 2.5 inches.

5.3.1.3 Gamma-Ray Backscattering - This experiment requires a definition of the shock standoff distance and the bow shock wave shape at low supersonic and hypersonic Mach numbers. Estimates of the standoff distance normalized by the base radius are presented in Figure 5.3-2. These data were obtained from analysis of shadowgraphs of shock shape about the VOYAGER configuration which was tested

COMPARISON OF STAGNATION TEMPERATURE CALCULATION

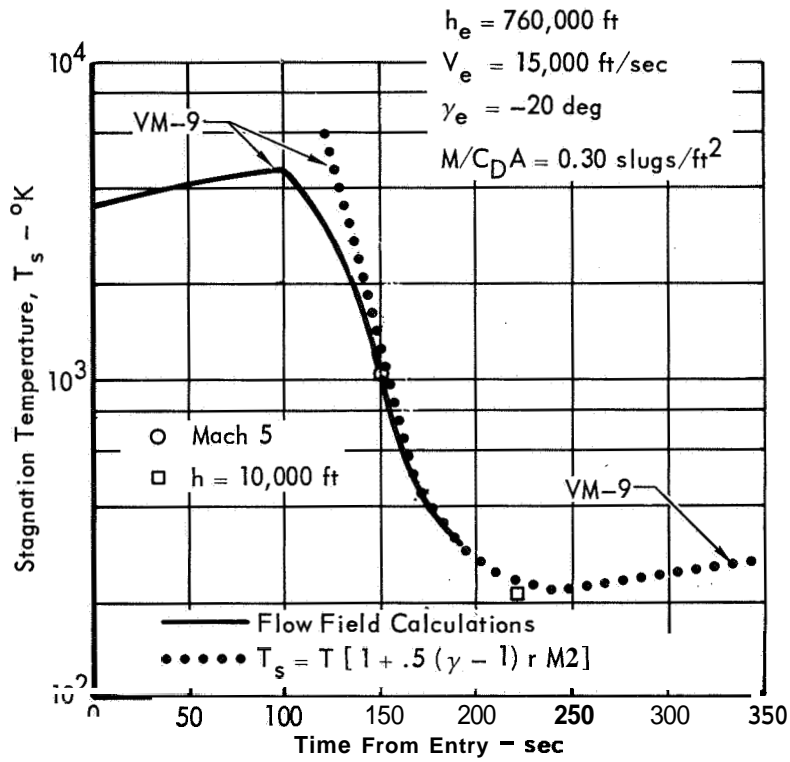
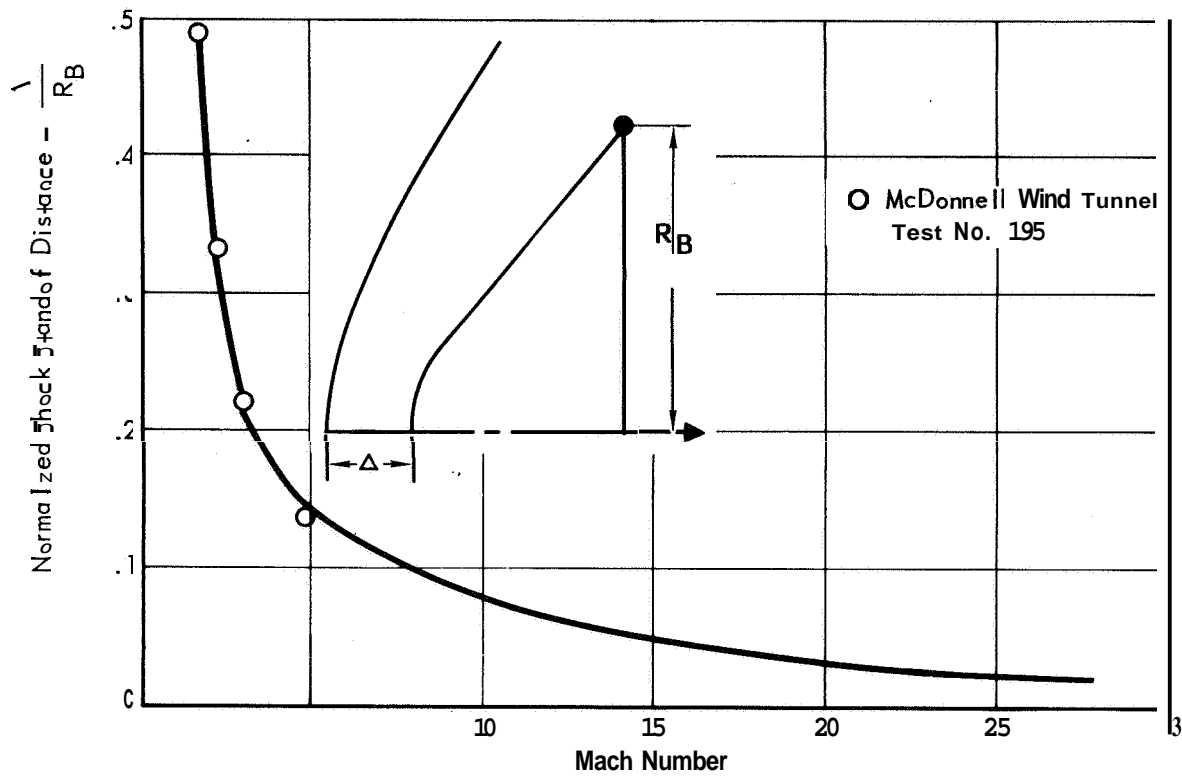


Figure 5.3-1

SHOCK STANDOFF DISTANCE FOR A 120° SPHERE-CONE



COMPARISON OF THEORETICAL AND EXPERIMENTAL SHOCK WAVE SHAPE

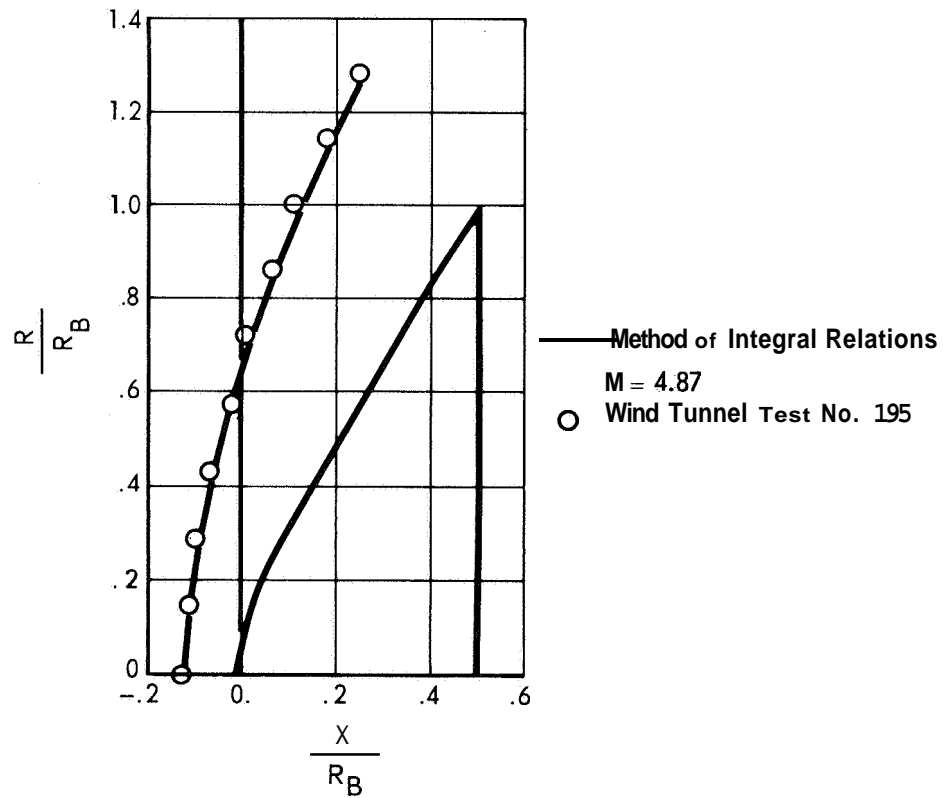


Figure 5.3-2

in the McDonnell wind tunnel facility. Beyond a Mach number of 4.87 the data is extrapolated by using calculations for standoff distance about a sphere and flow field calculations about a 120" sphere cone. The bow shock wave shape definition at lower Mach numbers can best be provided analytically by the method of integral relations described earlier. Figure 5.3-2 presents a comparison of this method with experimental data and, as shown, the agreement is good. Though the data is from tests performed in air, the computations can be done for other gas compositions by varying the specific heat ratio. For the VM atmospheres, the specific heat ratio has little effect on the standoff distance over the Mach range of interest.

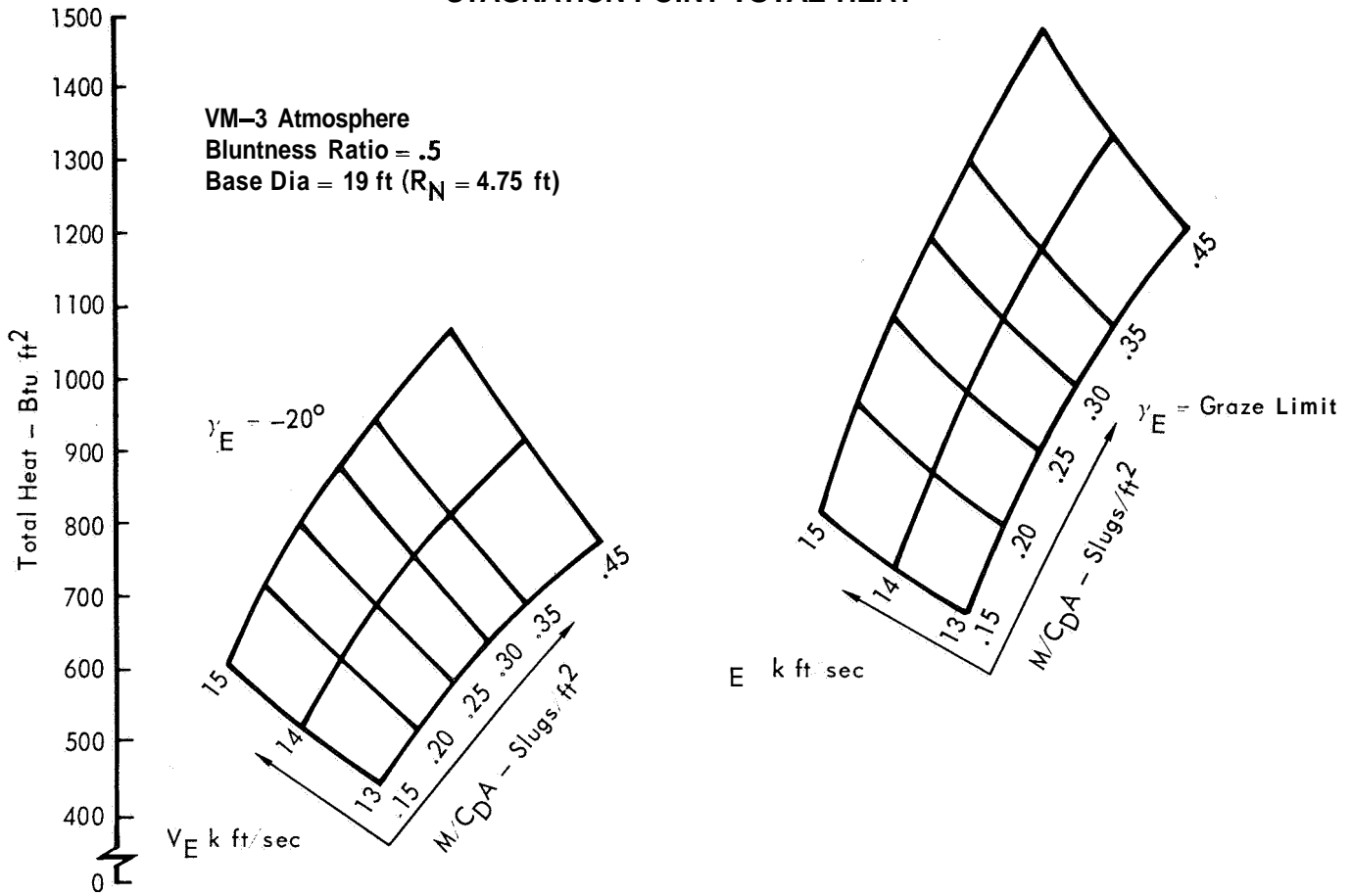
5.3.2 Heat Protection System - The Aeroshell heat protection system consists of a low density hardened Fiberfrax for the nose gap section, and a low density General Electric ESM 1004. silicone elastomeric ablator for the conical section. Selection of hardened Fiberfrax was made after our studies and tests indicated that the reaction products from an ablative nose cap would interfere with the ESP atmospheric composition measurements and degrade the TV window optics (as described in Section 5.3.2, Volume IV). The G.E. ESM 1004X was selected for the heat shield for the conical section because it showed the best overall material performance.

5.3.2.1 Nose Cap Heat Shield Requirements - The basic requirement for the nose cap heat shield is to thermally protect the Aeroshell substructure. In addition, reaction products of the heat shield must not contaminate the atmosphere measurements or degrade the TV window optics. The full nose cap configuration including heat shield, adhesive and backup structure must be RF transmissive for the radar altimeter.

5.3.2.2 Entry Heating Environment - Because of the relatively low entry velocities (13,000 to 15,000 ft/sec) into the low density Martian atmosphere, a relatively mild heating environment will be experienced by the nose cap region. The flight parameters which affect the magnitude of heating for a fixed geometric configuration are entry velocity, initial entry path angle, atmospheric model, and ballistic coefficient.

The manner in which these parameters influence the stagnation point heating rate and total heat load is shown in parametric form in Figure 5.3-3. Because of the large nose radius and consideration of possibly a $\pm 20^\circ$ variation in angle-of-attack throughout entry (RCS system malfunction), the entire nose cap can be considered as being subjected to the stagnation point heating rate value.

STAGNATION POINT TOTAL HEAT



STAGNATION POINT HEAT TRANSFER RATE

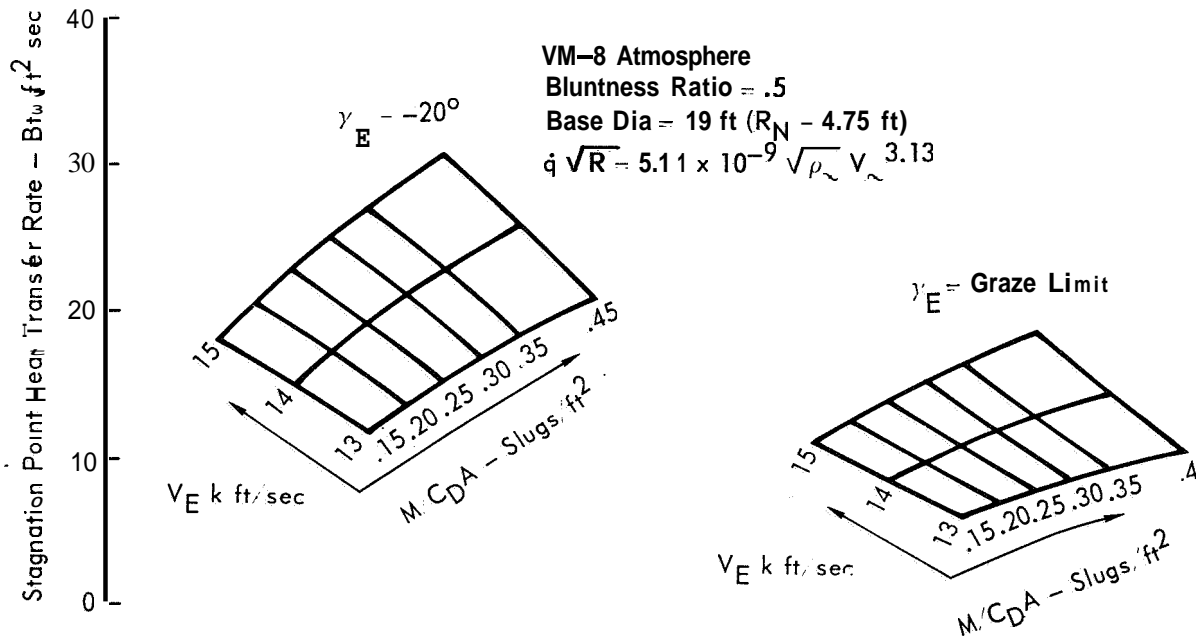


Figure 5.3-3

For instance, at maximum angle of attack, the tangency line local heating rate is 94% of stagnation point value. Although a large number of trajectories are possible, for the thermal analysis it will suffice to investigate the highest peak heating rate trajectory which causes the highest surface temperature,

$$\begin{aligned}
 V_E &= 15,000 \text{ ft/sec} \\
 \gamma_E &= -20^\circ \\
 \text{VM-8} &\text{ atm} \\
 m/C_D A &= .30 \text{ slug/ft}^2
 \end{aligned}$$

and highest total heat load trajectory, which causes the highest bondline temperature,

$$\begin{aligned}
 V_E &= 15,000 \text{ ft/sec} \\
 \gamma_E &= -14.07^\circ \\
 \text{VM-3} &\text{ atm} \\
 m/C_D A &= .30 \text{ slug/ft}^2
 \end{aligned}$$

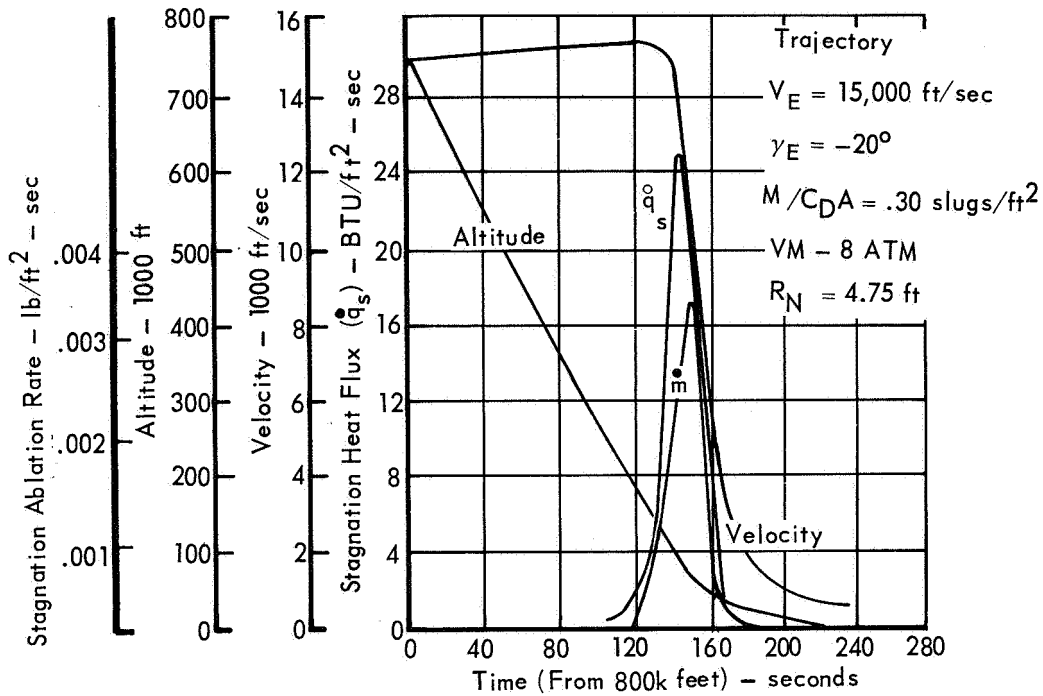
as shown in Figure 5.3-4.

5.3.2.3 Ablative Nose Cap Heat Shield - Use of the ablative material over the nose cap area is the simplest design and manufacturing approach to the thermal protection problem. However in order to use an ablative shield, a means to alleviate the contamination of stream gas by the ablation products is necessary to meet the ESP subsystem requirements. Existence of the ablation products in the boundary layer interferes with the atmospheric composition measurement and, the TV camera window optics by condensing and otherwise coating the window. Histories of stagnation point ablation rates for the highest peaking heating (steep entry) and the highest total heat load (shallow entry) trajectories are shown in Figure 5.3-4.

One way of eliminating the ablation product contaminants from the atmospheric measurement is to provide a protruding sampler probe which will extend beyond the boundary layer. Our studies show that in the nose cap region the boundary layer thickness is less than one inch thick most of the time during entry, while the minimum shock standoff distance is on the order of 2.5 inches. Thus protruding the probe about two inches would ensure against picking up any ablation products from the boundary layer at least for the low angle of attack case. A small probe would not significantly affect the Capsule aerodynamic characteristics.

Prevention of ablation product deposition on the TV window is more difficult. It has been shown in our ablation test programs and in the Gemini flights (as

HIGHEST PEAK HEATING TRAJECTORY



HIGHEST TOTAL HEAT LOAD TRAJECTORY

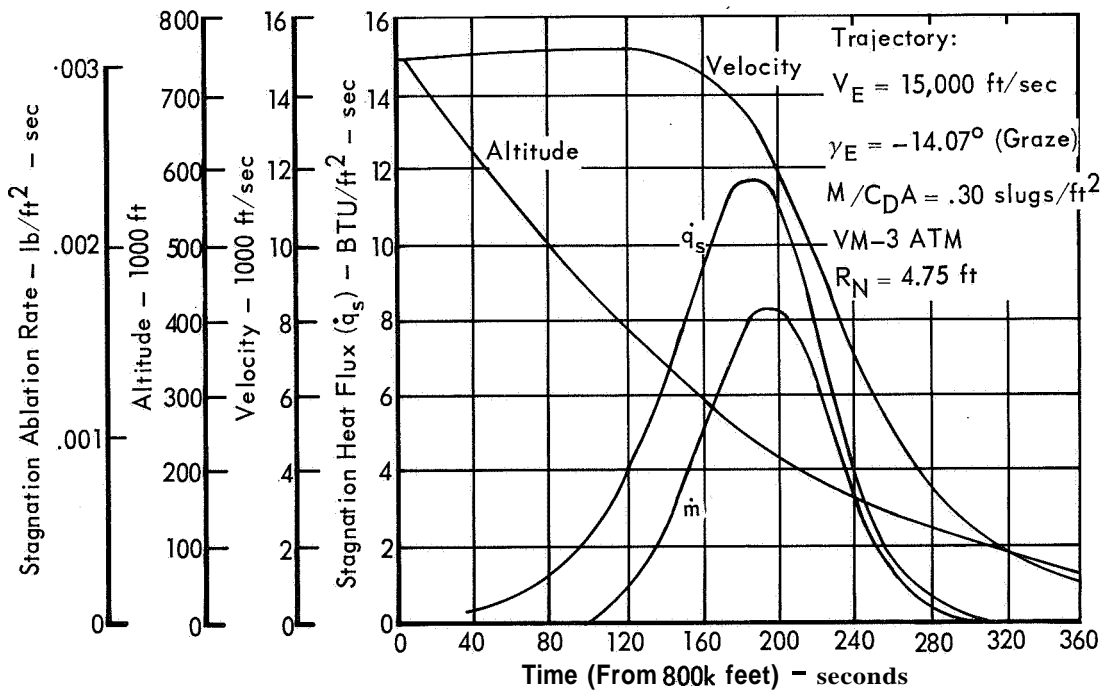


Figure 5.3-4

described in Section 2.2, Part E, Volume IV), as well as by others, that ablation products definitely deposit on a glass window downstream from an ablative heat shield.

To maintain adequate TV coverage during the entry phase with an ablative nose cap would require either the use of multiple layer windows which are removed at certain intervals or blocking of the ablation products by injecting a clean gas from the forward edge of the recessed window during entry. The first method requires accurate techniques for sensing and executing the operation. Also removal of the window can damage the ablative heat shield as the window pane is blown off rearward.

The second method is simpler than the first in executing the required operation. However, the additional hardware required for the second method is quite complicated and weight penalizing.

5.3.2.4 Non-Ablative Nose Cap Heat Shield - Since utilization of an ablative nose cap without introducing additional hardware design will prevent having good ESP atmospheric measurements and TV coverage, our baseline approach is to use a non-ablating material for the spherical cap areas in front of the TV window.

A material evaluation program was conducted to select a material which meets the following requirements :

- o No outgassing at the Capsule entry temperatures
- o Transmissive to the altimeter radar UHF frequency
- o Good thermal - structural efficiency
- o Not affected by ETO sterilization, long duration hard vacuum, and low temperature
- o State of the art material, and a simple existing fabrication process available for the large scale production.

Using these selection factors as guidelines, the following composite materials were evaluated.

- o Hardened Fiberfrax - low density composite of aluminosilicate fiber cemented with an inorganic binder
- o Foamed alumina coated with a high density alumina surface
- o Honeycomb sandwich structure fabricated from aluminum phosphate and fused quartz fabric reinforcement.

Certain ceramic materials such as boron nitride, fused silica, and Pyroceram were eliminated because of high density and complicated fabrication techniques.

The selected material is hardened Fiberfrax because it is satisfied all of the nose cap requirements and has a simple fabricated method for large scale construction.

5.3.2.5 Nose Cap Heat Shield Design - Having selected the preferred nose cap heat shield material, hardened Fiberfrax, the remaining task is to determine the required heat shield thickness to maintain the backup structure temperature at or below design limits. As shown in Figure 5.3-3, the backup structure is a phenolic fiberglass sandwich that is bonded to the hardened Fiberfrax shield with HT-435 high temperature adhesive. A maximum design temperature of 735" was selected for the backup structure based on thermal-stress considerations, To account for uncertainties in the material quality control and heat shield analysis a safety factor of 1.15 is applied to the design temperature rise. Thus, the nose cap shield is sized to limit the bondline (between the hardened Fiberfrax and the backup structure) temperature to 640°F for the spectrum of entry heating conditions possible due to the entry corridor and various atmospheric models.

5.3.2.5.1 Thermal Analysis and Material Requirement - Prediction of the temperature response of a passive (non-ablating) heat shield system, such as the preferred hardened Fiberfrax nose cap material, is rather straightforward, especially with the aid of high speed digital computers. The thermal analysis reported herein is based on one-dimensional heat conduction theory for a multiple slab model exposed to radiative and convective surface heatings. Verification of the analytical approach is shown in Figure 5.3-6, which shows a close correlation between the predicted and measured bondline temperature responses for the thermal performance tests. The test data correlated thermal properties for hardened Fiberfrax used in the analysis are listed below.

Density	25 lb/ft ³
Specific Heat	0.22 Btu/lb-°F
Thermal Conductivity	0.025 Btu/ft-hr°F at 100°F 0.080 Btu/ft-hr°F at 1000°F 0.0140 Btu/ft-hr°F at 2500°F
Emissivity	0.8

Based on the forementioned thermal analysis and property data, the trade-off between unit heat shield weight (density x thickness) and maximum bondline temperature is made and the results are shown in Figure 5.3-5 for the highest heat load entry trajectory. It is shown that to limit the bondline temperature rise to 640°F, it requires 0.67 lb/ft² of hardened Fiberfrax material. Since the entire nose cap area experiences approximately the same magnitude of heating, a constant thickness

**MAXIMUM BONDLINE TEMPERATURE vs CERAMIC NOSE CAP WEIGHT
THERMALMODEL**

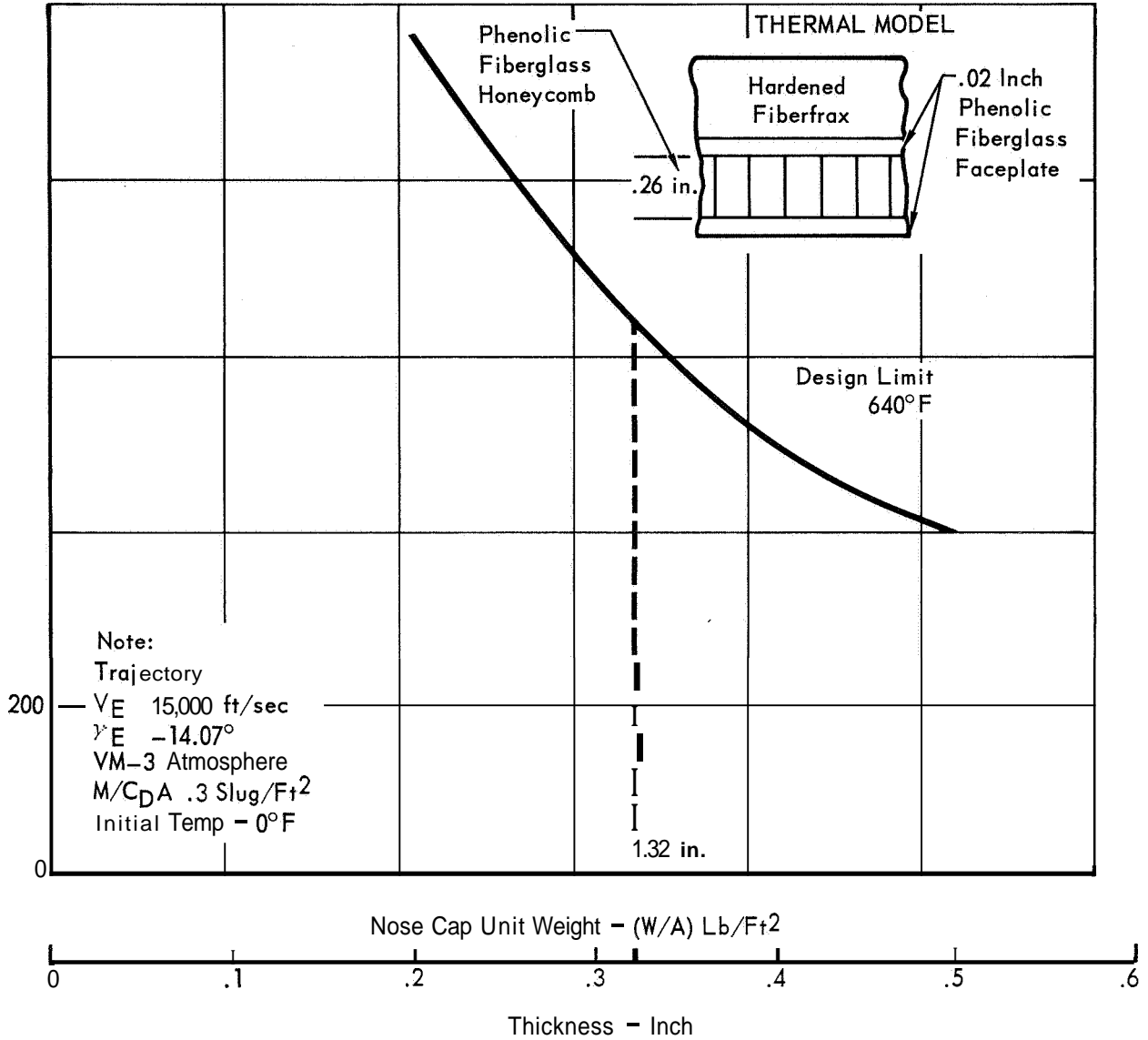
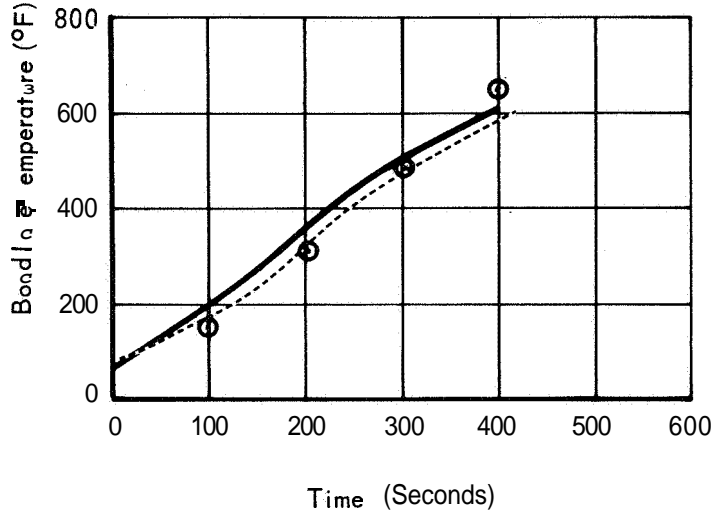


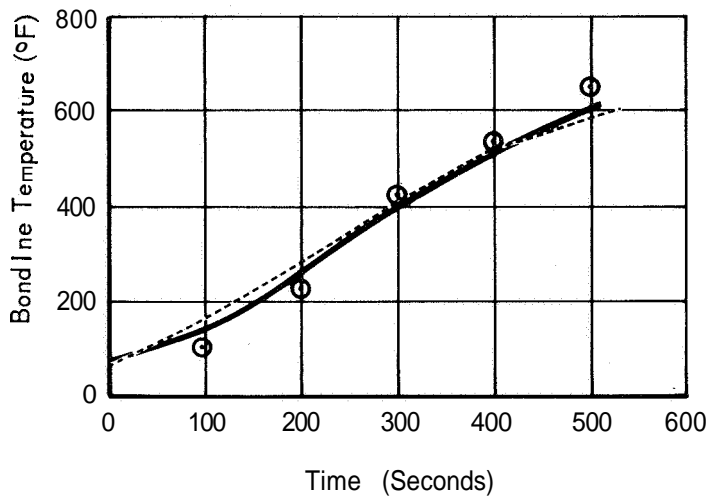
Figure 5.3-5

**THERMAL PERFORMANCE OF HARDENED FIBERFRAX
OXY-ACETYLENE TORCH FACILITY**

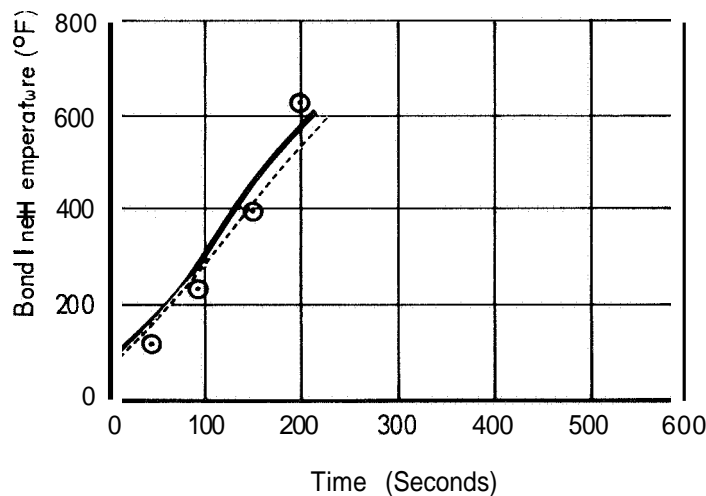


— First Test Data
 - - - Second Test Data
 ○ Computed Results

Fiberfrax - 466
 Density = 19.0 Lb/Ft³
 W/A = 0.604 Lb/Ft²
 $\dot{q}_{cw} = 12 \text{ Btu/Ft}^2 - \text{Sec}$



Fiberfrax - 61-B35
 Density = 29.0 Lb/Ft³
 W/A = 1.26 Lb/Ft²
 $\dot{q}_{cw} = 12 \text{ Btu/Ft}^2 - \text{Sec}$



Fiberfrax - 466-B40
 Density = 44.0 Lb/Ft³
 W/A = 1.11 Lb/Ft²
 $\dot{q}_{cw} = 12 \text{ Btu/Ft}^2 - \text{Sec}$

Figure 5.3-6

nose cap is recommended. The Fiberfrax surface, midpoint and bondline temperature histories are shown in Figure 5.3-7 for the steep and shallow entries.

Although the shallow entry trajectory provides the highest backface temperature, due to the long heat soak period, the steep entry results in the highest surface temperature. A peak temperature of 2100°F is shown in Figure 5.3-7 for the steep entry condition, but also note that the surface temperature is above 1600°F for only 20 seconds. Because of the rapid change in surface temperatures, a maximum of 70° F/sec, the steep entry will provide the greatest thermal shock problem. No indication of thermal shock effects, such as surface crazing, were evident in any of the thermal performance tests. In these tests the material was exposed to an instantaneous square heat pulse which is more severe, with respect to thermal shock, than the anticipated sinusoidal entry heat pulse.

5.3.6 ~~TV Window~~ - The TV window, located near the sphere-cone tangency line, serves as both an optical and thermal cover for the TV camera. Thus, it must be capable of withstanding both the heating and pressure loads encountered during entry, and at the same time minimizing backface radiation heating to the TV camera optics.

The preferred window material is Corning 7940 fused silica manufactured by the Corning Glass Company. It was selected on the basis of adequate temperature capability and good optical properties at high temperatures. The window material is optically good to 2000°F and structurally adequate to 2500°F. To reduce radiation heat transfer to the internal optics, the backface is coated with a heat control filter consisting of zinc sulfide and silicon oxide. The filter is optically transparent and can reflect a large portion of the infrared component of the radiation back to the source, and is stable to 2000°F.

A one-dimensional heat conduction analysis, similar to that used on the passive nose cap, was performed to determine the peak temperatures expected during entry and also the window thickness required to minimize backface radiation heating. The following thermal properties of fused silica were used in the analysis.

Density	165 lb/ft ³
Specific Heat	0.16 Btu/lb-°F at 0°F 0.25 Btu/lb-°F at 1500°F
Thermal Conductivity	0.765 Btu/ft-hr-°F at 0°F 1.150 Btu/ft-hr-°F at 1500°F
Emissivity	0.6

NOSE CAP MATERIAL PERFORMANCE

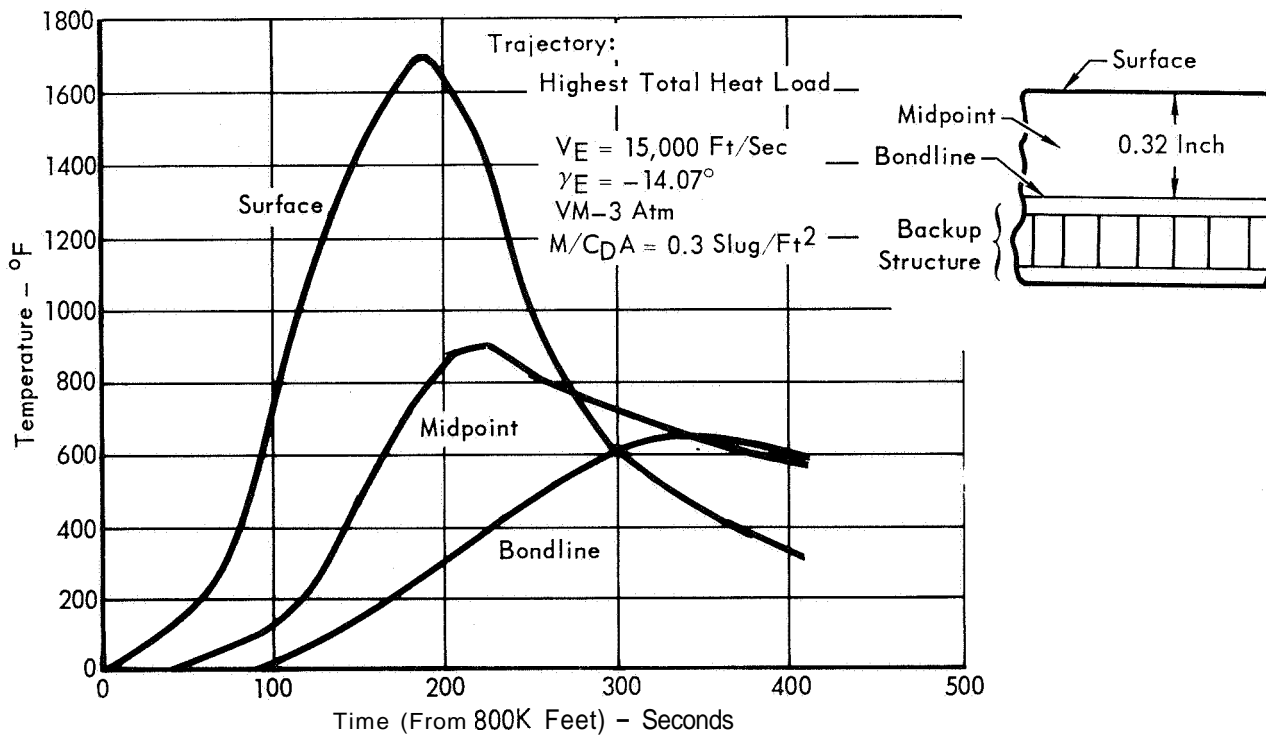
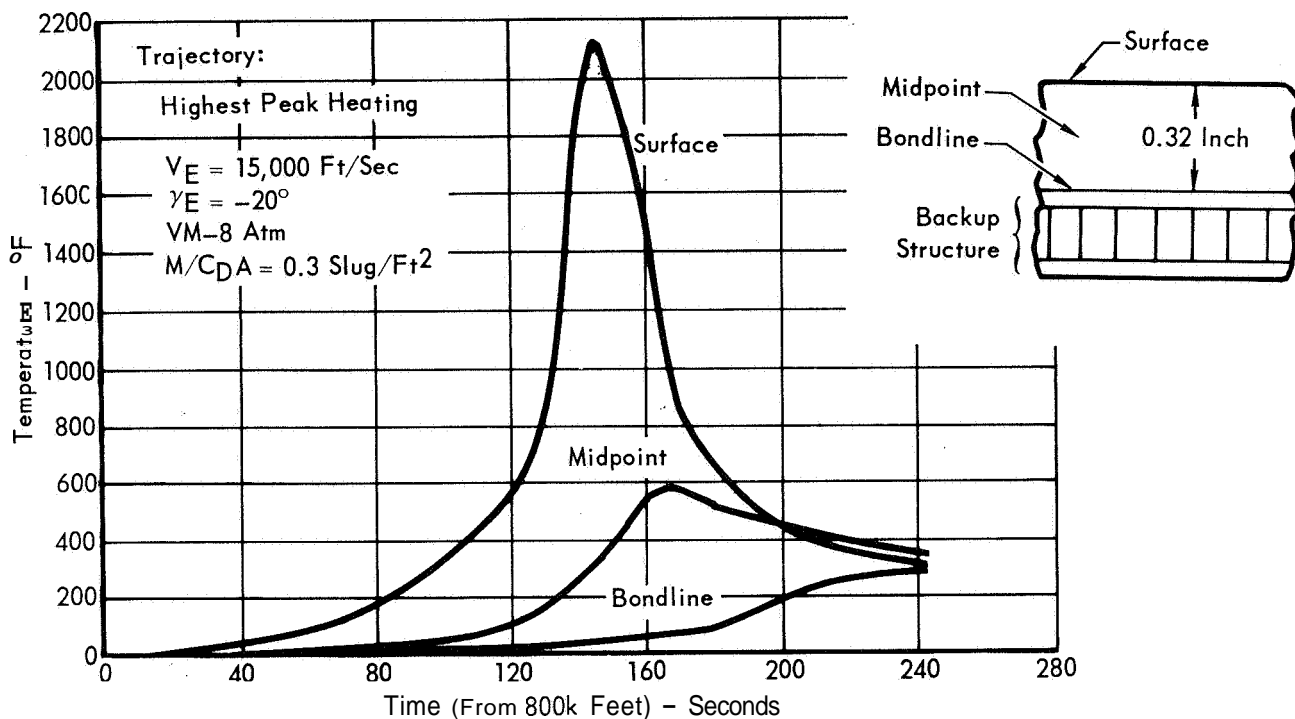


Figure 5.3-7

The temperature response from both the highest peak heating and highest total heat trajectory were investigated.

The variations of surface and backface temperatures with window thickness is shown in Figure 5.3-8. A window thickness of 0.375 inch was selected to provide enough support for the pressure loads and to prevent excessive temperature rise at the backface. In Figure 5.3-9 the temperature response at the surface, midpoint and backface is shown for the two limiting trajectories. Note that the peak temperature is only 1050°F and occurs for the shallow entry case instead of for the peak heating trajectory. This apparent anomaly is due to the relatively high thermal conductivity of glass which reduces the surface temperature gradients for the short steep entry.

To minimize the radiation heating to the internal TV optics, a heat control filter is applied on both the window backface and the TV camera lens. For the entry heat loads the estimated heat transfer to the lens is reduced to 60 BTU/ft². This results in a temperature rise of less than 50 F which is within the tolerance limit of the lens.

5.2.2.7 Heat Sink Plug for Atmospheric Measurement Probe - The heat sink plug for the atmospheric probe, located at the apex of the nose cap, serves as a heat sink material and structural support for the probe. Thus it must be capable of withstanding both heating and pressure loads encountered during entry. Also it must minimize the backface heating to the interior so that the temperature rise of the pressure transducer and conical monopole antenna can be kept at reasonable levels during the entry phase. From a wide variety of materials screened, beryllium was selected because of high thermal capacitance, good structural properties and flight proven history.

A one-dimensional heat conduction analysis, similar to that used on the nose cap, was performed to determine the temperature responses expected during entry and the thickness required to maintain the backface temperature below 400°F.

This backface temperature limitation was necessary because the heat sink plug is attached to the conical monopole antenna (of altimeter radar) whose maximum design temperature is 350°F.

The results of the analysis indicate that a material thickness of 0.5 inch will support the pressure loads and will limit the backface to 400°F for the worst heating entry condition.

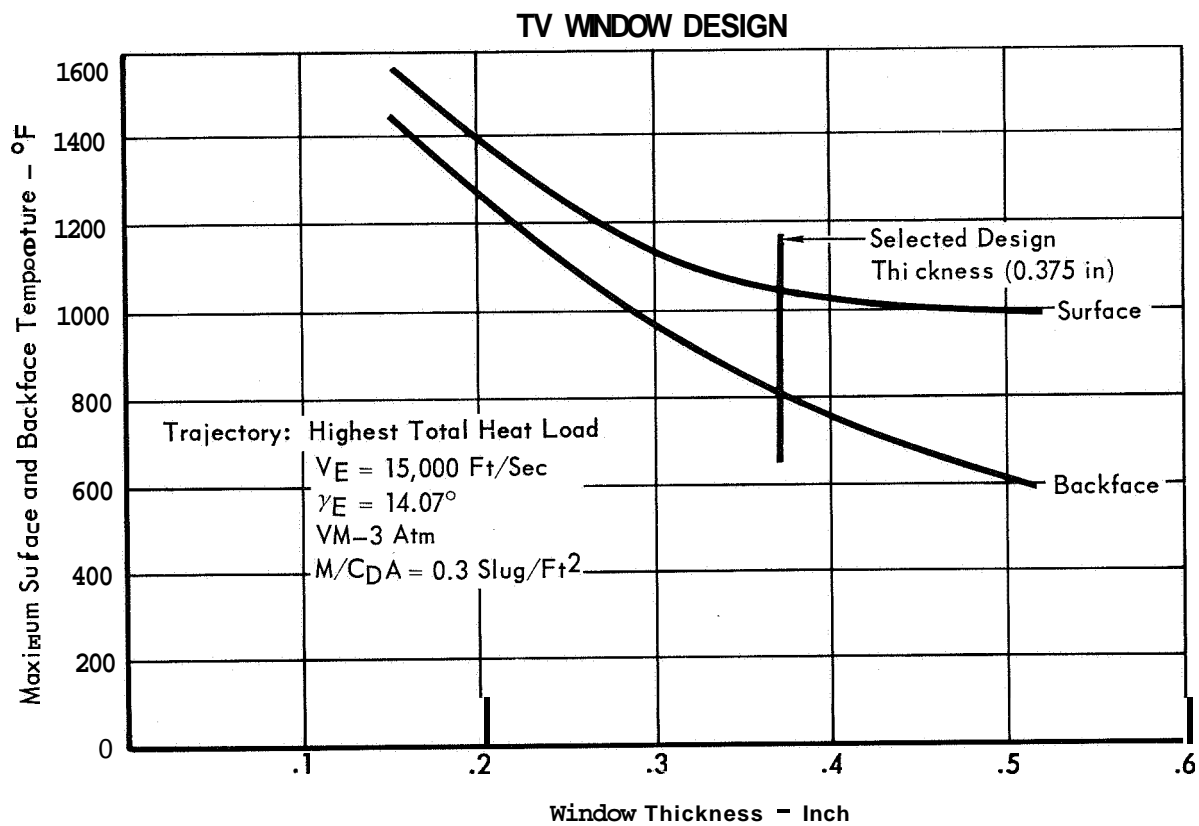


Figure 5.3-8

WINDOW MATERIAL PERFORMANCE

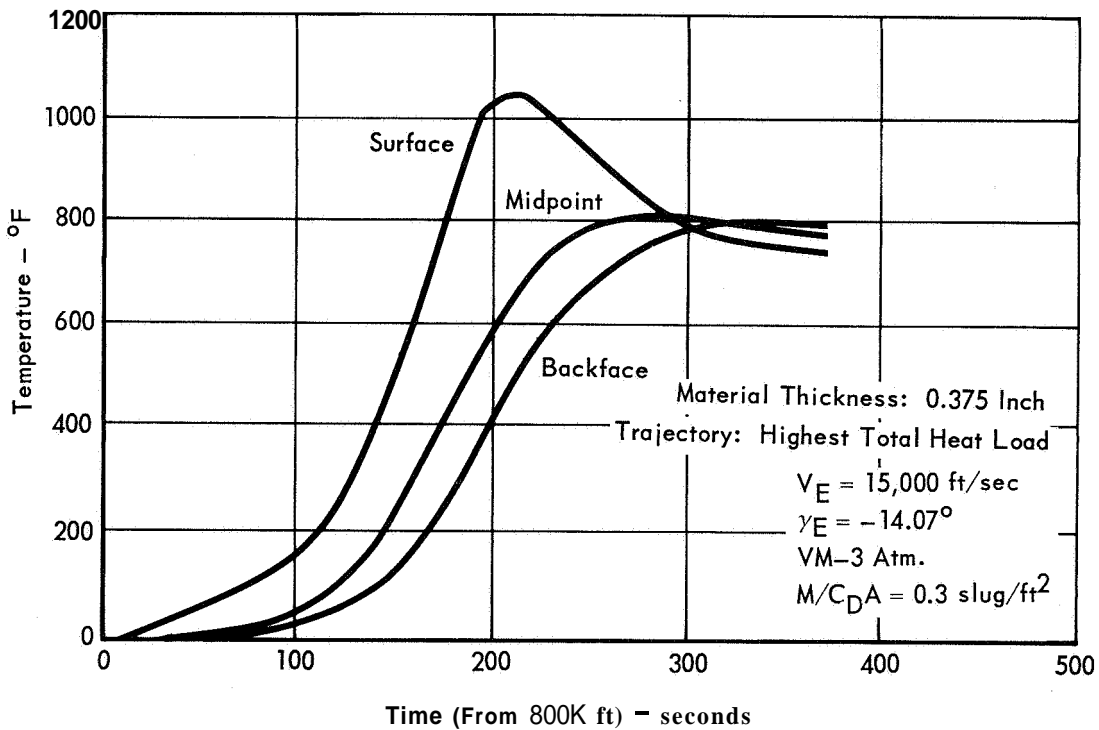
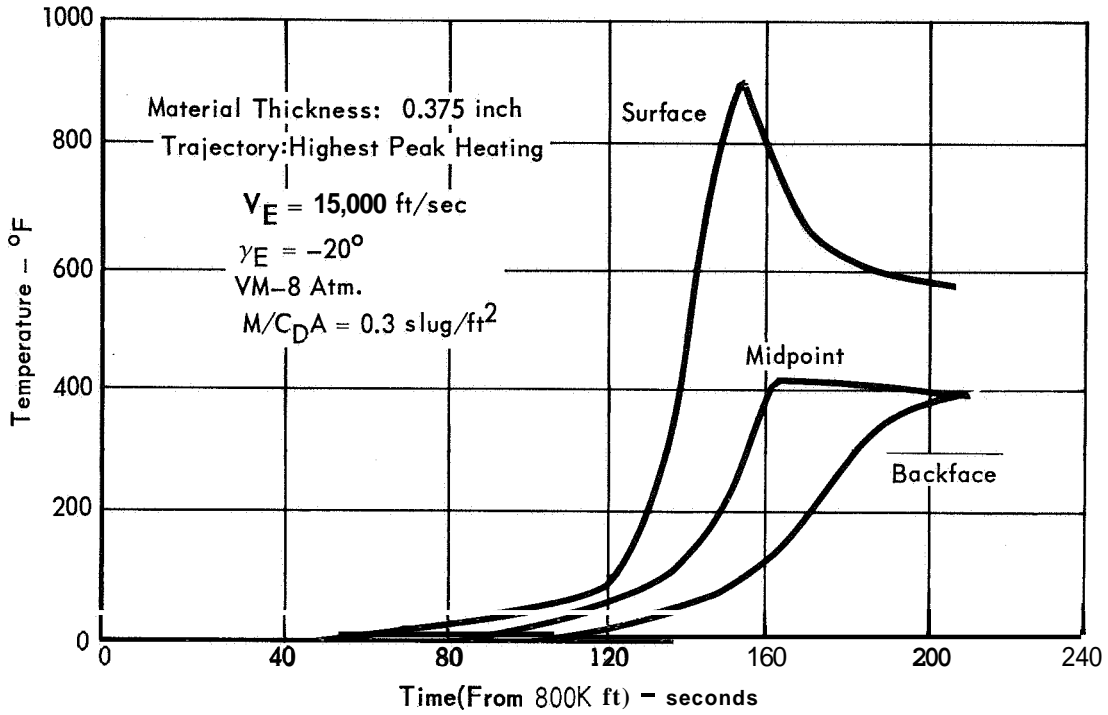


Figure 5.3-9

5.4 CAPSULE SEQUENCING - The sequencing and trajectory design alternatives of the Flight Capsule, coupled with the uncertainties of atmosphere and the time of atmospheric entry, create a wide range of operating conditions for the Entry Science Package (ESP). However, regardless of the atmosphere encountered or the descent trajectory design selected, the sequence of events for the ESP remain unchanged. The time spans of various Capsule events vary, thus changing the quantity of ESP data obtained during a particular phase, but the sequence remains unaltered.

The Flight Capsule, by definition, starts entry at a reference altitude of 800,000 feet. The 800,000 foot point cannot be determined by direct measurement (altimeter), and the uncertainty of indirect measurement (time from deorbit) is about \pm 60 seconds. In addition, warm-up of the instruments and both ends of the relay link is desired before actual data is obtained. To allow for entry time uncertainties and equipment warm-up, ESP operations are started 300 seconds prior to theoretical point of atmospheric entry. Actual entry will occur between 240 to 360 seconds after the start of ESP operation, thus allowing a minimum warm-up period of four minutes.

To this point we have been discussing the initial start of ESP operations. Some of the ESP's measurements must be performed from, or near, the point of entry through landing. Descent imaging and entry deceleration fall into this category. Other measurements, such as for stagnation temperature and atmospheric composition are performed below about Mach 5 after the temperature sensor outlet bleed line is opened. However the power, instrument electronics, and telecommunication channels for all ESP measurements are started at the same time because it simplifies the data handling and sequencing with no significant penalties either in power, data transmission, data buffer storage or instrument damage.

The alternatives of Capsule sequencing are constrained by the necessity to soft land the Capsule Bus and Surface Laboratory, on the surface. These constraints dictate a virtually inflexible Capsule sequence once the basic elements of the terminal descent are selected. By basic elements we mean parachutes, aeroshell separation after decelerator deployment, "fire-in-the-hole", "fire through the hole", or other terminal thrust alternative. For our preferred Capsule design we have selected the combination of parachute and terminal propulsion descent. The sequence of events for this design in the extremes of atmospheric models is shown in Figure 5.4-1. The relative inflexibility of the Capsule sequence for typical alternatives is discussed below:

ENTRY AND LANDING PHASE TIME LINE

Events

- ① Deceleration = .05g
- ② Mach 5
- ③ H = 23 kft (Chute Deploy)
- ④ H = 5 kft (Start-Terminal Descent)
- ⑤ Touchdown
- ⑥ End of F/C-S/C View, 34° Gnd. Slopes

Notes:

- 1. Orbit Size - 4400 x 23,400 km
- 2. $\theta_{DO} = 191^\circ$
- 3. $V_E = 15,000 \text{ ft/sec}$
- 4. $M/C_D A = .3 \text{ slugs/ft}^2$
- 5. Deflection Angle (δ) Adjusted to Meet Multipath Considerations
- 6. Time from Parachute Deployment to Capsule Bus Separation from Aeroshell = 12 sec.

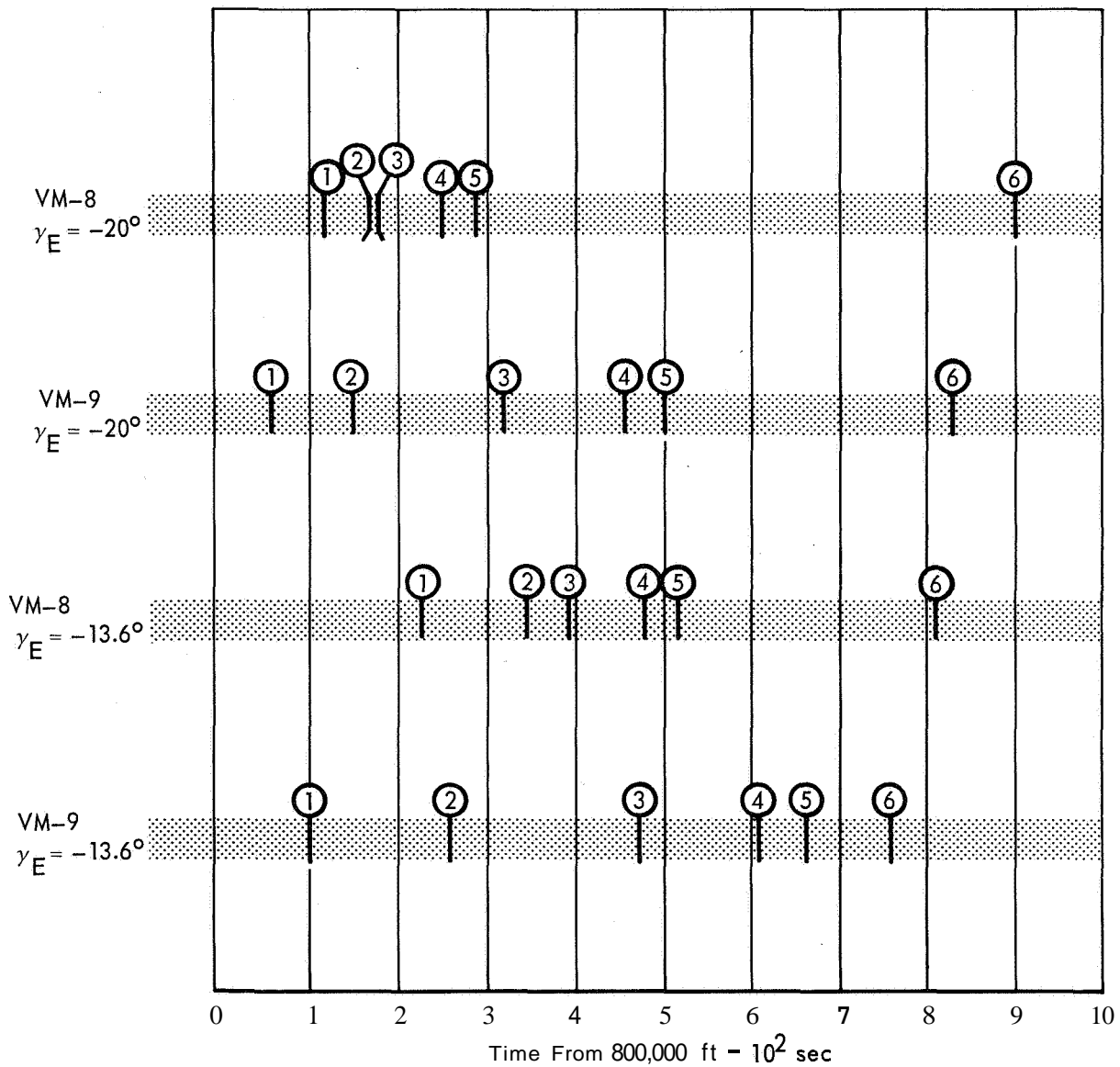


Figure 5.4-1

- Parachute Deployment— - The parachute is presently deployed at an altitude 23,000 feet. Deployment at higher altitudes would substantially exceed the Mach number capability of the parachute; deployment at lower altitudes would not allow sufficient time for the Aeroshell to impact prior to the operation of the landing radar, thus offering the possibility of the landing radar tracking the descending Aeroshell.
- Terminal Descent - Terminal descent is initiated at 5000 feet. Initiation of the terminal descent mode at a lower altitude runs the risk of impacting, prematurely, on a plateau, mountain or hill; higher altitudes require more fuel for terminal propulsion, and a larger and heavier parachute.

In summary, the optimization of the auxiliary aerodynamic decelerator and terminal descent propulsion subsystems has made the alternatives of Capsule sequencing for the benefit of the ESP, virtually non-existent. The quantity and quality of data obtained during a particular phase of the atmospheric descent will vary as a function of the atmosphere encountered, and the entry angle and velocity used.

5.5 AEROSHELL SEPARATION - The method selected for separating the Aeroshell and the Lander in the Martian atmosphere has a distinct effect on the quantity and quality of entry science data acquired. Separation alternatives and reasons for selection are described below.

5.5.1 Separation Alternatives - The preferred concept for Aeroshell separation was selected from four high value candidates which are briefly described below.

- Differential Drag: This was the selected concept and consists of an auxiliary aerodynamic decelerator (parachute) which is deployed at 23,000 ft. The Aeroshell is released 12 seconds later and falls away from the slower moving Lander/parachute combination.
- Fire-In-Hole: The terminal propulsion system, consisting of multiple throttleable rocket engines, is used to decelerate the Lander in retrograde direction by firing at the aft side of the Aeroshell, thus separating the Aeroshell and the Lander.
- Fire-Through-Hole: The terminal propulsion rocket engines fire through ports in the Aeroshell thus slowing the Aeroshell/Lander combination. Actual separation is delayed to a very low altitude (50 to 100 ft). No aerodynamic decelerator is used with this concept.
- Segmented Aeroshell: The Aeroshell is split (pyrotechnically or mechanically) into three or more segments which open up and are held open. The Lander is released and drops out. The Aeroshell is carried away above

the lander by the aerodynamic decelerator.

5.5.2 Comparison of Separation Alternatives - Each of the four separation alternatives has some disadvantages in terms of the quantity and/or quality of Entry Science data to be obtained using that particular system. Figure 5.5-1 shows a comparison of the disadvantages of each.

5.5.3 Selection Reasoning - Selection of the preferred concept of Aeroshell separation was made as a result of a major interdisciplinary trade study which is detailed in Section 4.6, Part B, Volume II of this report. While many factors were considered in making the selection, the effect of the selection on Entry Science, both directly and indirectly, was an important element in the final choice. For example, the contamination effects on TV lenses of the Fire-In-Hole separation counted heavily against it. Complicated aerodynamic characteristics and degraded science data due to exhaust gas flowback were important in deciding against the Fire-Through-Hole separation. While the segmented Aeroshell method of separation did not have many disadvantages from a science standpoint, the loss of TCM lock after separation did count against it somewhat. The only known disadvantage of the preferred concept is the oscillations induced by parachute deployment and this problem exists in three out of the four concepts. The Fire-Through-Hole concept was the lowest rated for both Entry Science and other non-science factors.

5.6 ATTITUDE CONTROL - Section 4.5 of Part D describes the preferred attitude reference and attitude control mechanizations for the various phases of the VOYAGER mission. This section discusses alternative mechanizations and their performance.

5.6.1 De-orbit - Reduction of the pointing angle uncertainty during de-orbit thrusting is desirable to reduce uncertainty in the initial entry conditions, and therefore improve the accuracy of the trajectory reconstruction. The total error during de-orbit thrusting is the result of the effects of three distinct error sources:

(1) initial alignment of the attitude reference before CB/FS separation, (2) reference drift during pre-de-orbit coast, and (3) attitude control system response to de-orbit disturbances. Attitude reference and attitude control performance are therefore equally important during de-orbit.

The alternative attitude reference systems considered are:

- Stable platform
- Strapdown gyros with Euler angle processing (the preferred design)
- Strapdown gyros with simple rate integration

Attitude reference alternatives were discussed in Section 5.2. The stable platform is heavier, more expensive and less reliable than the preferred design,

**COMPARISON OF AEROSHELL SEPARATION ALTERNATIVES
- ENTRY SCIENCE DATA OBTAINED**

FIRE IN-HOLE	FIRE-THROUGH-HOLE	SEGMENTED AEROSHELL	DIFFERENTIAL DRAG (PREFERRED CONCEPT)
<ul style="list-style-type: none"> o TV camera lenses must be covered during separation. No pictures during separation. Loss of reliability due to cover and sequencing. o Mass spectrometer will be sampling exhaust products during separation. o Accelerometer subjected to severe vibration during separation o Large oscillations during and after parachute deployment will affect TV pictures 	<ul style="list-style-type: none"> o No auxiliary aero. decelerator, therefore shortest period of subsonic operation, therefore least amount of subsonic data. o Stagnation temp. and pressure measurements and mass spectrometer sampling seriously affected by exhaust product flowback. o TV picture quality seriously affected by exhaust product flowback. o Accelerometer may be seriously affected by vibration of Aeroshell/Rocket interaction. 	<ul style="list-style-type: none"> o TCM lock with Spacecraft will be lost for a period during and immediately following separation. Transmission of data will not take place during that period o Large oscillations during and after parachute deployment will affect TV pictures. 	<ul style="list-style-type: none"> o Oscillations during and after parachute deployment will affect TV pictures

Figure 5.5-1

and was therefore eliminated. The simple rate-integration scheme has a higher drift rate than the preferred design, due to "coning" effects (kinematical coupling of angular rate about one body axis into Euler-angle rates about other axes). Reference drift therefore would exceed the design error budget in 13 minutes, as against 29 minutes for the preferred design. Such a reduction in the pre-deorbit coast time forces execution of the deorbit orientation maneuvers, with proportionate increase in attitude fuel expenditure. The simple strapdown concept is therefore eliminated.

- A single ring reaction control system (RCS), sized for maximum deorbit-motor disturbance torque (preferred design).
- Dual-ring RCS, each ring sized for the maximum deorbit disturbance, and firing on different deadbands.
- Thrust vector control (TVC) gimballed nozzle, jet vanes or fluid injection, plus a single RCS ring, sized for coast and/or entry attitude control.

The dual-ring RCS need not be discussed from a performance viewpoint in this subsection; for if the jets are properly sized, the backup ring will never fire, except in the event of a malfunction in the primary ring. As far as deorbit is concerned, then, the single/dual ring comparison is a weight and reliability question, and is discussed as such in Vol. IIC 15.7. Dual-ring performance with regard to atmospheric disturbances is discussed below.

The RCS versus TVC comparison made in Section 5.2 favored TVC, with pointing angle errors of 0.21, 0.27 and 0.35 degrees for gimballed nozzle, jet vanes, and RCS respectively. Installation of TVC, however, conflicts with the preferred method of thrust termination, nozzle blowoff. Although other method of solid rocket thrust termination are known, they are not considered sufficiently well-proven for VOYAGER. A TVC-plus-RCS system is also obviously more complicated than RCS alone.

5.6.2 Pre-Entry Coast - The dominant consideration in comparing attitude reference alternatives for this phase is the requirement to minimize power consumption during the six hours before entry. This calls for shutdown of the computer, resulting in selection of the simplest strapdown mechanization.

Attitude control during pre-entry coast is accomplished by the RCS, as modified by the previously mentioned considerations. Selection of the attitude deadband is a compromise between reference drift and impulse expenditure. With the selected 2.0 degree deadband, attitude uncertainty at entry is 15 degrees and impulse expenditure is 125 lb-sec. For an 0.5 degree deadband, attitude uncertainty at entry is reduced to 5 degrees, but impulse expenditure is increased to 320 lb-sec.

5.6.3 Entry and Atmospheric Flight - The early portion of the entry phase is essentially an extension of the pre-entry coast. Until an acceleration of $0.05g_e$ (1.61 ft/sec^2) is sensed by the axial g-switch (or the accelerometer backup), the RCS remains in an inertial hold mode, with the 2 deg deadband. The g-threshold discrete commands a mode change to three-axis rate damping, with a 3 deg/sec deadband.

Inertial Hold Regime - The angular reference direction for the inertial hold phase is set shortly after deorbit. It is assumed that this inertial orientation will be selected to minimize the angle of attack at the initiation of the entry rate damping. Because of the wide spread in atmospheric conditions, an angle must be selected that represents the average flight path orientation between the .05g point in the high density atmosphere extreme and the corresponding point in the low density extreme. The average angle will of course depend on the selected initial entry flight path. Illustrative calculations have been made for two extreme atmospheres, VM8 and VM-9, and two extremes of entry trajectory ($\gamma_e = -20^\circ$). The table below lists the angle of attack α and view angle (AB) occurring at 800K ft altitude and the .05g points of the two atmospheres assuming the inertial orientation of the Capsule is held to the average flight path and no reference uncertainty. The view angle is defined as the angle between the camera (roll) axis and the line of sight to the Martian horizon. The sign convention for both α and AB is positive upward, e.g., a positive AB leads to more "sky" in the pictures.

		800 KFT	.05g	.05g
		ALT	VM-9	VM8
$V_E = 15,000 \text{ ft/sec}$	α (Deg.)	-4.3	-1.7	1.5
$\gamma_E = -20 \text{ deg}$	AB (Deg.)	-3.2	-2.9	-4.6
$V_E = 13,000 \text{ ft/sec}$	α (Deg.)	-13	-5.4	5.4
$\gamma_E = -10.9 \text{ deg}$	AB (Den.)	-2.8	1.9	12.0

Hence, for the above conditions, the camera sees more of the Martian surface, than sky at all times except at the .05g point for either graze trajectory. Angle of attack at entry into the sensible atmosphere (.05g) is within ± 6 degrees for the cases shown.

The 3σ RSS reference uncertainty is estimated as 15degrees, which can be assumed to be ± 10.6 deg error in pitch and yaw. If it is desired to maintain camera view angles that give less "sky" than those previously shown, then the average inertial orientation can be biased down 10.6 deg. However, the actual

pitch error may also be downward, increasing the "sky" seen by the camera. This would result in the following view angles and initial angle of attack displacements :

		800 KFT ALT .	.05g VM-9	.05g VM-8
$V_E = 15,000$ ft/sec	α (Deg.)	-25.2	-22.9	-19.7
$\gamma_E = 20$	AB (Deg.)	-24.4	-24.1	-25.8
$V_E = 13,000$ ft/sec	α (Deg.)	-34.2	-26.6	-15.8
$\gamma_E = 10.9$ "	AB (Deg.)	-24.	-19.3	-9.2

For this assumed worst case condition, the wide angle camera (50 deg field of view) would barely see the horizon for the $\gamma_E = -20$ " entry conditions and the angles of attack are all relatively large which results in additional fuel consumption. The above examples, however, illustrate one approach. Other alternatives have also been considered which would reduce the boundary extremes. These are :

- Avoid graze entries.
Steep trajectories not only have smaller angular increments, but also a smaller initial angle of attack (smaller difference between depression angle and flight path angle at 800 Kft). Steep trajectories are also favored on the basis of other mission considerations - reduced multipath problems on the CB/FS telemetry link, reduced thermal loads, and smaller landing-site dispersions.
- Decrease the attitude deadband in the coast phase.
As mentioned above, an 0.5" deadband reduces the "coning" reference drift to 5" rss, or 3.5" in pitch. This reduces the downward bias which must be added to compensate for reference uncertainty, and also reduces the consequences of having an actual error opposite to the assumed error. The fuel penalty of 200 lb-sec in the coast phase may be more than offset by reduced fuel consumption during entry.
- Decrease the mode-switching g-level, to .03 or even .01 g. However, this proves to be a small reduction, i.e., the view angle spread between .01 g and .05 g is a maximum of 1.5 deg.

5.6.4 Rate-Damping Regime - According to the most recent wind tunnel data available, the selected VOYAGER configuration has stable pitch damping derivatives at all Mach numbers below 12.5. In considering attitude control alternatives for the entry phase, therefore, the primary decision is whether RCS damping is

necessary at all. If RCS damping is selected, subsidiary choices involve

- Jet orientation
- Jet sizing
- Single or dual ring
- Rate deadband value(s).

Figure 5.6-1 compares attitude envelopes with and without active damping, for VM-8 and VM-10 atmospheres, in a spectrum of wind conditions. For all runs shown in this table, a steep entry ($V_E = 15$ Kft/sec, $\gamma_e = -20^\circ$) was used. The initial angle of attack displacement is 5° in all cases. With these entry conditions, in a VM-8 model atmosphere, Mach number remains above 12.5 until an altitude of 52 Kft, which is below both the wind onset altitude (90 Kft) and the altitude at which maximum dynamic pressure occurs (60 Kft). This explains the large rate-envelope values shown for VM-8 runs at 100 Kft and 50 Kft, without RCS damping. Attitude and rate envelopes converge rapidly thereafter. In contrast, the VM-10 model with the above entry conditions hits maximum dynamic pressure at 108 Kft, drops below Mach number 12.5 at 100 Kft, and is therefore stable throughout the wind regime, from 90 Kft on down. Corresponding no-jet rate envelopes for VM-10 at high altitudes are therefore smaller than for the VM-8 model. In no case, however, are the rate envelopes at 100 Kft acceptable for TV imaging ($4^\circ/\text{sec}$ or less). The immediate conclusion is that RCS damping is required.

With the need for RCS damping demonstrated, the subsidiary questions may be taken up.

Orientation - The preferred RCS configuration places the pitch/yaw jets in an aft-firing orientation (slightly canted), since forward firing would require ports in the Aeroshell, and outward firing would sharply reduce the control torque.

Sizing - The preferred jet size is 22 pounds, which meets the deorbit torque requirement with a 50% reserve. This torque level is quite generous for control of mean and shear wind profiles. In a VM-10 shear-profile crosswind, for example, decreasing the jet size to 10 pounds only increases the maximum angle of attack envelope from 1.8° to 2.2° .

For control of transient wind disturbances (steps and gusts), however, large jets are desirable, to shorten the period of violent oscillation (during which much of the ESP data is degraded). Sample data illustrating the dependence of

WIND RESPONSE WITH AND WITHOUT RCS DAMPING
 (ENTRY CONDITIONS: $V = 15k$ ft/sec, $\gamma = -20^\circ$, $\alpha = 5^\circ$ AT 800k ft; AERODYNAMIC DAMPING ESTIMATED FOR c.g. AT BASE OF AEROSHELL)

RUN	ATMO VM-	WIND		RCS	AH ENVELOPE, deg			RATE ENVELOPE, deg/sec			IMPULSE lb-sec
		TYPE	AZIMUTH		100k ft	50k ft	25k ft	100k ft	50k ft	25k ft	
94	10	Mean	Head	No	3.0	0.005	0.03	33	0.9	0.4	-
99		Mean	Head	Yes	0.21	0.04	0.03	-	-	-	138.0
95		Mean	Cross	No	3.0	0.03	0.03	33	1.	0.3	-
98		Shear	Head	Yes	0.21	0.95	0.85	-	-	-	181.2
96		Shear	Cross	Yes	3.0	4.1	3.0	33	12.	7.5	-
97		Shear	Cross	Yes	0.21	1.7	0.63	-	-	-	216.8
95a	8	Mean	Cross	No	2.7	3.8	0.01	21	50.	0.5	-
96a		Shear	Cross	No	2.7	4.1	0.06	21	54.	1.7	-
97a		Shear	Cross	Yes	0.50	0.48	0.22	-	-	-	191.1

Figure 5.6-1

gust response upon jet size are given in the table below:

<u>Thrust</u>	<u>Max. Angle</u>	<u>Max. Rate</u>	<u>Settling Time</u>
10.0 lb.	28.1 deg.	66.7 deg/sec	50.0 sec.
16.5	27.2	63.4	17.6
30.0	25.1	56.1	8.4
45.0	22.9	48.0	5.0
60.0	20.7	39.7	3.8

Additional wind transient results are shown in Figure 5.6-2, which covers a range of altitudes, atmospheres, wind forms and azimuth angles, for a fixed jet size. For a few runs in this table, a positive (unstable) damping derivative value was used; for all others, the damping derivative was assumed zero (neutral dynamic stability). Capsule tumbling, which is regarded as catastrophic, is denoted by a maximum angle of "90+".

Dual Ring - Although high thrust levels are desired for control of severe transients, increasing jet size increases fuel consumption in less severe wind conditions (e.g., increasing jet thrust from 10 to 16.5 pounds on a VM-10 shear, crosswind run raised impulse expenditure from 319 to 342 lb-sec). A dual-ring RCS, therefore, seems attractive. The first ring would fire on the normal deadband, the second would fire on a higher deadband, and thus respond only to severe disturbances. Such a configuration should give the best combination of transient response and fuel economy. However, system weight is an over-riding consideration and therefore the single-ring RCS (which is 46 pounds lighter than the dual ring) was selected as the preferred design.

Varying Deadband (s) - Decreasing the RCS rate deadband (two deadbands for dual-ring RCS) naturally tends to decrease the oscillation envelope but may increase the impulse expenditure a disproportionate amount. Sample data for the VM-10 shear crosswind runs are:

<u>Deadband</u>	<u>Max. Envelope</u>	<u>Impulse Expended</u>
4 deg/sec	2.4 degrees	305 lb-sec
3	2.2	319
1	1.2	1453

Using a 4 deg/sec deadband, however, is crowding the TV smear boundary, which is estimated as 4 deg/sec for the narrow field camera. The design value of 3 deg/sec deadband keeps rates well below 4 deg/sec under all conditions except transient winds, and increases fuel consumption very little over 4 deg/sec deadband.

**RESPONSE TO LOW-ALTITUDE WIND TRANSIENTS:
SHARP-EDGED STEPS AND SHARP-EDGED RESONANT GUSTS**

(ENTRY CONDITIONS: $V = 15\text{kft/sec}$, $\gamma = -20^\circ$ AT 800 kft; 16.5-lb RCS)

RUN	ATMO- SPHERE VM-	WIND CONDITIONS				AERO. DAMPING	SYSTEM RESPONSE			
		h_w kft	V_w ft/sec	TYPE	AZIMUTH		θ_{\max} deg	$\dot{\theta}_{\max}$ deg/sec	T_c sec	I_c lb-sec
81	8	30	200	G	Head	0	2.64	18.3	3.5	52.5
82		30	200	G	Cross	0	9.47	66.4	13.4	215.7
47		20	200	S	Head	0	3.25	13.0	2.4	37.2
78		20	200	S	Cross	0	8.98	38.0	7.3	117.3
80a		20	200	G	Head	0	6.14	25.4	5.4	85.0
80b		20	200	G	Head	0.5	6.40	27.9	8.8	140.0
79a		20	200	G	Cross	0	16.84	73.8	14.5	234.3
79b		20	200	G	Cross	0.3	29.89	83.7	-	-
79c		20	200	G	Cross	0.5	90 t	-	-	-
83a		10	30	100	G	Head	0	23.29	54.2	11.5
83b	30		100	G	Head	0.3	24.2 1	58.7	36.0	586.8
84	30		100	G	Cross	0	24.69	56.8	12.3	211.2
43	20		100	S	Head	0	14.51	34.7	7.0	112.2
44	20		100	G	Head	0	26.84	61.8	13.3	219.3
65a	20		100	G	Head	0.1	27.15	63.4	17.4	289.9
107b	20		100	G	Head	0.2	27.61	65.3	27.8	452.3
65b	20		100	G	Head	0.3	90t	-	-	-

Notation - h_w = Wind Altitude
 V_w = Wind Velocity
S = Sharp-Edged Step
G = Sharp-Edged Resonant Gust
Aero. Damping = C_{mq} or C_{nr} , as appropriate (positive values are unstable)

θ = α or β , as Appropriate
 $\dot{\theta}$ = q or r , as Appropriate
 T_c = Time to Control to 3 deg/sec
 I_c = Impulse to Control to 3 deg/sec

Figure 5.6-2

Additional discussion of entry-phase attitude dynamics may be found in Volume 11, Part B, Section 2.3.4.

5.6.5 Parachute Deployment - The preferred design and operational sequence calls for RCS shutdown at parachute deployment, and separation of the RCS with the Aeroshell 12 seconds later. The stagnation-pressure sensor will also separate with the Aeroshell, terminating that experiment.

Continuation of RCS damping during parachute descent has been considered but does not appear feasible for two reasons:

- o The aft-firing yaw/pitch thrusters provide very little control torque about the primary center of rotation, located high in the parachute canopy.
- o The entire system parachute rigging and Capsule Lander - behaves as a compound pendulum. The oscillatory motion is therefore quite complex and it is difficult to say whether a simple rate-damping control law would in fact be stabilizing.

The parachute and rigging provide some damping of the primary mode (gross oscillation of the canopy), but little damping of the secondary mode (oscillation of the Capsule Lander about suspension point). In addition, the entire configuration is very tall (over 125 feet) and is thus quite sensitive to broadside gusts. For these reasons, the parachute descent phase is likely to be a period of large oscillations and high angular rates, which will degrade most ESP data. Radar altimeter readings will become the dominant data source for the trajectory reconstruction, due to the high noise level in the acceleration data.

Parachute dynamics are described in detail in Volume II B 5.10.

5.6.6 Terminal Descent - The preferred terminal descent sequence begins at about 5000 feet altitude, with ignition of the four 1620-pound bipropellant terminal descent engines. Parachute separation occurs shortly thereafter. These engines are throttleable over a 10:1 range, which provides both velocity and attitude control during the period from parachute separation to final cutoff, at an altitude of 10 feet and a final velocity less than 10 ft/sec. Detailed descriptions of the throttling control law and the resultant system response are given in Volume 11, Part B, Section 2.3.6.

An alternative all-propulsive mechanization, which eliminates the parachute, has also been considered. For this scheme, the engine thrust would be increased to 2000 pounds, ignition altitude increased to 15,000 feet, and the engines would fire through ports in the Aeroshell.

This would eliminate the high oscillations and uncertain dynamics of the parachute phase, and would be advantageous for imaging and acceleration data. The degree of degradation of TV image quality by rocket plumes would depend upon the relative location of the TV window and the rocket ports. A small amount of additional image degradation will be caused by engine-induced vibrations of the structure. With the Aeroshell in place, there will be very little intrusion of exhaust gases into the base-region atmospheric measurement apparatus, but the stagnation-pressure measurements will be somewhat degraded by engine plumes.

The choice between all-propulsive and aerodynamic decelerator-plus-propulsion, as well as the selection of the four-engine configuration from various other possibilities, is based upon tradeoff studies too complex to describe here (See Volume 11, Part B, Section 4.5 for details).

5.7 RADAR ALTIMETER - A radar altimeter is required to provide an altitude measurement for Entry Science data correlation. This altimeter has been described previously in Volume 11, Part B, Section 5.9 "Analysis" and Volume II, Part C, Section 10.1 "Functional Description" as part of the Capsule Bus equipment. A summary of the factors influencing altimeter selection are discussed below.

5.7.1 Constraints and Associated Design Alternatives - Development of the preferred Capsule Bus design for minimum complexity and maximum reliability subjected the altimeter design to the major constraints listed in Figure 5.7-1. Design alternatives which conform to these constraints are also listed.

5.7.2 Performance Alternatives - Maximum and minimum altitudes of operation will be set by the importance of the data at these altitudes and the increase in size, weight and power which can be tolerated. Altimeter accuracy must also be set by the subsystems dependent on the altimeter data and must consider weight and power increases for altimeter accuracy increases. Altitudes of operation from as low as 10 feet and up to 10^6 feet over the expected Martian surface could be obtained. Accuracies of better than 1%, \pm 5 feet are possible.

5.7.3 Selection of Preferred Design - Altimeter selection was influenced by the overall landing and mission constraints plus the altitude and accuracy required for Entry Science data correlation.

5.7.3.1 Constraint Design Alternatives - Switched fan beam antennas, steered narrow beams and single element antennas were candidates for providing the required coverage. Antenna switching and electronic beam steering were eliminated because of weight, complexity or development risk aspects. A single element antenna providing an approximation to the desired coverage is the lightest and most

ALTIMETER DESIGN CONSTRAINTS'

CONSTRAINTS	ALTIMETER DESIGN – ALTERNATIVES
1. Capsule Bus System will not have preferred roll orientation; rate damping only.	<ul style="list-style-type: none"> a) Single Element b) Electronic beam steering c) Switched antennas
2. Perform required function at pressures causing electrical breakdown	<ul style="list-style-type: none"> a) Dielectric insulation around components subjected to high voltage gradients b) Use low power, low voltage techniques c) Complete system pressurization
3. Operate before and after Aeroshell release	<ul style="list-style-type: none"> a) Provide RF window, primary and secondary antennas b) Use section of Aeroshell and secondary antenna c) Use two separate altimeters
4. Discriminate between Aeroshell and ground	<ul style="list-style-type: none"> a) Blank near returns while searching for surface b) Use loop tracking logic to unlock from opening targets c) Prevent altimeter operation until Aeroshell is sufficient distance away.

Figure 5.7-1

reliable. However, the low gain of this antenna increases the possibility of electrical breakdown. Elimination of breakdown can be most reliably obtained by covering the sections where high voltage gradients exist with a dielectric, such as teflon or silicon based materials, to exclude atmosphere.

The alternatives for operation before and after aeroshell release are (1) use of separate altimeters and antennas or (2) one altimeter and two antennas. The single altimeter-two antenna concept was selected from weight and antenna placement considerations. Use of the Aeroshell as an asymmetrical dipole to provide the desired coverage was eliminated based on the mechanical design of the Aeroshell, antenna fabrication, installation and checkout difficulties. A conical monopole antenna operating through an RF window in the Aeroshell nose cap provided the best coverage and most compatible installation.

Operation after Aeroshell release requires the altimeter to discriminate against the Aeroshell as a target. Methods of discrimination, such as built-in tracking loop logic which rejects opening targets such as the Aeroshell, require an excessively complex mechanization. Delaying operation until after the Aeroshell is a sufficient distance away would compromise the remainder of the mission. Near return blanking, such as that performed by pulsed radar systems, is the simplest and most reliable and has been selected as the preferred design.

5.7.3.2 Performance Required - Maximum altitude of operation was selected to be 200,000 ft., since studies show that Entry Science data correlation and iterative extrapolation back to 800,000 ft. could still be made accurately. Operation at higher altitudes required penetration of possible blackout plasmas, or operation at 500,000 to 600,000 ft., before blackout occurred. Operation down to 50 feet is desired to provide a functional backup to the Landing Radar range beam. Operation at altitudes lower than 50 ft. requires increased complexity with attendant unreliability and two separate antennas. An accuracy of $1\% \pm 400$ feet for Entry Science atmospheric data correlation was selected as an optimum compromise based on a computer study which determined degradations in Entry Science data accuracy as a function of altimeter accuracy and altitude.

5.7.3.3 Frequency and Modulation Selection - An operating frequency selection imposed certain considerations on the modulation techniques available. From a maximum returned power criteria, when using omnidirectional antenna coverage, a frequency from 10 to 500 MHz appeared best. Selection of the conical monopole, however, constrained the frequency to be 1 GHz or higher. Simple non-coherent pulse, frequency modulated/continuous wave (FM/CW), FM/CW Bessel Sideband,

Interrupted Continuous Wave (ICW) and Pseudo Random Code were the modulation techniques considered. Selection of the 5 microsecond single non-coherent pulse technique was based on obtaining the best performance for the least complexity (see definition of ratings given in Section 5.9, Part B, Volume 11).

5.7.4 Problems and Options - The present altimeter selection uses simple techniques and space proven equipment. No state-of-the-art advances will be required to obtain a usable system. Design development to insure sufficient electrical breakdown protection must be performed during Phase C development.

5.8 POST TOUCHDOWN OPERATION - Mission profile study results indicate that a period of time is available after touchdown during which the orbiting Spacecraft is in view of the landed Capsule. The entry and landing phase operations time line diagram contained in Section 5.5 (Figure 5.5-1) indicates that the CBS low rate UHF communications link with the SC will be available for a minimum of 100 seconds to a maximum of 600 seconds after touchdown for the baseline orbit size and de-orbit anomaly, and worst entry velocity conditions. The ESP VHF communications link with the SC is designed to maintain an adequate signal margin at least to touchdown for the worst case combination of entry and atmosphere conditions. Since the low rate data from the ESP is interleaved on the CBS UHF link, surface atmosphere properties can be obtained from the ESP base region pressure and temperature sensors quite easily and involves simply not turning these instruments off. Composition data can also be obtained from mass spectrometer measurements. The sample is obtained in a different manner than during descent since, without any dynamic pressure, pumping is required for fresh samples. Due to the small pumping capacity of the mass spectrometer, a small time constant associated with obtaining fresh samples requires an alternate small diameter, short tube. Thus, in the interest of obtaining fresh atmosphere samples after touchdown, the mass spectrometer molecular leak inlet will be switched to a small capillary sampling tube.

MODULATION TECHNIQUE RATING

NUMBERS SHOW VALUE UNITS

MODULATION TYPE		SELECTED CONCEPT		FM/CW ZEMO IF	FM/CW 3E SEL SIDEBAND	ICW HIGH-PRF WITH AMBIGUITY RESOLUTION	FSK PSEUDO-RANDOM CODE (CORRELATION)
SELECTION FACTORS	SIMPLE PULSE, WITH PULSE WIDTH SWITCHING	3	Reduced accuracy, increased TX RX coupling, decreased maximum range.	1	Degrades risetime, reduces accuracy.	3	
Omni-directional Antenna Coverage Constraint							
Accuracy	Best accuracy if pulse width switch used.	4	Ranging, step error, return noise, leakage noise.	2	Phase linearity, phase distortion of ground return.	3	
Maximum/Minimum Altitude	Breakdown susceptible, pulse-width switching required.	2					
High Voltage Breakdown	Most susceptible, design must overcome.	2					
Complexity/Reliability		3					
Operation through Aeroshell and after Aeroshell Release	Natural aeroshell discrimination.	4					
Ambiguity Resolution		3					
Weight		3					
Previous Use and Development Risk	All techniques and concepts previously used. Much development done.	4					
Input Power		3					
Total Rating		31		22	21	24	25

Figure 5.7-2

PART F

FUTURE MISSION OPTIONS

The desirability of carrying out entry science measurements and observations on the later missions stems primarily from:

- a. The new place and time of each successive landing,
- b. The new questions raised by previous results,
- c. The opportunity for improved performance based on a proven range of uncertainties, better identification of interfering difficulties, and engineering monitoring data on equipment performance,
- d. The extent to which the ESP measurements can supplement the Orbiter and Surface Laboratory results of each mission,
- e. The number of important measurements and observations not included in the first ESP because of weight and priority considerations.

The entry TV observations of the new landing sites will be useful in defining the area around the lander; the atmospheric profile can be determined for a different time of day, season, and location; and additional instruments and measurements can be added based on the early mission results.

The results of the 1973 entry composition measurements will no doubt have significant effect on the desired future mission sampling technique and also on the instruments mass ranges and accuracies desired. Also, since the density profile is expected to undergo large diurnal variations, the measurement of the density profile at a different time during the day for the later missions will provide further information leading to a precise definition of the atmosphere.

The prime objectives for descent TV on future missions will still be landing site identification and detail pictures of the surface area around this site. However, the methods employed to procure these pictures will differ somewhat since we will have a better idea on the properties of the atmosphere. We will know when the communications blackout and peak heating occur and this will precisely define when the pictures can be taken. Planning can therefore, be directed at insuring optimum coverage and resolutions using the best descent profile, a high bandwidth data recorder employed, and high density sampling conducted at altitudes where it will give the most desirable pictures. Reduced surface condition uncertainties and/or a small weight increment can permit imaging to examine small detail down to

within a few feet of the surface, without having to worry about the camera system interfering with capsule landing mechanisms. For future missions with a mobile laboratory, the descent images can back up those obtained from the laboratory for purposes of deriving initial displacement vector commands. For future missions with a stationary laboratory, the descent images promise to increase the inter-pretability of those obtained from the surface. The photometric measurements of surface reflectivity can be optimized, particularly with regard to a better spectral evaluation. The same statement can be made concerning spectral investigations of atmospheric attenuation.

These jobs can be accomplished with small variations on the selected approach. Alternately, it may be feasible to reduce the instrument package to only a single vidicon. Or a two vidicon system could be employed with one camera gathering descent information while the second is reserved for a rapid post-landing, panoramic scan of the surroundings. Still another choice would be to perform this high data rate panoramic scan just prior to touchdown. A wide angle optical system would be used with images taken in a very short period and immediately transmitted to the Orbiter.

Of the priority-addition experiments discussed in Parts A, D, and E, those which could most easily be worked into the selected design at minimum weight and maximum confidence in obtaining useful results include: a) the UV and X-ray absorption experiment, and b) the differential nose pressure measurement. Confidence in getting useful results with the mass spectrometer arranged to yield data from the beginning of continuum flow to post touchdown is realistically somewhat less, but still high. However, the ceramic nose cap of the selected design concept considerably simplifies the problem, and installation is straight-forward. Similarly, the installation of γ backscatter instrumentation (5 lbs) is straightforward. For the highly desirable post touchdown imaging, spacecraft ESP receiving antenna positioning and the weight of an 8 pound facsimile camera, plus installation, represent somewhat more of a problem. However, this capability utilizing the ESP UHF Spacecraft-relay communications link is a highly desirable backup to Surface Laboratory imaging.

Additional experiments or ESP accommodations for future ESP missions are illustrated by, a) composition measurements in the molecular flow regime, b) radiometers for use during parachute descent, c) capability for recording and retransmitting images obtained during blackout, with maintenance of suitable imaging interval, and d) capability to handle accelerometer data during touchdown, for

supplemental soil mechanics information.

The selected ESP design concept is amendable to either deletion or modification and retention for future missions (or retention without modification). Retention of the TV and telecommunications system as basic items, with affordable flexibility for modification and addition of other measurements, is desirable.